Dissertation

Determination of Vapor Pressures of Hazardous Materials with Transpiration Method, Coupled to Chromatographic Techniques

Greta Bikelytė

2021

Dissertation zur Erlangung des Doktorgrades
der Fakultät für Chemie und Pharmazie
der Ludwig-Maximilians-Universität München

Determination of Vapor Pressures of Hazardous Materials with Transpiration Method, Coupled to Chromatographic Techniques

Greta Bikelytė

aus

Vilnius, Lithuania

2021

Erklärung

Diese Dissertation wurde im Sinne von § 7 der Promotionsordnung vom 28. November 2011 von Herrn Prof. Dr. Thomas M. Klapötke betreut.

Eidesstattliche Versicherung

Diese Dissertation wurde eigenständig und ohne unerlaubte Hilfe erarbeitet.

München,03.06.2022

_____

Greta Bikelytė

Dissertation eingereicht am: 01.07.2021

1. Gutachter: Prof. Dr. Thomas M. Klapötke

2. Gutachter: Prof. Dr. Konstantin L. Karaghiosoff

Mündliche Prüfung am: 10.08.2021

Dedicated to my family

Acknowledgments

First of all, I would like to thank my supervisor, **Prof. Dr. Thomas M. Klapötke** for the opportunity to do my fast-track Ph.D. in his research group. I am very proud to belong to his group and I greatly appreciate that he believed in me while I was still an ERASMUS student in the third year of my bachelor studies in Vilnius University. Professor Klapötke was very supportive during the scholarship and fast-track assessment periods and throughout the whole doctoral studies. Professor Klapötke always had an interest in the not-so-common topic of my research project and made me feel welcome in the group by always appreciating the fact that I came to this group from a background of physics. The support and the scientific freedom allowed my project to move forward and I was able to gain successes in my research. Once again, thank you very much.

I would also like to thank the members of the Ph.D. examination commission for reading my project report and taking a significant part in my journey to achieve my degree.

Additionally, I would like to express my gratitude to my thesis reviewer **Prof. Dr. Konstantin L. Karaghiosoff**, who was extremely helpful during the time of my research project, devoted hours of his time to consult on various scientific matters and always provided great opportunities to visit companies and meet knowledgeable people working on analytical chemistry.

I would like to thank German Academic Exchange Service (DAAD) for financial support throughout the period of my research project under the grant no. 57299294. **Ms. Laura Mendelssohn** is gratefully acknowledged for the overall help and care for my well-being during my academic stay in Germany. The scholarship made this amazing opportunity possible and I will be forever grateful for the support.

The research project would have never had a successful course without the help of **Dr. Martin Härtel**. Back in 2015, Martin agreed to supervise my ERASMUS internship and during that time introduced me to the specifics of the chemistry lab, gave me invaluable lessons on the analytical techniques as well as the transpiration method. As the Martin‘s project time came to an end, he offered me to become his successor and continue the vapor pressure measurements

in the group of Prof. Klapötke. I gladly accepted this opportunity. Since then, Martin was extremely helpful, guiding through the intricacies of the transpiration method, provided ideas, advices and his expertise, and was an integral part of my positive experience during the period of my doctoral studies. I can say with confidence, that during these past 6 years I not only learned so much from him, but I also gained a friend.

I would also like to thank **Prof. Sergey Verevkin** for kind advice and insight into the problematics of the vapor pressure measurements through our extensive email correspondence and I had a pleasure meeting him in XXII International Conference on Chemical Thermodynamics in Saint Petersburg, Russia.

Dr. Burkhard Krumm is also gratefully acknowledged for numerous discussions and his contribution to a successful establishment of quantitative NMR experimental procedure, which allowed me to introduce very precise analytical technique to my routine analysis.

I would like to thank **Ms. Irene Scheckenbach** for her warmth, care and support when it came to bureaucratic inconveniences that came along with a foreigner studying in Germany.

I am also grateful for two of my students – **Audrius Sadaunykas** and **Andreas Neuer** – for their time, patience and efforts to help me achieve major results in my research project. Both of them gave invaluable support and brought joy to my everyday routine.

For scientific collaborations and input towards the success of my research project I want to thank **Alex G. Harter, Stefanie Heimsch, Max Born, Jasmine Lechner, Jelena Reinhardt, Dr. Teresa Küblböck**, **Dr. Marco Reichel, Marcus Lommel**.

Additionally, successful fast-track Ph.D. assessment test would not have been possible without the **Prof. Dr. Achim Hartschuh**, who allowed me do my internship in his group. Accordingly, I would like to thank my internship supervisor **Veith Giegold**.

I would also like to particularly thank **Maurus Völkl** for his helping hand in academic and everyday life as well as for making my journey full of laughs, meaningful conversations, board game afternoons, explorations of remote places and countless online calls. **Stefan Huber** deserves a heartfelt acknowledgement for being a source of laughs and aid at all times.

All former and current members of the work group of Prof. Klapötke are also gratefully acknowledged.

I would also like to thank my partner **Markus** for every second that he has been by my side. A great part of my achievements would not have been possible without him and his family that welcomed me and made me feel at home.

Finally, I would like to thank the most important people **– My Dear Family –** for all the support throughout this endeavour. Thank You for believing in me. All I have done is for You.

Table of contents

1. Introduction

In the late evening of the 22nd of May, 2020, a suicide bomber detonated a shrapnel-loaded homemade explosive (HME) device after a highly attended Ariana Grande`s concert in the Manchester Arena, Manchester, England [1]. During a 6-month period before the incident, the organizers of the attack purchased the necessary ingredients to prepare and assemble the improvised explosive device (IED). The terrorists avoided the exposure of their own identities and, using the names of their families and friends, ordered and purchased widely available precursor materials required to synthesize a significant amount of a powerful explosive material - triacetone triperoxide (TATP) [2]. An independent assessment of the institutional actions revealed that the involved individuals had not been under an active investigation prior to the incident, but in the months before the attack certain activity drew the attention of the intelligence and a meeting for the reconsideration was scheduled to take place, but it had not been held as of the date of the attack [3]. Insufficient preventative measures lead to a tragic terror attack, killing 22 and injuring over 800 civilians [4]. Unfortunately, this is only a single example out of multitude IED-related attacks involving casualties. In between October 2010 and September 2020, globally more than 170 000 people (civilians and armed actors) were killed or injured by IEDs, corresponding to approximately 48% of all reported victims of explosive violence [5]. According to Explosives Incident Report (EIR) of the United States Bomb Data Center (USBDC), solely in the USA, in the year of 2019, 84 of the explosives incidents and 656 of the recoveries involved IEDs [6]. These statistics show that IEDs pose a significant threat and international conversations about the installment of more efficient preventative measures in a whole chain of IED threats are regularly introduced [7]. In 2008, the European Union approved an Action Plan on Enhancing the Security of the Explosives [8], which prioritized the step-up of the explosives-related research and set specific goals including aggregation and spread of the research results on IEDs precursors and detection technologies, further research on the IEDs, their properties and the detection of explosives and their precursors. Major improvements in the detection technology of trace and bulk amounts of explosives have been achieved since [9-13]. Further information on several most important detection techniques will be discussed in the Chapter 1.1.

The explosive trace detection (ETD) plays a significant role not only in the efforts to combat the terrorism by the use of the IEDs, but also it is important in many other fields, including

forensics, environmental monitoring, as well as the manufacture and storage of explosives [9]. In the past, detection of the explosives has been approached in two ways: detection in condensed and gaseous phase (particles and vapor). The detection of the explosives in the gaseous phase has always been problematic even for the most volatile compounds since the detection might be intercepted by environmental conditions, careful packaging of the explosive material, sample accumulation and adhesion on the surfaces, and many others [9; 14; 15]. Moreover, a wide array of explosive materials of interest also vary significantly in their physical and chemical properties and it makes them more or less susceptible to different detection technologies [16].

One of the parameters that can differ considerably depending on the type of the explosive of interest is the vapor pressure [14; 17].

Many common high explosives possess extremely low vapor pressures (in the range of ppt at room temperature), which is a difficult task to overcome for some of the detection devices, such as sniffers or stand-off vapor detection techniques. On the other hand, some utilized explosive materials have considerably high vapor pressures (TATP, etc. [18]), which reduces the difficulty of the vapor phase detection, but introduces a time dependency when it comes to the detection of the traces, deposited on the exterior of the packaging [13]. Various additives and impurities in the explosive mixtures, depending on their properties, may further reduce the vaporization of the explosive material, or, instead, possess high vapor pressure themselves and aid in the detection. For all of these reasons, in order to fully comprehend the detection characteristics of novel vapor detection devices, the vapor pressures of the target compounds need to be understood [14]. In addition, sufficient information about this property allows the estimation of maximum possible concentration of the molecules in the gas phase at a given temperature and, correspondingly, their condensable fraction, which is also of a great importance for the monitoring of the fate and the pathways of atmospheric pollutants in the environment [19]. Furthermore, volatility of the molecules can contribute to the development of computational approaches dealing with modeling of vapor plumes in confined areas to improve screening procedures and placement of sensors [9]. And lastly, the vapor pressure is vital for the development of detection standards and evaluation of the emerging detection techniques [14].

Experimental vapor pressures of explosive materials have been measured extensively in the past, however many of the reported values are in a disarray [14; 17]. The reason behind it often

lies in the great variation of used determination techniques (when an inappropriate vapor pressure measurement technique is chosen for the application) or the insufficient purity of the samples used. It is generally recognized that for low vapor pressure compounds, such as explosives, the most suitable are gas-saturation (transpiration), Knudsen effusion and Langmuir methods [20-22]. Additionally, there is constant strive to develop suitable techniques for vapor pressure measurements at near-room-temperature conditions for extreme low-volatility compounds, which was not possible with some of the classical techniques [22; 23]. Further information on the vapor pressure measurement techniques will be discussed in the Chapter 2.

Experimental values obtained with mentioned methods allow the determination of the vapor pressure-temperature (*p*-*T*) relationship. Generally, the relationship is described by an exponential function, but when the *p*-*T* data is plotted as a natural logarithm of the vapor pressure versus the reciprocal temperature, for relatively short temperature ranges a linear dependency is observed (**Figure 1**).

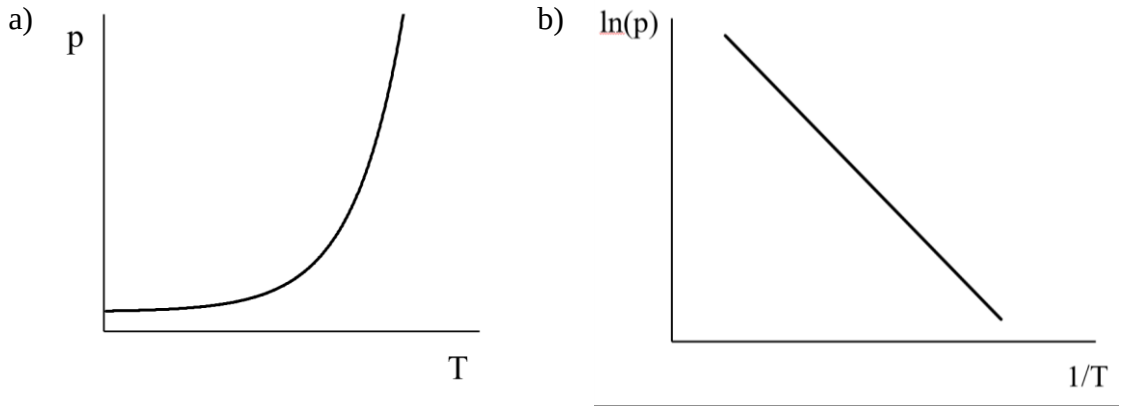

Figure 1. Vapor pressure and temperature dependencies: a) $f(T) = p$; b) $f(1/T) = \ln(p)$.

Knowledge of the *p*-*T* relationship allows the determination of other thermodynamical parameters such as molar enthalpies and entropies of the phase transition. These phase boundary thermodynamic properties help tracking the energy paths in chemical reactions and physical processes. One recent example of implementation of phase transition thermodynamics was demonstrated by its recent application for contact cooling of the computer servers [24]. The servers are operated in a bath of a non-conductive low-boiling thermal fluid. At the boiling temperature, any additional computer hardware-generated thermal energy is efficiently transferred and consumed to elevate a specific amount of the cooling liquid into the gaseous

phase which eventually gets carried away and condensed outside of the computer system, keeping the hardware operation at optimum conditions. Besides practical implementations, knowledge of compound-specific thermodynamic properties such as enthalpies of phase transitions are highly desirable for the transformation of the values of molar enthalpies of formation from condensed to the gaseous state. Some theoretical aspects of these thermodynamic concepts in terms of this project will be discussed in the 2.6.

1.1. Explosive trace detection (ETD) techniques

There are two main approaches when it comes to the detection of the explosive materials: bulk and trace detection. Bulk detection usually focuses on the determination of the anomalies in the composition of the materials. The methods include the determination of density variation, nitrogen content, neutron emission spectrum, etc. [25]. However, this chapter will focus on the detection of trace amounts of explosive material, which usually is sub-microgram scale, non-detonable and not visible with a naked eye. Two different types of sampling procedures are applied in the detection technology – surface (condensed phase) or vapor (gaseous phase) sampling. In the comprehensive review by *Moore* [13], a classification of detection methods according to their sampling protocol was graphically illustrated (**Figure 2**) and thoroughly discussed. Plenty of reviews on current advances of trace detection technology were published since, including a two-part work by *Brown et al.* [11; 12], works by *To et al.* [9], *Giaonnoukos et al.* [26] and others.

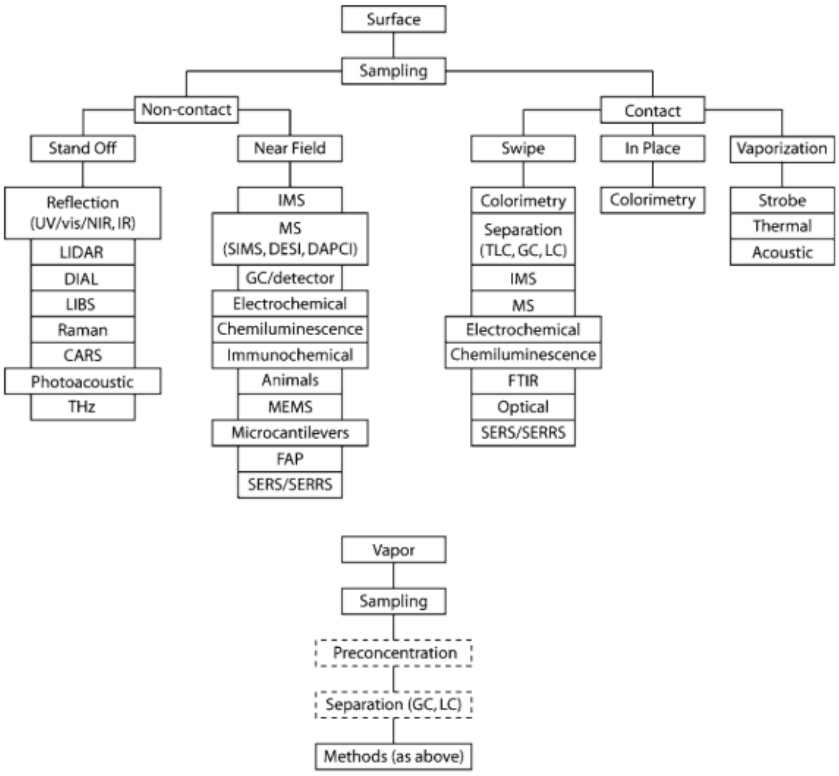

Figure 2. Non-exhaustive overview of trace explosive detection technologies according to their sampling protocol. Reprinted with permission from [13]. Copyright 2008 Springer.

Before the detector is applied in practice, it has to be evaluated for its detection limits and performance. For this reason, vapor generators are often necessary in order to deliver the analyte vapors to the device being tested. Consequently, the vapor-generating systems must be calibrated and able to deliver vapors reproducibly and of a precise concentration. However, for low-vapor pressure compounds, such as explosives, the task is not so straight-forward. The evaporation processes for solid explosives are inherently slow and, therefore, it has to be accelerated by exposure to elevated temperatures. These temperatures have to be maintained constant throughout the whole system to avoid possible molecular adsorption or condensation on the cold-spots, which would result in a generation of fluctuating or not-defined vapor concentrations. Also, in some cases it is assumed that the output concentration is governed by the theoretical saturated vapor pressure values, however, in reality, the saturation is not achieved. Many of these aspects and various types of vapor-generating devices have been previously discussed in the work by *Grate et al.* [27].

The European Civil Aviation Conference (ECAC) periodically prepares and updates a list of ETD devices, which are in accordance with ECAC and European Union (EU) performance

standards [28]. As of the current date, the majority of approved devices are ion mobility spectrometers (IMS) and mass spectrometers (MS). These technologies, animal olfactory systems and several detection techniques concerned in terms of vaporization (devices that screen analytes in gaseous phase or require the vaporization of the sample for analysis) are discussed below. All of the techniques introduced below, have been applied for the detection of explosives or other hazardous materials.

1.1.1. Animal olfactory systems

Several species of animals, including dogs, rats, honey bees and pigs have been used for the detection of drugs, explosives, weapons, mines, live human bodies, tobacco, cash, and cadavers [26]. The benefit of the sophisticated animal olfactory systems in the field of the detection are namely sensitivity, near real-time response, localization, and the ability to simultaneously analyse several different analytes. For many years canines have been the gold standard for vapor detection and other detection methods have been judged in comparison with trained sniffer dogs (**Figure 3**) [13]. The basis for this is their extremely sensitive olfactory system and their acute scent recognition − interpretation ability [26]. Because of their superior performance, other detection technologies have attempted to mimic their sophisticated olfactory systems [29; 30]. Nevertheless, certain drawbacks are associated with the employment of the explosives detection dogs (EDDs): the efficiency of the detection procedure depends on the environmental conditions, distractions, dog personality, dog-handler interaction. Moreover, dogs are not capable of universal detection (usually trained only for one type of threat) and a major limiting factor is the costly and time-consuming training and handling [31]. The training of the dogs is a delicate procedure which is based on stimulus−reward techniques, and those often employ the energetic compounds and their simulant compounds, precursors, breakdown products, or taggants [26].

The training of the canines also involves the utilization of the gas-generators. However, the testing procedure for EDDs is considerably different from the test protocol for the instrumental detection systems. Firstly, the emphasis in the detection dog training is not necessarily on the detection of a particular explosive compound, but on the vapors that the canine olfactory system *can* detect [27]. Hence, the training devices have to deliver vapor from samples with the contents of a realistic explosive device. Secondly, it is also important to train the EDDs to detect not only the compounds in trace concentrations, but also to expose the trainee to a vapor

"cloud", which may originate from a bulk amount of material. Failure to do so might result in an inability to locate or detect the explosive device altogether [32]. When a real explosive sample is too dangerous to use, non-hazardous vapor sources encompassing explosive materials suspended on a solid or liquid support can be employed in the training of EDDs [33]. Since the performance of the canine detection systems is superior to other ETD detectors to this day (**Figure 3**), the development of the canine training aids remains an important field of research.

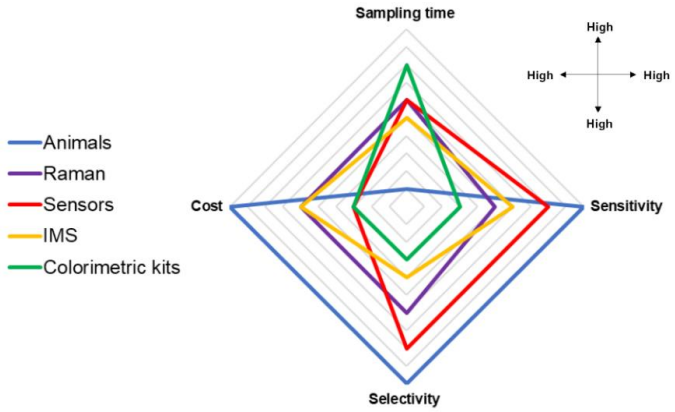

Figure 3. Visual comparison of various explosive trace detection (ETD) technologies. Reprinted with permission from [9]. Copyright (2020) American Chemical Society.

1.1.2. Electronic Noses

Electronic noses are *artificial* olfactory systems usually composed of a gas sensor array, gas transmission path, a microprocessor and an identification method [34]. Interaction of the array of sensors with various vapors produce a pattern of electrical responses that are compared with the integrated database and subsequently identified.

Currently, the most common sensor types used in electronic noses include metal oxide semiconductor (MOS) because of their mature technology and low price, but certain limitations (i.e. high working temperatures) encouraged the development and application of other sensor types such as electrochemical (EC), conducting polymer (CP), quartz crystal microbalance (QCM), surface acoustic wave (SAW), and optical sensors. Generally, such analytical devices as mass (MS) and ion mobility spectrometers (IMS), gas chromatographs (GC) can also be considered as electronic noses since they contain gas detection systems and chemical determination technologies [26].

1.1.3. Micro- and nano- technology

Microfabrication technology has advanced immensely in past decades and allowed the development of lab-on-a-chip devices. Micro-electro-mechanical systems (MEMS) are an approach which benefits from the miniaturization of detection devices (electronic noses, etc.) to achieve portable, cost-effective systems, containing a microprocessor and mechanical components. One of the technologies, applicable for MEMS is the use of microcantilevers [35]. Microcantilevers can be coated with a variety of different materials to match the specific application. The working principle of the microcantilevers sensors is based on the mechanical movement and deformations of the components. Upon absorption of the sample, the detection is observed in one of two ways: either the absorption causes a deflection which is identified by a change in the differential surface stresses of microcantilever surfaces, or, the absorbed mass changes the frequency of the vibration of the reflected light beam.

Nanotechnology has been employed for this purpose as well. Nanomaterials are an extensively researched field and its advantages are the possibility to easily tune their intrinsic parameters, such as electric, optical, catalytic, magnetic and mechanical properties specifically to the application [9]. There is a multitude of various types of nanosensoric devices, one of them being semiconductors. Metal oxide semiconductors (MOS) are the most commonly used sensors since they exhibit superior performance in comparison to other semiconductive gas sensors [36]. Gas sensing mechanisms in MOS sensors are an elaborate topic and several different theories exist. The electrical properties of the semiconductor are influenced in the microscopic (based on electron depletion and hole accumulation theories) and macroscopic (adsorption/desorption theory) scales. On the macroscale, upon chemical or physical adsorption of the gas specimen, a change in the resistance is induced due to the change of the charge carrier concentration [36]. MOS detection systems based on chemical adsorption record a change of the semiconductor response (voltage, current or conductivity) initiated by a chemical reaction. Physical adsorption is the adsorption of gas molecules onto sensor surface by Coulomb forces, hydrogen bonding and other intermolecular forces without chemical changes [36]. Currently, due to the rapid development of the MOS sensors and advanced chip packaging technology, the size of MOS sensors can be very small which makes them suitable for portable electronic nose systems [34].

Nanotechnology is also successfully applied in the electrochemical gas sensors. A commercially available example of electrochemical gas sensors is the Vaporsens device (from Vaporsens Inc., USA). This device uses nanofibers that are formed by self-assembly of chemically tuned organic molecules. The network of nanofibers ensures a large surface area,

that captures molecules in a gaseous phase by molecular diffusion and surface adsorption. The selective functional groups of the nanofiber backbone interact with the compounds under investigation and can either donate or withdraw the electrons, inducing a change in the internal resistance of the nanofiber instrument and resulting in an increase or a decrease of an applied electrical current [37].

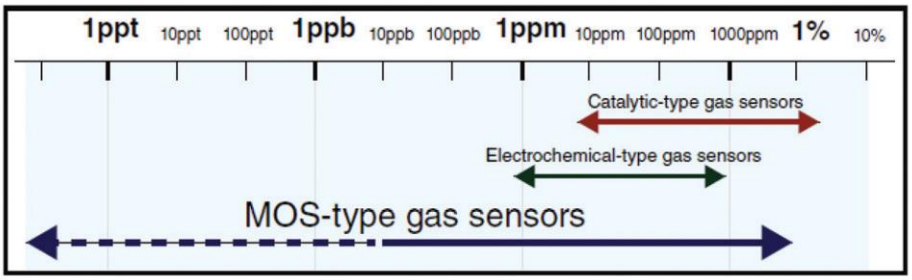

Figure 4. The range of the detectable gas concentration of several common gas sensors. Reprinted with permission from [36]. Copyright (2019) Royal Society of Chemistry.

1.1.4. Ion Mobility Spectrometry (IMS)

According to the US Transportation Security Association (TSA), the ETD devices based on the ion mobility spectrometry are the only types of detectors, considered to be included into the Air Cargo Screening Technology List, which serves as an official guide for the regulated authorities on which ETD technologies are qualified for the use according to the Standard Security Program [38].

The working principle of the IMS devices relies on the separation of the ionized analytes under a weak electric field in an ambient pressure. The sample is usually introduced in a condensed phase and is thermally desorbed to produce a gaseous sample from specially designed swabs or by sampling vapors directly from the environment. In a typical IMS device (**Figure 5**), after the gaseous sample is ionized in an ionization chamber, it passes through the ion gate in portions and travels into a drift tube, where under the influence of the electric field, the carrier gas and opposing flow of the drift gas, different molecules are retained and separated according to their mobility, which corelates to their ion size, shape and charge. The drift time and the detector signal intensity allow the identification of the analytes from a library with predetermined drift characteristics. The simple instrumentation and quick process time are some of the benefits that resulted in the IMS popularity in explosive trace detection.

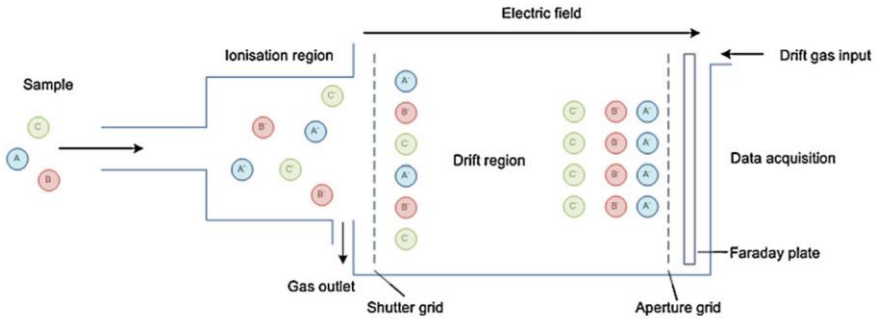

Figure 5. A graphical representation of a simplified ion mobility spectrometer. Reprinted with permission from [10]. Copyright (2012) Elsevier.

Ion mobility spectrometers suffer from several limitations, including non-linear response, limited selectivity, dependency on the humidity, common use of radioactive ionization sources, the need of extensive sampling and, lastly, competitive (matrix affected) and collision driven ionization processes [39]. There is a constant search for novel solutions to ensure efficient collection and selective extraction of the samples and the research results are promising for low vapor pressure materials [9].

The performance of the IMS device can be enhanced by hyphenating the device with gas chromatography (GC), single and tandem mass spectrometry (MS, MS/MS) and other techniques [40; 41; 42]. Gas chromatography in the GC-IMS provides an additional separation before entering the ionization step of the IMS device, which, in turn, reduces the matrix effects, ion interactions, the number of false positives and, consequently, increases the overall sensitivity. Moreover, the hyphenation grants the possibility of a three-dimensional identification (according to the GC run time, IMS intensity and IMS drift time) [26].

In the devices containing the IMS and MS technologies, IMS enables a fast separation of isomers, isobars and conformers in the complex mixtures and provides improved detection results [40].

1.1.5. Mass Spectrometry (MS)

Mass spectrometry has been the preferred technique in the chemical analysis because of its sensitivity, selectivity, rapid operation and applicability to a wide range of analytes. Similar to the IMS, the sample molecules in the MS are ionized in the ionization source and transferred into a chamber where they are separated according to their intrinsic properties. Unlike the IMS,

mass spectrometry differentiates the molecules depending not on their mobility, but on their mass-to-charge ratio (*m/z*). The device, responsible for the discrimination of the molecules, is called mass analyzer and typical examples are time-of-flight, quadrupole mass filter, orbitrap, ion trap, Fourier transform ion cyclotron resonance and electrostatic analyzers. In a mass spectrometer with a linear quadrupole mass analyzer, which was employed in this project as well, the core element is a square assembly of four cylindrical rods which produce a quadrupolar electrodynamic field induced by alternating electric potentials. A periodically changing electric charge forces the ions to oscillate in trajectories depending on their *m/z* ratios and alternating voltages [43]. The sample ions are detected only if their oscillation radius does not reach the quadrupole rods. Ions oscillating with a bigger radius impact the quadrupole rods and are "filtered out" (**Figure 6**). Other types of mass analyzers have been extensively reviewed elsewhere [44].

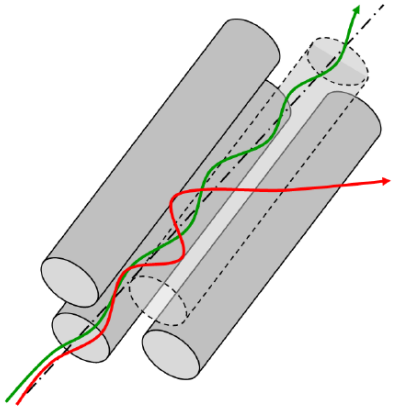

Figure 6. A basic schematic of a quadrupole mass analyzer. Green line represents detected ions and red line ions that are "filtered out" [45].

Other integral components of the MS include the detector and a vacuum pump. For a long time, combination of these elements resulted in bulky and power-consuming analytical devices, which were mainly used in a laboratory environment, but in last decades major developments resulted in the miniaturization of some of the main components and converted the MS into a portable device [46-48]. Portable hyphenated GC-MS devices have been reported in the past and they benefit in similar aspects as in the case of GC-IMS, discussed above [49].

Constant research and development of new sampling and ionization procedures resulted in improvements in the sensitivity of the MS technology and enabled detection of low vapor

pressure explosive materials making a contactless detection a feasible prospect in the future of ETDs [50; 51].

1.1.6. Surface-enhanced Raman Spectroscopy (SERS)

Raman spectroscopy relies on the vibrational fingerprinting of molecules and materials [52]. The very weak Raman effect, which results in a low signal intensity, remains the primary problem in applications of Raman spectroscopy. One way to circumvent the problem is to use Surface-enhanced Raman Spectroscopy (SERS). SERS detection technology has been of a particular interest in the field of trace explosives detection because it can recognize the structural information of substances at the molecular level. In SERS, a laser scans the surface of a microscopically roughened metal substrate for adsorbed analytes of interest. The analyte molecules interact with the laser light and the vibrational modes, associated with the absorption of the incident light, enters a resonance and are enhanced in the vicinity of the metal substrates. The enhanced intensities can reach 10^2-10^{14} times in comparison to their non-resonant Raman intensities. These enhanced vibrational signals are detected and interpreted to identify a particular molecule. The SERS substrates can be designed specifically for the intended application so that only particular types of analytes would be absorbed. These properties can be tuned by choosing an appropriate metal surface itself, the degree of roughness, the degree of oxidation of the surface, the acid/base properties of the surface and the use of coatings [53].

In many SERS applications the sample must be physically removed and/or put into the close contact with the substrate. However, the achieved sensitivity (up to a single molecule detection) and high selectivity show a great method potential for the ETD detection in the gaseous phase [54]. For the detection of the vapors of the most explosives, a gold based substrate has been employed [55], since it provides a strong and specific binding, while other metals show low absorption [56]. Unfortunately, a continuous gas-phase explosive trace detection using SERS has been problematic because of a “memory effect” caused by “sticky” explosive molecules. A possible solution is an employment of a microfluidic technology, which mimics animal olfactory system (**Figure 7**) [29; 57]. In such a structure gaseous molecules are efficiently transferred into the mucous layer, which preconcentrates the airborne analyte molecules and thereby enhances their detection.

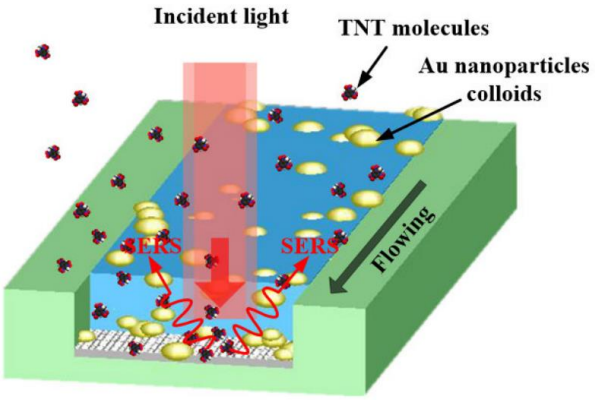

Figure 7. Graphical representation of the gas phase ETD device, based on the SERS technology in combination with microfluidic technology, by [57] and licensed under CC BY 4.0.

1.1.7. Cavity ring down spectroscopy (CRDS)

In Cavity Ring Down Spectroscopy (CRDS), the device contains a cavity surrounded with high reflectivity mirrors.

A laser pulse in the near-infrared or ultraviolet part of the spectrum is released upon the vapor residing in the cavity (**Figure 8**).

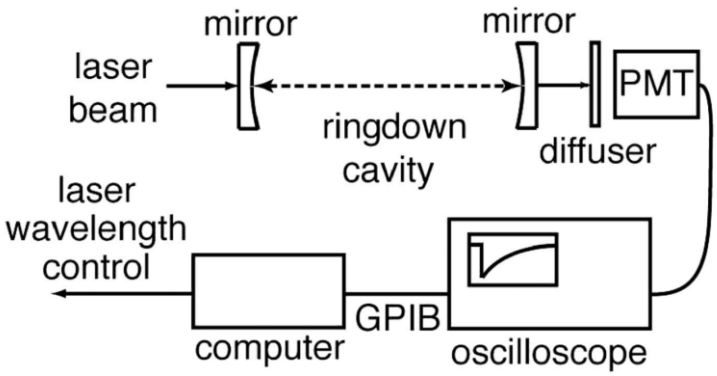

Figure 8. Schematic of the experimental CRDS apparatus. Here PMT: photomultiplier tube; GPIB: general purpose interface bus. Reprinted with permission from [58]. Copyright (2007) OSA.

The light travels a distance measured in kilometres and the interaction with the vapor results in the absorption of the characteristic wavelengths. The absorption occurs by either electronic transitions in the ultraviolet mode, or vibrational transitions in the infrared range [58]. After the laser light is turned off, the degradation of the laser signal is monitored over a period of time using the photomultiplier tube (PMT), that would transfer the CRD signal into computer

interface with a software that would analyze photon decay and compare with a signal degradation profile, observed in an empty cavity. The signal decay characteristics of the vapor filled cavity are observed and assigned to a specific compound. The CRDS devices are commercially available and have been tested on several explosive materials (TNT, TATP, RDX, PETN, Tetryl) [59; 60].

2. Determination of vapor pressures

As mentioned earlier (Chapter 1), vapor pressures are of high importance in various fields. Over the last century, vast amounts of research were focused on the determination of vapor pressures of various types of compounds and their mixtures in different phases. Nevertheless, most of the known vapor pressure data has been determined for industrial applications. For this reason, only a small fraction of the vapor pressures, relevant for other applications are available [61]. The lack of experimental vapor pressure values is especially relevant for the investigation of the fate of the atmospheric aerosols, because the vapor pressure is the primary determinant for the condensable mass of the organic aerosol, and this condensate participates in the absorption and scattering of radiation [19]. However, due to their large number, the measurement of the vapor pressure of all atmospheric organic compounds is impractical. Consequently, many vapor pressure estimation methods have been developed in the past [19]. However, because these methods are usually developed based on the available experimental data on non- or monofunctional compounds, they often do not suit more complex analytes. In the case of more sophisticated estimation methods, knowledge of an experimentally determined descriptor is often required which may include boiling point, vapor pressure of the parent hydrocarbon, critical point, melting temperature, topological, geometric, electronic, hybrid, elemental and many other descriptors, as reviewed in the works of *Naef and Acree* [62] and *Barley and McFiggans* [61]. The use of methods utilizing such descriptors is limited by their availability. Alternatively, the values can be estimated by further prediction methods, which potentially introduce an additional source of error [62].

In their work, *Barley and McFiggans* [61] point out another important issue that many of the more complex group contribution methods bear. For many models, the estimation will work very well for the compounds that the model was derived from, but the method will perform very poorly for the compounds out of the training set, since their intrinsic structural features are underrepresented in the estimation method. This problem is especially unforgiving for higher molecular weight, low vapor pressure compounds (such as explosives) since there are relatively few compounds with vapor pressures below 0.1 Pa available in the literature. Moreover, as scientists usually report data in bulk for structurally similar compounds, measured by the same experimentalists and the same equipment, the fitted parameters in the estimation models might reflect a present bias. Thus, it is really important to develop estimation methods using multiple

independent experimental datasets from a collection of diverse sources employing reliable vapor pressure determination techniques.

A wide variety of the vapor pressure measurement techniques have been implemented and they have been documented thoroughly over many decades including reviews by *Ambrose* (1975) [63], *Delle Site* (1996) [20] and recent work by *Verevkin et al.* (2018) [64]. Available data on the experimental values of the vapor pressures have shown that the vapor pressure results often differ depending on what experimental method is utilized for the purpose. Certain methods have their own advantages and disadvantages and they have been discussed in a study by *Verevkin* (2005) [21]. Therefore, it is essential to choose the correct technique for the application.

For semi-volatile compounds, the molecules that have evaporated from the surface of the compound collide with each other and, consequently, occupy a relatively small volume and are constantly re-absorbed into the surface. At equilibrium state, the evaporation and re-absorption rates are equal. However, for the compounds with a low vapor pressure, such as explosives, the amount of the molecules above the surface is small and if there is a sufficient unoccupied volume above the sample surface, the molecular collisions become unlikely and the molecules do not re-enter the sample in the condensed state. If the molecules are efficiently removed from the proximity of the sample before they are re-absorbed, it is possible to measure the rate at which evaporation is taking place by determining the loss in mass of the source sample, or by determining the amount of substance collected [63]. This principle has been utilized in several vapor pressure measurement techniques. Some of them, including Langmuir, Knudsen and transpiration (gas-saturation) methods have been considered to be most suited for the low vapor pressure materials [21; 22; 61]. These methods are concisely discussed in this chapter.

2.1.Knudsen effusion method

In the Knudsen effusion method, sample material is situated in a closed cell with a small orifice into a vacuum [65]. At a constant temperature sample vapors reach an equilibrium and effuse out of the enclosed chamber, which results in an observable mass loss. The vapor pressures can be investigated by analyzing the sample vapor after it effused from the cell (i.e. by collecting the vapors on a cooled surface or QCM, by determination of resulting mechanical torque or response in the mass spectrometry) or by the determination of the mass difference of the

experimental cell and its contents (i.e. by weighing, thermogravimetrically) [21]. Mass loss is monitored periodically before and during the experiment with a sensitive technique that can be external or internal to the device.

The resulting vapor pressure p_{sat} is derived from a Knudsen effusion equation (eq 1), which concerns not the evaporation from the sample, but the effusion from the cell:

$$p_{sat} = \frac{dm}{K\, d\tau}\sqrt{\frac{2\pi RT}{M}} \tag{1}$$

Here p_{sat} is the vapor pressure, in Pa; $dm/d\tau$ is the mass loss, in kg s^{-1}; T is temperature, in K, R is the universal gas constant equal to 8.3144 $J{\cdot}mol^{-1}{\cdot}K^{-1}$, M is the molar mass of the compound in the gaseous phase, in kg mol^{-1}; K is a product of Clausing coefficient K_C and the area of the orifice S. The Clausing coefficient is introduced to consider the thickness of the cell walls that causes the orifice to have a cylindrical form and yield a non-zero probability that the sample molecules will strike the cylinder's wall instead of escaping into the vacuum [63].

To avoid deviations, arising from the higher vapor pressure samples (>1 Pa) and the low Knudsen number K_N (K_N defines the ratio between the mean free path of the molecule λ and the orifice diameter), the experiments usually involve measurements with three or more orifices of varying diameter [64].

The limitations to the application of the Knudsen effusion method for low volatility compounds lie in the sensitivity of the gravimetric techniques. To determine the vapor pressures reliably, a sufficient amount of the sample has to evaporate and that can be problematic for the extremely-low vapor pressure materials. As an alternative, the experimental temperature can be increased to raise the evaporation rate, but that could induce decomposition or safety issues with the thermolabile compounds, such as explosives. Furthermore, the use of this method requires substances of an extremely high purity, since any high volatile impurity may falsify the results.

Prominent examples where Knudsen effusion method was used for the determination of vapor pressures of explosives are the works of *Edwards* [66; 67] and *Cundall et al.* [68; 69].

2.2. Langmuir method

In contrast to the Knudsen effusion method discussed above, in the Langmuir method samples are usually placed into open crucibles with a well-defined surface area and the substance of interest evaporates into a vacuum or into an inert purge gas. As a result, the rate that the substance is evaporating is faster. Consequently, the sufficient amount of the sample, required for a reliable measurement of the mass-loss leaves the sample faster and the experimental temperature can be reduced. The method is often coupled with the thermogravimetry and can operate with isothermal and gradient temperature programs.

The calculation of the vapor pressure can be executed via the modified Knudsen effusion equation (1), where for the Langmuir experiment:

$$K = \alpha\gamma S \tag{2}$$

Here α is the empirical condensation (accommodation) coefficient, γ is the roughness of the surface and S is the area of the sample. Due to the fact that the condensation (accommodation) coefficient is not uniform, in order to obtain absolute vapor pressure values using this approach, the device has to be calibrated with a substance of a similar structure.

The isothermal thermogravimetric analysis (TGA), which, in principle, is a form of Langmuir method, was recently used for the determination of the method suitability for the determination of the absolute vapor pressures of explosives [70]. The findings showed that the coefficient α drifted with each experimental run, therefore, the method is not suitable for the determination of the absolute vapor pressure on its own. On the other hand, if the measured molar enthalpies of phase transitions obtained with this method agree with the experimental results, established with other reliable vapor pressure methods, the coefficient α could be derived and TGA results could be recalculated into absolute vapor pressures and could compliment already known experimental vapor pressures.

The Langmuir method was also employed for the determination of the vapor pressures of explosives, notably in the study by *Rosen and Dickinson* [71].

2.3.Transpiration method

The transpiration method has been acknowledged to be a reliable method for the determination of experimental vapor pressures [61]. The basic working principle of the method is based on

the transportation of the analyte-saturated gas stream from sample-coated support under isothermal conditions followed by external collection and quantification of the condensed material. Some of the advantages of this method include the independency on small amount of impurities, since the volatile organic compound impurities or moisture can be eliminated from the experimental setup by a thermal conditioning step and for other compounds the impurity induced error in the quantification of the collected sample can be prevented by application of analytical separation techniques, such as gas or liquid chromatography. Moreover, the method performs well at both ambient and elevated temperature ranges and the measurements can be executed under different carrier gas (for certain applications or measurements at elevated temperatures, inert gas atmosphere can prevent sample decomposition). The relatively inexpensive experimental setup and ease of operation are also some of the great advantages of transpiration method [20; 21; 64].

The transpiration method has been used for an array of different compounds and has shown an excellent agreement with the well-established vapor pressures of reference materials, determined using other methods. For these reasons the transpiration method was established in our work group and ever since it demonstrated being well-suited for the determination of vapor pressures of hazardous materials, including the energetic as well as toxic compounds [18; 72-75]. A thorough discussion on many of the practical aspects for this method has been reported in the study by *Härtel* [70]. The basic experimental setup of the transpiration method, established in the work of *Härtel* [70], was implemented in this project as well. However, some new improvements were realized in this work and will be discussed in this chapter along with some other important aspects.

In the scope of this project, a new approach on the drying of the carrier gas was implemented. The previously used gas drying tower–a glass-pipe, which was filled with phosphorus pentoxide coated on a silica support (Sicapent®, SigmaAldrich, cat. #79610)– had performed well, but not ideally in terms of capturing the moisture in the gas transfer system. In practice, especially when long-term measurements of extremely low volatility compounds were taking place, the cooling trap (**7**, Figure 9) would collect an observable amount of water which would crystalize in the condensation tube. As an alternative, a new drying module, consisting of one T-type particulate filter SS-4TF-05 and two SS-FCB coalescing-particle filters by company *Swagelok,* was installed. The drying system was connected using PFA tubing. The new implementations completely eliminated the water condensation problem for experiments of any duration.

The final setup for transpiration experiments is depicted in the **Figure 9**.

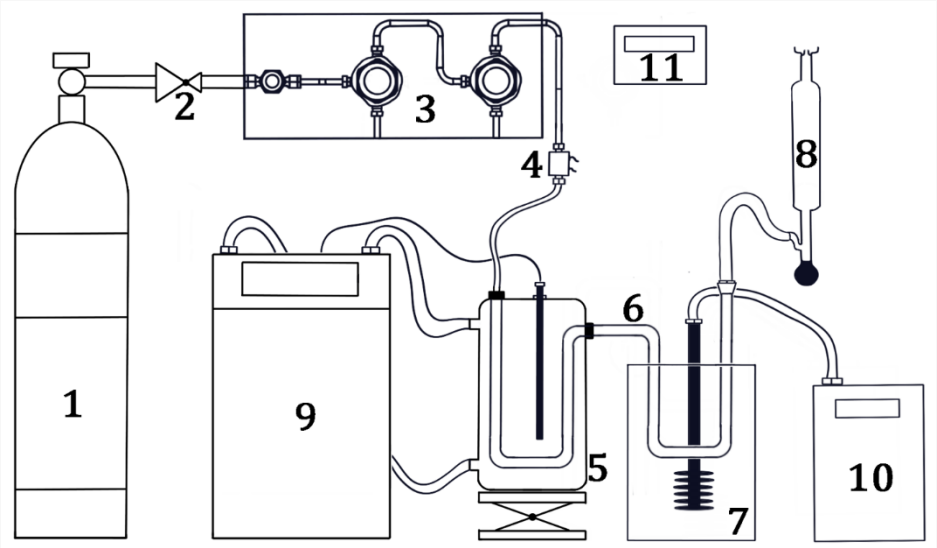

Figure 9. The final experimental setup of the transpiration method used in this work: nitrogen reservoir **1**, pressure reduction valve **2**, drying module **3**, mass flow controller **4**, saturator **5**, condensation tube **6**, cooling trap **7**, soap-film flowmeter **8**, thermostat **9**, immersion cooler **10** and thermobarometer **11.** Reprinted with the permission from [76]. Copyright (2021) American Chemical Society.

2.4. Quantification by chromatography

In this work, the determination of the mass of the condensed analytes, collected during the transpiration experiment was executed using chromatographic techniques.

2.4.1. Vacuum Outlet-GCMS

Since this work deals with the determination of the thermodynamic properties of the materials in the gaseous phase, the gas chromatography coupled to a MS seemed like an obvious choice for an analytical method. However, the analysis of thermolabile analytes, such as energetic materials using a conventional GCMS device can be tricky, since the device is operating at elevated temperatures and the decomposition of the compounds under investigation must be avoided in order to achieve reliable results. For this reason, a vacuum outlet-GCMS method (VO-GCMS) was employed in our group and successfully implemented for the determination of the vapor pressures of selected energetic materials [18; 72; 73; 74]. In this technique, a wide inner diameter capillary column is connected to the mass spectrometer to permit a gradual

expansion of the detector vacuum along the capillary column. The consequently reduced pressure in the capillary column raises the carrier gas velocity along the analytical column and thus reduces the elution temperature of the compounds under investigation. However, without an additional system modification, the significant increase in the gas flow through the analytical column would compromise vacuum build up in the detector. In order to prevent the detector vacuum from a collapse, a small diameter restriction column is securely connected to the inlet of the analytical column and placed at the injector. The restriction allows the control of the carrier gas flow and operation at a constant pressure mode [73].

In this work, vacuum outlet operation was established by employment of a Shimadzu® GCMS QP2010 SE device that was equipped with an Atas® Optic 4 injector which is able to fit a custom-made stainless-steel liner. The custom liner of 5 mm outer diameter and 0.5 mm wall thickness is necessary to house an SGE SilTite® μ-union column connector with an outer diameter of 3.5 mm. A column configuration in the GCMS software Labsolutions GCMSsolution v4.11 was manipulated to allow the head pressure to be set to 760 kPa. More detailed information can be found in the work of *Härtel* [70].

In this work, an array of compounds was analysed using VO-GCMS and the specific methods are discussed at relevant chapters. Unfortunately, the VO-GCMS system has its limitations when it comes to the quantification of labile and low-vapor pressure materials such as explosives. As previously performed study by *Härtel* has shown, several common explosive materials (PETN, RDX, etc.) could not be detected or quantified with required reproducibility. A milder method of chromatography, such as liquid chromatography, in which the compounds do not need to be transferred into gaseous phase by exposure to elevated temperatures, was chosen for further analysis.

2.4.2. HPLC-DAD

High performance liquid chromatography with diode array detector (HPLC-DAD) was newly established at our group in the framework of the vapor pressure measurements as a method of quantification, so it is important to discuss some aspects of the application. In a standard HPLC device (**Figure 10**), during an operation cycle a sample solution is introduced into a pump-regulated continuous flow of the mobile phase and enters a thermostated separation column, where sample components, upon interaction with the column packing material (stationary

phase), are separated according to various parameters, such as hydrogen bonding, polarizability, etc. The now-separated molecules in mobile phase medium enter the detector, which records specific physical parameters of the mobile phase that are changed in a presence of the analyte, such as UV-absorbance, light scattering, mass spectrum, etc. The detector response is processed by a software to get a time-resolved chromatogram. Depending on whether the used detector is destructive (mass spectrometry, charged aerosol detector, etc.), or non-destructive (refractive index, fluorescence, UV, etc.), the remnants of the sample are then further processed to be retrieved or recycled.

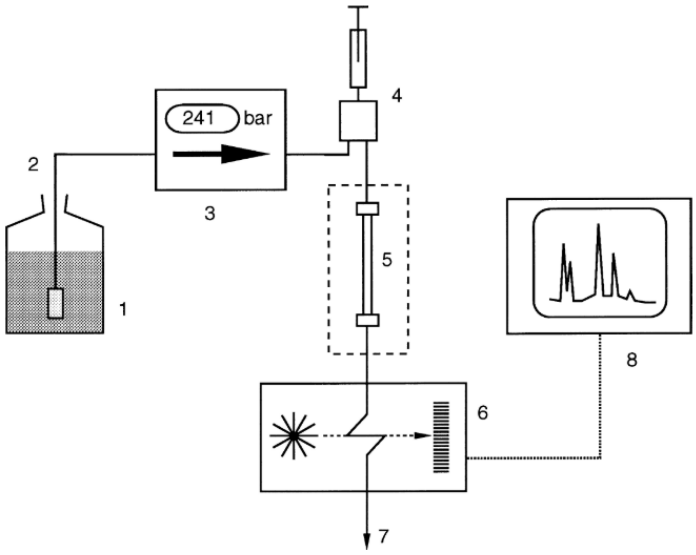

Figure 10. Schematic diagram of a HPLC unit. Solvent reservoir **1**, transfer line **2**, pump **3**, sample introduction system **4**, thermostatted column **5,** detector **6**, waste **7**, data acquisition **8**. Reprinted with a permission from [77]. Copyright (2010) John Wiley and Sons, New York, NY.

In this work, the HPLC was operated in a reverse phase mode, where the stationary phase contains a non-polar material and the mobile phase is a mixture of polar solvents, most commonly comprised from water, methanol or/and acetonitrile. The benefit of this operation mode is the abundance of the relatively cheap and high purity polar organic solvents and the possibility to use water. It is of a great importance to use high grade solvents, since the impurities may induce various matrix effects, compromise the detection of the analytes, lower the signal to noise ratio (S/N) or contaminate the system. Moreover, all solvents should be freshly filtered and preferably degassed.

In the reverse phase mode, polar molecules, such as explosives, will prefer the polar mobile phase ("like-attracts-like") and will leave the column with little interaction, while non-polar molecules will be retained stronger [78]. Nevertheless, a careful development of the method by selection of optimum water-organic solvent ratios for isocratic or gradient methods allow the efficient use of non-polar analytical columns for the analysis and quantification of relatively polar compounds. In this work, instead of the most common reverse phase column with non-polar C_{18} packing, a biphenyl column was primarily used because of its compatibility with highly aqueous conditions (up to 100%) and enhanced $\pi-\pi$ interactions with aromatic molecules (*Phenomenex Kinetex*®, 2.6 µm Biphenyl, 100 Å, 150 × 4.6 mm). For certain analytes, a slightly more polar column with cyano- functional group, which is able to operate in both normal and reverse modes, was equipped for the analysis (*Restek ROC*®, 3 µm Cyano, 100 Å, 150 × 3.0 mm). In this project, chromatographic samples contained only the compound under the investigation, a specific amount of reference material (for internal standard quantification) and high purity solvent that is identical or similar to the mobile phase of the chosen method. Since the materials used for the vapor pressure measurement as well as the reference materials were of a high purity, the method development mainly included the reduction of the method duration while maintaining the proper separation of the peaks.

In this work, a non-destructive diode array detector (DAD), which records changes in the sample absorbance in the UV/VIS spectral region, was utilized for the quantification of the analyte, collected during the transpiration experiment. UV/VIS absorbance detectors are some of the most commonly used detectors for the HPLC systems since they can provide a wide linear range, they are relatively unaffected by the temperature or flow changes and are also suited for the gradient elution [79]. In diode array detectors (DAD) a light source (deuterium for wavelengths from 190 nm to approximately 400 nm and wolfram for wavelengths 400 nm to 900 nm) generates a light beam which is directed through a flow cell of specific dimensions, containing the sample of interest (**Figure 11**). Upon interaction with molecules in the sample, certain wavelengths of the incident light are absorbed as the electrons undergo excitation in a form of a transition from molecular orbitals $\pi \rightarrow \pi^*$, $n \rightarrow \pi^*, n \rightarrow \sigma^*$. In theory, the excitation would result in the light absorption of a discrete wavelength, however, the molecules in a solution absorb a part of the energy as vibrational energy and it significantly broadens the absorption bands [80]. The transmitted light interacts with a diffraction grating which disperses

the light beam into its spectral components and different wavelengths are simultaneously captured by an array of photodiodes that convert the light intensity into an electrical signal [81].

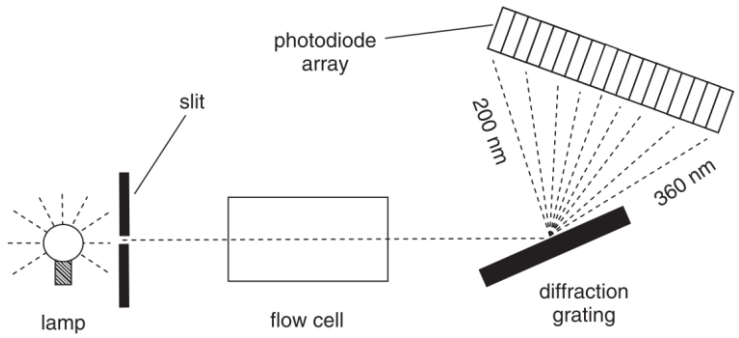

Figure 11. Schematic representation of a DAD detector. Dashed lines show the optical path. Reprinted with permission from [78]. Copyright (2010) John Wiley and Sons, New York, NY.

The observed absorbance can be calculated according to the Beer–Lambert law:

$$\mathrm{A} = \log(\frac{I_0}{I}) = \epsilon l c \tag{3}$$

Here A is the absorbance, which is equal to the logarithm of the ratio between incidence light intensity I_0 and the intensity of the transmitted light I; ϵ is the molar extinction coefficient, a parameter dependent on the particular sample molecule and the wavelength of the absorbed light, in $M^{-1} \cdot cm^{-1}$; l is the the optical path (cell) length, in cm; and c is the molar concentration of the species, in M. This relationship is only valid if the light photon interacts with no more than a single absorbing molecule and that can be ensured by a sufficient dilution of the sample and a short path length. The length should be carefully considered since the increase in cell length l increases the limits of detection (LOD), but large cell volume might contribute to the peak dispersion [82].

The absorption of the UV light is present in the compounds containing certain chromophores with signature absorption bands that can be obtained from the literature. Some of the chromophores include bromine, iodine or sulfur atoms, structures containing two conjugated double bonds, aromatic rings, carbonyl and nitro groups, double bonds adjacent to an atom with a lone electron pair, and other examples which cover most of the energetic and the majority of the organic compounds [77]. The absorption wavelength and intensity of these groups can also be altered by neighboring groups in the molecule, solvent pH and solvent polarity. However, when the chromophores for certain molecules are absent, the absorption detection may still be

applied using the inverse UV chromatography, where an UV absorbent material is added to the mobile phase resulting in an artificial elevation of the baseline and non-absorbing molecules are detected as negative peaks since they absorb less than the mobile phase [80].

The HPLC-DAD analysis generates a 3D spectroscopic image for the analyzed sample (**Figure 12a**). Each cross section along a specific wavelength contains an individual 2D chromatogram which can be processed and integrated (**Figure 12b**).

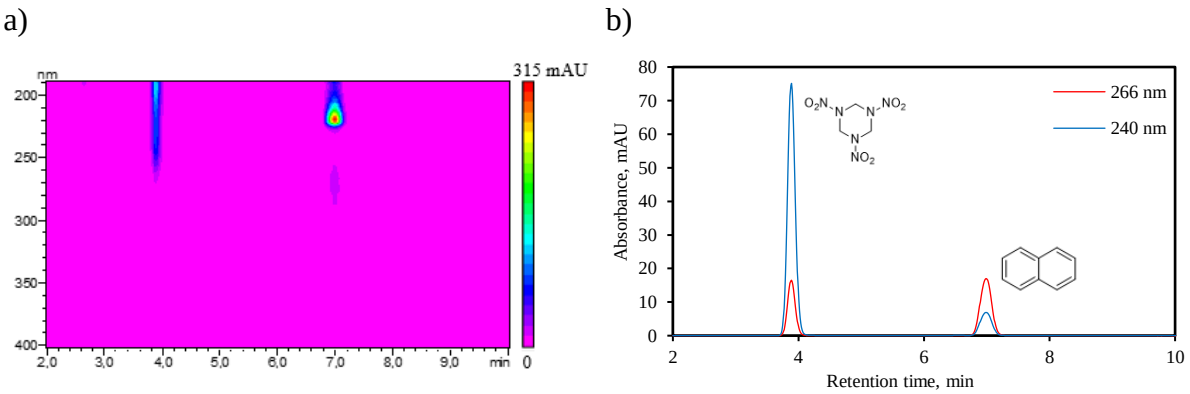

Figure 12. Spectroscopic analysis of a single sample containing the compounds RDX (retention time 3.9 min) and naphthalene (retention time 7.0 min), executed using a HPLC-DAD device. a) 3D contour (retention time vs. detector wavelength vs. absorbance); b) 2D contours (retention time vs. absorbance) for wavelengths 266 nm (red) and 240 nm (blue).

In order to quantify the analytes reliably, a device calibration has to be performed and regularly monitored. For quantification results to be viable, the same chromatographic method has to be used for each analysis and, for each compound, the detector responses (peaks) have to be processed at a fixed wavelength. If possible, the processing wavelength should be set at the absorbance maximum, where there is little change in absorbance with a change in wavelength, rather than on a steeply sloped portion of the absorbance curve [80]. Figure 12b illustrates how the change of the processing wavelengths influences the chromatogram.

The internal standard calibration was the method of choice for the quantification of the compounds investigated in this work. In this method, several different samples (5 or more) of known concentrations for analyte and reference material are prepared. The device chromatograms result in two peaks with two integral areas (I_a for the analyte and I_r for the reference). The calibration is achieved by determination of the calibration coefficients slope X and offset Y for the linear relationship between ratios of the masses of the analyte m_a and the

reference m_r and their integral areas (equation 4). For satisfactory analytical quantification, coefficient of determination R^2 for the equation 4 should be equal to 0.9996 or higher.

$$\frac{I_a}{I_r} = X\frac{m_a}{m_r} + Y \tag{4}$$

$$m_a = \frac{m_r}{X}\left(\frac{I_a}{I_r} - Y\right) \tag{5}$$

A small rearrangement of the equation 4 into equation 5 allows the determination of the unknown mass of the analyte in the sample, with a known concentration of the reference material. This calibration method is advantageous for samples, which require intricate preparation, since it is not sensitive to the errors introduced by several dilution steps (while it would be detrimental for the quantification using external standard calibration method).

To make sure that internal standard calibration is independent from sample concentrations it is important to evaluate the detector response linearity. For this reason, a solution containing both the analyte and the reference is diluted step-wise to produce a set of samples of various concentrations. The sample concentration range where the original ratio of integral areas is constant can be used for quantification. In this work, linearity and calibration measurements were executed in triplicates to simultaneously confirm the proper reproducibility.

2.5. Purity Assessment by ^{1}H-qNMR

The transpiration method's independency on the small amount of volatile impurities in the sample is one of the major advantages of the method. However, it is of great importance to accurately determine the purity of the compounds, used for the chromatographic device calibration, since the absolute purity is essential for correct calibration. There are various ways for the assessment of the compound purity. Many scientific journals do not require absolute purity values and claim elemental analysis (EA), clean nuclear magnetic resonance (NMR) or chromatographic spectra as adequate measures. Liquid chromatography (LC), coupled with mass spectrometry and/or UV absorption detector are some of the most commonly used analytical methods employed for this purpose, often used in quality control (QC) and are present in almost every analytical laboratory. However, such analysis may not detect inorganic impurities, solvent residues or other materials that have the same retention time as the analyte.

Moreover, quantification using LC is limited by the availability of high-grade reference materials and requires lengthy work-flow.

Many of these problems can be solved with quantitative nuclear magnetic resonance spectroscopy (qNMR), which has gained popularity and found widespread application [83]. qNMR validation studies have confirmed it to be suited for Good Laboratory and Manufacturing Practices (GLP/GMP) and it became standard technique in many fields [84].

A non-exhaustive list of the attractive features associated with this method include (i) its high accuracy and precision, (ii) robustness, (iii) fast work-flow, (iv) non-destructive analysis with the possibility to recover the analytes, (v) possibility to obtain structural and quantitative data simultaneously, (vi) small sample size and (vii) ability to recognize dynamic properties, such as chemical exchange (e.g., tautomerism) or rotational/conformational isomerism [85; 86; 87; 88]. A brief overlook on this method and the experimental protocol used in this work are discussed in this chapter.

2.5.1. Theory behind qNMR

NMR spectroscopy is, by definition, a quantitative spectroscopic tool because the intensity and the area of a resonance line is directly proportional to the number of resonant nuclei (spins) [89]. Due to this proportionality, the measurements are not affected by response factors (while it is inevitable in most of the LC detectors, such as UV absorption detector) and no compound-specific calibration is required, enabling a simultaneous determination of more than one analyte in the mixture [90]. Furthermore, for ^{1}H-qNMR there are almost no restrictions in compound class, as long as the analytes contain protons, while detection of UV-transparent and poorly ionizable molecules would be problematic in LC-UV/-MS devices. The analyte repertoire can also be successfully expanded to phosphorus and fluorine nuclei containing compounds, because of their 100% natural abundance and ½ spin quantum number.

In order to ensure the proper proportionality between the sample contents and the NMR response, several experimental conditions have to be met. According to *Schönberger* [91], the conditions correspond to, so-called, “six commandments” or **SCSSRS** (**Table 1**).

Table 1. SCSSRS: the qNMR experiment conditions, required for a successful quantification [91].

The signals of the compound of interest must not interfere with other signals	**S**electivity

The components of the samples should not react with each other	**C**hemical inertness
Not dissolved material will not be detected in the qNMR experiment	**S**olubility
Analytes must be stable in the sample solution throughout the whole experiment	**S**tability
Complete relaxation must be ensured for all of the relevant nuclei, in order to obtain maximum signal response	**R**elaxation
Signals should be sharp, sufficiently separated and defined by an adequate amount of data points	**S**ufficient resolution

More often than not, the quantification in the qNMR experiment is aided by an introduction of an internal standard, which is usually a precisely weighed amount of a certified reference material (CRM) that also has to adhere to the **SCSSRS** requirements. In this way the instrumental parameter fluctuation induced errors are minimized, because the analyte and the reference material are subjected to identical experimental conditions. However, if contamination of the analyte must be avoided, external standards can be used. Besides the conditions, listed in the Table 1, reference materials for qNMR experiments should fulfil these requirements [92]:

- High absolute purity with known uncertainty
- High availability
- Only few signals
- Precisely weighable (non-hygroscopic and non-volatile)
- Low toxicity
- Low cost

One of great advantages of qNMR technique is a relatively simple sample preparation. If the materials of interest are homogeneous, only a duplicate analysis (two samples with one measurement for each sample) are sufficient for a reliable purity determination. The compounds under investigation and the reference materials are usually weighed by a sensitive scale to ensure the least possible weighing contribution to the overall uncertainty pool of the purity result. The upper limit of the weighed sample is usually determined by the solubility in the NMR solvent and the lowest limit is determined by the scale parameters. Additionally, CRM analytical certificates usually provide a minimum recommended sample size for the provided certified uncertainty. Typically, roughly 5 to 15 mg of material is weighed for a 5 mm NMR tube with 0.5 mL solvent. If the sample contains mixtures or a complicated matrix, it is normal that not all components are completely soluble in the NMR solvent.

Prepared samples have to be measured with certain NMR spectrometer parameters, which ensure that the **SCSSRS** conditions are met. Many of the parameters are thoroughly discussed in the literature [87; 93]. In principle, in every NMR experiment the nuclei of the sample undergo excitation upon a radio pulse. After the pulse is terminated the nuclei are given a specific period of time (acquisition time) to allow the relaxation, that produces a detectable resonant radio frequency, which takes form as an exponentially decaying sine wave, called free induction decay (FID).

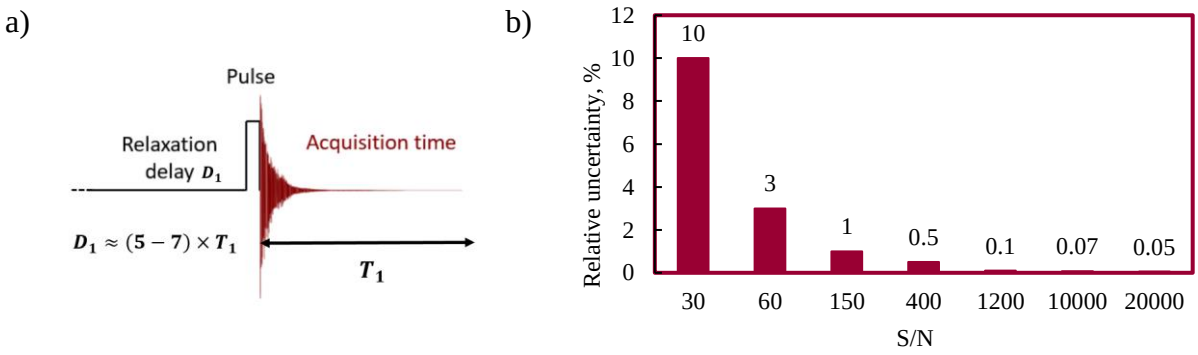

Figure 13. a) NMR experiment sequence. Reprinted from [91]. b) The influence of the signal-to-noise ration on the relative measurement uncertainty [91].

In routine qualitative NMR analysis, 30° pulse angle is sufficient, however, in the qNMR method, it is essential that the maximum pulse angle of 90° is applied to ensure the maximum signal to noise ratio. An insufficient signal to noise ratio (S/N) can result in significant increase of measurement uncertainty (**Figure 13**) [94]. In addition, an appropriate acquisition time has to be chosen. The acquisition time must be long enough to record the fully decayed FID signal while too long acquisition time will acquire only an unnecessary noise when no signal is present. A suitable value for the acquisition time is approximately 7 seconds. During this period, a high number of data points should be acquired to ensure a sufficient description of the resonant behavior of the nuclei. The selection of the relaxation delay time (D1), which takes place before the next excitation stage takes place, is governed by nuclei-specific relaxation times T1 (spin-lattice relaxation) and T2 (spin-spin relaxation). The D1 should cover at least 5 to 7 times the length of T1 (which is generally longer than T2) so that absolute abundance of the excited nucleus would return to the ground state. One qNMR experiment contains multiple excitation cycles and results in a sum of the recorded FID signals which is then further processed and decoded into an interpretable spectrum with the help of the Fourier transformation.

After careful baseline and (preferably manual) phase corrections, zero-filling and peak integration, the calculation of the absolute purity of the sample P_S is executed according to the following equation [95]:

$$P_S = \frac{I_{analyte}}{I_{CRM}} \cdot \frac{N_{CRM}}{N_{Analyte}} \cdot \frac{M_{Analyte}}{M_{CRM}} \cdot \frac{m_{CRM}}{m_S} \cdot P_{CRM} \quad (6)$$

Here P_S is the purity of the sample as mass fraction, P_{CRM} is the purity of CRM as mass fraction, $I_{analyte}$ is the integral of an analyte signal, I_{CRM} is the integral of the CRM signal, N_{CRM} is the number of CRM nuclei corresponding to the integrated signal, $N_{Analyte}$ is the number of analyte nuclei corresponding to the integrated signal, $M_{Analyte}$ is the molar mass of the analyte, M_{CRM} is the molar mass of the CRM, m_S is the mass of the sample and m_{CRM} is the mass of the CRM. The way these parameters were determined and how did they contribute to the overall uncertainty of the purity result will be discussed in the following sections.

2.5.2. Uncertainty evaluation of qNMR experiment

The uncertainty of the obtained purity value using the equation 6 is influenced by every variable individually and must be carefully assessed. General overview of the uncertainty sources, contributing to the purity determination using qNMR experiment is depicted in Figure 14.

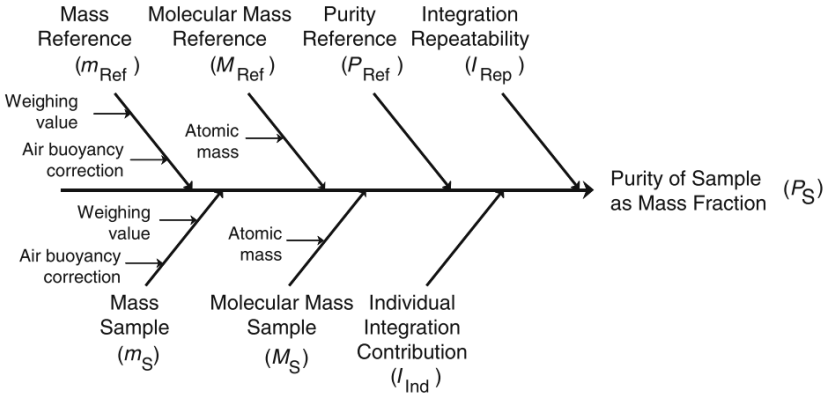

Figure 14. The contributors to the uncertainty of the qNMR purity assessment. Reprinted with permission from [96]. Copyright (2013) Springer**.**

Resulting combined standard uncertainty of qNMR experiment can be calculated according to the equation:

$$u_c(P_{Sample}) = P_{Sample} \cdot \sqrt{\begin{matrix} u_{rel}^2(m_S) + u_{rel}^2(m_{CRM}) + u_{rel}^2(M_S) + u_{rel}^2(M_{CRM}) \\ +u_{rel}^2(P_{CRM}) + u_{rel}^2(I_{Rep}) + u_{rel}^2(I_{Ind}) \end{matrix}} \quad (7)$$

The definitions of the variables in equation 7 are described in the eq. 6 and figure 14. In this chapter detailed procedure will be discussed with calculation examples for the compound anthracene.

Uncertainties introduced by sample weighing

Accurate determination of the mass of the samples is extremely important part in the qNMR sample preparation. Before the weighing procedure takes place, external disturbances (i.e. electrostatic charges, air drafts, sample evaporation or water adsorption) should be maintained at the minimum. If samples are weighed under controlled environment, the main error sources in the weighing procedure come from the technical specifications of the balance and the effect of air buoyancy [97]. Since the electronic balances do not display the true mass, but rather the force that the sample exerts on the device, knowing the buoyancy factor Bu allows the correction of the weighed value w_S to generate the true mass m_S of the sample, which is later inserted in the purity calculation (eq. 6). Weight correction is done with equations 8 and 9.

$$m_S = Bu \cdot w_S \quad (8)$$

$$Bu = \frac{1 - (\rho_a/\rho_r)}{1 - (\rho_a/\rho_s)} = \frac{\rho_s(\rho_r - \rho_a)}{\rho_r(\rho_s - \rho_a)} \quad (9)$$

Here ρ_a is the air density, in kg · m^{-3}; ρ_r is the density of the analytical balance reference weights, which is provided in the manufacturer specifications, in kg · m^{-3}; ρ_s is the sample density (experimental or literature known values), in kg · m^{-3}. Density of air ρ_a is dependent on the ambient conditions and can be calculated according to the equation 10:

$$\rho_a = \frac{3.4848 \cdot p - 9.024 \cdot h_r \cdot e^{0.0612 \cdot T}}{273.15 + T} \cdot 10^{-3} \quad (10)$$

Here p is the ambient pressure, in Pa; h_r is the relative air humidity, in %; and T is the temperature, in °C. For the qNMR measurements of anthracene, two samples were prepared. Corresponding values calculated according to the equations 8, 9 and 10 are reported in the Table 2. Example calculation for the true mass values of the weighed anthracene samples.

Table 2. Example calculation for the true mass values of the weighed anthracene samples.

		ρ_s [a]	w [b]	m [c]	$w - m$
		$kg \cdot m^{-3}$	mg	mg	mg
Sample 1	Anthracene	1250	10.538	10.546	0.008
	CRM	1321	11.008	11.016	0.008
Sample 2	Anthracene	1250	9.950	9.957	0.007
	CRM	1321	10.776	10.784	0.008

[a] Sample density, obtained from the compound packaging, [b] weighed value, [c] calculated true mass, according to the equation 8.

The various technical parameters, that influence the weighing result of the electronic balance w are usually defined in the device specifications and include repeatability REP (dependent on the gross weight of the container and sample), non-linearity NL (dependent on the net weight of the sample), sensitivity offset ST (dependent on the net weight of the sample) and temperature coefficient TC (dependent on the net weight of the sample and maximum temperature fluctuation within measurement). Detailed explanations of these parameters and alternative calculation procedures can be found in the work by *Reichmuth et al.* [97].

The combined absolute uncertainty u_c of the determination of the true mass of the sample components m_S and m_{CRM} (under assumption that the $w \approx m$) is calculated according to the equation 11.

$$u_c(m) = \sqrt{m^2 \left(\frac{u(Bu)}{Bu}\right)^2 + m^2 \left(\frac{u(w)}{w}\right)^2} = \sqrt{m^2 \left(\frac{u(Bu)}{Bu}\right)^2 + u^2(REP) + u^2(NL) + u^2(ST) + u^2(TC)} \quad (11)$$

where uncertainty of the buoyancy is calculated by equation 12, derived from equation 9:

$$u(Bu) = = \frac{\rho_s}{\rho_r(\rho_s - \rho_a)} \sqrt{\left(\frac{-\rho_r \cdot \rho_a}{\rho_s(\rho_s - \rho_a)}\right)^2 u^2(\rho_s) + \left(\frac{\rho_a}{\rho_r}\right)^2 u^2(\rho_r) + \left(\frac{(\rho_r - \rho_s)}{(\rho_s - \rho_a)}\right)^2 u^2(\rho_a)} \quad (12)$$

Absolute uncertainty $u(\rho_s)$ is assumed to be equal to approximately 1% of the absolute ρ_s value, uncertainty $u(\rho_a)$ can be determined as a standard deviation of the average ρ_a,

depending on the experimental environment and $u(\rho_r)$ value for steel alloy has been determined to be approximately 10 kg · m^{-3} [96].

Uncertainty of the molecular mass

Molecular masses and their uncertainties of the compounds of interest can be determined using periodically updated IUPAC technical report on the standard atomic weights with most recent values available online [98].

The standard uncertainties of the reported values can be calculated from the rectangular distribution. Here are some examples of the atomic weight and associated uncertainties calculations for hydrogen A_H and helium A_{He}:

$$A_H[1.007\ 84,\ 1.008\ 11] = \frac{1.00784 + 1.00811}{2} = 1.007975$$

$$u(A_H) = \frac{1.00784 - 1.00811}{2\sqrt{3}} = 0.000078$$

$$A_{He}[4.002\ 602(2)] = 4.002\ 602$$

$$u(A_{He}) = \frac{0.0000002}{\sqrt{3}} = 0.00000012$$

The combined uncertainty for anthracene ($C_{14}H_{10}$) would be a result of:

$$u\left(M_{C_{14}H_{10}}\right) = \sqrt{10 \times u^2(A_H) + 14 \times u^2(A_C)}$$

Uncertainty of the purity of the CRM

The purity of the CRM is usually determined by the manufacturer and provided in the certificate of the analysis. Attention should be paid to what is the confidence level of the reported purity and, if necessary, values should be transferred into standard uncertainties.

Uncertainties associated with the integration

The standard uncertainty of the individual integration contribution $u(I_{Ind})$ is based on the series of post-acquisition procedures which ideally are done by different operators and at different times. For the determination of $u(I_{Ind})$ in this work, spectra were processed and integrated 5 times, the absolute integral values were used to generate standard deviations yielding 4

contributors for a two-sample qNMR experiment. Uncertainty of the repetition $u(I_{Rep})$ is the standard deviation of the calculated purity values (according to equation 6).

The uncertainties for anthracene from various contributing factors were evaluated (Figure 15) and inserted into equation 7 to calculate the final values of combined standard uncertainty as a mass fraction $u_c(P_{Sample}) = 0.003$.

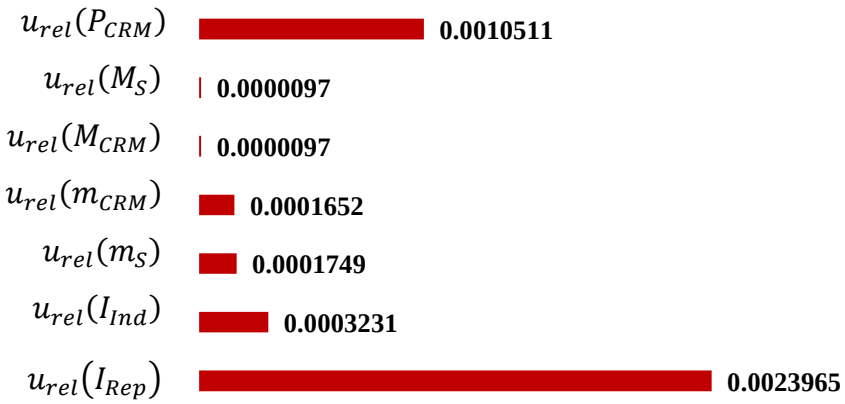

Figure 15. Comparison of the relative standard uncertainties that contributed to the calculation of the combined standard uncertainty of qNMR experiment.

Figure 15 illustrates that the biggest uncertainty contributions in this particular experiment were caused by repeatability (which may be caused by a slight inhomogeneity of the bulk material) and the purity uncertainty of the CRM, while the lowest contributor is the uncertainty of the molecular mass. The final purity for the anthracene can be reported as follows:

$$P_{Anthracene} = 0.992 \pm 0.003 \text{ (m/m)}$$

In this project, the uncertainty associated with the obtained purity result contribute to the overall uncertainty of the vapor pressure measurement and is inserted in the relevant calculations.

2.5.3. Experimental procedure applied in this work

In this work the qNMR purity determination was executed according to the following procedure. Between 2 and 20 mg of analyte and around 10-25 mg of certified reference material (CRM), were weighed with a *Mettler Toledo* XP26DR scale (0.002/0.01 mg) and dissolved in 1 mL of $CDCl_3$ (99.80 % deuterated, *Eurisotop*, D007HAG). The solution was left in an ultrasonic bath for 10 min until analyte and internal standard were completely dissolved. The sample was transferred into a 5 mm NMR-tube. The sample was measured with a *Bruker*

AVANCE 400 MHz instrument with z-gradient using a 90° pulse with a pulse width of 11.85 µs. In total 65,536 data points were acquired. Samples were not spinned and acquisition time (AT) was set to 6.5012 s. Relaxation delay (D1) of 60 s was chosen to ensure that the relaxation duration would be exceeded 5-7 times. Each measurement contained 64 scans.

The processing was done with *MestReNova* v. 12.0.1-20560 software. Before Fourier transformation, linear group delay was applied and zero filling to 2048 K was executed once. After careful manual phase correction and baseline correction by "Bernstein Polynomial" of 5th order, integration was performed manually (integral calculation method - "Edited sum"). Integration was applied excluding the ^{13}C satellites. Two samples were produced for each analyte and their spectra were independently processed 5 times.

2.6. Notes on molar heat capacities, the temperature adjustment of enthalpies of phase transition and the associated uncertainties

The theoretic background of the transpiration method was discussed in the study of *Härtel* [70]. There it was mathematically demonstrated that the slope of the linear relationship between natural logarithm of vapor pressures and the reciprocal temperature describes the molar enthalpy of phase transition at average temperature and is expressed by the Clausius-Clapeyron equation (9):

$$\frac{R \cdot d(\ln(p_{sat}))}{d(1/T)} = \Delta_{l/cr}^{g} H_m^{\circ}(T_{avg}) \tag{13}$$

Here p_{sat} is the saturated vapor pressure, in Pa; T is the experimental temperature, in K; T_{avg} is the average temperature, in K; $\Delta_{l/cr}^{g} H_m^{\circ}$ is the standard molar enthalpy of phase transition, in J · mol^{-1}.

Nonetheless, it is important to adjust the $\Delta_{l/cr}^{g} H_m^{\circ}$ value to a reference temperature (298.15 K, etc.) to be able to compare it with different sets of data or use in the other calculations (i.e. in the adjustment of molar enthalpy of formation). The adjustment to the reference temperature is done by equation 14:

$$\Delta_{l/cr}^{g} H_m^{\circ}(T_{ref}) = \Delta_{l/cr}^{g} H_m^{\circ}(T_{avg}) - \Delta_{l/cr}^{g} C_{p,m}^{\circ} \cdot \Delta T \tag{14}$$

Here T_{ref} is the reference temperature, in K; $\Delta_{l/cr}^{g}C_{p,m}^{\circ}$ is the standard isobaric molar heat capacity difference $C_{p,m}^{\circ}(g) - C_{p,m}^{\circ}(l/cr)$ and $C_{p,m}^{\circ}$ is the standard isobaric molar heat capacity, in $J \cdot mol^{-1} \cdot K^{-1}$; ΔT is the length of the extrapolation path equal to $T_{avg} - T_{ref}$, in K [99]. The required heat capacities can be determined experimentally, obtained from the literature or estimated by various methods. In this chapter different approaches how to determine the necessary values to perform the temperature adjustment $\Delta_{l/cr}^{g}C_{p,m}^{\circ}\Delta T$ according to the equation 14 and associated uncertainties will be discussed and illustrated with some examples.

2.6.1. Temperature adjustment of the molar enthalpy of phase transition to 298.15 K and the associated uncertainties

The uncertainty of the $\Delta_{l/cr}{}^{g}H_{m}^{\circ}(T_{ref})$, from equation 14 can be calculated according to [100]:

$$u_{final}\left(\Delta_{l/cr}{}^{g}H_{m}(T_{ref})\right) = u\left(\Delta_{l/cr}{}^{g}H_{m}\right) + \Delta(\Delta_{l/cr}{}^{g}C_{p} \times \Delta T) \quad (15)$$

This chapter will concern the theory behind the calculation of the term $\Delta\left(\Delta_{l/cr}{}^{g}C_{p} \times \Delta T\right)$, which depends on how the heat capacity values were obtained and the availability of their uncertainties. Generally, the uncertainty of the temperature adjustment can be calculated according to the equation 16 [99]:

$$\Delta\left(\Delta_{l/cr}{}^{g}C_{p} \times \Delta T\right) = u(C_{p,m}^{o}) \times \Delta_{l/cr}^{g}C_{p,m}^{o} \times \Delta T \quad (16)$$

Various situations concerning the calculation of term $\Delta\left(\Delta_{l/cr}{}^{g}C_{p} \times \Delta T\right)$ are discussed and application examples (grey boxes) are provided below.

I. Values for $C_{p,m}^{\circ}(l/cr)$ and $C_{p,m}^{\circ}(g)$ are obtained experimentally or available in the literature

i. Uncertainties of absolute values are available.

$$u(C_{p,m}^{o}) = u\left(C_{p,m}^{o}(\mathrm{l/cr})\right) + u\left(C_{p,m}^{o}(\mathrm{g})\right) = \sqrt{\left(\frac{\Delta(C_{p,m}^{o}(\mathrm{l/cr}))}{C_{p,m}^{o}(\mathrm{l/cr})}\right)^{2} + \left(\frac{\Delta(C_{p,m}^{o}(\mathrm{g}))}{C_{p,m}^{o}(\mathrm{g})}\right)^{2}} \quad (17)$$

ii. Uncertainties of absolute values of $C_{p,m}^{o}$(l) or $C_{p,m}^{o}$(cr) are not available

If uncertainties are not available, the *Chickos et al.* (2016) [101] group contribution uncertainty should be assumed for the condensed phase heat capacities since the group contribution method uncertainty should be greater than any experimental uncertainty.

$$u\left(C_{p,m}^{o}(\mathrm{l})\right) = \frac{14.4\ J \cdot mol^{-1} \cdot K^{-1}}{C_{p,m}^{o}(\mathrm{l})} \quad (18) \qquad u\left(C_{p,m}^{o}(cr)\right) = \frac{17.0\ J \cdot mol^{-1} \cdot K^{-1}}{C_{p,m}^{o}(\mathrm{cr})} \quad (19)$$

For the ideal gas heat capacities, the uncertainty for the experimental values is assumed in the work by *Chickos et al.* [99].

$$u\left(C_{p,m}^{o}(g)\right) = \frac{4\ J \cdot mol^{-1} \cdot K^{-1}}{C_{p,m}^{o}(g)} \quad (20)$$

Table 3. Sample application for compound anthracene for literature available $C_{p,m}^{\circ}$ values and their uncertainties (I.i).

$C_{p,m}^{\circ}(cr)$	$C_{p,m}^{\circ}(g)$	$-\Delta_{cr}^{g}C_{p,m}^{\circ}$
J·mol^{-1}·K^{-1}	J·mol^{-1}·K^{-1}	J·mol^{-1}·K^{-1}
211.7±2.5 [102]	184.7±1.0 [103]	27.0

$$u(C_{p,m}^{o}) = \sqrt{\left(\frac{2.5}{211.7}\right)^2 + \left(\frac{1}{184.7}\right)^2} = 1.3\%$$

$$\Delta\left(\Delta_{cr}^{g}C_{p,m}^{o} \times \Delta T\right) = 0.013 \times 0.027\ kJ \cdot mol^{-1} \cdot K^{-1} \times 47.5\ K = 0.017\ kJ \cdot mol^{-1}$$

Table 4. Sample application for compound naphthalene for literature available $C_{p,m}^{\circ}$values without their uncertainties (I.ii).

$C_{p,m}^{\circ}(cr)$	$C_{p,m}^{\circ}(g)$	$-\Delta_{cr}^{g}C_{p,m}^{\circ}$
J·mol^{-1}·K^{-1}	J·mol^{-1}·K^{-1}	J·mol^{-1}·K^{-1}
165.7[102; 104]	133.0 [105]	32.7

$$u(C_{p,m}^{o}) = \sqrt{\left(\frac{17}{165.7}\right)^2 + \left(\frac{4}{133.0}\right)^2} = 10.7\%$$

$$\Delta\left(\Delta_{cr}^{g}C_{p,m}^{o} \times \Delta T\right) = 0.107 \times 0.033\ kJ \cdot mol^{-1} \cdot K^{-1} \times 20.5\ K = 0.072\ kJ \cdot mol^{-1}$$

II. Values for $C_{p,m}^{\circ}(l/cr)$ are available, but $C_{p,m}^{\circ}(g)$ is not

When the ideal gas molar heat capacity is not available, $-\Delta_{l/cr}^{g}C_{p,m}^{\circ}$ can be calculated from the molar heat capacity of liquid/crystalline phase according to the equation published in the work of *Chickos et al.* (1993) [99]:

$$-\Delta_{l}^{g}C_{p,m}^{\circ} = 10.58 + 0.26 \times C_{p,m}^{\circ}(l) \quad (21)$$

$$-\Delta_{cr}^{g}C_{p,m}^{\circ} = 0.75 + 0.15 \times C_{p,m}^{\circ}(cr) \quad (22)$$

Several ways how to approach the uncertainties of the temperature adjustment, influenced by the application of equations 21 and 22, exist, also depending if it concerns the sublimation or the vaporization of the material.

i. Uncertainty estimation for heat capacities of solids according to *Acree and Chickos* (2010) [106]

According to the work of *Acree and Chickos* [106], instead of uncertainty evaluation for the heat capacities, the uncertainty of the whole term $\Delta\left(\Delta_{cr}^{g}C_{p,m}^{o} \times \Delta T\right)$ can be assumed as one third of the total value of temperature adjustment, resulting in equation 23:

$$\Delta(\Delta_{cr}^{g}C_{p,m}^{o} \times \Delta T) = \frac{\left[0.75 + 0.15 \times C_{p,m}^{\circ}(cr)\right] \times \Delta T}{3 \times 1000} \tag{23}$$

This uncertainty, generally, includes not only the uncertainty of correlation, but also the deviations, introduced when a group contribution method is used to estimate the values of $C_{p,m}^{\circ}(cr)$.

ii. Uncertainty estimation for heat capacities of solids according to *Chickos et al.* (1993) [99]

The introduction of the additional correlation (whether it is correlation 21 or 22) results in an additional source of uncertainties and the equation 16 should be expanded to include them:

$$\Delta\left(\Delta_{l/cr}^{g}C_{p,m}^{o} \times \Delta T\right) = u\left(\Delta_{l/cr}^{g}C_{p,m}^{o}\right) \times \Delta_{l/cr}^{g}C_{p,m}^{o} \times \Delta T \tag{24}$$

$$u\left(\Delta_{l/cr}^{g}C_{p,m}^{o}\right) = \sqrt{(u_1^2 + u_2^2)} = \sqrt{\left(\frac{\Delta(C_{p,m}^{o}(\mathrm{l/cr}))}{C_{p,m}^{o}(\mathrm{l/cr})}\right)^2 + \left(\frac{\Delta(\Delta_{l/cr}^{g}C_{p,m}^{o}}{\Delta_{l/cr}{}^{g}C_{p}}\right)^2} \tag{25}$$

Here u_1 represents the standard relative uncertainty of the known molar heat capacity in the condensed phase $C_{p,m}^{\circ}(l/cr)$ and u_2 is the standard relative uncertainty introduced by the molar heat capacities difference correlation equation (equations 21 or 22).

According to the work of *Chickos and Acree* (1993) [99], the standard deviation of the correlation equation 21 is equal to 33 $J \cdot mol^{-1} \cdot K^{-1}$.

In the calculation applications for the uncertainty values for solid material TATP (Table 5), the achieved temperature adjustment uncertainty value is greater for the concept explained in the chapter II.ii. than the uncertainty elucidated in the section II.i. Therefore, the II.ii. approach is preferred for crystalline materials.

iii. Uncertainty estimation for heat capacities of liquids according *Chickos et al.* (1993) [99]

According to the work of *Chickos and Acree* (1993) [99], the standard deviation of relationship 22 for liquids is equal to 15 $J \cdot mol^{-1} \cdot K^{-1}$.

Table 5. Calculation application for compound TATP for temperature adjustment when $C^{\circ}_{p,m}(g)$ values are not available and uncertainties are estimated according to the methods in sections **II.i.** snd **II.ii**.

$C^{\circ}_{p,m}(cr)$	$C^{\circ}_{p,m}(g)$	$-\Delta^{g}_{cr}C^{\circ}_{p,m}$
J·mol^{-1}·K^{-1}	J·mol^{-1}·K^{-1}	J·mol^{-1}·K^{-1}
271.8 [107]	n.a.	41.5

II.i. $\Delta\left(\Delta^{g}_{cr}C^{o}_{p,m} \times \Delta T\right) = \frac{(0.75+0.15\times 271\ J\cdot mol^{-1}\cdot K^{-1})\times 4.5\ K}{3\times 1000} = 0.06\ kJ \cdot mol^{-1}$

II.ii. $u\left(\Delta^{g}_{cr}C^{o}_{p,m}\right) = \sqrt{\left(\frac{17}{271.8}\right)^2 + \left(\frac{33}{41.5}\right)^2} = 79.8\%$

$\Delta\left(\Delta^{g}_{cr}C^{o}_{p,m} \times \Delta T\right) = 0.798 \times 0.0415\ kJ \cdot mol^{-1} \cdot K^{-1} \times 4.50\ K = 0.14\ kJ \cdot mol^{-1}$

Table 6. Calculation application for compound methyl salicylate for temperature adjustment when $C^{\circ}_{p,m}(g)$ values are not available and uncertainties are estimated according to the method **II.iii**.

$C^{\circ}_{p,m}(l)$	$C^{\circ}_{p,m}(g)$	$-\Delta^{g}_{l}C^{\circ}_{p,m}$
J·mol^{-1}·K^{-1}	J·mol^{-1}·K^{-1}	J·mol^{-1}·K^{-1}
248.8 [108]	n.a.	75.3

$u\left(\Delta^{g}_{l}C^{o}_{p,m}\right) = \sqrt{\left(\frac{14.4}{248.8}\right)^2 + \left(\frac{15}{75.3}\right)^2} = 20.7\%$

$\Delta\left(\Delta^{g}_{l}C^{o}_{p,m} \times \Delta T\right) = 0.207 \times 0.0753\ kJ \cdot mol^{-1} \cdot K^{-1} \times 9.0\ K = 0.14\ kJ \cdot mol^{-1}$

III. No data on $C^{o}_{p,m}$(l/cr) or $C^{o}_{p,m}$(g) available

When no data on the isobaric heat capacities is available, a suitable estimation method can be applied. Options, used in this work include a group contribution method by *Acree and Chickos* (2016) [101] for certain selection of functional groups and, alternatively, elemental composition method by *Hurst et al.* [109]. In the case of the method by *Acree and Chickos*, the uncertainties

of $C_{p,m}^{o}$(l) and $C_{p,m}^{o}$(cr) are provided in the equations 18 and 19. The uncertainties for the estimation of the $\Delta_{cr}^{g}C_{p,m}^{o}$ are provided in the sections II.ii and II.iii.

If the heat capacity estimation is done by elemental composition method of *Hurst et al.* [109], the relative standard deviation for organic liquids containing miscellaneous elements (which often are not included in the array of functional groups with heat capacity values in the group contribution methods) is equal to 15 % and for solids, 12.7%.

Table 7. Calculation application for compound methyl salicylate for temperature adjustment when $C_{p,m}^{\circ}(l/cr)$ values are estimated according to the group contribution method by *Acree and Chickos.*

$C_{p,m}^{\circ}(l)$	$C_{p,m}^{\circ}(g)$	$-\Delta_{l}^{g}C_{p,m}^{\circ}$
J·mol^{-1}·K^{-1}	J·mol^{-1}·K^{-1}	J·mol^{-1}·K^{-1}
280.8	n.a.	83.6

$$u\left(\Delta_{l}^{g}C_{p,m}^{o}\right) = \sqrt{\left(\frac{14.4}{280.8}\right)^{2} + \left(\frac{15}{83.6}\right)^{2}} = 0.19$$

$$\Delta\left(\Delta_{l}^{g}C_{p,m}^{o} \times \Delta T\right) = 0.19 \times 83.6\ J \cdot mol^{-1} \cdot K^{-1} \times 9.0\ K = 0.14\ kJ \cdot mol^{-1} \cdot K^{-1}$$

Table 8. Calculation application for compound DEMP for temperature adjustment when $C_{p,m}^{\circ}(l/cr)$ values are estimated according to the elemental composition method by *Hurst.*

$C_{p,m}^{\circ}(l)$	$C_{p,m}^{\circ}(g)$	$-\Delta_{l}^{g}C_{p,m}^{\circ}$
J·mol^{-1}·K^{-1}	J·mol^{-1}·K^{-1}	J·mol^{-1}·K^{-1}
259.2	n.a.	78.0

$$u\left(\Delta_{l}^{g}C_{p,m}^{o}\right) = \sqrt{(0.15)^{2} + \left(\frac{15}{78}\right)^{2}} = 0.25$$

$$\Delta\left(\Delta_{l}^{g}C_{p,m}^{o} \times \Delta T\right) = 0.25 \times 78.0\ J \cdot mol^{-1} \cdot K^{-1} \times 11.0\ K = 0.21\ kJ \cdot mol^{-1} \cdot K^{-1}$$

3. Aims of this work

The absence of the sufficient and reliable experimental data and an evident disarray in the existent literature on the thermodynamic properties of various hazardous materials is problematic since this information is essential for the description of their vaporization behavior in fields of security, environment and for monitoring in the energy pathways in chemical and physical processes.

In this work, the task of providing reliable data on the thermodynamics of relevant hazardous materials were to be realized by determination of high-quality experimental vapor pressures by means of the well-established transpiration method coupled to high precision analytical devices.

First of all, a newly-implemented chromatographic technique HPLC-DAD was to be utilized for the experiments on several reference materials of well-defined vapor pressures in order to prove the validity of updated experimental setup. The transpiration experimental setup, located in the group of Prof. Klapötke, was previously tested on the compounds naphthalene and anthracene using the GCMS device and showed an excellent agreement with literature data. In the current project, the same compounds were to be tested to investigate the consistency of obtainable results also using the HPLC-DAD analytical method. Moreover, additional compounds of extremely low volatility were to be tested to investigate the method capabilities and limitations.

To facilitate the generation of reliable thermodynamic data, a high accuracy purity assessment method - quantitative nuclear magnetic resonance (^{1}H-qNMR) - was to be established and tested. A proper process for the uncertainty estimation for the obtained results was to be developed and incorporated into the assessment procedure of the overall uncertainties for measured vapor pressures using the transpiration method.

Subsequently, a literature analysis for the most relevant compounds for this project was to take place. As a result, vaporization behavior of several chemical warfare agent (CWA) simulants were to be measured in order to achieve reliable thermodynamic data that is relevant for the development of the detection technologies for extremely toxic vapor without using the CWA materials. The research was to be followed by the vapor pressure determination for one of the most common explosive materials RDX that has been previously investigated in multiple instances yielding deviating results. Thermodynamic properties of its environmental

decomposition product and common home-made explosive TNX were also to be determined since there is a scarcity of reliable experimental results on this compound. Another group of energetic materials, a family of propellants alkyl- nitroxyethyl nitramines (NENAs), were to be investigated for their vaporization behavior since there was no literature data available for compounds that are currently in-use and manufactured on an industrial scale. Further research was to be focused on measurements of several azido group containing compounds that are generally avoided in most scientific laboratories because of their high mechanical sensitivities. Information on the thermodynamic properties of these compounds is desirable, since the high-quality experimental results enable the development of estimation techniques for other parameters that would normally require experimental evaluation. Also, vapor pressures of an organic compound containing a geminal diazido- group was to be investigated for the first time.

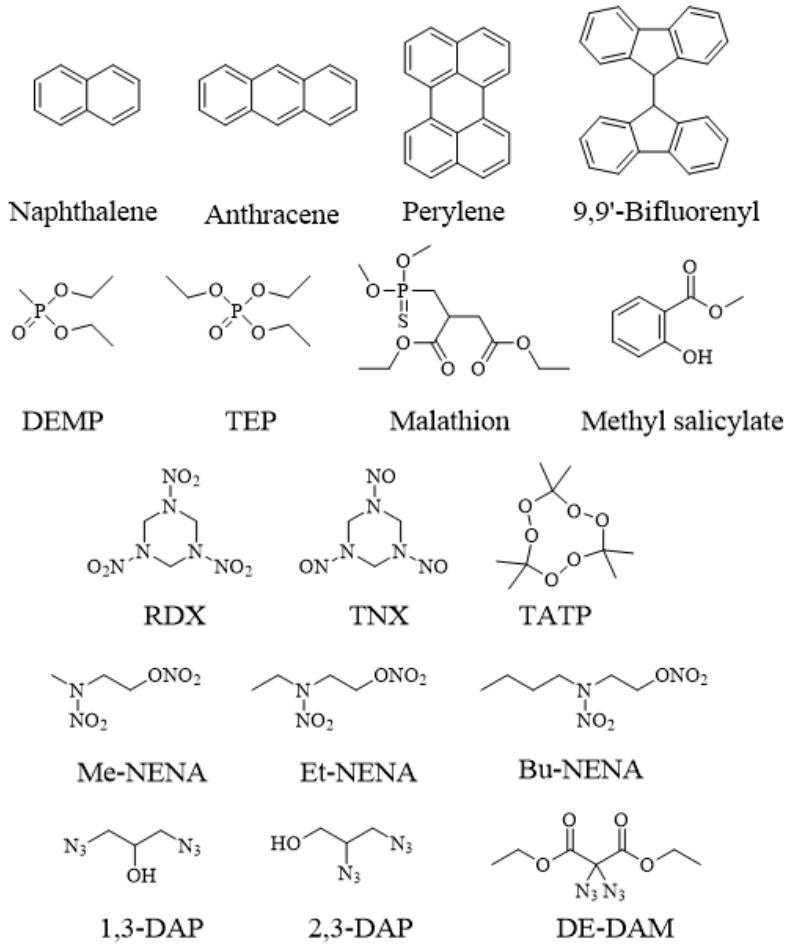

Figure 16. Compounds, investigated within the scope of the project in terms of their vapor pressures.

Finally, in the scope of the cooperation project with the Fraunhofer Institute for Chemical Technology and German Federal Police, one of the objectives of this work was to investigate the sublimation processes of a newly developed mixture containing the phlegmatized primary explosive - triacetone triperoxide (TATP). Since the developed mixtures were to be used as training aids for explosive detection dogs, it was important to determine the vapor pressures in order to assess the differences in the sublimation behavior between the phlegmatized mixture and the neat compound.

4. Summary and conclusions

Vapor pressures of hazardous materials have been measured extensively in the past, however, many of the reported values are in a disarray. The main objective of this work was to obtain new and reliable experimental vapor pressure data for various hazardous materials in order to establish a good understanding behind the thermodynamics in terms of a phase change. Therefore, this research focused on the determination of experimental vapor pressures using the transpiration method.

In order to properly evaluate the purity of analyzed compounds, a ^{1}H-qNMR method (quantitative nuclear magnetic resonance) was successfully established in the working group of Prof. Klapötke. The method allowed a reliable determination of the mass fraction purity of various compounds with uncertainties as low as 0.002 (m/m).

For the purpose of broadening the repertoire of compounds suitable for vapor pressure measurements using the transpiration method, a previously implemented VO-GCMS device was accompanied by a recent installment of a HPLC-DAD analytical device that enabled measurements of low vapor pressure and thermolabile compounds. In order to prove the validity of newly introduced analytical method, the volatility of several reference materials with well-defined vapor pressures (naphthalene and anthracene) were measured using the transpiration method. The close agreement with the previously reported data proved the method reliability in terms of determination of thermodynamic properties. The experiment on reference materials were expanded to low vapor pressure materials (perylene and 9,9'-bifluorenyl) to investigate the reproducibility of the transpiration experiment results at extremely low vapor pressures. The successful outcome proved the method to be suitable for low vapor-pressure materials. The results were reported in the **Article 1 [1]** .

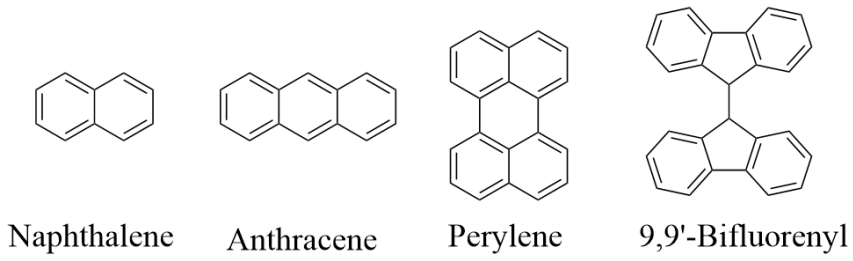

Figure 17. Chemical structures of the reference compounds under investigation.

The research was followed by the measurements of vaporization behavior of several chemical warfare agent (CWA) simulants that could contribute to the determination of detection limits of corresponding CWA detection devices (**Article 1 [1]**). The new results complemented the literature data and expanded the *p-T* database to uninvestigated temperature ranges, mostly focusing on the ambient temperatures. Whilst the *p-T* values, obtained in this work, agreed with most of literature values for compounds TEP and DEMP and methyl salicylate, the results of malathion showed a different trend from what was observed in the literature.

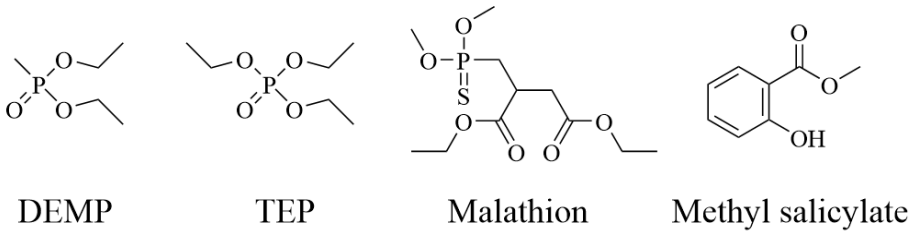

Figure 18. Chemical structures of Chemical Warfare Agent (CWA) simulants, investigated in this work.

In **Article 2 [2]**, new experimental vapor pressures for one of the most commonly used explosive RDX and its environmental decomposition product TNX, which is also known as common home-made explosive, were reported. Results were compared with existing *p-T* data in the literature. In case of RDX, several studies have already investigated the sublimation behavior, however, available *p-T* data was inconsistent. New reported experimental vapor pressures introduced more certainty in the thermodynamic description of this important compound. As for TNX, only one set of experimental vapor pressures has been recorded in the past and the results differ considerably from the *p-T* data reported in this work. Since the vapor pressures of TNX are significantly higher than of its mother compound, it could allow more efficient detection of the past or current presence of explosive RDX in environmental conditions.

Figure 19. Cover picture in the journal *Propellants, Explosives, Pyrotechnics* (2020): transpiration method set-up.

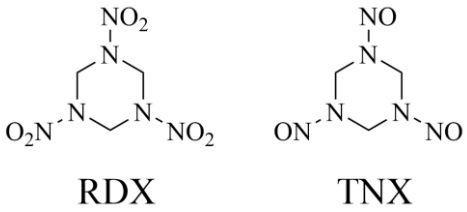

Figure 20. Compounds studied in this work: hexahydro-1,3,5-trinitro1,3,5-triazine (RDX) and hexahydro-1,3,5-trinitroso-1,3,5-triazine (TNX).

In **Article 3 [3]**, the experimental vapor pressures and the resulting molar enthalpies of phase transitions for alkyl− NENAs were reported for the first time. In the case of Me-NENA, because the substance melts at near-ambient temperature, both the sublimation and vaporization behaviors were investigated. To verify the validity of the derived molar enthalpies of phase transition for Me-NENA, the experimental value for molar enthalpy of fusion at 298.15 K was determined using DSC and was compared to the theoretical value, derived from the vapor pressure results obtained in this work. The resulting value agreed with the derived value confirming the consistency of the experimental results. The determined vapor pressures of Et-NENA and Bu-NENA indicated an unexpected phenomenon: the absolute vapor pressures of Me- and Et-NENAs were nearly indistinguishable, with Et-NENA having slightly higher vapor pressure values. It can be speculated that in the case of a shorter alkyl group, the chemical structure and the corresponding charge distribution in Me-NENA induce an additional dipole moment affecting the intermolecular interactions. The results of this study fill an evident gap in the knowledge of the thermodynamic properties of the alkyl-NENA compounds and may assist in the optimization of the manufacturing process of propellant mixtures.

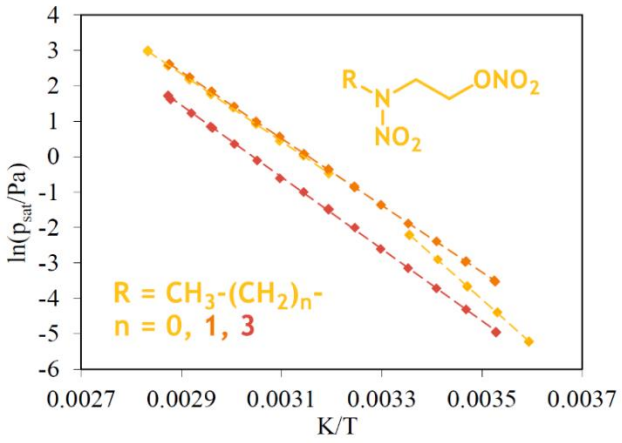

Figure 21. Comparison of the experimental vapor pressure values of alkyl-NENA compounds measured in this work [3].

Further investigations focused on the vaporization behavior of compounds from a rarely thermodynamically investigated organic polyazido group: 1,3-DAP, 2,3-DAP and DE-DAM. It is the first time the thermodynamic properties are reported for a compound, containing a geminal diazido- group (DE-DAM). The reported thermodynamic data (**Article 4 [4]**) could contribute to achieve a better understanding of the vaporization behavior of the azido- group containing organic compounds and improve the existent thermochemical parameter estimation methods for the compounds containing multiple azido groups.

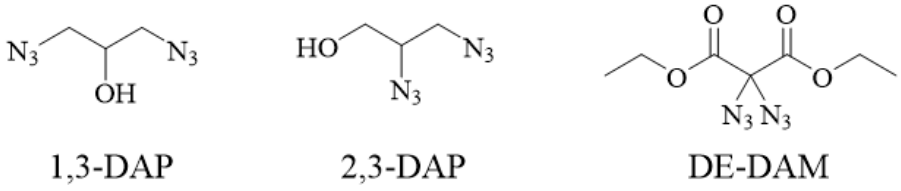

Figure 22. Organic polyazido compounds that were analyzed in this work: 1,3-DAP, 2,3-DAP and DE-DAM.

Finally, in the frame of a cooperation with institute of Fraunhofer ICT and German Federal Police, a newly established way of phlegmatization of one of the most common home-made primary explosive – TATP – contributed to the development of a new detection aid for the explosive detection dogs. The cooperation project included the investigation of the developed mixtures containing TATP and activated charcoal in terms of their vapor pressures, which were compared to the results of neat TATP and reported in the **Article 5 [5]**. It was observed that lowering the amount of TATP in the mixture with activated charcoal decreases the vapor

pressure p_{sat} at 298.15 K and increases the molar enthalpy of sublimation at 298.15 K, which can be attributed to absorption phenomena. These results agree with the results of the process mass spectrometer measurements, which indicated that TATP/activated charcoal-mixture has a lower volatility than the pure bulk material. Moreover, it was demonstrated that the volatility of the TATP in the TATP/activated charcoal-mixtures is rather sensitive to the compound concentration.

Figure 23. Left: phlegmatized activated charcoal-TATP mixture on a filter paper, right: structure of the TATP [5].

References in this Chapter

[1] G. Bikelytė, M.A. Härtel, T.M. Klapötke, B. Krumm, A. Sadaunykas, J. Chem. Thermodyn. 143 (2020) 106043.
[2] G. Bikelytė, M.A. Härtel, T.M. Klapötke, Propellants Explos. Pyrotech. 45 (2020) 1573-1579.
[3] G. Bikelytė, M.A.C. Härtel, M. Holler, A. Neuer, T.M. Klapötke, J. Chem. Eng. Data (2021) 66(4), 1709-1716.
[4] G. Bikelytė, A.G. Harter, M.A.C. Härtel, S.B. Heimsch, T.M. Klapötke, Fluid Ph. Equilibria (2021) 549: 113222.
[5] I. Wilhelm, G. Bikelytė, M. Wittek, M.A.C. Härtel, T.M. Klapötke, Propellants Explos. Pyrotech. (2022) 47(2): e202100057.

5. Results and discussion

5.1. Measurements of CWA simulants (Article 1)

Article 1: Experimental thermochemical data of CWA simulants: Triethyl phosphate, diethyl methylphosphonate, malathion and methyl salicylate

The results were published in the *Journal of Chemical Thermodynamics* [110] and are reprinted with permission. Copyright 2020 Elsevier. DOI: doi.org/10.1016/j.jct.2019.106043.

J. Chem. Thermodynamics 143 (2020) 106043

Contents lists available at ScienceDirect

J. Chem. Thermodynamics

journal homepage: www.elsevier.com/locate/jct

Experimental thermochemical data of CWA simulants: Triethyl phosphate, diethyl methylphosphonate, malathion and methyl salicylate

Greta Bikelytė, Martin A.C. Härtel, Thomas M. Klapötke *, Burkhard Krumm, Audrius Sadaunykas

Department Chemie, Ludwig-Maximilians-Universität München, Butenandtstr. 5-13 (D), 81377 München-Großhadern, Germany

ARTICLE INFO

Article history:
Received 26 April 2019
Received in revised form 19 December 2019
Accepted 29 December 2019
Available online 31 December 2019

Keywords:
Vapor pressure
CWA simulants
Gas-saturation
Enthalpy of vaporization

ABSTRACT

This work focuses on the determination of important thermochemical properties of several chemical warfare agent (CWA) simulants: diethyl methylphosphonate (DEMP, CAS 683-08-9, **1**), triethyl phosphate (TEP, CAS 78-40-0, **2**), malathion (CAS 121-75-5, **3**) and methyl salicylate (MS, 119-36-8, **4**). Enthalpies of vaporization $\Delta_l^g H_m^o$ (298.15 K) (**1**: 56.8 ± 0.8 kJ mol^{-1}; **2**: 63.9 ± 0.9 kJ mol^{-1}; **3**: 101.4 ± 1.8 kJ mol^{-1}; **4**: 59.3 ± 0.8 kJ mol^{-1}) and vapor pressures p_{sat} (298.15 K) (**1**: 43.9 Pa; **2**: 12.5 Pa; **3**: 1.4 mPa; **4**: 14.5 Pa) were determined by the transpiration method in the ambient temperature range. The results were compared with existing literature values and critically evaluated. Data of DEMP **1**, TEP **2** and MS **4** show agreement with most literature vaes, while results of malathion **3** show a significant disagreement with the scarce available literature *p-T* data.

1. Introduction

With respect to the recent attacks involving chemical warfare agents (CWA) (Ghouta, Syria, 2013 [1]; Salisbury, UK, 2018 [2]) there is a great interest in acquiring knowledge on the thermodynamical processes related to these compounds. Volatilization mechanisms are especially important when it comes to the development of detection systems for hazardous materials. However, CWA toxicity and usage restrictions (controlled by Chemical Weapons Convention, Schedule II, etc.) create difficulties when it comes to investigations of their detectability [3]. For this reason CWAs are usually exchanged with simulants mimicking composition, physical and/or chemical properties, but of a significantly lower toxicity. Moreover, CWA simulants are an essential tool for the design of new detectors. There are several studies published, analyzing the suitability of the compounds to simulate most common CWAs, such as VX, mustard gas, G-agents [4,5]. Many CWA simulants face a lack of consistency when it comes to literature values of vapor pressures. Consequently, this study is focused on the determination of vapor pressures and related thermodynamic properties of 4 CWA simulants: diethyl methylphosphonate (DEMP **1**), triethyl phosphate (TEP **2**), malathion **3** and methyl salicylate (MS **4**) (Fig. 1).

2. Materials and methods

Caution! Malathion is highly toxic and should be handled with caution! Proper protective measures (gloves, safety googles, laboratory coats, etc.) should always be used during handling of the compound.

2.1. Purity

The purity of the compounds used in this study was tested by EA and ^{1}H-qNMR techniques. Three of the substances (DEMP **1**, TEP **2** and MS **4**) were purchased from a *Sigma-Aldrich* and malathion **3** was prepared according to a known literature procedure [6]. Purity data are disclosed in the Table 1. For further information on purity assessment please see Supporting Information.

2.2. Transpiration method

In this study, the experiments were conducted using the gas-saturation method. Previously we have applied the transpiration method on mononitrotoluenes [7], peroxides [8], nitrate esters [9], aliphatic nitroalkanes [10], organothiophosphates [11].

The transpiration experiment can be explained as follows (Fig. 2): between 0.5 and 1 g of analyte material was mixed with around 35 g of glass beads and placed in a custom-made glass vessel (saturator, ***5***) that is connected to a thermostat (*Huber* Ministat 230 with external class A PT-100 temperature sensor inside the saturator vessel), surrounded by a circulating thermo-fluid (ethylene glycol, 50% aqueous). The saturator is kept at a constant

* Corresponding author.
E-mail address: tmk@cup.uni-muenchen.de (T.M. Klapötke).

https://doi.org/10.1016/j.jct.2019.106043
0021-9614/

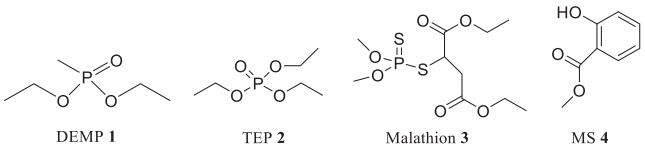

Fig. 1. Chemical structures of compounds under investigation: DEMP **1**, TEP **2**, malathion **3**, MS **4.**

temperature (±0.1 K) and connected to a gas inlet. Nitrogen gas (1) (*Air Liquide*, Stickstoff HG Flüssig, 99.999 vol% purity, <3 ppm O_2/H_2O v/v), flows through a pressure reduction valve (2) and a drying column (3) that is filled with phosphorus pentoxide, coated on a silica support (Sicapent™, *Sigma-Aldrich*, cat. #79610). The gas flow, regulated by a mass flow controller (***4***) (MC-100 CCM, *Natec Sensors GmbH*), is directed into the saturator. As the gas travels through the saturator it reaches the saturation equilibrium with the analyte and enters a glass condenser tube (***6***), which is positioned in a Dewar vessel (cooling trap, ***7***), containing *iso*-propanol that is cooled with an immersion cooler (*Huber* TC45E) to −30 °C. The gas stream is cooled and analyte condenses on the walls of the condenser tube. The exact flow rate of the gas stream is measured with a soap film flow meter (*Hewlett Packard* No.: 0101–0113, ***8***) under ambient conditions (T_{amb}, p_{amb}), which are determined by a thermobarometer (*Greisinger* GFTB 200). The analyte in the condenser tube is collected for a defined interval of time, after which the tube is removed from the saturator and a known amount of standard solution is introduced in order to determine the mass of collected analyte m_a using chromatographic techniques. In this work, the quantification of all CWA simulants was executed with a VO-GC/MS [12] (*Shimadzu* GC/MS QP2010 SE).

The experimental method allows the calculation of the absolute vapor pressure of the analyte p_{sat} at a temperature of the saturator T_{exp} using the Ideal Gas Law:

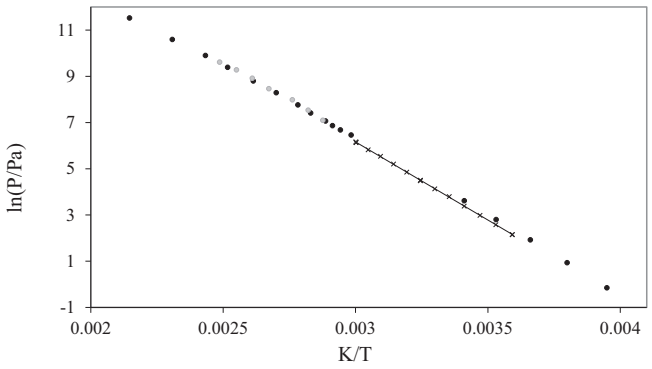

Fig. 3. Experimental vapor pressure values of DEMP **1** in comparison with literature values. Here ● – from Butrow et al. [20], ● – from Kosolapoff [21], × and solid line – from this work.

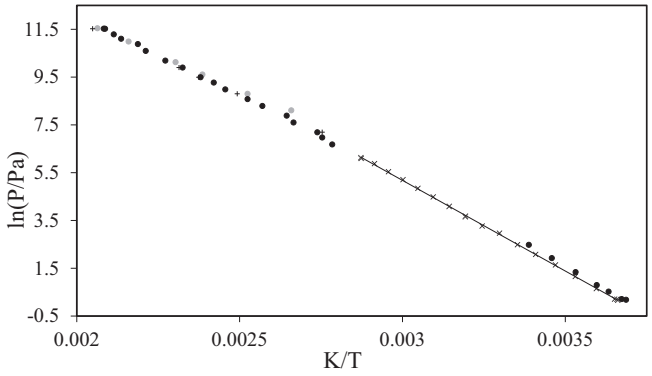

Fig. 4. Experimental vapor pressure values of TEP **2** in comparison with literature values. Here ● – from Brozena et al. [27], ● – from Cavalier [28], + – from Evans et al. [29], × and solid line – from this work.

Table 1
Origin and purity of the compounds investigated.

Substance	CAS#	Producer	Product-#	Purity	Final purity ($U(P_{An})$)[b]
DEMP **1**	683-08-9	*Sigma-Aldrich*	268119	0.97[a]	0.985 (±0.006)
TEP **2**	78-40-0	*Sigma-Aldrich*	838728	0.998[a]	0.980 (±0.002)
Malathion **3**	121-75-5	–	–	–	0.978 (±0.003)
MS **4**	119-36-8	*Sigma-Aldrich*	76631	>0.990[a]	0.991 (±0.002)

[a] Mass fraction purity as stated by manufacturer.
[b] Mass fraction purity was determined by the ^{1}H-qNMR technique. Expanded uncertainties are reported with a confidence level of 0.95 (k = 2) and further detailed in the Supporting Information.

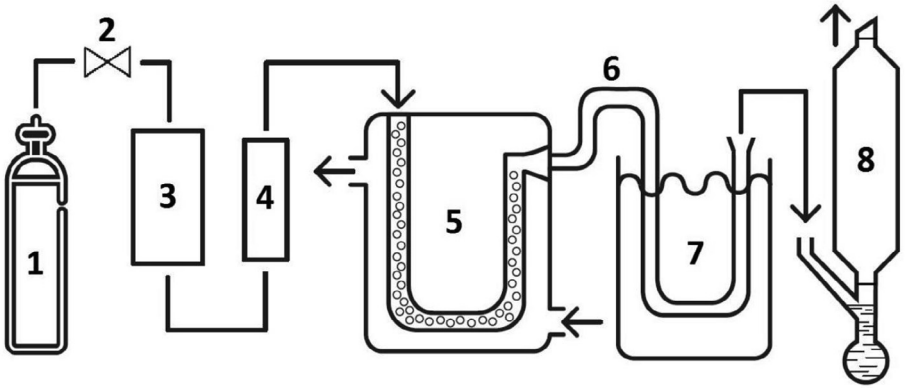

Fig. 2. Transpiration method experimental setup: 1 – nitrogen reservoir; 2 – pressure reduction valve; 3 – P_4O_{10} drying tower; 4 – mass flow controller; 5 – saturator; 6 – condenser pipe; 7 – cooling trap; 8 – soap film flowmeter.

$$p_{sat}(T_{\exp}) = \frac{m_a R T_{amb}}{M V_{amb}}. \quad (1)$$

The authors also assume the validity of Daltons Law of Partial Pressures and that the volume of the analyte (V_a) in gaseous phase is negligibly small in comparison to the volume of the carrier gas (V_{N_2}) :

$$V_{N_2} >> V_a, \text{ in } V_{amb} = V_{N_2} + V_a$$

p_{sat}: vapor pressure of the analyte [Pa], T_{exp}: temperature of the saturator [K], m_a: the mass of the analyte collected in the condenser tube [kg], T_{amb}: ambient temperature [K], V_a: volume of the analyte [m^3], V_{N2}: volume of the carrier gas [m^3], V_{amb}: volume of the carrier gas measured at ambient conditions [m^3], R: universal gas constant 8.314462 [J mol^{-1} K^{-1}], M: molecular weight [kg mol^{-1}].

These assumptions allow the determination of V_{amb} from the flow rate of the gas stream and the duration of the measurement.

Table 2
Molar heat capacities and their differences at T = 298.15 K.

Compound	$C^o_{p,m}(l)$		$-\Delta^g_l C^o_{p,m}$
	Calc. J mol^{-1} K^{-1}	Exp. J mol^{-1} K^{-1}	J mol^{-1} K^{-1}
DEMP **1**	259.2[a]	n.a.	78.0[c]
TEP **2**	306.7[a]	n.a.	90.3[c]
Malathion **3**	491.9[a]	n.a.	138.5[c]
MS **4**	275.3[b]	–	82.2[c]
	–	(268.4) [16]	(80.4)
	–	(248.8) [17]	(75.3)

Values in parentheses were not used for calculation of molar heat capacity differences. n.a.: not available. a) calculated according to the empirical increment approach by Hurst et al. [15]. b) derived from the molecular increments procedure described by Chickos et al. [14]. c) calculated by $-\Delta^g_l C^o_{p,m} = 10.58 + C^o_{p,m}(l) \times 0.26$ [13].

The experimental vapor pressure values obtained are expressed by a fitting function, based on the *Clarke-Glew* equation [7]:

$$\ln\left(\frac{p_{sat}}{p^o}\right) - \frac{\Delta^g_l C^o_{p,m}}{R} \ln\frac{T}{T_0} = A - \frac{B}{T}. \quad (2)$$

p^o: reference pressure (1 Pa), $\Delta^g_l C^o_{p,m}$: molar heat capacity difference at constant pressure from liquid to gaseous state [J mol^{-1} K^{-1}], T: temperature [K], T_0: reference temperature [298.15 K], A/B: fitting coefficients (A: [ ], B: [K]).

The enthalpies of vaporization at the temperature T are calculated by:

$$\Delta^g_l H^o_m(T) = RB + \Delta^g_l C^o_{p,m} T. \quad (3)$$

$\Delta^g_l H^o_m(T)$: molar enthalpy of vaporization at temperature T [J mol^{-1}].

Available literature data was analyzed using the same approach as analyzing the experimental vapor pressures, measured in this work.

For the validation of the experimental set-up used, vapor pressures of 4 reference materials – naphthalene, anthracene, perylene and 9,9′-bifluorenyl were measured. For the results and experimental details, refer to the Supporting Information.

2.3. Molar heat capacities

The molar heat capacity at constant pressure $C^o_{p,m}(l)$ at 298.15 K of analyte **4** was derived from the molecular increments procedure described by Chickos et al. [13,14] (Table 2). Values for the remaining analytes **1**–**3** were calculated according to the empirical increment approach by Hurst et al. [15], with respect to their phosphorus content. For further information on the calculations of molar heat capacities by the method of Hurst et al. [15] refer to Supporting Information (Section S4).

Table 3
Results of DEMP **1**: absolute vapor pressures p_{sat} and thermodynamic properties of vaporization obtained by the transpiration method in this work.

Diethyl methylphosphonate: $\Delta^g_l H^o_m$ (298.15 K) = 56.8 ± 0.8 kJ mol^{-1}
$\ln p_{sat}/p^0 = \frac{300.0}{R} - \frac{80064.0}{RT} - \frac{78.0}{R} ln \frac{T}{298.15K}$

T_{exp}[a] [K]	m[b] [mg]	V_{N2}[c] [dm^3]	T_{amb}[d] [K]	Gasflow [dm^3 h^{-1}]	p_{sat}[e] [Pa]	$U(p_{sat})$[f] [Pa]	$\Delta^g_l H^o_m$ [kJ mol^{-1}]	$\Delta^g_l S^o_m$ [J mol^{-1} K^{-1}]
278.3	0.17	0.35	297.3	1.4	8.26	0.37	58.35	131.5
278.4	0.12	0.24	300.6	0.9	8.64	0.39	58.35	131.8
278.4	0.25	0.49	299.9	1.9	8.57	0.39	58.35	131.7
283.3	0.24	0.30	298.6	1.2	13.2	0.6	57.97	130.4
288.2	0.28	0.24	299.1	0.9	19.8	0.9	57.59	128.9
293.2	0.42	0.24	299.1	0.9	29.4	1.3	57.19	127.5
298.1	0.64	0.24	299.0	0.9	44.3	2.0	56.81	126.3
303.1	0.90	0.24	299.1	0.9	62.4	2.8	56.42	124.8
308.2	1.30	0.24	297.5	0.9	89.8	4.1	56.03	123.5
308.2	1.31	0.24	296.4	0.9	90.6	4.1	56.03	123.6
308.2	1.27	0.23	298.0	0.9	88.6	4.0	56.03	123.4
313.1	1.85	0.24	298.5	0.9	128	6	55.64	122.3
318.1	2.64	0.24	297.3	0.9	183	8	55.25	121.3
323.2	3.73	0.24	295.8	0.9	255	12	54.86	120.1
328.1	4.88	0.24	296.9	0.9	337	15	54.47	118.7
333.1	6.70	0.24	297.2	0.9	462	21	54.08	117.6
333.1	6.70	0.23	297.1	0.9	464	21	54.08	117.7
333.2	6.91	0.23	297.4	0.9	479	22	54.08	117.9

The uncertainties for T, V and m are standard uncertainties. Uncertainty of the enthalpy of vaporization is the expanded uncertainty with a confidence level of 0.95 (k = 2), calculated including uncertainties of vapor pressure, uncertainties from the fitting equation and the uncertainty of temperature adjustment to T = 298.15 K. Detailed information on the methods of calculations was published previously [18,19].

[a] Saturation temperature ($u(T)$ = 0.1 K).
[b] Mass of transferred sample condensed at 243 K.
[c] Volume of nitrogen ($u(V)$ = 0.005 dm^3) used to transfer m ($u(m)/m$ = 1.5%) of the sample.
[d] T_{amb} is the temperature of the soap film flowmeter used for measurement of the gas flow.
[e] Vapor pressure at temperature T, calculated from the m and the residual vapor pressure at the condensation temperature, calculated by an iteration procedure; po = 1 Pa.
[f] Relative expanded uncertainty with confidence level 0.95 (k = 2) for p was calculated to be $U(p)/p$ = 4.52% (see Supporting Information).

There are two literature sources stating experimental heat capacities [16,17] of MS **4**. Both of these papers have been published by the same working group one year apart and in both publications molar heat capacities of liquids were measured with a differential scanning calorimeter. Even though the measurements were executed in the same temperature range and repeated 3 times, the resulting heat capacity values differed by approximately 9%. Because of the observed inconsistency, in this study the molar heat capacity value, obtained by the calculation according to Chickos et al. [13], is used for further calculations.

3. Results and discussion

3.1. Vapor pressures

3.1.1. Diethyl methylphosphonate (DEMP **1**)

The vaporization behavior of DEMP **1** was measured in this work in the temperature range of 278.3–333.2 K. The absolute vapor pressures p_{sat} and thermodynamic properties of vaporization obtained by the transpiration method are compiled in Table 3. From these results, values of enthalpy of vaporization (56.8 ± 0.8 kJ mol^{-1}) and vapor pressure at 298.15 K (43.9 Pa) were

Table 4
Compilation of data on enthalpies of vaporization $\Delta_l^g H_m^o$ of DEMP **1.**

Experiment[a]	Method[b]	*T*-Range K	T_{avg} K	$\Delta_l^g H_m^o(T_{avg})$ kJ mol^{-1}	$\Delta_l^g H_m^o$(298.15 K)[c] kJ mol^{-1}	p_{sat}[d] Pa
Butrow et al. 2009 [20]	Comb	253.2–465.9	337.3	54.2	56.8 ± 1.5	55.6
Stephenson et al. 1987 [22]	O	343.0–403.0	372.1	51.8	[57.5]	[55.3]
Kosolapoff 1955 [21]	ISO	347.7–402.2	372.8	53.3	59.2 ± 3.8	47.8
This Work 2019	T	278.3–333.2	304.8	56.2	56.8 ± 0.8	43.9
					56.9 ± 0.7[e]	49.1[f]

Values in brackets were not used in further analysis.
[a] First author and year of publication.
[b] Methods: T = transpiration, ISO = isoteniscope method, O = equation only, Comb = combination of results from DSC and transpiration measurements.
[c] Enthalpies of vaporization were adjusted according to Chickos et al. [13] with values of $\Delta_l^g C_{p,m}^o$ and $C_{p,m}^o$(l), stated in Table 2. Uncertainty for enthalpy of vaporization is expressed as expanded uncertainty with confidence level of 0.95 (k = 2).
[d] Vapor pressure at 298.15 K.
[e] Weighted average value, calculated using uncertainty as the weighing factor.
[f] Average value.

Table 5
Results of TEP **2**: absolute vapor pressures p_{sat} and thermodynamic properties of vaporization obtained by the transpiration method in this work.

Triethyl phosphate: $\Delta_l^g H_m^o$ (298.15 K) = 63.9 ± 0.9 kJ mol^{-1}
$\ln p_{sat}/p^0 = \frac{325.7}{R} - \frac{90841.7}{RT} - \frac{90.3}{R} ln \frac{T}{298.15K}$

T_{exp}[a] [K]	m[b] [mg]	V_{N2}[c] [dm^3]	T_{amb}[d] [K]	Gasflow [dm^3 h^{-1}]	p_{sat}[e] [Pa]	$U(p_{sat})$[f] [Pa]	$\Delta_l^g H_m^o$ [kJ mol^{-1}]	$\Delta_l^g S_m^o$ [J mol^{-1} K^{-1}]
273.1	0.04	0.46	303.5	1.85	1.18	0.05	66.18	147.9
273.3	0.30	3.48	300.7	2.32	1.23	0.06	66.16	148.0
273.9	0.02	0.24	297.7	0.96	1.23	0.06	66.11	147.4
278.1	0.06	0.45	298.2	1.82	1.92	0.09	65.73	146.0
283.2	0.10	0.46	303.5	1.85	3.18	0.15	65.27	144.3
288.2	0.17	0.46	299.1	1.83	5.16	0.24	64.82	142.8
293.4	0.27	0.46	303.6	1.85	8.00	0.37	64.35	140.9
298.2	0.40	0.46	300.1	1.84	12.0	0.6	63.91	139.3
303.2	0.65	0.46	303.8	1.85	19.5	0.9	63.46	138.3
308.2	0.88	0.46	301.6	1.84	26.3	1.2	63.01	135.9
313.1	1.33	0.46	302.2	1.85	39.6	1.8	62.57	134.7
313.2	0.96	0.33	301.0	1.33	39.8	1.8	62.56	134.7
313.2	0.68	0.24	298.0	0.95	38.7	1.8	62.56	134.4
318.1	2.01	0.46	300.1	1.84	60.0	2.8	62.12	133.6
318.2	1.98	0.46	303.6	1.85	59.4	2.8	62.11	133.4
323.2	1.59	0.25	302.2	0.99	88.9	4.1	61.66	132.4
328.2	3.03	0.33	302.7	0.99	127	6	61.21	131.1
333.2	4.15	0.31	302.6	0.99	183	9	60.76	130.0
338.2	4.46	0.24	300.6	0.96	255	12	60.30	128.7
343.1	6.29	0.24	301.4	0.97	358	17	59.86	127.6
348.0	7.83	0.24	302.2	0.97	446	21	59.41	125.7
348.2	10.83	0.33	302.8	1.32	453	21	59.40	125.7
348.2	8.08	0.24	302.9	0.97	460	21	59.40	125.9

The uncertainties for T, V and m are standard uncertainties. Uncertainty of the enthalpy of vaporization is the expanded uncertainty with a confidence level of 0.95 (k = 2), calculated including uncertainties of vapor pressure, uncertainties from the fitting equation and the uncertainty of temperature adjustment to T = 298.15 K. Detailed information on the methods of calculations was published previously [18,19].
[a] Saturation temperature ($u(T)$ = 0.1 K).
[b] Mass of transferred sample condensed at 243 K.
[c] Volume of nitrogen ($u(V)$ = 0.005 dm^3) used to transfer m ($u(m)/m$ = 1.5%) of the sample.
[d] T_{amb} is the temperature of the soap film flowmeter used for measurement of the gas flow.
[e] Vapor pressure at temperature T, calculated from the m and the residual vapor pressure at the condensation temperature, calculated by an iteration procedure; p^o = 1 Pa.
[f] Relative expanded uncertainty with confidence level 0.95 (k = 2) for p was calculated to be $U(p)/p$ = 4.64% (see Supporting Information).

derived. This work and literature values are illustrated in Fig. 3 and compared in Table 4. Deviation of experimental literature values from *p*-*T*-equation derived from *p*-*T*-data obtained in this work (Table 3) is illustrated in Fig. S9.

Butrow et al. [20] measured vapor pressures of DEMP **1** with two different methods: differential scanning calorimetry (DSC) and by the transpiration method. From the results, established with both methods, a vapor pressure value at 298.15 K was extrapolated (55.6 Pa). This result does not match the value, derived from this work (43.9 Pa). However, enthalpy of vaporization at 298.15 K, calculated from the study of Butrow et al. [20] matches with the enthalpy of vaporization, calculated in this work (both 56.8 kJ mol^{-1}). Transpiration measurement results from Butrow et al. [20] were also disclosed in the publication by Brozena et al. [23]. Here the authors claim results to be in a good agreement with the results of Kosolapoff [21] in the pressure range above 10 Torr (1333.2 Pa). Moreover, they express the need of experimental measurements of vapor pressures over a wider ambient temperatures range, which is fulfilled by this work.

In the work of Kosolapoff [21] vapor pressures were determined using an isoteniscope apparatus in the temperature range from 343.15 K to 402.15 K. As the authors indicate, the apparatus was not precise at low vapor pressures. Therefore, the values at lowest experimental temperatures are considered unreliable. These concerns were addressed in the work of Butrow et al. [20] as well. For these reasons, results of this study should be used with great

Table 6
Compilation of data on enthalpies of vaporization $\Delta_l^g H_m^o$ of TEP **2.**

Experiment[a]	Method[b]	*T*-Range K	T_{avg} K	$\Delta_l^g H_m^o(T_{avg})$ kJ mol^{-1}	$\Delta_l^g H_m^o$(298.15 K)[c] kJ mol^{-1}	p_{sat}[d] Pa
Brozena et al. 2014 [27]	Comb	271.3–480.2	365.9	58.9	63.7 ± 2.8	14.7
Evans et al. 1930 [29]	E	363.2–488.2	417.2	51.0	61.9 ± 5.4	17.3
Cavalier 1899 [28]	E	376.2–484.7	425.7	48.5	60.0 ± 5.8	26.2
This Work 2019	T	273.1–348.2	309.3	63.1	63.9 ± 0.9	12.5
					63.8 ± 0.8[e]	17.7[f]

[a] First author and year of publication.
[b] Methods: T = transpiration, E = ebulliometry, Comb = combination of results from DTA, Knudsen-effusion and transpiration measurements.
[c] Enthalpies of vaporization were adjusted according to Chickos et al. [13] with values of $\Delta_l^g C_{p,m}^o$ and $C_{p,m}^o$(l), stated in Table 2. Uncertainty for enthalpy of vaporization is expressed as expanded uncertainty with confidence level of 0.95 (k = 2).
[d] Vapor pressure at 298.15 K.
[e] Weighted average value, calculated using uncertainty as the weighing factor.
[f] Average value.

Table 7
Results of malathion **3**: absolute vapor pressures p_{sat} and thermodynamic properties of vaporization obtained by the transpiration method in this work.

Malathion: $\Delta_l^g H_m^o$ (298.15 K) = 101.4 ± 1.8 kJ mol^{-1}
$\ln p_{sat}/p^0 = \frac{423.7}{R} - \frac{142673.8}{RT} - \frac{138.5}{R} ln \frac{T}{298.15K}$

T_{exp}[a] [K]	m[b] [mg]	V_{N2}[c] [dm^3]	T_{amb}[d] [K]	Gasflow [dm^3 h^{-1}]	p_{sat}[e] [mPa]	$U(p_{sat})$[f] [mPa]	$\Delta_l^g H_m^o$ [kJ mol^{-1}]	$\Delta_l^g S_m^o$ [J mol^{-1} K^{-1}]
298.2	0.03	136	297.1	6.11	1.44	0.07	101.37	189.8
303.2	0.04	102	296.3	4.56	2.68	0.12	100.69	187.2
303.2	0.04	106	297.2	5.21	2.74	0.13	100.69	187.3
303.2	0.03	84.6	296.3	4.24	2.67	0.12	100.68	187.1
308.1	0.01	20.9	297.0	6.10	5.08	0.23	100.00	184.9
308.1	0.06	89.2	296.3	5.15	4.96	0.23	100.00	184.7
313.1	0.10	77.9	297.8	4.58	9.69	0.44	99.31	182.9
318.0	0.03	10.9	297.3	6.10	17.3	0.8	98.63	180.6
323.0	0.04	9.08	296.5	5.14	30.5	1.4	97.94	178.5
328.0	0.05	7.44	297.3	5.19	52.7	2.5	97.25	176.3
328.0	0.06	8.55	297.7	4.58	54.0	2.4	97.25	176.5
332.9	0.05	4.31	296.9	5.17	84.6	3.9	96.56	173.8
333.0	0.04	3.82	296.5	4.58	87.3	4.0	96.56	174.0
333.0	0.04	3.28	296.4	3.93	85.4	3.9	96.56	173.8
337.9	0.05	2.77	298.3	5.20	144	7	95.87	171.9
342.9	0.04	1.28	296.6	5.14	245	11	95.19	170.2
347.9	0.04	0.83	296.5	3.33	395	18	94.50	168.2
352.8	0.07	0.83	296.8	3.33	632	29	93.81	166.3
357.8	0.11	0.83	296.5	3.32	982	45	93.11	164.3
362.8	0.10	0.50	296.6	1.99	1501	69	92.43	162.4
362.8	0.07	0.34	296.8	1.36	1506	69	92.43	162.4
362.8	0.04	0.22	296.9	0.89	1500	69	92.42	162.4

[a] Saturation temperature ($u(T)$ = 0.1 K).
[b] Mass of transferred sample condensed at 243 K.
[c] Volume of nitrogen ($u(V)$ = 0.005 dm^3) used to transfer m ($u(m)/m$ = 1.5%) of the sample.
[d] T_{amb} is the temperature of the soap film flowmeter used for measurement of the gas flow.
[e] Vapor pressure at temperature T, calculated from the m and the residual vapor pressure at the condensation temperature calculated by an iteration procedure; p^p = 1 Pa.
[f] Relative expanded uncertainty with confidence level 0.95 (k = 2) for p was calculated to be $U(p)/p$ = 4.58% (see Supporting Information). The uncertainties for T, V and m are standard uncertainties. Uncertainty of the enthalpy of vaporization is the expanded uncertainty with a confidence level of 0.95 (k = 2), calculated including uncertainties of vapor pressure, uncertainties from the fitting equation and the uncertainty of temperature adjustment to T = 298.15 K. Detailed information on the methods of calculations was published previously [18,19].

care. With respect to the preceding elucidations, in our work only *p-T* data above 347 K was used for the derivation of the vaporization enthalpy and vapor pressure at 298.15 K.

It should be mentioned that results, published in Stephenson et al. [22], are presented only by Antoine equations and lack information about the source of the primary data, purity information and experimental methods. For these reasons the values from the data provided were not included in the calculation of average values.

Multiple sources cite the work of Neale et al. [24] and corresponding value of enthalpy of vaporization (56.5 kJ mol^{-1}). However, the exact origin of the data used is not disclosed. For this reason, it is not included in average calculations. In Cox et al. [25] this value has an uncertainty of ±1.0 kJ mol^{-1}. However, in the work of Ovchinnikov et al. [26], which supposed to be citing book of Cox et al. [25], the uncertainty is claimed to be ±4.0 kJ mol^{-1}. Nevertheless, the value agrees with the result achieved in this work (56.8 ± 0.8 kJ mol^{-1}).

From the results, presented in the Table 4, an uncertainty-weighted average value for the enthalpy of vaporization was determined to be 56.9 ± 0.7 kJ mol^{-1} and an arithmetic average for vapor pressure at 298.15 K is 49.1 Pa.

3.1.2. Triethyl phosphate (TEP **2**)

The vaporization behavior of TEP **2** was measured in this work in the temperature range of 273.1–348.2 K. The absolute vapor pressures p_{sat} and thermodynamic properties of vaporization obtained by the transpiration method are compiled in Table 5. From these results, values of enthalpy of vaporization (63.9 ± 0.9 kJ mol^{-1}) and vapor pressure at 298.15 K (12.5 Pa) were derived. Results from this work are illustrated in Fig. 4 and compared to literature values in Table 6. Deviation of experimental literature values from *p-T*-equation derived from *p-T*-data obtained in this work (Table 5) is illustrated in Fig. S10.

There are several *p-T* datasets of TEP **2** available in the literature: Evans et al. [29] and Cavalier [28] measured boiling points, work of Brozena et al. [27] combines vapor pressures measured with 3 different methods: differential thermal analysis (DTA), Knudsen effusion and by transpiration. In the latter work, measurements were executed in different temperature ranges and compiled into one *p-T* equation. Few remarks have to be made about the results, achieved by different methods individually. Transpiration measurements were executed only at two temperatures and therefore do not allow proper assessment of linearity and estimation of error. In the case of the DTA measurements, values below p = 650 Pa were found to be erroneous, therefore, were excluded from the final equation. Moreover, the temperature errors at the low temperature range of DTA experiment are significant (errors up to 2.4 K). Consequently, these results should be used with caution.

From the boiling point measurements by Evans et al. [29], the extrapolated vapor pressure value at 298.15 K is 17.3 Pa. The study also cites the work of Cavalier [28] and claims that determined boiling points are too low (vapor pressure is too high). The extrapolated vapor pressure value at 298.15 K from the work of Cavalier [28] is 26.2 Pa.

In the work of Panneerselvam et al. [30], the correlation gas-chromatographic technique was used to determine the enthalpy of vaporization of TEP **2**. The value of 55.73 kJ mol^{-1} (at 298.15 K) was achieved. This result does not agree with the results, derived in this work (63.9 ± 0.9 kJ mol^{-1}).

From the *p-T* datasets mentioned above, average uncertainty-weighted value of enthalpy of vaporization (63.8 ± 0.8 kJ mol^{-1}) and arithmetic average vapor pressure at 298.15 K (17.7 Pa) are calculated and reported in Table 6.

3.1.3. Malathion **3**

The vaporization behavior of malathion **3** was measured in this work in the temperature range of 298.2–362.8 K. The absolute vapor pressures p_{sat} and thermodynamic properties of vaporization obtained by the transpiration method are compiled in Table 7.

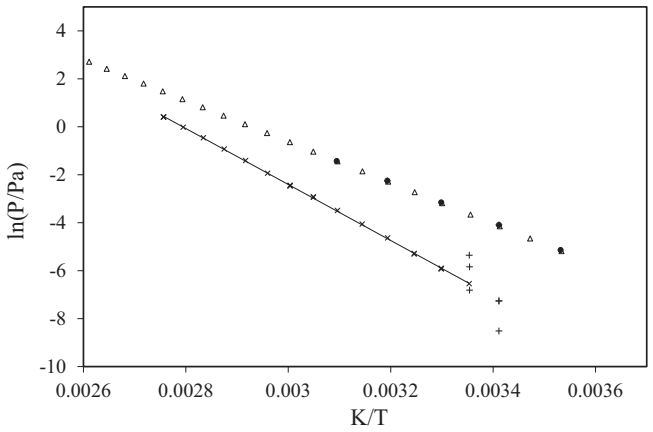

Fig. 5. Experimental vapor pressure values of malathion **3** in comparison with literature values. Here Δ – from Stephenson et al. [22], ● – from Schrader [31], + – from [32–37], × and solid line – from this work.

Table 8
Compilation of data on enthalpies of vaporization $\Delta_l^g H_m^o$ of malathion **3**.

Experiment[a]	Method[b]	*T*-Range K	T_{avg} K	$\Delta_l^g H_m^o(T_{avg})$ kJ mol^{-1}	$\Delta_l^g H_m^o$(298.15 K)[c] kJ mol^{-1}	p_{sat}[d] mPa
Hinckley et al. 1990 [32]	GCR	298.2	–	–	–	4.7
Stephenson et al. 1987 [22]	O	283.0–419.0	345.8	71.2	77.4	24.6
Kim et al. 1984 [34]	T	298.2	–	–	–	1.1
	GC	293.2	–	–	–	0.7
Woolford 1975 [32]	–	298.2	–	–	–	2.9
Gückel et al.1973 [35]	G	293.2	–	–	–	0.7
Perkow 1968 [36]	–	293.2	–	–	–	16.7
	–	313.2	–	–	–	105
Eichler 1965 [37]	–	293.2	–	–	–	0.2
Schrader 1963 [31]	–	283.2–323.2	302.5	70.6	71.1 ± 1.3	27.2
This Work 2019	T	298.2–362.8	328.7	97.0	101.4 ± 1.8	1.37

[a] First author and year of publication.
[b] Methods: GCR = gas-chromatography retention, GC = gas-chromatography, T = transpiration, G = gravimetric, E = ebulliometry, O = equation only.
[c] Enthalpies of vaporization were adjusted according to Chickos et al. [13] with values of $\Delta_l^g C_{p,m}^o$ and $C_{p,m}^o$(l), stated in Table 2. Uncertainty for enthalpy of vaporization is expressed as expanded uncertainty with confidence level of 0.95 (k = 2).
[d] Vapor pressure at 298.15 K.

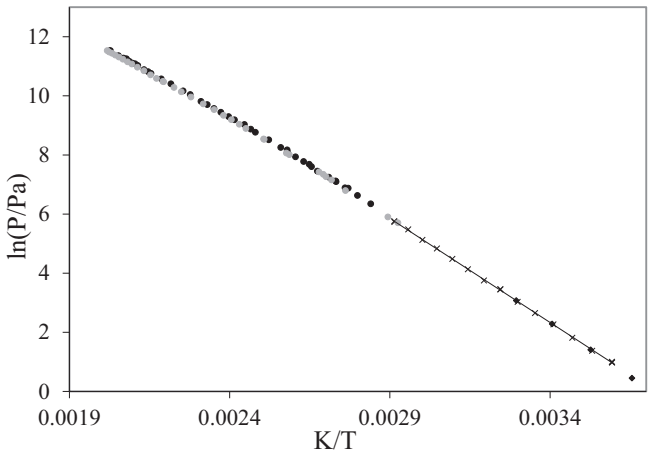

Fig. 6. Experimental vapor pressure values of MS **4** in comparison with literature values. Here ◆ – from Tevault et al. [40], ● – from Matthews et al. [41], ● – Ramsay et al. [42], × and solid line – from this work.

From these results, values of enthalpy of vaporization (101.4 ± 1.8 kJ mol^{-1}) and vapor pressure at 298.15 K (1.37 mPa) were derived. Literature values are compared to this work in Table 8 and illustrated in Fig. 5. Deviation of experimental literature values from *p-T*-equation derived from *p-T*-data obtained in this work (Table 7) is illustrated in Fig. S11.

Literature data on the vapor pressures of malathion **3** are scarce. One *p-T* dataset is in the book of Schrader [31]. However, no information on the details of the measurements are disclosed. As seen in Table 8 and illustrated by Fig. 5, both the enthalpy of vaporization and extrapolated vapor pressure at 298.15 K (71.1 ± 1.3 kJ mo l^{-1} and 27.2 mPa, respectively) differ significantly from the results derived in this work (101.4 ± 1.8 kJ mol^{-1} and 1.37 mPa, respectively).

Several single measurement points are available in the literature. The work of Hinckley et al. [32] provides a vapor pressure value at 298.15 K, experimentally determined by the gas-chromatographic retention method. The study describes the purity of multiple materials; however, malathion **3** is an exception and no absolute value is provided. The GC method in general has a relatively high standard deviation [38,39]. Therefore, this value should be used cautiously.

In the work of Hinckley et al. [32], along with experimental values of vapor pressure, a value at 298.15 K from a private letter of M. H. Woolford to W.F. Spencer (1975) is provided. The article does not give any information to allow a proper justification of this value as no details on the purity or method are provided.

In the work of Kim et al. [34], vapor pressure of malathion **3** was measured with gas-saturation and gas-chromatographic techniques and resulting values were disclosed at single temperatures (298.15 and 293.15 K, respectively). The authors assumed that the material, collected by the gas-saturation method was quantified with a deviation of around 10%, which is excessive. The authors also indicate that, according to their recovery and trapping experiments, malathion **3** had low total recovery and trapping efficiencies. For this reason the authors speculated, that the gas-saturation method could have a potential drawback when measuring vapor pressures at elevated temperatures.

Also, the study of Kim et al. [34] cites several single literature values, which include vapor pressure value of 0.2 mPa at 293.15 K from a handbook with undisclosed experimental details by Eichler et al. [37] and 0.7 mPa at 293.15 K from Gückel et al. [35]. In the work of Gückel et al. [35], the evaporation rate data were derived gravimetrically and vapor pressure value was derived from the resulting evaporation rate.

Table 9
Results of MS **4**: absolute vapor pressures p_{sat} and thermodynamic properties of vaporization obtained by the transpiration method in this work.

Methyl salicylate: $\Delta_l^g H_m^o$ (298.15 K) = 59.3 ± 0.8 kJ mol^{-1}
$\ln p_{sat}/p^0 = \frac{304.9}{R} - \frac{84257.8}{RT} - \frac{83.6}{R} ln \frac{T}{298.15K}$

T_{exp} [a] [K]	m [b] [mg]	V_{N2} [c] [dm^3]	T_{amb} [d] [K]	Gasflow [dm^3 h^{-1}]	p_{sat} [e] [Pa]	$U(p_{sat})$ [f] [Pa]	$\Delta_l^g H_m^o$ [kJ mol^{-1}]	$\Delta_l^g S_m^o$ [J mol^{-1} K^{-1}]
278.3	0.07	0.45	296.4	1.81	2.65	0.11	60.99	131.6
278.3	0.06	0.36	297.1	1.43	2.69	0.11	60.99	131.6
278.3	0.04	0.24	297.0	0.96	2.72	0.11	60.99	131.8
283.2	0.11	0.45	296.0	1.81	3.96	0.17	60.58	129.6
288.3	0.17	0.45	296.0	1.81	6.15	0.26	60.16	128.1
293.2	0.14	0.24	296.5	0.94	9.66	0.40	59.75	126.9
298.2	0.21	0.24	296.5	0.95	14.1	0.6	59.32	125.2
303.2	0.30	0.24	296.7	0.95	20.6	0.9	58.91	123.8
308.2	0.46	0.24	297.9	0.95	31.5	1.3	58.49	122.8
308.2	0.46	0.24	298.1	0.95	31.6	1.3	58.49	122.8
313.2	3.09	1.19	298.6	1.83	42.6	1.8	58.08	120.9
318.1	0.91	0.24	296.7	0.95	62.3	2.6	57.66	119.9
323.1	1.29	0.24	296.8	0.95	88.6	3.7	57.25	118.7
328.2	1.84	0.24	296.4	0.95	126	5	56.82	117.6
333.2	2.47	0.24	296.3	0.95	168	7	56.41	116.2
338.2	3.48	0.24	297.2	0.94	240	10	55.99	115.4
343.1	4.52	0.24	298.2	0.95	309	13	55.57	113.9
343.2	4.95	0.25	297.5	0.95	317	13	55.57	114.1

[a] Saturation temperature ($u(T)$ = 0.1 K).
[b] Mass of transferred sample condensed at 243 K.
[c] Volume of nitrogen ($u(V)$ = 0.005 dm^3) used to transfer m ($u(m)/m$ = 1.5%) of the sample.
[d] T_{amb} is the temperature of the soap film flowmeter used for measurement of the gas flow.
[e] Vapor pressure at temperature T, calculated from the m and the residual vapor pressure at the condensation temperature, calculated by an iteration procedure; p^o = 1 Pa.
[f] Relative expanded uncertainty with confidence level 0.95 (k = 2) for p was calculated to be U(p)/p = 4.18% (see Supporting Information). The uncertainties for T, V and m are standard uncertainties. Uncertainty of the enthalpy of vaporization is the expanded uncertainty with a confidence level of 0.95 (k = 2), calculated including uncertainties of vapor pressure, uncertainties from the fitting equation and the uncertainty of temperature adjustment to T = 298.15 K. Detailed information on the methods of calculations was published previously [18,19].

Table 10
Compilation of data on enthalpies of vaporization $\Delta_l^g H_m^o$ of MS **4**.

Experiment[a]	Method[b]	*T*-Range	T_{avg}	$\Delta_l^g H_m^o(T_{avg})$	$\Delta_l^g H_m^o$(298.15 K)[c]	p_{sat}[d]
		K	K	kJ mol^{-1}	kJ mol^{-1}	Pa
Tevault et al. 2014 [40]	T	273.5–303.5	288.1	60.4	59.6 ± 1.1	14.3
Stephenson et al. 1987 [22]	O	288.0–333.0	309.8	56.9	[57.8]	[17.0]
Matthews et al. 1950 [41]	E	352.1–493.6	419.2	52.4	62.5 ± 3.8	13.7
Ramsey et al. 1885 [42]	E	341.9–495.6	425.0	52.7	62.5 ± 4.0	12.9
This Work 2019	T	278.3–343.2	307.2	58.6	59.3 ± 0.8	14.5
					59.6 ± 0.6[e]	13.9[f]

Values in brackets were not used in further analysis.
[a] First author and year of publication.
[b] Methods: T = transpiration, E = ebulliometry, O = equation only.
[c] Enthalpies of vaporization were adjusted according to Chickos et al. [13] with values of $\Delta_l^g C_{p,m}^o$ and $C_{p,m}^o$(l), stated in Table 2. Uncertainty for enthalpy of vaporization is expressed as expanded uncertainty with confidence level of 0.95 (k = 2).
[d] Vapor pressure at 298.15 K.
[e] Weighted average value, calculated using uncertainty as the weighing factor.
[f] Average value.

Two *p*-*T* values published in Perkow et al. [36] have no experimental details disclosed, but almost identically match the results of the work of Schrader et al. [31]. Very similar results are provided in the book of Stephenson et al. [22], where vapor pressures are expressed with an Antoine equation over temperature range T = (283.0–419.0) K. As mentioned before, work of Stephenson et al. [22] lacks information about the source of the primary data, purity information and experimental methods.

Due to the questionable quality of available literature data, the results of this work are of high relevance and are recommended for future calculations.

*3.1.4. Methyl salicylate (MS **4**)*

The vaporization behavior of MS **4** was measured in this work in the temperature range of 278.3–343.2 K. The absolute vapor pressures p_{sat} and thermodynamic properties of vaporization obtained by the transpiration method are compiled in Table 9. From these results, values of enthalpy of vaporization (59.3 ± 0.8 kJ mol^{-1}) and vapor pressure at 298.15 K (14.5 Pa) were derived. These results are compared to literature values in Table 10 and illustrated in Fig. 6. Deviation of experimental literature values from *p*-*T*-equation derived from *p*-*T*-data obtained in this work (Table 9) is illustrated in Fig. S12.

In 1885 Ramsey and Young [42] measured MS **4** boiling point temperatures at different pressures using a self-made apparatus and used this data to calculate vapor pressures. An extrapolated vapor pressure value at 298.15 K is 12.9 Pa. Some 65 years later Matthews et al. [41] attempted to replicate Ramsey and Young [42] experiment and measured vapor pressures over a similar temperature range. Matthews et al. [41] managed to achieve a value of 13.7 Pa at 298.15 K. Vapor pressures, determined in these studies, cover the high temperature range of available literature data.

Tevault et al. [40] researched vapor pressures of CWAs and their simulants in 2014 using the transpiration method and focused on measuring vapor pressures around ambient temperatures. In contrast to this work, the experiment in the publication by Tevault et al. [40] was executed over a narrow temperature range (273.5–303.5 K) and the measurement was performed only at 5 different temperatures, one of which was below MS **4** melting temperature and was excluded from further calculations in this work. The value of vapor pressure at 298.15 K was determined to be 14.3 Pa. These results closely match to the results, achieved in this work (14.5 Pa at 298.15 K). Work of Stephenson et al. [22] suggests three Antoine equations for *p*-*T* data without stating the method of measurements, no sources of information or sample purity. For these reasons they are not included into further analysis. For comparison, the Table 10 includes the results of one of the given equations.

Average uncertainty-weighted value of enthalpy of vaporization (59.6 ± 0.6 kJ mol^{-1}) and arithmetic average of vapor pressure at 298.15 K (13.9 Pa) were calculated from the results, stated in the Table 10.

The absolute vapor pressures measured in this work compliment literature values and cover a range of temperatures from 278.3 to 343.2 K and complete the database of *p*-*T* values of compound MS **4** in a liquid phase.

4. Conclusions

In this work the vapor pressures of four CWA simulants were studied. The new results complement the currently available data and expands the *p*-*T* database to uninvestigated temperature ranges, mostly focusing on the ambient temperatures. The current study also analyses available literature data and provides a critical review. Whilst the *p*-*T* values, obtained in this work, are in agreement with most of literature values for TEP **1** and DEMP **2** and MS **4**, malathion **3** is in disagreement. The results obtained can be used for the determination of detection limits necessary for CWA detectors.

CRediT authorship contribution statement

Greta Bikelytė: Conceptualization, Methodology, Validation, Formal analysis, Investigation, Data curation, Writing - original draft, Writing - review & editing, Visualization. **Martin A.C. Härtel:** Conceptualization, Methodology, Validation, Writing - original draft, Writing - review & editing, Supervision. **Thomas M. Klapötke:** Conceptualization, Resources, Supervision, Writing - original draft, Project administration, Funding acquisition. **Burkhard Krumm:** Methodology, Writing - original draft. **Audrius Sadaunykas:** Investigation, Formal analysis, Writing - original draft.

Declaration of Competing Interest

The authors declare that they have no known competing financial interests or personal relationships that could have appeared to influence the work reported in this paper.

Acknowledgments

Financial support of this work by the Ludwig-Maximilian University of Munich (LMU), the Office of Naval Research (ONR)

[grant no. ONR.N00014-19-1-2078], the Strategic Environmental Research and Development Program (SERDP) [contract no. WP19-1287] and the DAAD (German Academic Exchange Service) [grant no. 57299294] is gratefully acknowledged. We express gratitude to Mr. Jörn Martens, M. Sc., for help with the preparation of malathion. Audrius Sadaunykas was provided an ERASMUS scholarship, funding his research stay in the laboratories of Prof. Klapötke. We would like to thank Prof. Dr. Sergey Verevkin (University of Rostock) for help with establishing the transpiration method at our laboratory.

Appendix A. Supplementary data

Supplementary data to this article can be found online at https://doi.org/10.1016/j.jct.2019.106043.

References

[1] Attacks on Ghouta. Analysis of alleged use of chemical weapons in Syria, 2015. Available from: https://www.hrw.org/sites/default/files/reports/syria_cw0913_web_1.pdf.
[2] Sergei Skripal: former Russian spy poisoned with nerve agent, say police, 2018. Available from: https://www.theguardian.com/uk-news/2018/mar/07/russian-spy-police-appeal-for-witnesses-as-cobra-meeting-takes-place.
[3] M.A. Althoff, A. Bertsch, M. Metzulat, T.M. Klapötke, K.L. Karaghiosoff, Talanta 174 (2017) 295–300.
[4] S.L. Bartelt-Hunt, D.R. Knappe, M.A. Barlaz, Crit. Rev. Environ. Sci. Tec. 38 (2008) 112–136.
[5] J. Leppert, Schnelle Detektion luftgetragener chemischer Kampfstoffe mittels TD-GC-MS, Dissertation, Rheinischen Friedrich-Wilhelms-Universität Bonn, 2015.
[6] V.R. Arava, V. Nadkarni, V. Jasti, Process for the preparation of malathion and its intermediate, Google Patents (2012).
[7] G. Bikelytė, M. Härtel, J. Stierstorfer, T.M. Klapötke, A.A. Pimerzin, S.P. Verevkin, J. Chem. Thermodyn. 111 (2017) 271–278.
[8] M.A. Härtel, T.M. Klapötke, B. Stiasny, J. Stierstorfer, Propellants, Explos. Pyrotech. 42 (2017) 623–634.
[9] M.A. Härtel, T.M. Klapötke, J. Stierstorfer, L. Zehetner, Propellants, Explos. Pyrotech. (2019).
[10] M.A.C. Härtel, T.M. Klapötke, V.N. Emel'yanenko, S.P. Verevkin, Thermochim. Acta 656 (2017) 151–160.
[11] M.A. Althoff, K. Grieger, M.A. Härtel, K.L. Karaghiosoff, T.M. Klapötke, M. Metzulat, J. Phys. Chem. A 121 (2017) 2603–2609.
[12] M. Härtel, Studies Towards the Gas-Phase Detection of Hazardous Materials by Vapor Pressure Measurements with the Transpiration Method in Combination with Vacuum Outlet GC/MS, Dissertation LMU München, 2017.
[13] W. Acree, J.S. Chickos, J. Phys. Chem. Ref. Data 39 (2010) 043101.
[14] W. Acree Jr, J.S. Chickos, J. Phys. Chem. Ref. Data 45 (2016) 033101.
[15] J.E. Hurst, B. Keith Harrison, Chem. Eng. Commun. 112 (1992) 21–30.
[16] N.d. Kolossowsky, W. Udowenko, C.R. Hebd, Seanes Acad. Sci. 197 (1933) 519–520.
[17] N.d. Kolossowsky, W. Udowenko, Zhur. Obshchei Khim. (1934) 1027–1033.
[18] V.N. Emel'yanenko, S.P. Verevkin, J. Chem. Thermodyn. 85 (2015) 111–119.
[19] S.P. Verevkin, A.Y. Sazonova, V.N. Emel'yanenko, D.H. Zaitsau, M.A. Varfolomeev, B.N. Solomonov, K.V. Zherikova, J. Chem. Eng. Data 60 (2014) 89–103.
[20] A.B. Butrow, J.H. Buchanan, D.E. Tevault, J. Chem. Eng. Data 54 (2009) 1876–1883.
[21] G. Kosolapoff, J. Chem. Soc. (1955) 2964–2965.
[22] R.M. Stephenson, S. Malanowski, D. Ambrose, Handbook of the Thermodynamics of Organic Compounds, Elsevier, 1987.
[23] A. Brozena, P.L. Abercrombie-Thomas, D. Tevault, Report: Vapor Pressure Data and Analysis for Selected Organophosphorus Compounds, CMMP, DPMP, DMEP, and DEEP: Extrapolation of High-Temperature Data, Edgewood Chemical Biological Center Aberdeen Proving Ground [US], 2018.
[24] E. Neale, L. Williams, V. Moores, J. Chem. Soc. (1956) 422–427.
[25] J.D. Cox, G. Pilcher, Thermochemistry of Organic and Organometallic Compounds, Academic Press, 1970.
[26] V. Ovchinnikov, V. Brus' ko, A. Sobanov, Thermochim. Acta 233 (1994) 153–166.
[27] A. Brozena, J.H. Buchanan, R.W. Miles Jr, B.R. Williams, M.S. Hulet, J. Chem. Eng. Data 59 (2014) 2649–2659.
[28] M.J. Cavalier, Ann. Chem. Phys. (1899) 449–576.
[29] D.P. Evans, W.C. Davies, W.J. Jones, J. Chem. Soc. (1930) 1310–1313.
[30] K. Panneerselvam, M. Antony, T. Srinivasan, P.V. Rao, Thermochim. Acta 466 (2007) 49–56.
[31] G. Schrader, Die Entwicklung neuer insektizider Phosphorsäure-Ester, Verlag Chemie, 1963.
[32] D.A. Hinckley, T.F. Bidleman, W.T. Foreman, J.R. Tuschall, J. Chem. Eng. Data 35 (1990) 232–237.
[33] A. Hildebrandt, S. Lacorte, D. Barceló, Anal. Bioanal. Chem. 387 (2007) 1459–1468.
[34] Y.-H. Kim, J.E. Woodrow, J.N. Seiber, J. Chromatogr. A 314 (1984) 37–53.
[35] W. Gückel, G. Synnatschke, R. Rittig, Pestic. Sci. 4 (1973) 137–147.
[36] W. Perkow, Die Insektizide, Hüthig, 1968.
[37] W. Eichler, Handbuch der Insektizidkunde VEB Verlag Volk und Gesundheit, Berlín, 1965.
[38] S.P. Verevkin, Phase Changes in Pure Component Systems: Liquids and Gases, 1st ed., Elsevier B.V, Amsterdam, Netherlands, 2005.
[39] A. Delle Site, J. Phys. Chem. Ref. Data 26 (1997) 157–193.
[40] D.E. Tevault, L.C. Buettner, K.L. Crouse, Report: Vapor Pressure of Methyl Salicylate and n-Hexadecane, Edgewood Chemical Biological Center Aberdeen Proving Ground [US], 2014.
[41] J. Matthews, J. Sumner, E. Moelwyn-Hughes, Trans. Faraday Soc. 46 (1950) 797–803.
[42] W. Ramsay, S. Young, J. Chem. Soc. Trans. 47 (1885) 640–657.

JCT 2019-321

Experimental Thermochemical Data of CWA Simulants: Triethyl Phosphate, Diethyl Methylphosphonate, Malathion and Methyl Salicylate

Greta Bikelytė, Martin A. C. Härtel, Thomas M. Klapötke, Burkhard Krumm, Audrius Sadaunykas

SUPPORTING INFORMATION

Table of Contents

S1. Purity assessment

1.1 ^{1}H – qNMR

Between 2 and 20 mg of analyte and around 10-25 mg of certified reference material (CRM), in this case – ethylene carbonate (*Sigma-Aldrich*, 01380, 99.90% mass fraction purity), were weighed with a *Mettler Toledo* XP26DR scale (0.002/0.01 mg) and dissolved in 1 mL of $CDCl_3$ (99.80 % deuterated, *Eurisotop*, D007HAG). The solution was left in an ultrasonic bath for 10 min until analyte and standard were completely dissolved. The sample was transferred into a 5 mm NMR-tube. The sample was measured with a *Bruker* AVANCE 400 MHz instrument with z-gradient using a 90° pulse with a pulse width of 11.85 µs. In total 65,536 data points were acquired. Samples were not spinned and acquisition time (AT) was set to 6.5012 s. Relaxation delay (D1) of 60 s was chosen to ensure that the relaxation duration would be exceeded 5-7 times. Each measurement contained 64 scans.

The processing was done with *MestReNova* v. 12.0.1-20560 software. Before Fourier transformation, linear group delay was applied and zero filling to 2048 K was executed once. After careful manual phase correction and baseline correction by "Bernstein Polynomial" of 5th order, integration was performed manually (integral calculation method - "Edited sum"). Integration was applied excluding the ^{13}C satellites. Two samples were produced for each analyte and their spectra were independently processed 5 times. The chemical purity was calculated manually according to the work of *Schönberger* [1].

Expanded relative uncertainty of achieved purity value contains several major contributors [1]. Uncertainty of the purity of the certified reference material (CRM) ($u(P_{CRM})$) is stated on the producer certificate. Uncertainty of molecular mass of the analyte ($u(M_{An})$), as well as the uncertainty of molar mass of CRM ($u(M_{CRM})$) were calculated combining atomic mass uncertainties of individual atoms [2]. Weighed values of analyte (w_{An}) and CRM (w_{CRM}) were buoyancy–corrected. Combined uncertainty of the true mass $u(m_{CRM})$ was calculated considering the specifications of the scale and environmental conditions of the weighing room [3]. Processing of the NMR spectra introduced the uncertainties of integration ($u(Int)$) and repetition ($u(Rep)$). Calculated combined relative uncertainty $u(P_{An})$ was included in the calculation of the overall vapor pressure measurement uncertainty. Combined relative uncertainty was also multiplied by confidence level factor k=2 to achieve a value with a confidence level of 0.95 [4]. Resulting expanded uncertainty $U(P_{An})$ is reported in the Table 1 of the manuscript.

1.2 Elemental analysis

Elemental analysis (CHNS) was performed with an *Elementar Vario Micro* instrument.

1.3 Purity assessment results

Results of the purity assessment are presented in the following. The signals used for purity calculation are underlined.

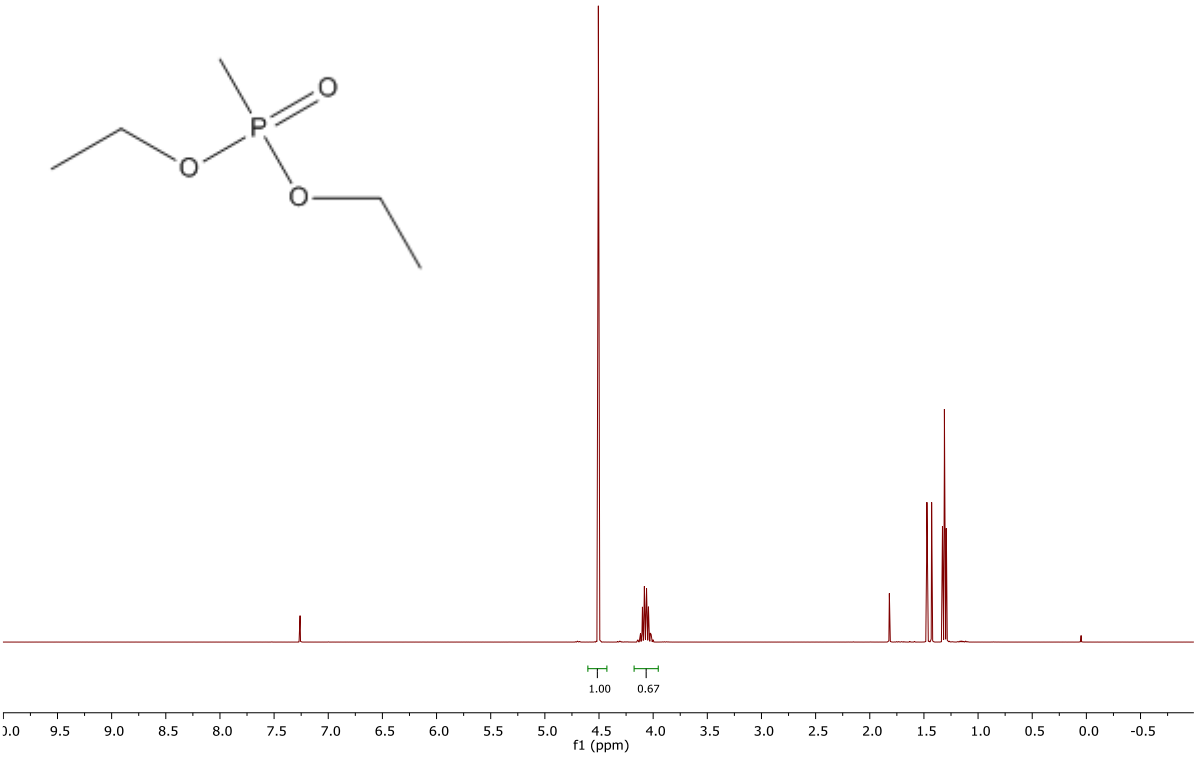

Fig. S1. ^{1}H-qNMR spectrum of DEMP **1**.

^{1}H – qNMR	DEMP **1**. ($CDCl_3$, 400.13 MHz): δ = 4.07 (m, 4H, C*H*$_2$), 1.45 (d, 3H, C*H*$_3$-P), 1.31 (t, 6H, C*H*$_3$), ppm. Ethylene carbonate as reference material. ($CDCl_3$, 400.13 MHz): δ = 4.51 (s, 4H, C*H*$_2$).
EA	Calc.: C 39.48, H 8.61 %; Found: C 39.15, H 8.29 %.

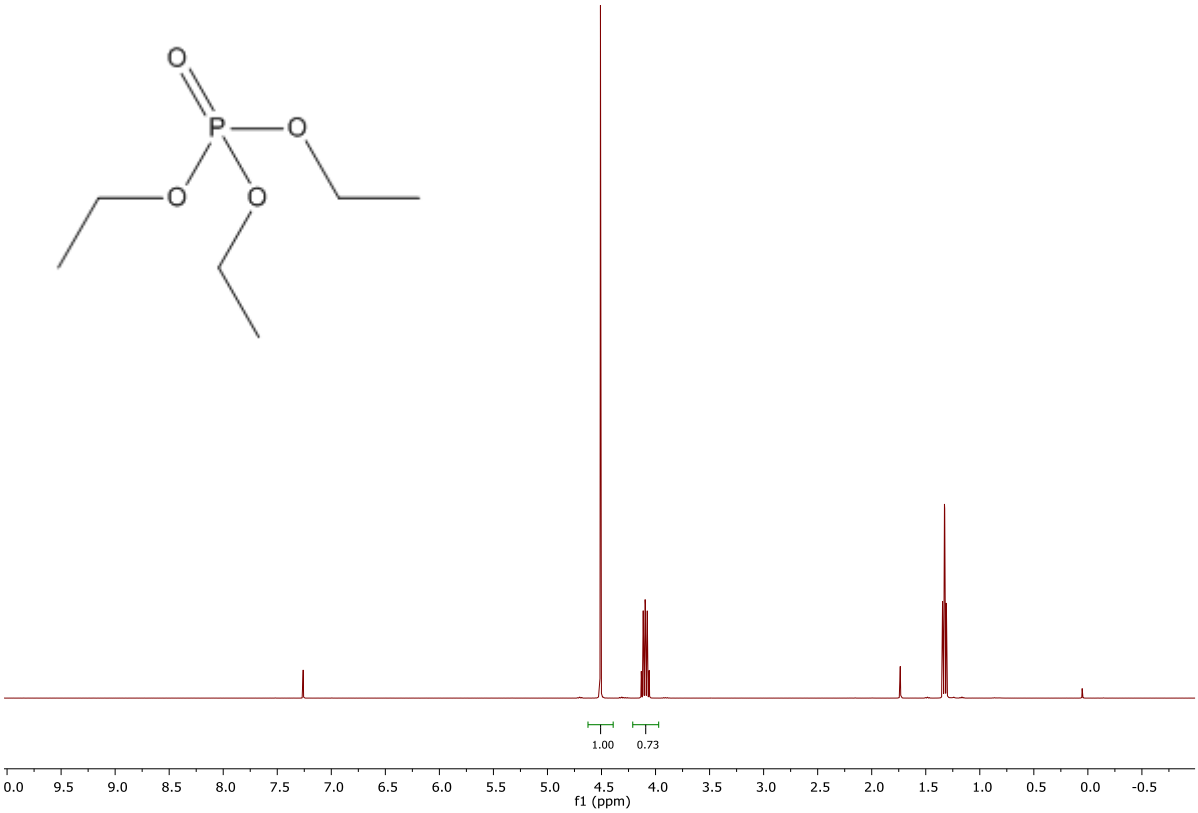

Fig. S2. ^{1}H-qNMR spectrum of TEP **2**.

^{1}H – qNMR	TEP **2**. ($CDCl_3$, 400.13 MHz): δ = 4.10 (m, 6H, C*H*$_2$), 1.33 (t, 9H, C*H*$_3$) ppm. Ethylene carbonate as reference material. ($CDCl_3$, 400.13 MHz): δ = 4.51 (s, 4H, C*H*$_2$).
EA	Calc.: C 39.56, H 8.30 %; Found: C 39.43, H 7.93 %.

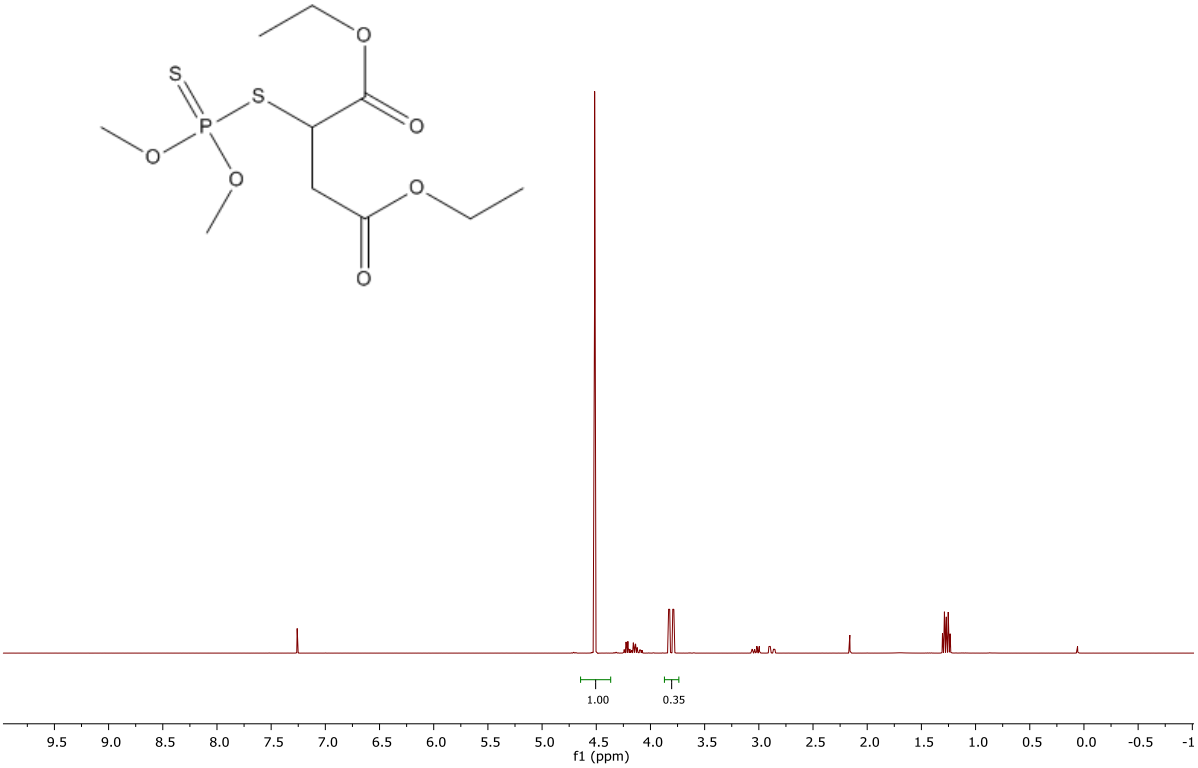

Fig. S3. ^{1}H-qNMR spectrum of malathion **3**.

^{1}H – qNMR Malathion **3**. ($CDCl_3$, 400.13 MHz): δ = 4.16 (m, 5H), 3.81 (d, 6H, C*H*$_3$), 2.97 (q, 2H, C*H*$_2$), 1.27 (p, 6H, C*H*$_3$) ppm.
Ethylene carbonate as reference material. ($CDCl_3$, 400.13 MHz): δ = 4.51 (s, 4H, C*H*$_2$).

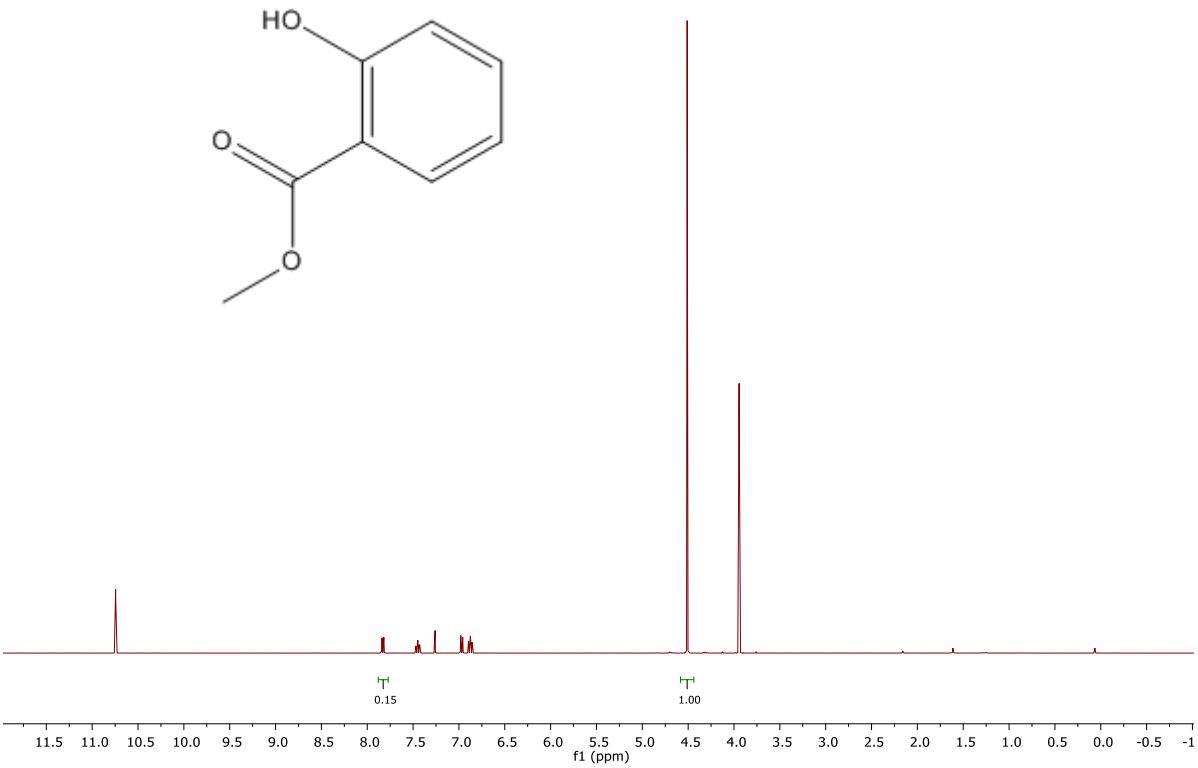

Fig. S4. ^{1}H-qNMR spectrum of MS **4**.

^{1}H – qNMR	MS **4**. ($CDCl_3$, 400.13 MHz): δ = 10.74 (s, 1H, O*H*), 7.83 (d, 1H, C*H*), 7.45 (t, 1H, C*H*), 6.97 (d, 1H, C*H*), 6.87 (t, 1H, C*H*), 3.94 (s, 3H, CH_3) ppm. Ethylene carbonate as reference material. ($CDCl_3$, 400.13 MHz): δ = 4.51 (s, 4H, CH_2).
EA	Calc.: C 63.15, H 5.30 %; Found: C 63.06, H 5.14 %.

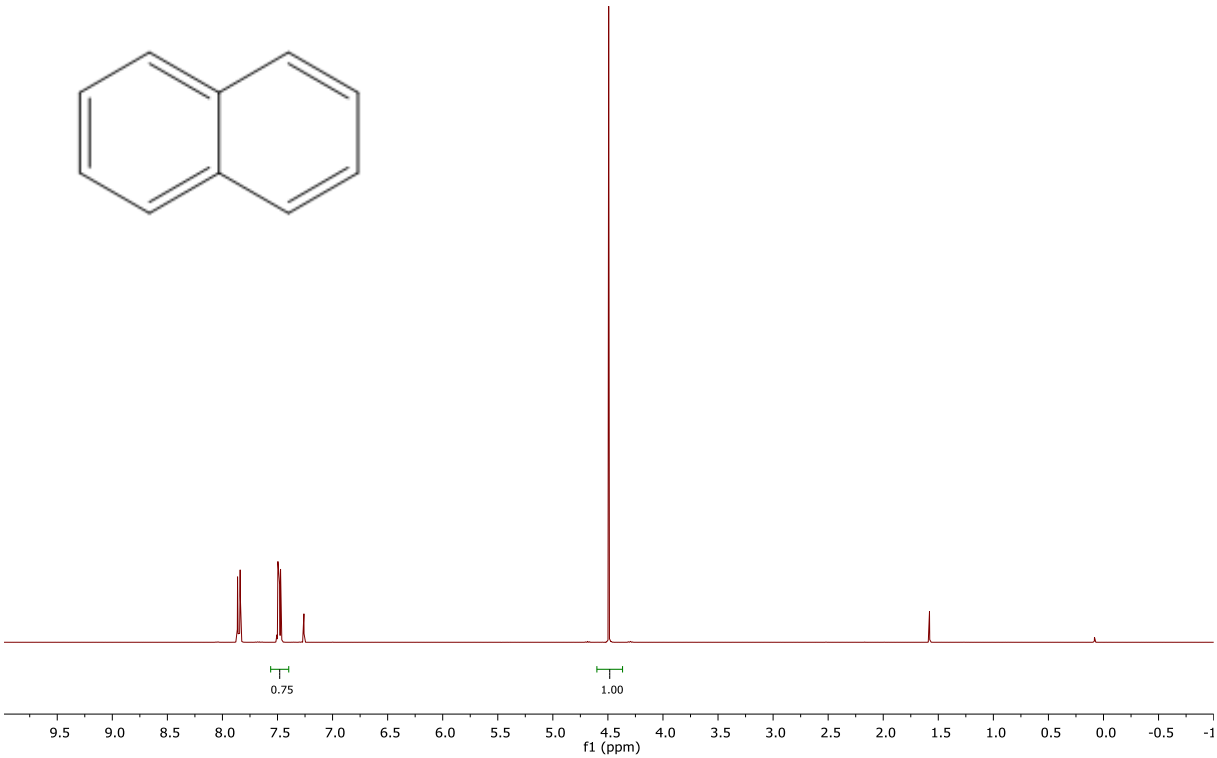

Fig. S5. ^{1}H-qNMR spectrum of naphthalene.

^{1}H – qNMR	Naphthalene. ($CDCl_3$, 400.13 MHz): δ = 7.85 (m, 4H, C*H*), 7.48 (m, 4H, C*H*) ppm. Ethylene carbonate as reference material. ($CDCl_3$, 400.13 MHz): δ = 4.51 (s, 4H, CH_2).
EA	Calc.: C 93.71, H 6.29 %; Found: C 93.60, H 6.16 %.

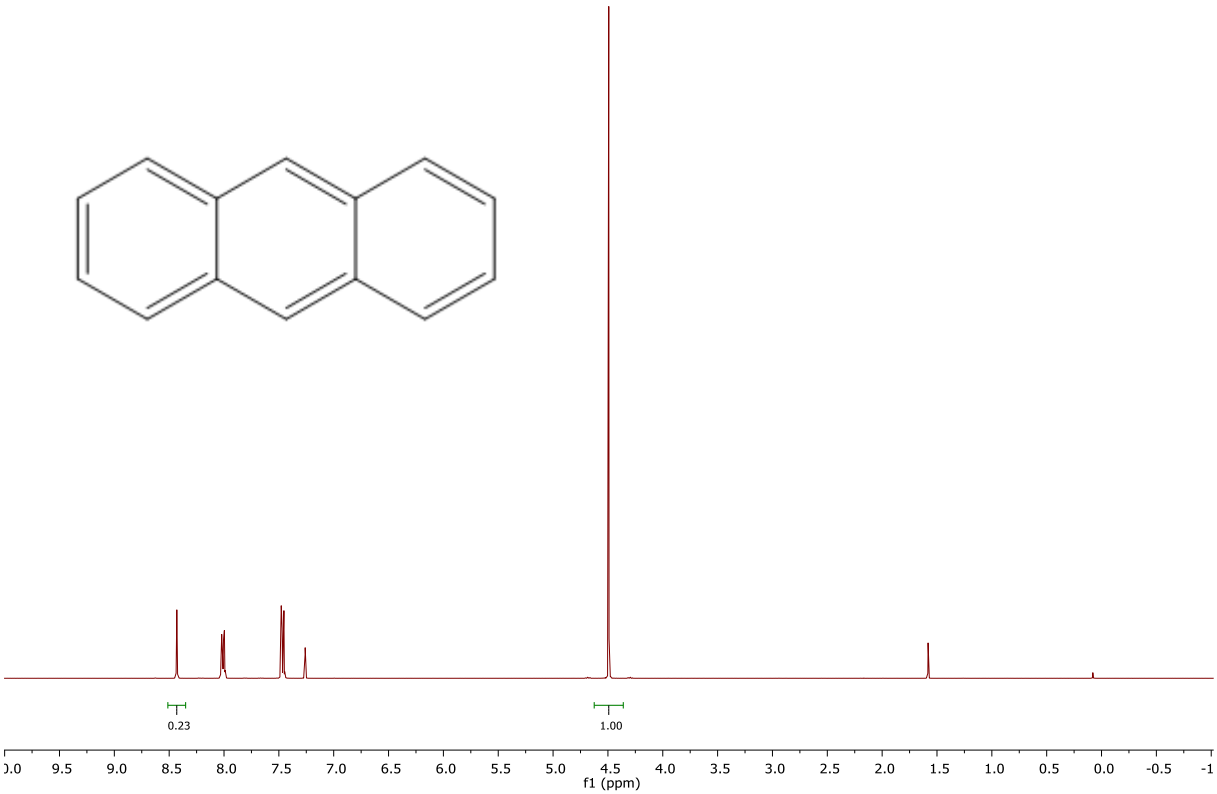

Fig. S6. ^{1}H-qNMR spectrum of anthracene.

^{1}H – qNMR	Anthracene. ($CDCl_3$, 400.13 MHz): δ = 8.43 (s, 2H, C*H*), 8.01 (m, 4H, C*H*), 7.46 (m, 4H, C*H*) ppm. Ethylene carbonate as reference material. ($CDCl_3$, 400.13 MHz): δ = 4.49 (s, 4H, CH_2).
EA	Calc.: C 94.43, H 5.66 %; Found: C 94.19, H 5.51 %.

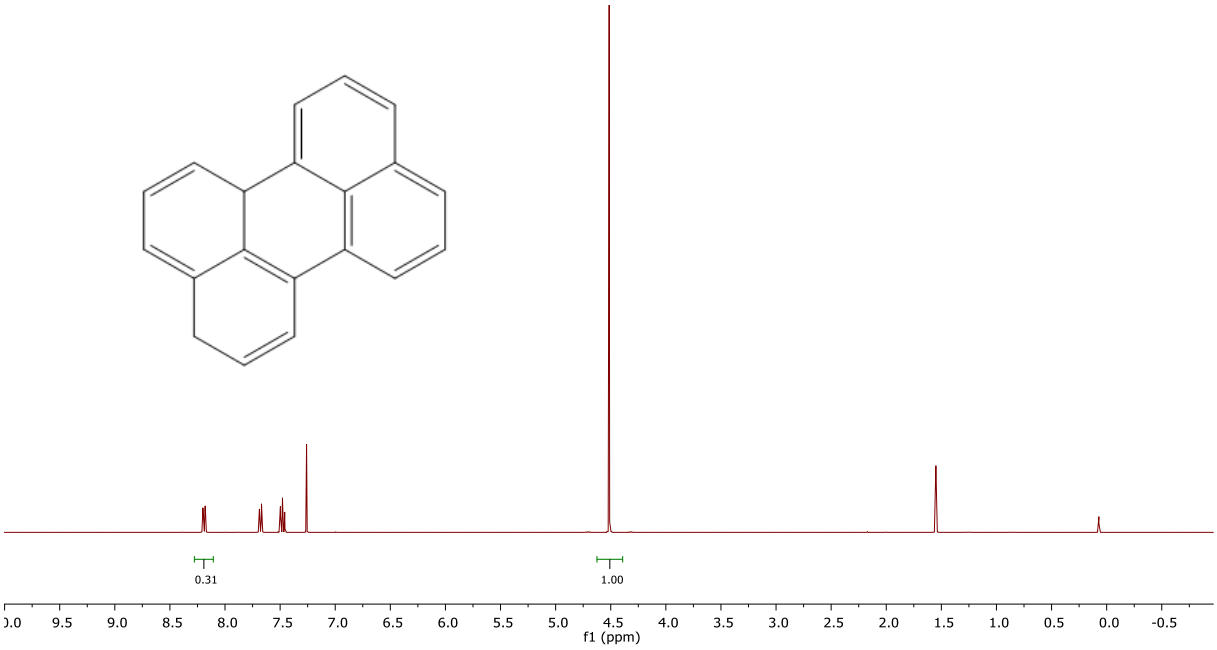

Fig. S7. ^{1}H-qNMR spectrum of perylene**.**

^{1}H – qNMR	Perylene. ($CDCl_3$, 400.13 MHz): δ = 8.19 (d, 4H, C*H*), 7.68 (d, 4H, C*H*), 7.48 (t, 4H, C*H*) ppm.
	Ethylene carbonate as reference material. ($CDCl_3$, 400.13 MHz): δ = 4.51 (s, 4H, CH_2).
EA	Calc.: C 95.21, H 4.79 %; Found: C 95.26, H 4.67 %.

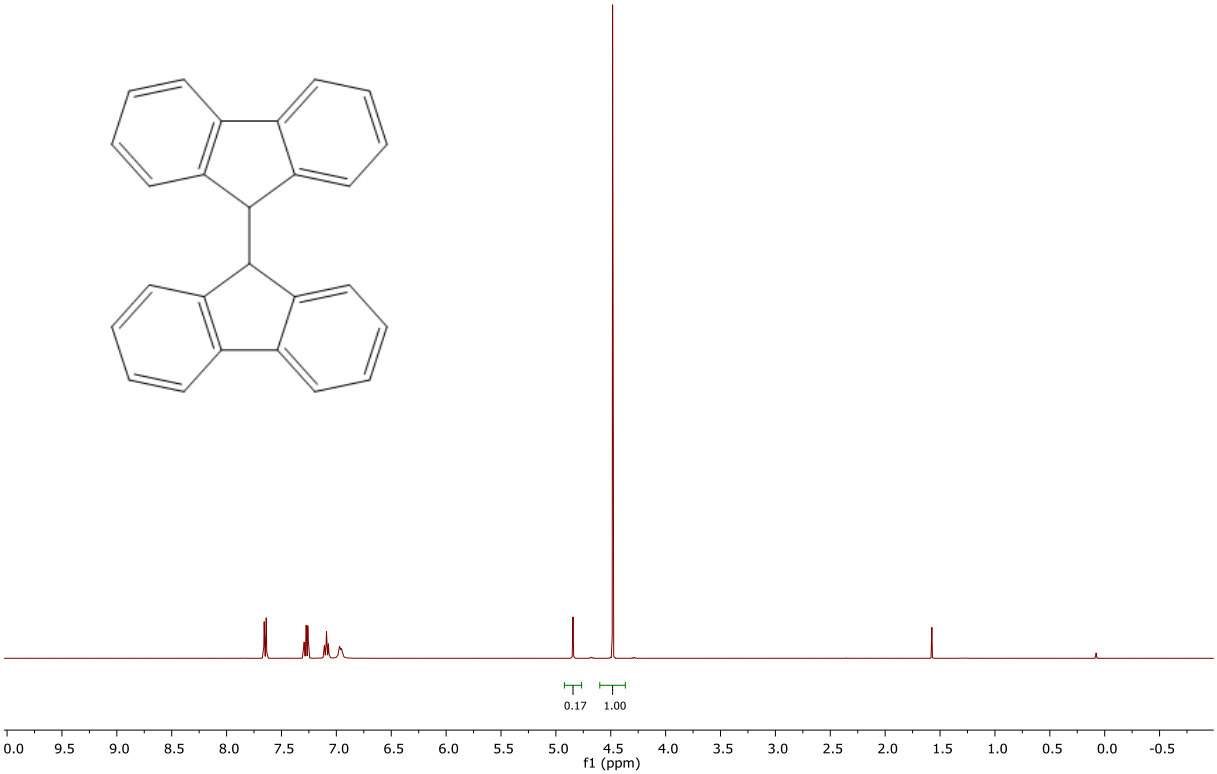

Fig. S8. ^{1}H-qNMR spectrum of 9,9'-bifluorenyl**.**

^{1}H – qNMR	9,9'-Bifluorenyl. ($CDCl_3$, 400.13 MHz): δ = 7.65 (d, 4H, C*H*), 7.27 (t, 4H, C*H*), 7.09 (t, 4H, C*H*), 6.96 (m, 4H, C*H*), 4.48 (s, 2H, C*H*) ppm. Ethylene carbonate as reference material. ($CDCl_3$, 400.13 MHz): δ = 4.48 (s, 4H, CH_2).
EA	Calc.: C 94.51, H 5.49 %; Found: C 94.51, H 5.11 %.

S2. Estimation of standard vapor pressure uncertainties

The calculation of standard uncertainties of vapor pressure measurements was partially based on the previously reported process by *Verevkin et al.* [5]. Calculation of combined standard uncertainty includes the uncertainty of mass of the analyte ($u(m_{An})$), mass of the reference material ($u(m_{Ref})$), volumes of the pycnometers ($u(V_{Pyc})$), volumes of the standard solutions ($u(V_{Std})$), uncertainties introduced by standard addition into the sample ($u(V_{Add})$), GC analysis (for calibration and determination) ($u(GC)$), transporting gas volume uncertainty ($u(V_{gas})$), saturator and ambient temperatures uncertainties ($u(T)$) and the uncertainty of purity of the materials ($u(P_{An})$), explained above. Experimental vapor pressures measured in this work are reported together with expanded uncertainties of confidence level 0.95 (k = 2).

S3. Estimation of uncertainties of molar enthalpies of phase transition at 298.15 K

The calculation of uncertainties of molar enthalpies of phase transition at 298.15 K is partly based on the previously published procedure by *Verevkin et al.* [6]. The uncertainty of temperature adjustment of enthalpy of phase transition to 298.15 K was modified in this work.

The temperature adjustment relies on the change of the molar heat capacity at constant pressure from liquid/crystalline to gaseous phase $\Delta_{l/cr}^{g}C_{p,m}^{o}$ and the length of the extrapolation path $\Delta T = T_{avg} - T_{ref}$ [7]. The absolute uncertainty of temperature adjustment $\Delta\left(\Delta_{l/cr}^{g}C_{p,m}^{o} \times \Delta T\right)$ is calculated according to an equation [7]:

$$\Delta\left(\Delta_{l/cr}^{g}C_{p,m}^{o} \times \Delta T\right) = u(C_{p,m}^{o}) \times \Delta_{l/cr}^{g}C_{p,m}^{o} \times \Delta T \quad \text{(S2)}$$

Here $u(C_{p,m}^{o})$ – combined relative uncertainty of molar heat capacity at constant pressures.

Ideally, the compounds under investigation would have experimental molar heat capacities at constant pressures and their uncertainties of condensed and gaseous phases available in the literature. In that case, the term $u(C_{p,m}^{o})$ is a combined relative uncertainty of relative uncertainty of molar heat capacity at constant pressure of liquid or solid $u(C_{p,m}^{o}\,(\mathrm{l/cr}))$ and relative uncertainty of molar heat capacity at constant pressure of gas $u(C_{p,m}^{o}\,(\mathrm{g}))$. In this work, this approach was applied for the cases of naphthalene, anthracene and perylene.

Here an example of application for anthracene is provided. For molar heat capacities and corresponding uncertainties refer to Table S2.

$$u\left(C_{p,m}^{o}\right) = \left\{\left[\frac{\Delta(C_{p,m}^{o}(cr))}{C_{p,m}^{o}(cr)}\right]^{2} + \left[\frac{\Delta(C_{p,m}^{o}(g))}{C_{p,m}^{o}(g)}\right]^{2}\right\}^{\frac{1}{2}} =$$

$$= \left\{\left[\frac{2.5\ J\ mol^{-1}K^{-1}}{211.7\ J\ mol^{-1}K^{-1}}\right]^{2} + \left[\frac{1\ J\ mol^{-1}K^{-1}}{184.7\ J\ mol^{-1}K^{-1}}\right]^{2}\right\}^{\frac{1}{2}} = 1.3\%$$

$$\Delta\left(\Delta_{cr}^{g}C_{p,m}^{o} \times \Delta T\right) = u\left(C_{p,m}^{o}\right) \times\ \Delta_{cr}^{g}C_{p,m}^{o} \times \Delta T = 0.013\ \times 0.027\ kJ\ mol^{-1}K^{-1} \times 47.5\ K$$
$$= 0.0167\ kJ\ mol^{-1}$$

If the uncertainties of experimental molar heat capacity values are not available, $u(C_{p,m}^{o})$ is assumed to be the uncertainty of the molar heat capacity at constant pressure as if it was determined by group contribution method, described in the work of *Chickos and Acree* [8]. The reasoning behind this is that the uncertainty of the estimated value of $C_{p,m}^{o}$, in most cases, is greater than any experimental uncertainty.

A different procedure must be applied for compounds that have only the molar heat capacity for condensed states available in the literature. In that case, $\Delta_{l/cr}^{g}C_{p,m}^{o}$ can be calculated from correlation equations, published in the work of *Chickos et al.* [7]:

$$-\Delta_{l}^{g}C_{p,m}^{\circ} = 10.58 + 0.26 \times C_{p,m}^{\circ}(l) \quad \text{(S3)}$$

$$-\Delta_{cr}^{g}C_{p,m}^{\circ} = 0.75 + 0.15 \times C_{p,m}^{\circ}(cr) \quad \text{(S4)}$$

As a result, the uncertainty of temperature adjustment is not only dependent on the $C_{p,m}^{o}$ values, but also on the uncertainty of the correlation equations S3 and S4:

$$\Delta\left(\Delta_{l/cr}^{g}C_{p,m}^{o} \times \Delta T\right) = u\left(\Delta_{l/cr}^{g}C_{p,m}^{o}\right) \times \Delta_{l/cr}^{g}C_{p,m\times}^{o}\Delta T \quad \text{(S5)}$$

Here $u\left(\Delta_{l/cr}^{g} C_{p,m}^{o}\right)$ is the combined relative uncertainty of change of molar heat capacity at constant pressures for sublimation or vaporization.

The absolute uncertainties for correlation equations S3 and S4 were reported to be equal to 15 J mol^{-1} K^{-1} for liquids and 25 J mol^{-1} K^{-1} for solids. The combination of the uncertainty of experimental molar heat capacity value $u\left(C_{p,m}^{o}\right)$ and the uncertainty of correlation equations $u(\Delta_{l/cr}^{g} C_{p,m}^{o}, Chickos\ correl.equation)$ result in equation S6.

$$u\left(\Delta_{l/cr}^{g} C_{p,m}^{o}\right) = u\left(C_{p,m}^{o}\right) + u(\Delta_{l/cr}^{g} C_{p,m}^{o}, Chickos\ correl.equation) \quad \text{(S6)}$$

This uncertainty calculation procedure can be used for both vaporization and sublimation case. However, in more recent work of *Chickos and Acree* [9] the uncertainty, associated with temperature adjustment of enthalpy of sublimation (when the equations S3 and S4 are in use) is reported to be 1/3 of total temperature adjustment. This results in greater uncertainty values than as if the uncertainties were calculated according the equations S2 and S6. For this reason, for sublimation the uncertainty of 1/3 of temperature adjustment should be used. In this work, this procedure was applied for the calculations of uncertainty for 9,9'-bifluorenyl.

Here an example of application for 9,9'-bifluorenyl is provided. For molar heat capacities and corresponding uncertainties refer to Table S2.

$$\Delta\left(\Delta_{cr}^{g} C_{p,m}^{o} \times \Delta T\right) = \frac{\{0.75 + 0.15 \times C_{p,m}^{\circ}(cr)\} \times \{T_{avg} - 298.15\}}{3 \times 1000}$$
$$= \frac{\{0.75 + 0.15 \times 425.8\ J\ mol^{-1}K^{-1}\} \times \{395.6\ K - 298.15\ K\}}{3 \times 1000}$$
$$= 2.10\ kJ\ mol^{-1}$$

When the condensed phase and ideal gas molar heat capacities are not available in the literature, the condensed phase molar heat capacities can be estimated by several methods. For many organic and organometallic compounds, group contribution method, described in the works of *Chickos and Acree* [8; 9], can be applied. Associated uncertainties for group contribution method $u\left(C_{p,m}^{o}(\mathrm{l/cr}), Chickos\ group\ contr.\right)$ were reported to be 14.4 J mol^{-1} K^{-1} and 17.0 J mol^{-1} K^{-1} for liquids and solids, respectively [8]. Accordingly, these uncertainties must be included in the calculations of uncertainties of temperature adjustment:

$$u\left(\Delta_{l/cr}^{g} C_{p,m}^{o}\right) = u\left(C_{p,m}^{o}(\mathrm{l/cr}), Chickos\ group\ contr.\right) + u(\Delta_{l/cr}^{g} C_{p,m}^{o}, Chickos\ correl.equation) \quad \text{(S7)}$$

In this work, this approach was applied for methyl salicylate (MS **4**). The calculation was done as follows (for molar heat capacities refer to Table 2):

$$u\left(\Delta_{l}^{g} C_{p,m}^{o}\right) = \left\{\left(\frac{14.4\ J\ mol^{-1}K^{-1}}{280.8\ J\ mol^{-1}K^{-1}}\right)^{2} + \left(\frac{15\ J\ mol^{-1}K^{-1}}{83.6\ J\ mol^{-1}K^{-1}}\right)^{2}\right\}^{\frac{1}{2}} = (0.003 + 0.032)^{\frac{1}{2}}$$
$$= 0.19 = 19\%$$

$$\Delta\left(\Delta_{l}^{g} C_{p,m}^{o} \times \Delta T\right) = 0.19 \times 83.6\ J\ mol^{-1}K^{-1} \times 9.03\ K = 0.143\ kJ\ mol^{-1}$$

Unfortunately, the group contribution method by *Chickos and Acree* [9] is not universal for all functional groups and other methods have to be applied. For phosphorus containing compounds molar heat capacities can be estimated by elemental contribution method, described in the work of *Hurst et al.* [10] (example of application is given in Chapter S4). Reported relative uncertainties for compounds containing miscellaneous (*Misc.*) elements $u\left(C_{p,m}^{o}(\mathrm{l/cr}), Hurst\ el.composition\right)$ for liquids and solids are, respectively, 15 and 12.7 percent.

The estimated molar heat capacity can be inserted in equations S3 and S4 and resulting uncertainty equation S7 must be updated to be:

$$u\left(\Delta_{l/cr}^{g} C_{p,m}^{o}\right) = u\left(C_{p,m}^{o}(\mathrm{l/cr}), Hurst\ el.composition\right) + u\left(\Delta_{l/cr}^{g} C_{p,m}^{o}, Chickos\ correl.equation\right) \quad \text{(S8)}$$

This approach was applied for estimation of molar heat capacities at constant pressure for DEMP **1**, TEP **2** and Malathion **3**. Here an example of application for DEMP **1** is provided. For molar heat capacities and corresponding uncertainties refer to Table S2.

$$u\left(\Delta_{l}^{g} C_{p,m}^{o} \times \Delta T\right) = \left\{(0.15)^2 + \left(\frac{15\ J\ mol^{-1}K^{-1}}{78\ J\ mol^{-1}K^{-1}}\right)^2\right\}^{\frac{1}{2}} = (0.023 + 0.037)^{\frac{1}{2}} = 0.244 = 24.4\%$$

$$\Delta\left(\Delta_{l}^{g} C_{p,m}^{o} \times \Delta T\right) = 0.244 \times 78\ J\ mol^{-1}K^{-1} \times 6.62\ K = 0.126\ kJ\ mol^{-1}$$

S4. Calculation of molar heat capacities for compounds containing phosphorus

Molar heat capacities for compounds DEMP **1**, TEP **2** and Malathion **3** were calculated according to the empirical increment approach by *Hurst et al.* [10], with respect to their phosphorus content. For liquid compounds, investigated in this work the molar heat capacity calculation relies on the correlation:

$$C_{p,m}^{\circ}(l) = \left(\sum_{i=1}^{n} C_i \times N_i\right) + 26.19 \times N_{Misc} \quad \text{(S1)}$$

Here $C_{p,m}^{\circ}(l)$: molar heat capacity for liquid [J mol^{-1} K^{-1}] at 298.15 K; C_i: constant associated with element *i*; N_i: number of elements *i*; N_{Misc}: number of elements, not associated with specific constant; *n*: number of elements in the compound, which have designated constants.

The chemical formula of compound DEMP **1** is $C_5H_{13}O_3P$. C_i constants for individual elements include $C_H = 9.20$ J mol^{-1} K^{-1}, $C_C = 13.08$ J mol^{-1} K^{-1}, $C_O = 16.00$ J mol^{-1} K^{-1}. Phosphorus does not have a specific constant and belongs to *Misc.* category.

Resulting molar heat capacity for DEMP **1** at 298.15 K:

$$C_{p,m}^{\circ}(l) = 9.20 \times 13 + 13.08 \times 5 + 16.00 \times 3 + 26.19 \times 1 = 259.19\ \text{J mol}^{-1}\ \text{K}^{-1}.$$

The standard deviation for molar heat capacities of organic liquids containing *Misc.* components reported to be 15 %. This uncertainty was included into calculation of uncertainty of enthalpies of phase transition for DEMP **1**, TEP **2** and malathion **3**.

S5. Vapor pressure deviation plots for compounds DEMP **1**, TEP **2**, malathion **3** and MS **4**

Experimental results obtained in this work and available literature vapor pressures for DEMP **1**, TEP **2**, malathion **3**, MS **4,** and their deviations from the fitting equations, derived in this work (Tables 3, 5, 7, 9) are plotted in Figures S9, S10, S11, S12.

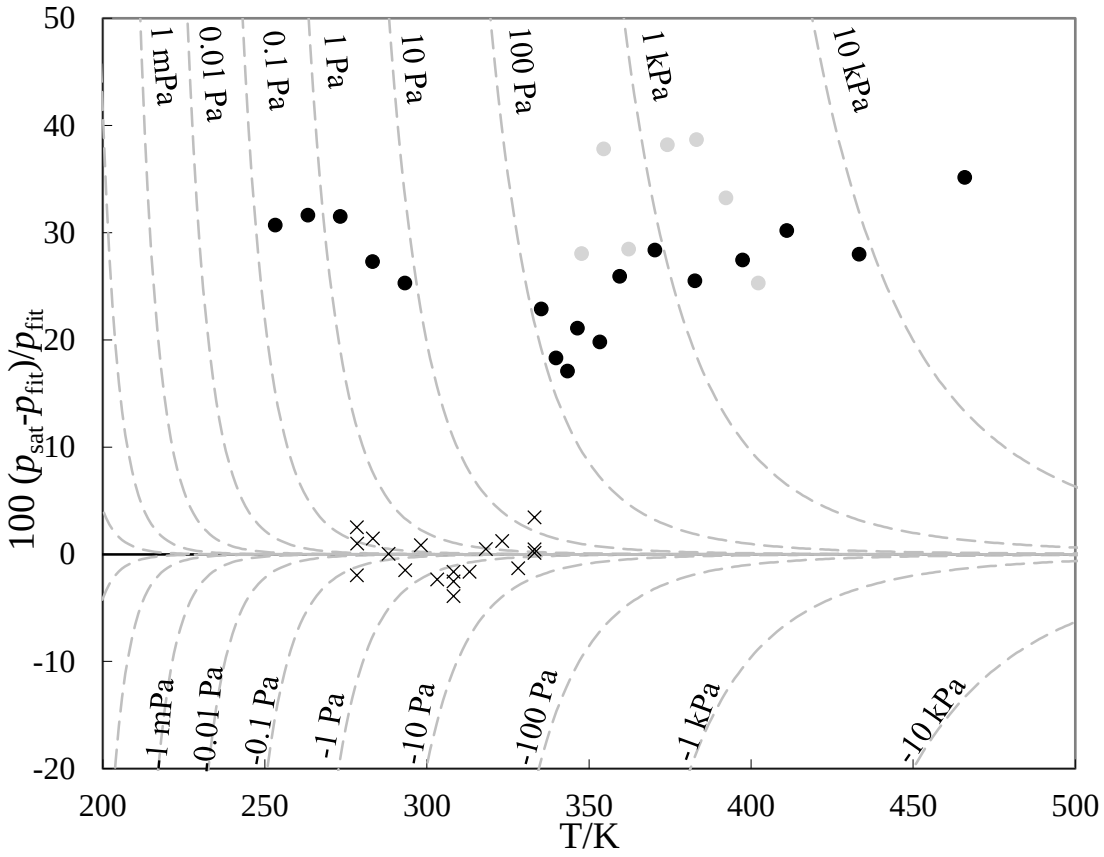

Fig. S9. Experimental vapor pressure deviations from the derived fitting equation for DEMP **1** in Table 3. Here ● – from *Butrow et al.* [11], ● – from *Kosolapoff* [12], × - this work.

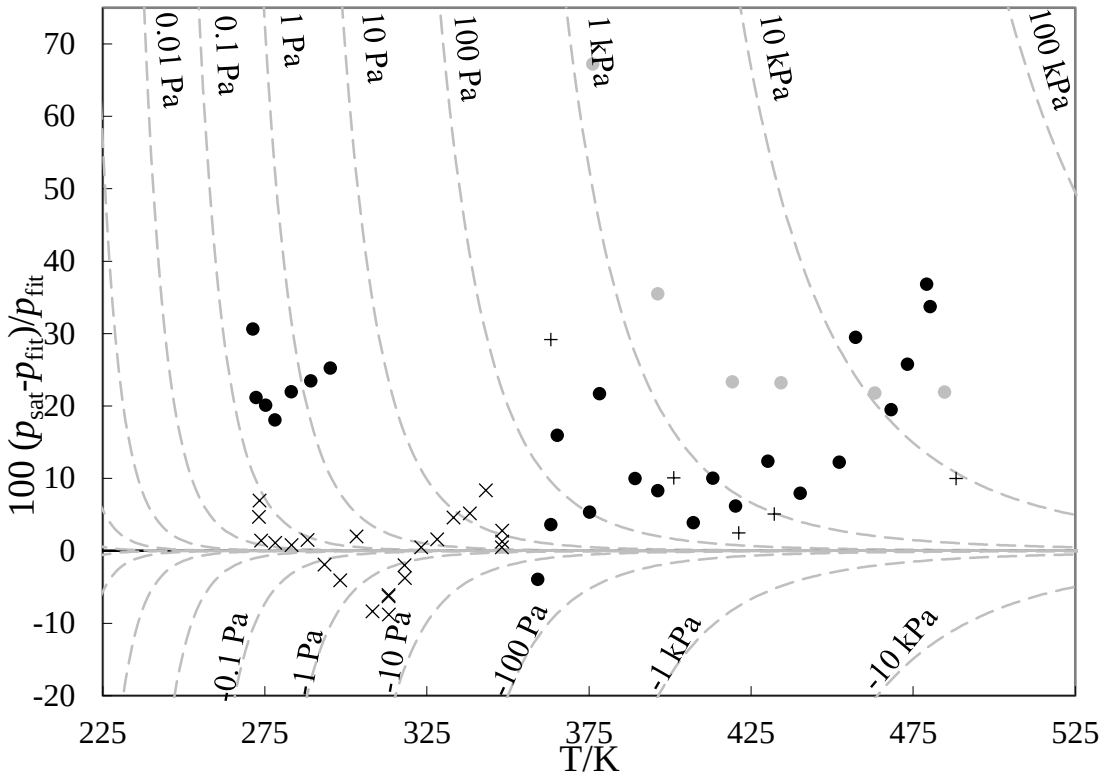

Fig. S10. Experimental vapor pressure deviations from the derived fitting equation for TEP **2** in Table 5. Here ● – from *Brozena et al.* [13], ● – from *Cavalier* [14], + – from *Evans et al.* [15], × - this work.

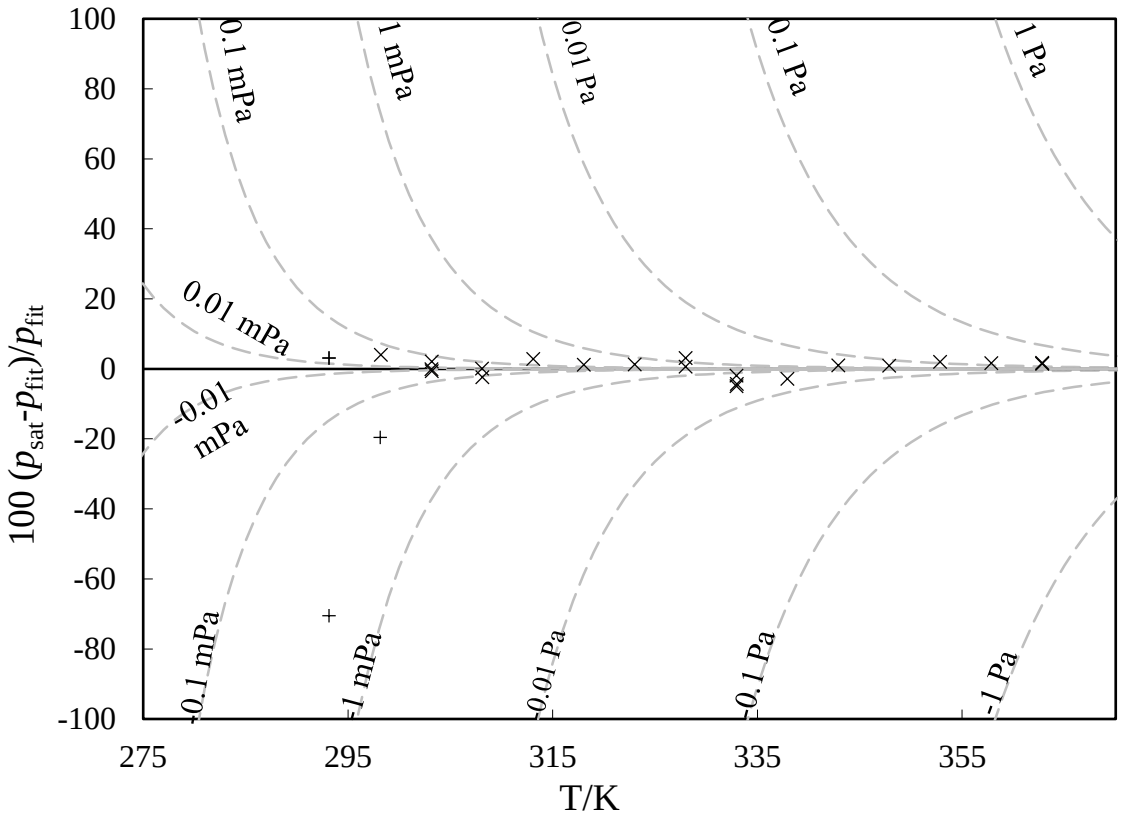

Fig. S11. Experimental vapor pressure deviations from the derived fitting equation for malathion **3** in Table 7. Here + – from single temperature results of [16; 17; 18], × - this work. The results from *Stephenson et al.* [19],

Schrader [20], *Hinckley et al.* [21], *Woolford* [21] and *Perkow* [22] are not depicted since the results differ significantly from our fitting equation.

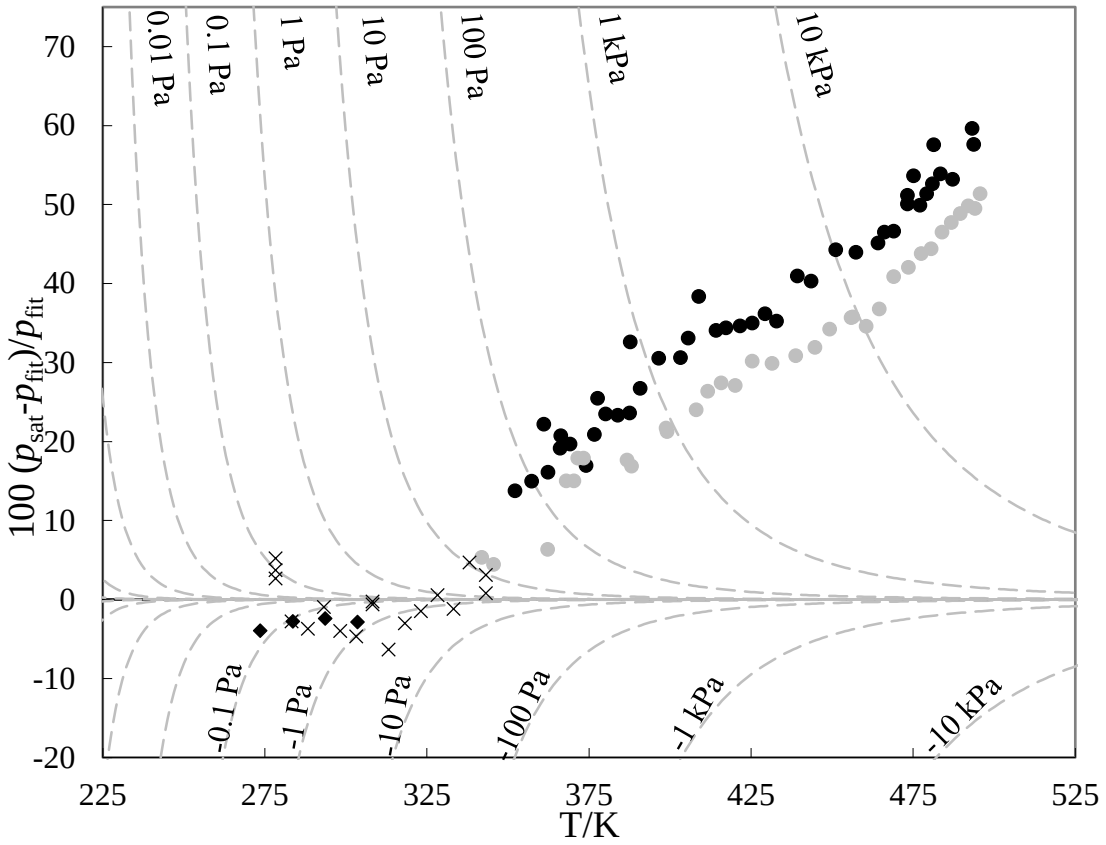

Fig. S12. Experimental vapor pressure deviations from the derived fitting equation for MS **4** in Table 9. Here ♦ – from *Tevault et al.* [23], ● – from *Matthews et al.* [24], ● – *Ramsay et al.* [25], × - this work.

S6. Reference materials

Transpiration experimental setup with VO-GC/MS was previously validated by vapor pressure measurements of reference materials in our work group [26]. In order to validate the experimental setup in connection with HPLC-DAD, measurements of several medium-volatility reference materials, including naphthalene and anthracene, were executed and compared with reliable results, available in the literature. Furthermore, two low-volatility compounds, perylene and 9,9'-bifluorenyl were investigated as well. Their results are presented in the following section.

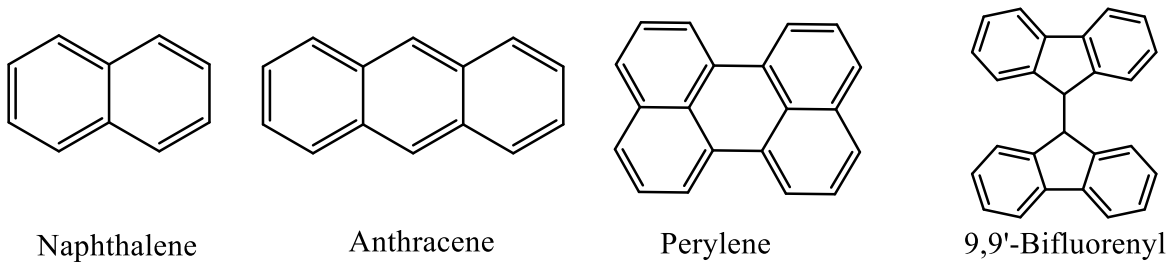

Fig. S13. Chemical structures of reference compounds under investigation.

Table S1. Origin and purity of the compounds investigated.

Substance	CAS#	Producer	Product-#	Purity	Final purity ($U(P_{An})$)[b]
Naphthalene	91-20-3	Bayer	LLB LEV-C709	„pure“	0.993 (±0.003)
Anthracene	120-12-7	Acros Organics	104861000	0.99[a]	0.992 (±0.005)
Perylene	198-55-0	Sigma-Aldrich	394475	≥0.995[a]	0.992 (±0.003)
9,9’-Bifluorenyl	1530-12-7	abcr GmbH	AB 331655	0.98[a]	0.997 (±0.002)

[a] Mass fraction purity as stated by manufacturer. [b] Mass fraction purity was determined by the ^{1}H-qNMR technique. Expanded uncertainties are reported with a confidence level of 0.95 (k = 2), further detailed in section S1.

6.1 Molar heat capacities

Molar heat capacities for reference compounds were obtained from the literature or derived by procedure described in works of *Chickos et al.* [8; 9] (Table S2). Values of molar heat capacities of condensed phase (at 298.15 K) for naphthalene and anthracene were provided in the studies by *McCullough et al.* [27] and *Radomska et al.* [28]. Remaining heat capacities for perylene and 9,9’-bifluorenyl were obtained from the works of *Wong et al.* [29] and *Rakus et al.* [30]. The ideal-gas heat capacity for naphthalene was obtained from *Thermodynamics Research Center* [31], values for anthracene and perylene were available from the work of *Dorofeeva et al.* [32]. No values for ideal-gas molar heat capacities of 9,9’- bifluorenyl were available at the time of publication.

Table S2. Molar heat capacities and their differences at 298.15 K.

Compound	$C^{\circ}_{p,m}(cr)$[a]	$C^{\circ}_{p,m}(cr)$	$C^{\circ}_{p,m}(g)$[b]	$-\Delta^{g}_{cr}C^{\circ}_{p,m}$[c]	$-\Delta^{g}_{cr}C^{\circ}_{p,m}$[d]
	Calc.	Exp.			
	J mol^{-1} K^{-1}	J mol^{-1} K^{-1}	J mol^{-1} K^{-1}	J mol^{-1} K^{-1}	J mol^{-1} K^{-1}
	1	2	3	4	5
Naphthalene	157.0			24.3	32.81[e,f]
		165.7±2.5 [27; 28]	133.0 [31]	25.6	32.7
Anthracene	209.0			32.1	
		211.7±2.5 [28]	184.7±1.0 [32]	32.5	27.0[e]
Perylene	277.4			42.4	
		274.9±0.3 [29]	255.4 ±2.5 [32]	42.0	19.5[e]
9,9'-Bifluorenyl	371.4		n.a.	56.5	n.a.
		425.8 [30]		64.6[e]	

[a] Derived from the molecular increments procedure described by *Chickos et al.* [8; 9] [b] Literature values on ideal-gas heat capacities. [c] Calculated by $-\Delta^{g}_{cr}C^{\circ}_{p,m} = 0.75 + C^{\circ}_{p,m}(cr) \times 0.15$. [9] [d] Differences of adiabatic heat capacity of condensed phase (Column 2) and reported ideal-gas heat capacity (Column 3). [e] Values were used for further processing. [f] Value obtained from the work of *Růžička et al.*[33]. n.a.: not available.

The value of $-\Delta^{g}_{cr}C^{\circ}_{p,m}$ for naphthalene was obtained from a set of recommended thermodynamical values, derived in study of *Růžička et al.* [33].

6.2 Naphthalene

Table S3. Naphthalene: absolute vapor pressures p_{sat} and thermodynamic properties of sublimation obtained by the transpiration method in this work.

Naphthalene: $\Delta^{g}_{cr}H^{\circ}_{m}$ (298.15 K) = 72.1 ± 0.9 kJ mol^{-1}

$$\ln p_{sat}/p^{0} = \frac{294.5}{R} - \frac{81916.0}{RT} - \frac{32.8}{R} ln \frac{T}{298.15\mathrm{K}}$$

T_{exp}[a]	m[b]	V_{N2}[c]	T_{amb}[d]	Gasflow	p_{sat}[e]	$U(p_{sat})$[f]	$\Delta^{g}_{cr}H^{\circ}_{m}$	$\Delta^{g}_{cr}S^{\circ}_{m}$
[K]	[mg]	[dm³]	[K]	[dm³ h^{-1}]	[Pa]	[Pa]	[kJ mol^{-1}]	[J mol^{-1} K^{-1}]
293.3	0.30	0.98	296.4	2.80	6.68	0.32	72.29	166.6
293.3	0.13	0.45	296.3	0.89	6.64	0.32	72.29	166.5
293.3	0.19	0.61	295.7	0.89	6.87	0.33	72.29	166.8
298.2	0.57	1.16	296.4	2.79	10.3	0.5	72.13	165.5
303.2	0.54	0.62	296.3	1.87	17.6	0.8	71.97	165.5
308.1	0.70	0.49	296.4	1.84	28.2	1.3	71.81	165.1
313.1	1.83	0.83	296.4	2.77	43.1	2.1	71.64	164.4
318.0	0.73	0.22	296.4	0.88	64.5	3.1	71.48	163.7
318.0	0.75	0.22	296.4	0.88	66.4	3.2	71.48	163.9

318.1	2.30	0.69	296.2	2.75	65.0	3.1	71.48	163.7
318.1	0.73	0.22	296.4	0.89	64.2	3.1	71.48	163.6
323.0	3.57	0.69	296.4	2.76	101	5	71.32	163.4
328.0	4.02	0.52	296.7	1.84	149	7	71.15	162.9
332.9	5.25	0.46	296.0	1.84	220	11	70.99	162.4
337.9	4.53	0.26	296.4	0.88	331	16	70.83	162.1
342.9	6.54	0.28	296.5	0.88	452	22	70.67	161.2
342.9	5.28	0.22	296.4	0.86	471	22	70.67	161.5
343.1	5.26	0.22	296.5	0.87	464	22	70.66	161.2
347.8	7.53	0.22	296.3	0.87	668	32	70.50	161.1

[a] Saturation temperature ($u(T)$ = 0.1 K). [b] Mass of transferred sample condensed at 243 K. [c] Volume of nitrogen ($u(V)$ = 0.005 dm^3) used to transfer m ($u(m)/m$ = 1.5 %) of the sample. [d] T_{amb} is the temperature of the soap film flowmeter used for measurement of the gas flow. [e] Vapor pressure at temperature T, calculated from the m and the residual vapor pressure at the condensation temperature calculated by an iteration procedure; $p°$ = 1 Pa. [f] Relative expanded uncertainty with confidence level 0.95 (k=2) for p was calculated to be $U(p)/p$ = 4.77%.

The uncertainties for T, V and m are standard uncertainties. Uncertainty of the enthalpy of sublimation is the expanded uncertainty with a confidence level of 0.95 (k =2), calculated including uncertainties of vapor pressure, uncertainties from the fitting equation and the uncertainty of temperature adjustment to T = 298.15 K. Detailed information on the methods of calculations was published previously [5; 34].

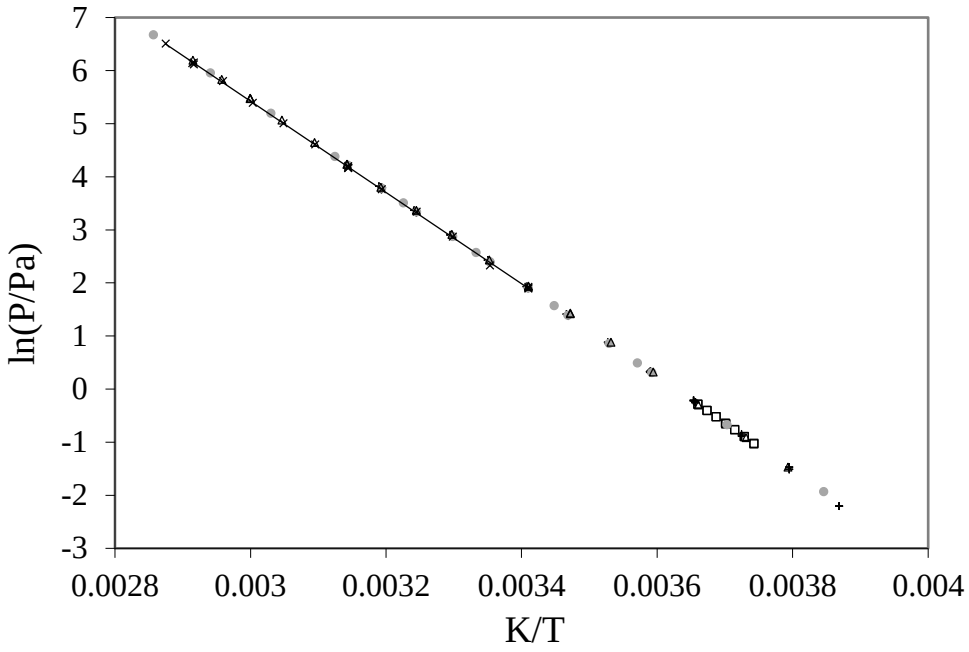

Fig. S14. Experimental vapor pressure of naphthalene in comparison with literature values. Here ◊ – from *Althoff et al.* [26], ● – from *Růžička et al*. [33] recommended values, + – from *Růžička et al.* [33] experimental values, Δ – from *Ambrose et al.* [35], □ – from *Monte et al.* [36], × and solid line – from this work.

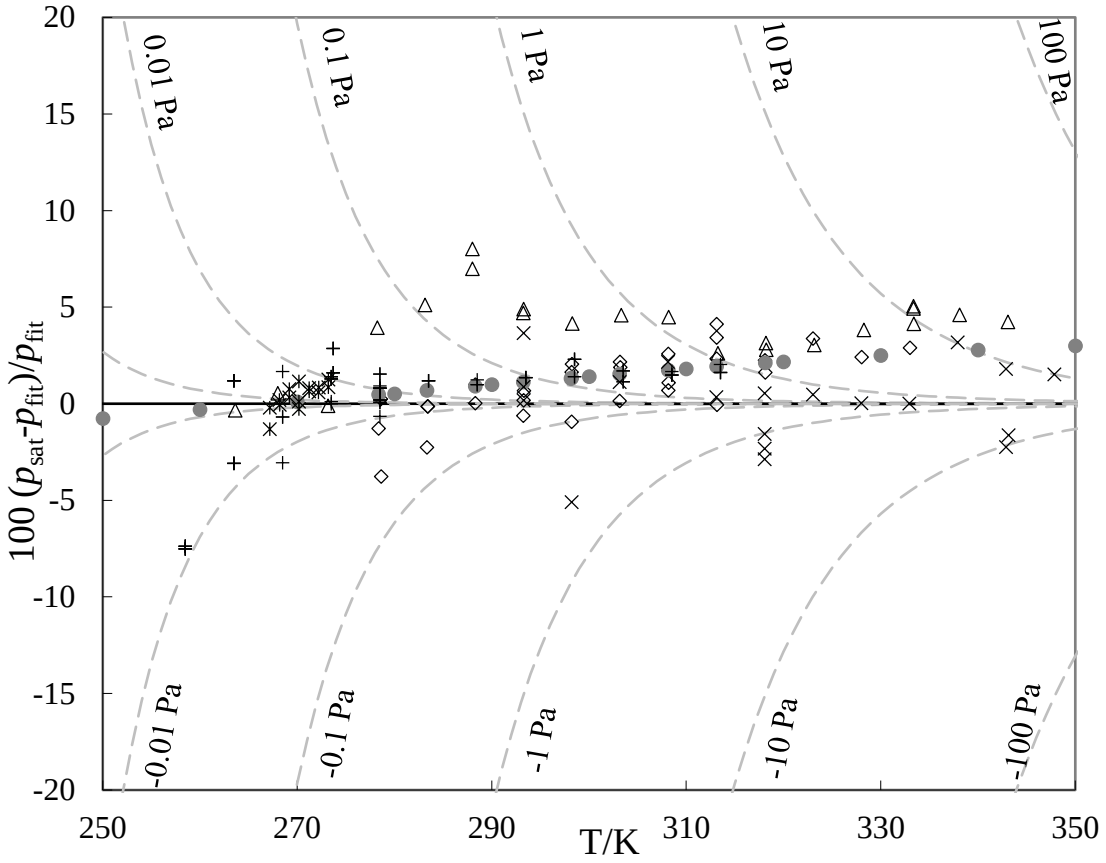

Fig. S15. Experimental vapor pressure deviations from the derived fitting equation for naphthalene in Table S3. Here ◊ – from *Althoff et al.* [26], ● – from *Růžička et al.* [33] recommended values, + – from *Růžička et al.* [33] experimental values, Δ – from *Ambrose et al.* [35],∗ – from *Monte et al.* [36], × - this work.

Table S4. Compilation of data on enthalpies of sublimation $\Delta_{cr}^{g}H_{m}^{\circ}$ of naphthalene.

Experiment[a]	Method[b]	T-Range	T_{avg}	$\Delta_{cr}^{g}H_{m}^{\circ}(T_{avg})$	$\Delta_{cr}^{g}H_{m}^{\circ}$(298.15K)[c]	p_{sat}[d]
		K	K	kJ mol^{-1}	kJ mol^{-1}	
Althoff *et al.* 2017 [26]	T	278.4 – 333.0	300.3	72.7	72.8±0.7	10.9
Monte *et al.* 2006 [36]	S	267.2 – 273.2	270.2	74.6	73.6±4.9	11.5
Růžička *et al.* 2005 a [33]	S	258.5 – 313.5	279.8	73.4	72.9±0.7	11.0
Růžička *et al.* 2005 b [33]	S	150.0 – 353.4	240.3	74.4	[72.1±0.6]	[10.9]
Ambrose *et al.* 1975 [35]	S	263.6 – 343.1	303.6	72.2	72.3±0.6	11.2
This Work 2019	T	293.3 – 347.8	318.6	71.5	72.1±0.9	10.8
					72.6±0.4[e]	11.1[f]

Values in brackets were not used in further analysis. [a] First author and year of publication. [b] Methods: T = transpiration, S = static method. [c] Enthalpies of sublimation were adjusted with value of $\Delta_{cr}^{g}C_{p.m}^{\circ}$, stated in Table S2. No uncertainty for $-\Delta_{cr}^{g}C_{p,m}^{\circ}$, reported in the work of *Růžička et al.* [33] was provided, therefore, it was not included into calculation of final uncertainty of enthalpy of sublimation. Uncertainty for enthalpy of sublimation is expressed as expanded uncertainty with confidence level of 0.95 (k = 2). [d] Vapor pressure at 298.15 K. [e] Weighted average value, calculated using uncertainty as the weighing factor. [f] Average value. a – experimental, b – recommended.

In this work, vapor pressures of naphthalene were measured with the transpiration method in the temperature range of 293.3 – 347.8 K. As well as in the work, performed previously in our group [26], results of this study are compared with three vapor pressure datasets, achieved with static method by *Monte et al.* [36], *Růžička et al.* [33] and *Ambrose et al.* [35]. *Růžička et al.*

[33] compiled a recommended *p-T*-dataset for naphthalene by correlating multiple literature data in accordance to their properties and related thermal data. All *p-T*-data under discussion is depicted in a *Clausius-Clapeyron* plot in Figure S14, which illustrates an excellent agreement of the results achieved in this work with other literature datasets. Deviation of experimental literature values from *p-T*-equation derived from *p-T*-data obtained in this work (Table S3) is illustrated in Figure S15.

Enthalpies of sublimation at 298.15 K of naphthalene derived from literature results and this work are compiled in Table S3. The value determined in this study (72.1 ± 0.9 kJ mol^{-1}) is in agreement with the measurements by *Monte et al.* [36], *Ambrose et al.* [35], *Althoff et al.* [26] and the recommended data by *Růžička et al.* [33]. In addition to the recommended *p-T*-data, *Ruzicka et al*. [33] provides own experimental data and extrapolates vapor pressure value at 298.15 K (11.0 Pa). This value match closely to the results of this work. Work of *Althoff et al.* [26] provides an uncertainty-weighted average value for enthalpy of sublimation at 298.15 K (72.8 ± 0.2 kJ mol^{-1}), calculated based on the literature data mentioned above and it agrees with the enthalpy of sublimation at 298.15 K, derived in this work (72.1 ± 0.9 kJ mol^{-1}). With the results of this study included, a new uncertainty-weighted value of enthalpy of sublimation at 298.15 K was calculated (72.6 ± 0.4 kJ mol^{-1}).

6.3 Anthracene

Table S5. Anthracene: absolute vapor pressures p_{sat} and thermodynamic properties of sublimation obtained by the transpiration method in this work.

Anthracene: $\Delta_{cr}^{g}H_m^{\circ}(298.15\ K) = 100.1 \pm 1.3$ kJ mol^{-1}

$$\ln p_{sat}/p^0 = \frac{304.9}{R} - \frac{108148.1}{RT} - \frac{27.0}{R} ln \frac{T}{298.15K}$$

T_{exp} [a] [K]	m [b] [mg]	V_{N2} [c] [dm³]	T_{amb} [d] [K]	Gasflow [dm³ h^{-1}]	p_{sat} [e] [Pa]	$U(p_{sat})$ [f] [mPa]	$\Delta_{cr}^{g}H_m^{\circ}$ [kJ mol^{-1}]	$\Delta_{cr}^{g}S_m^{\circ}$ [J mol^{-1} K^{-1}]
323.0	0.14	85.8	296.3	3.62	0.022	0.9	99.43	180.3
323.0	0.12	76.2	296.3	4.53	0.021	0.9	99.43	180.0
323.0	0.04	26.7	297.6	4.01	0.021	0.9	99.43	180.1
328.0	0.20	79.2	300.5	4.92	0.036	2	99.29	179.4
333.1	0.35	75.8	298.6	4.58	0.065	3	99.16	179.3
338.0	0.24	32.2	298.6	4.58	0.103	4	99.02	178.3
343.0	0.25	19.2	299.5	4.59	0.180	8	98.89	178.3
347.8	0.13	6.02	296.6	4.82	0.308	13	98.76	178.4
347.8	0.13	6.03	296.5	4.82	0.298	13	98.76	178.1
347.9	0.13	6.05	300.1	4.84	0.306	13	98.75	178.3
348.0	0.26	11.9	298.1	4.51	0.300	13	98.75	178.1
353.0	0.26	7.09	297.2	4.48	0.499	21	98.62	177.9
357.9	0.25	4.59	297.3	4.59	0.768	32	98.48	177.2

362.9	0.23	2.75	299.3	4.46	1.170	49	98.35	176.6
367.9	0.20	1.52	297.1	4.56	1.810	76	98.22	176.2
372.7	0.25	1.20	301.0	4.78	2.984	126	98.08	176.5
372.8	0.24	1.13	296.9	4.54	2.899	122	98.08	176.2

[a] Saturation temperature ($u(T)$ = 0.1 K). [b] Mass of transferred sample condensed at 243 K. [c] Volume of nitrogen ($u(V)$ = 0.005 dm^3) used to transfer m ($u(m)/m$ = 1.5 %) of the sample. [d] T_{amb} is the temperature of the soap film flowmeter used for measurement of the gas flow. [e] Vapor pressure at temperature T, calculated from the m and the residual vapor pressure at the condensation temperature calculated by an iteration procedure; $p°$ = 1 Pa. [f] Relative expanded uncertainty with confidence level 0.95 (k=2) for p was calculated to be $U(p)/p$ = 4.22%.
The uncertainties for T, V and m are standard uncertainties. Uncertainty of the enthalpy of sublimation is the expanded uncertainty with a confidence level of 0.95 (k = 2), calculated including uncertainties of vapor pressure, uncertainties from the fitting equation and the uncertainty of temperature adjustment to T = 298.15 K. Detailed information on the methods of calculations was published previously [5; 34].

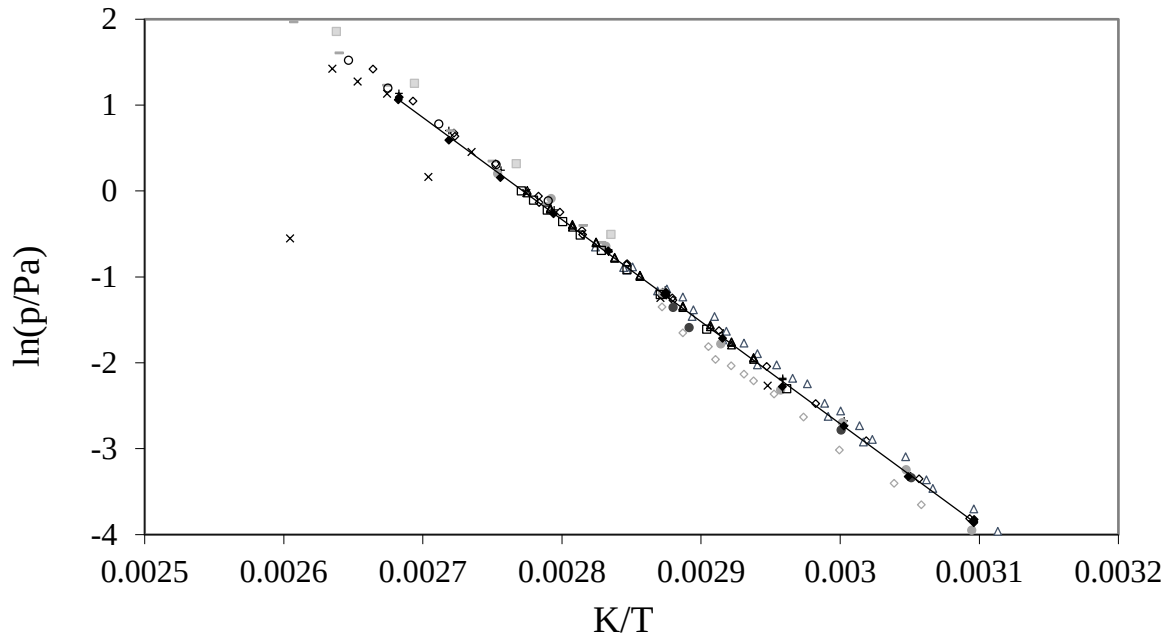

Fig. S16. Experimental vapor pressure of anthracene in comparison with literature values data: × – from *Siddiqi et al.* [37], ◊ – from *Santos et al.* [38],+ – from *Althoff et al.*[26], ◊ – from *Goldfarb et al.* [39], ▬ – from *Bender et al.* [40], △ – from *Chen et al.* [41], Δ – from *Ribeiro da Silva et al.* [42], ● – from *Oja et al.* [43], ● – from *Hansen et al.* [44], ○ – from *Macknick et al.* [45], □ – from *De Kruiff* [46], ■ – from *Malaspina et al.* [47] and ♦ and solid line – from this work.

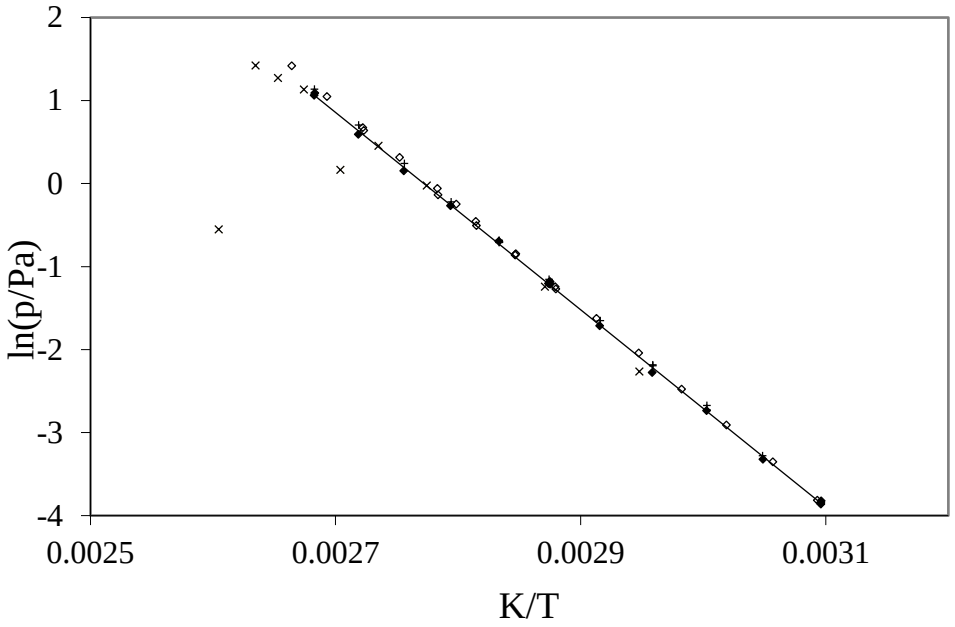

Fig. S17. Experimental vapor pressure of anthracene. Comparison of own experimental results with the literature data: × – from *Siddiqi et al.* [37], ◊ – from *Santos et al.* [38],+ – from *Althoff et al.*[26] and ♦ and solid line – from this work.

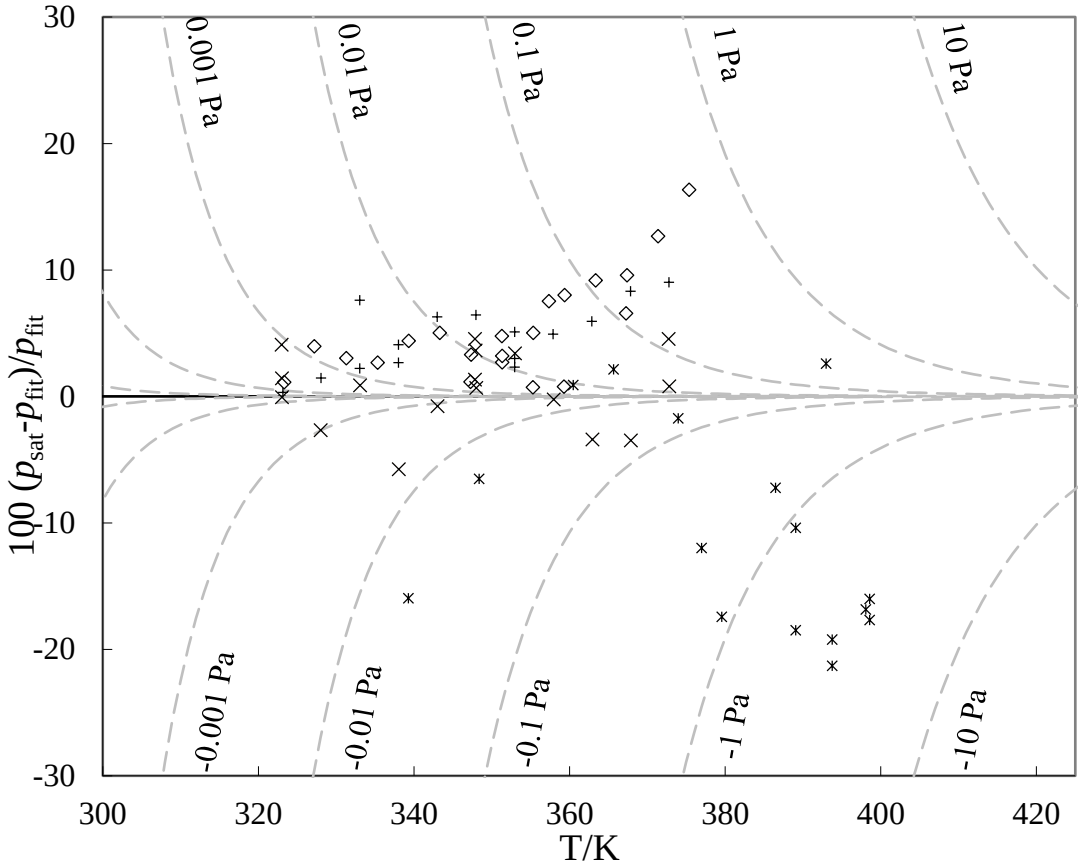

Fig. S18. Experimental vapor pressure deviations from the fitting equation for anthracene in Table S5. Here ∗ – from *Siddiqi et al.* [37], ◊ – from *Santos et al.* [38],+ – from *Althoff et al.*[26], × - this work.

Table S6. Compilation of data on enthalpies of sublimation $\Delta_{cr}^{g}H_{m}^{\circ}$ of anthracene.

Experiment[a]	Method[b]	T-Range	T_{avg}	$\Delta_{cr}^{g}H_m^{\circ}(T_{avg})$	$\Delta_{cr}^{g}H_m^{\circ}$(298.15K)[c]	p_{sat}[d]
		K	K	kJ mol^{-1}	kJ mol^{-1}	mPa
Althoff *et al*. 2017 [26]	T	323.2 – 372.8	346.4	99.9	101.2±1.1	0.94
Santos *et al.* 2011 [38]	K	323.3 – 375.4	350.8	100.5	101.9±1.2	0.90
Siddiqi *et al*. 2009 [37]	K	339.3 – 398.6	379.4	96.1	98.1±2.9[e]	1.01[e]
This Work 2019	T	323.0 – 372.8	345.7	98.8	100.1±1.3	0.96
					101.0±0.7[f]	0.95[g]

[a] Author and year of publication. [b] Methods: T = transpiration, K = Knudsen-effusion. [c] Enthalpies of sublimation were adjusted with value of $\Delta_{cr}^{g}C_{p.m}^{\circ}$, stated in Table S2. Uncertainties for enthalpies of sublimation are expressed as expanded uncertainty with confidence level of 0.95 (k = 2). [d] Vapor pressure at 298.15 K. [e] For data analysis the apparently erroneous data points (p_{sat}/T_{exp}): 1.18 Pa / 369.85 K and 0.577 Pa / 383.95 K were disregarded. [f] Weighted average value, calculated using uncertainty as the weighing factor. [g] Average value.

In this work, anthracene vapor pressures were measured with the transpiration method in the temperature range of 323.0 – 372.8 K. The complete experimental *p*-*T*-dataset is compiled in the Table S5. From these results a vapor pressure value at 298.15 K was extrapolated (0.96 mPa) and the enthalpy of sublimation at 298.15 K was calculated to be 100.1±1.3 kJ mol^{-1}.

In the literature, two recent reviews on the thermodynamical sublimation properties of anthracene exist. The work of *Roux et al.* [48] evaluates over 20 literature sources on enthalpies of sublimation of anthracene, available at the time. The study addresses the problem that most of literature sources have no sufficient information on the purity of the compound. Moreover, some of the datasets show excessive measurement errors. For these reasons, the results should be used with an utmost caution. From selected set of literature sources the author determined a recommended value of enthalpy of sublimation for anthracene (101.9±1.3 kJ mol^{-1}). This value agrees with the value, derived in this work (100.1±1.3 kJ mol^{-1}) within the range of uncertainties.

The work of *Althoff et al.* [26], which was previously performed in our group, presents new experimental values and a compilation of data from multiple literature sources [39; 40; 41; 42; 43; 44; 45; 46; 49], including the most recent ones (by *Santos et al.* [38] and *Siddiqi et al.* [37]). The study by *Althoff et al.* [26] compares own experimental results with literature values and concludes that recommended values of enthalpy of sublimation and vapor pressure (at 298.15 K) for anthracene should be respectively, 100.9±0.3 kJ mol^{-1} and 0.95 mPa. The value of enthalpy of sublimation determined in the study by *Althoff et al.* [26] (101.2±1.1 kJ mol^{-1}) agrees with the results, achieved in this work (100.1±1.3 kJ mol^{-1}).

After careful review of the literature sources, the studies of *Althoff et al.* [26] and *Roux et al.* [48], a set of literature data [37; 38; 39; 40; 41; 42; 43; 44; 45; 46; 47] were selected to be valuable sources of experimental vapor pressure data. Graphic representation of selected literature *p*-*T*-data together with own experimental values is shown in Figure S16. Figure S17 presents the results of selected recent literature datasets by *Althoff et al.* [26], *Sidiqqi et al.* [37], *Santos et al.* [38] and this work and illustrates a good agreement. Corresponding thermodynamic properties are compiled in Table S6. Deviation of experimental literature values from *p*-*T*-equation derived from *p*-*T*-data obtained in this work (Table S5) is illustrated in Figure S18.

6.4 Perylene

Table S7. Perylene: absolute vapor pressures p_{sat} and thermodynamic properties of sublimation obtained by the transpiration method in this work.

Perylene: $\Delta_{cr}^{g}H_m^{\circ}(298.15\ K) = 128.8 \pm 2.0\ kJ\ mol^{-1}$

$$\ln p_{sat}/p^0 = \frac{308.5}{R} - \frac{134654.1}{RT} - \frac{19.5}{R} ln \frac{T}{298.15K}$$

T_{exp}[a] [K]	m[b] [µg]	V_{N2}[c] [dm³]	T_{amb}[d] [K]	Gasflow [dm³ h^{-1}]	p_{sat}[e] [mPa]	$U(p_{sat})$[f] [mPa]	$\Delta_{cr}^{g}H_m^{\circ}$ [kJ mol^{-1}]	$\Delta_{cr}^{g}S_m^{\circ}$ [J mol^{-1} K^{-1}]
372.7	4.62	44.2	297.4	2.54	1.02	0.07	127.39	188.8
372.7	5.75	54.9	296.7	3.01	1.02	0.07	127.39	188.8
372.7	7.16	70.3	297.0	4.11	1.00	0.07	127.39	188.6
377.7	4.89	26.2	297.2	5.12	1.83	0.13	127.29	188.9
377.7	16.7	92.2	296.9	5.13	1.77	0.12	127.29	188.6
382.6	5.67	17.6	296.8	5.06	3.15	0.22	127.19	188.8
382.7	26.7	88.9	297.0	5.11	2.94	0.20	127.19	188.2
387.6	4.53	8.94	297.0	3.01	4.97	0.34	127.10	188.0
387.6	7.39	15.3	296.8	5.11	4.71	0.33	127.10	187.6
387.7	9.48	18.8	297.2	5.11	4.95	0.34	127.09	188.0
392.6	1.77	2.10	295.6	5.05	8.17	0.56	127.00	187.8
392.6	1.10	1.26	295.7	5.05	8.46	0.58	127.00	188.1
392.6	0.88	1.02	296.6	4.08	8.43	0.58	127.00	188.1
392.6	16.2	19.5	296.9	5.13	8.12	0.56	127.00	187.7
392.6	12.8	15.0	297.3	5.07	8.34	0.58	127.00	187.9
397.6	8.34	6.15	297.3	4.10	13.3	0.9	126.90	187.5
397.6	6.54	4.66	296.6	2.02	13.7	0.9	126.90	187.8
397.6	9.11	6.84	296.8	5.07	13.0	0.9	126.90	187.4
402.5	8.68	3.85	296.7	4.82	22.0	1.5	126.80	187.6
402.6	3.98	1.76	297.0	3.01	22.2	1.5	126.80	187.6
402.6	8.33	3.72	297.4	4.96	22.0	1.5	126.80	187.5
402.6	15.7	7.00	297.1	4.94	22.0	1.5	126.80	187.5
407.6	4.16	1.15	297.2	3.01	35.3	2.4	126.71	187.4
407.6	15.6	4.54	297.2	4.96	33.6	2.3	126.71	187.0
412.5	15.7	2.88	297.1	4.94	53.2	3.7	126.61	186.8
417.5	6.50	0.75	297.0	3.02	84.3	5.8	126.51	186.7

417.5	15.7	1.81	296.9	4.94	84.8	5.9	126.51	186.8
422.5	21.8	1.72	297.4	5.13	124	9	126.42	186.2
422.5	17.9	1.35	297.4	4.04	130	9	126.42	186.5
422.6	16.0	1.25	297.5	3.01	125	9	126.41	186.1

[a] Saturation temperature ($u(T) = 0.1$ K). [b] Mass of transferred sample condensed at $T = 243$ K. [c] Volume of nitrogen ($u(V) = 0.005$ dm^3) used to transfer m ($u(m)/m = 1.5$ %) of the sample. [d] T_{amb} is the temperature of the soap film flowmeter used for measurement of the gas flow. [e] Vapor pressure at temperature T, calculated from the m and the residual vapor pressure at the condensation temperature calculated by an iteration procedure; $p° = 1$ Pa. [f] Relative expanded uncertainty with confidence level 0.95 (k=2) for p was calculated to be $U(p)/p = 6.89$ %.

The uncertainties for T, V and m are standard uncertainties. Uncertainty of the enthalpy of sublimation is the expanded uncertainty with a confidence level of 0.95 ($k = 2$), calculated including uncertainties of vapor pressure, uncertainties from the fitting equation and the uncertainty of temperature adjustment to $T = 298.15$ K. Detailed information on the methods of calculations was published previously [5; 34].

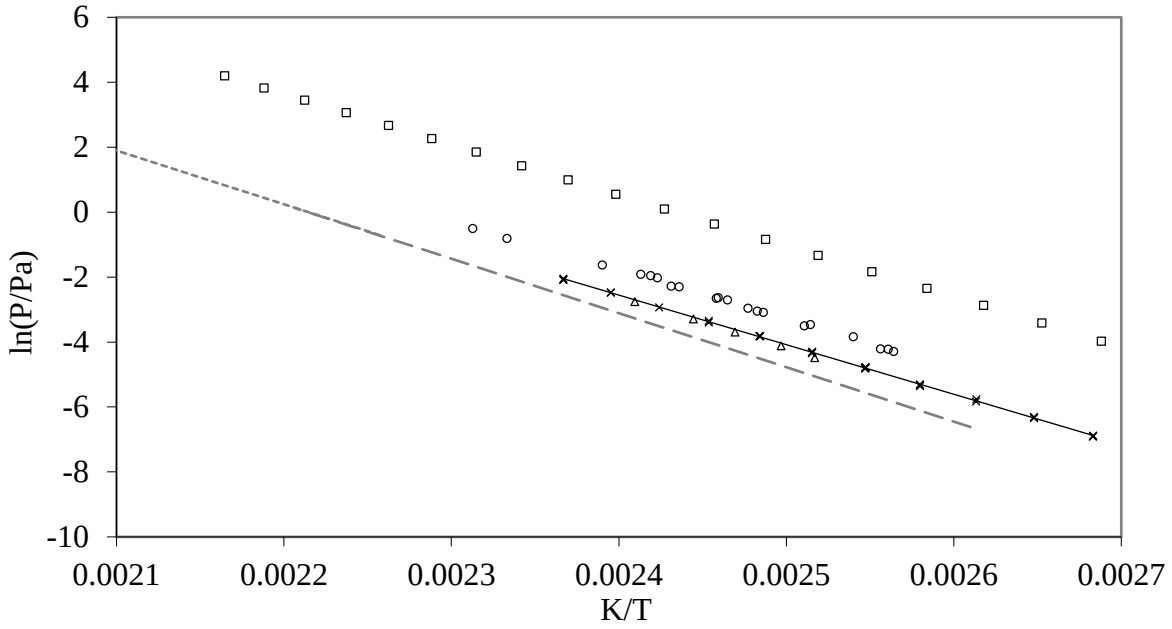

Fig. S19. Experimental vapor pressure of perylene in comparison with literature values. Here ○ – from *Goldfarb et al.* [39], Δ – from *Oja et al*. [43], dotted line – from *Gigli et al.* [50], dashed line – from *Hoyer et al.* [51], □ – from *Inokuchi et al*. [52] and × and solid line – from this work.

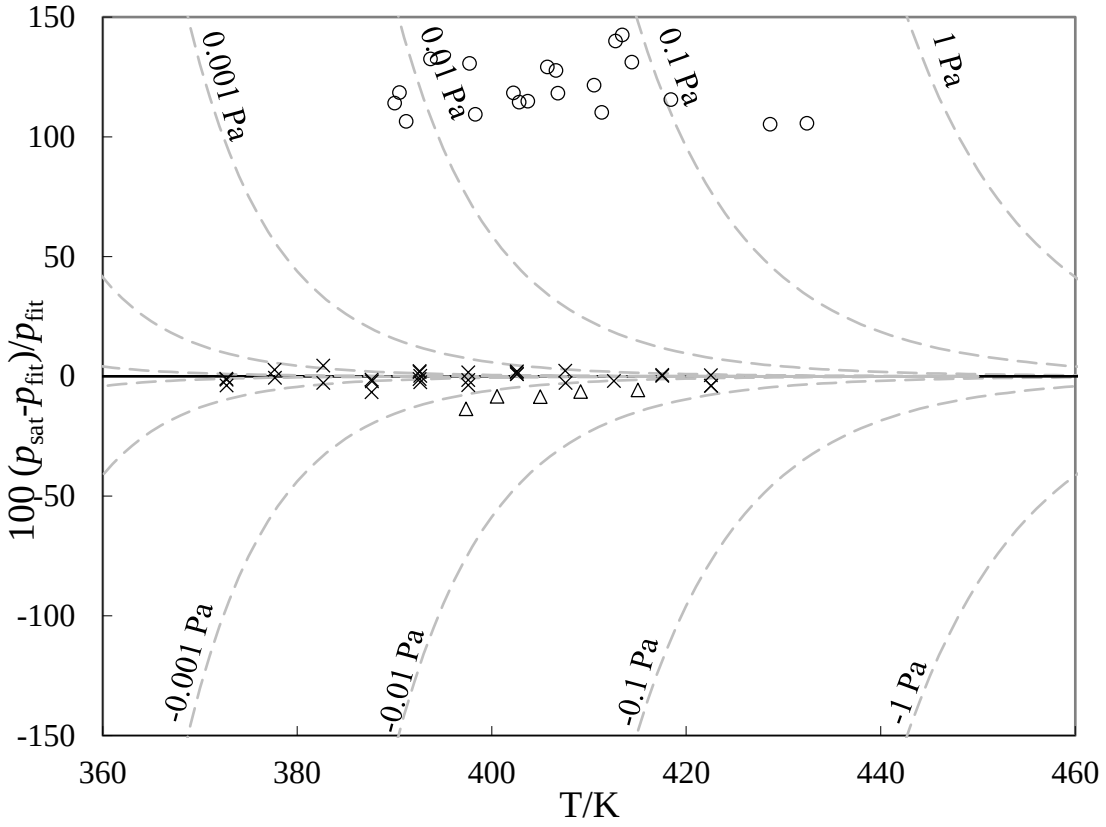

Fig. S20. Experimental vapor pressure deviations from the fitting equation for perylene in Table S7. Here: ○ – from *Goldfarb et al.* [39], Δ – from *Oja et al*. [43], × - this work. The results of *Inokuchi et al*. [52], *Gigli et al.* [50] and *Hoyer et al.* [51] were not included since only a fitting equation was provided.

Table S8. Compilation of data on enthalpies of sublimation $\Delta_{cr}^{g}H_{m}^{\circ}$ of perylene.

Experiment[a]	Method[b]	T-Range	T_{avg}	$\Delta_{cr}^{g}H_{m}^{\circ}(T_{avg})$	$\Delta_{cr}^{g}H_{m}^{\circ}$(298.15K)[c]	p_{sat}[d]
		K	K	kJ mol^{-1}	kJ mol^{-1}	nPa
Goldfarb *et al.* 2008 [39]	K	390.0 – 432.4	406.2	126.2	128.3±3.6	76.6
Chikos *et al.* 2002 [53]	HSA	298.2	-	-	[138.1±6.2]	-
Oja *et al.* 1998 [43]	K	397.3 – 415.0	405.3	132.6	134.7±6.6	16.2
Nass *et al.* 1995 [54]	T	313.2 – 453.2	-	-	[123.2]	[554]
Gigli *et al.* 1973 [50]	K, O	443.0 – 518.0	479.4	137.8	[141.4]	[4.6]
Hoyer *et al.* 1958 [51]	K, O	383.2 – 453.2	417.0	139.0	[141.3]	[4.6]
Inokuchi *et al.*1952 [52]	K, O	-	415.2	129.6	[131.9]	[512]
This Work 2019	T	372.7 – 422.6	396.0	127.0	128.8±2.0	33.2
					129.1±1.7[e]	42.0[f]

Values in brackets were not used in further analysis. [a] Author and year of publication. [b] Methods: T = transpiration, K = Knudsen-effusion, HSA = headspace analysis, O = equation only. [c] Enthalpies of sublimation were adjusted with value of $\Delta_{cr}^{g}C_{p.m}^{\circ}$, stated in Table S2. Uncertainties are expressed as expanded uncertainty with confidence level of 0.95 (k = 2). [d] Vapor pressure at 298.15 K. [e] Weighted average value, calculated using uncertainty as the weighing factor. [f] Average value.

In this work perylene vapor pressures were measured with transpiration method in a temperature range of 372.7 – 422.6 K. The complete experimental *p*-*T*-dataset is compiled in Table S7. From these results a vapor pressure value at 298.15 K was extrapolated (33.2 nPa) and the enthalpy of sublimation at 298.15 K was determined to be 128.8±2.0 kJ mol^{-1}.

In the literature there are several *p-T*-datasets available. The compilation of literature and own *p-T* data is presented in Table S8. The literature includes 5 vapor pressure measurements with Knudsen-effusion method by *Goldfarb et al.* [39], *Oja et al.* [43], *Gigli et al.* [50], *Inokuchi et al.* [52] and *Hoyer et al.* [51] and one transpiration experiment by *Nass et al.* [54]. Literature and own experimental *p-T* datasets are represented in Figure S19. Deviation of experimental literature values from *p-T*-equation derived from *p-T*-data obtained in this work (Table S7) is illustrated in Figure S20. These graphs illustrate great inconsistencies among the literature data. The derived values of enthalpies of sublimation at 298.15 K cover a range from 128.3±3.6 kJ mol^{-1} by *Goldfarb et al*. [39] to 141.4 kJ mol^{-1} by *Gigli et al.* [50].

In year 2008 *Roux et al.* [48] reviewed literature data on the enthalpies of sublimation of perylene. The authors determined a recommended value for perylene (135.9±2.6 kJ mol^{-1}) from studies by *Oja et al.* [43] and *Inokuchi et al.* [52]. However, work of *Inokuchi et al*. [52] lacks information on the purity and no temperature range for given *p-T* equation is given.

Few other literature sources also face fundamental shortcomes. *Nass et al.* [54] presents an extrapolated vapor pressure value at 298.15 K from the measurement in the temperature range of 313.2 - 453.2 K. However, there is no information on the absolute vapor pressures values. For these reasons, results by *Inokuchi et al.* [52] and *Nass et al.* [54] were not included in further analysis.

As Figure S19 illustrates, vapor pressures from the works of *Hoyer et al*. [51], *Gigli et al. [50]*, *Oja et al.* [43], *Goldfarb et al.* [39] are relatively close to each other. Results by *Gigli et al*. [50] and *Hoyer et al.* [51] create an extensive dataset of vapor pressures over a wide range of temperatures with similar results. However, the study by *Hoyer et al.* [51] gives no purity information and discloses only the fitting equation. The work by *Gigli et al*. [50] has the same problem as there are also no absolute *p-T* values reported.

Vapor pressure results from the work of were extrapolated to 298.15 K and the resulting value (76.6 Pa) is significantly higher than the value derived from this work (33.2 nPa). However, the value of enthalpy of sublimation at 298.15 K (128.3±3.6 kJ mol^{-1}) in the work of *Goldfarb et al.* [39] closely matches the result, achieved in this work (128.8±2.0 kJ mol^{-1}). Vapor pressures measured by *Oja et al.* [43] in the temperature range of 397.3 – 415.0 K show relatively similar results as the vapor pressures, measured in this work in the same temperature range (see Figure S19). The calculated enthalpy of sublimation at 298.15 K (134.7±6.6 kJ mol^{-1}) agrees with the value derived in this work within the expanded uncertainties.

The work of *Chickos et al.* [53] provides another value of enthalpy of sublimation at 298.15 K (138.1±6.2 kJ mol^{-1}), which was derived from headspace analysis. This work does not provide absolute vapor pressures, therefore, it was excluded from calculation of average values.

Uncertainty-weighted average of the enthalpy of sublimation of perylene at 298.15 K is 129.1±1.7 kJ mol^{-1} and arithmetic average of vapor pressures extrapolated at 298.15 K is 42.0 nPa.

6.5 9,9’-Bifluorenyl

Table S9. 9,9’-Bifluorenyl: absolute vapor pressures p_{sat} and thermodynamic properties of sublimation obtained by the transpiration method in this work.

9,9'-Bifluorenyl: $\Delta_{cr}^{g}H_{m}^{\circ}(298.15\ K) = 139.5 \pm 3.0\ kJ\ mol^{-1}$

$$\ln p_{sat}/p^{0} = \frac{384.5}{R} - \frac{158777.8}{RT} - \frac{64.6}{R} ln \frac{T}{298.15K}$$

T_{exp} [a] [K]	m [b] [mg]	V_{N2} [c] [dm³]	T_{amb} [d] [K]	Gasflow [dm³ h^{-1}]	p_{sat} [e] [mPa]	$U(p_{sat})$ [f] [mPa]	$\Delta_{cr}^{g}H_{m}^{\circ}$ [kJ mol^{-1}]	$\Delta_{cr}^{g}S_{m}^{\circ}$ [J mol^{-1} K^{-1}]
372.2	8.89	59.3	296.7	3.19	1.12	0.08	134.73	209.8
372.2	14.1	89.2	297.4	4.84	1.18	0.08	134.72	210.2
372.3	12.2	82.1	297.2	4.79	1.11	0.08	134.72	209.6
377.3	22.6	83.8	296.8	4.78	2.01	0.14	134.40	208.9
382.2	10.4	21.6	296.8	4.80	3.60	0.25	134.08	208.4
387.2	11.2	14.2	296.8	4.71	5.88	0.40	133.76	207.0
392.2	21.2	16.4	297.0	4.70	9.68	0.66	133.43	205.9
397.1	21.5	9.22	297.1	2.07	17.4	1.2	133.12	205.9
397.2	30.2	12.8	297.3	3.02	17.6	1.2	133.11	205.9
397.2	23.7	10.1	296.9	4.68	17.5	1.2	133.11	205.8
402.1	51.0	13.5	297.2	4.69	28.3	1.9	132.79	204.9
407.1	23.7	3.89	296.9	4.67	45.5	3.1	132.47	204.0
407.2	24.8	3.99	297.1	4.60	46.5	3.2	132.47	204.1
412.1	23.5	2.32	297.2	4.64	75.8	5.2	132.15	203.5
417.1	18.0	1.15	297.0	4.62	117	8	131.83	202.5
422.1	18.3	0.73	297.0	2.94	187	13	131.50	201.9
422.1	27.0	1.16	297.0	4.62	175	12	131.50	201.3

[a] Saturation temperature ($u(T) = 0.1$ K). [b] Mass of transferred sample condensed at $T = 243$ K. [c] Volume of nitrogen ($u(V) = 0.005$ dm^3) used to transfer $m(u(m)/m = 1.5$ %) of the sample. [d] T_{amb} is the temperature of the soap film flowmeter used for measurement of the gas flow. [e] Vapor pressure at temperature T, calculated from the m and the residual vapor pressure at the condensation temperature calculated by an iteration procedure; $p^{\circ} = 1$ Pa. [f] Relative expanded uncertainty with confidence level 0.95 (k=2) for p was calculated to be $U(p)/p = 6.87\%$.

The uncertainties for T, V and m are standard uncertainties. Uncertainty of the enthalpy of sublimation is the expanded uncertainty with a confidence level of 0.95 ($k = 2$), calculated including uncertainties of vapor pressure, uncertainties from the fitting equation and the uncertainty of temperature adjustment to $T = 298.15$ K. Detailed information on the methods of calculations was published previously [5; 34].

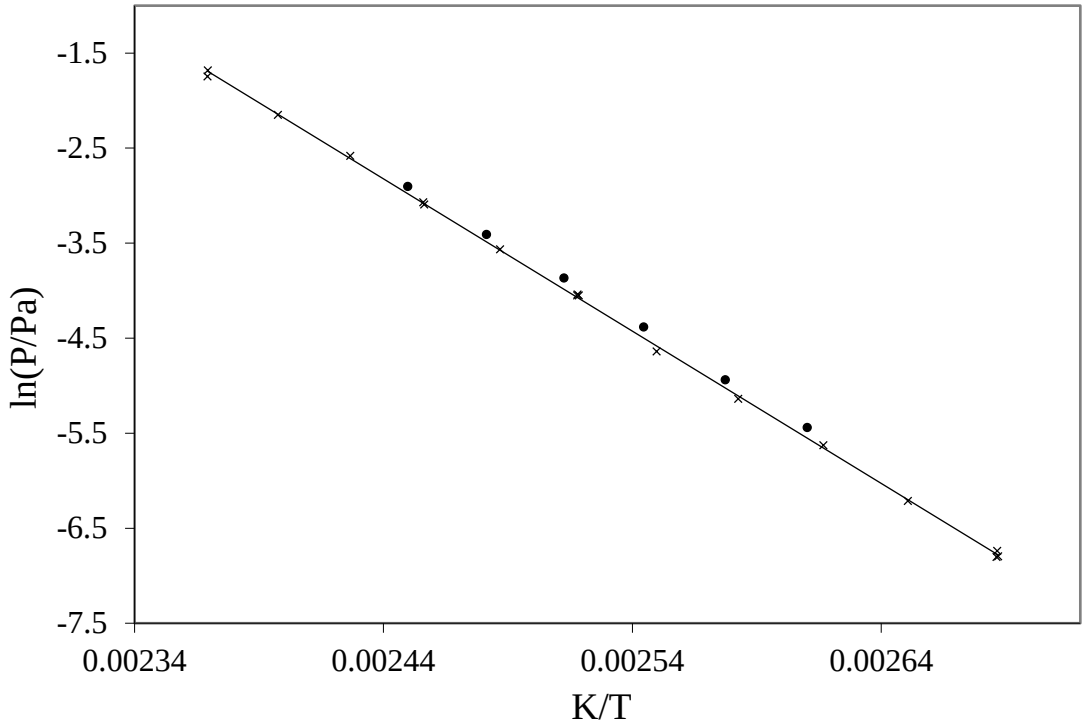

Fig. S21. Experimental vapor pressure of 9,9'-bifluorenyl. Comparison of own experimental results with the literature data: ● – from *Rakus et al.* [30], × and solid line – from this work.

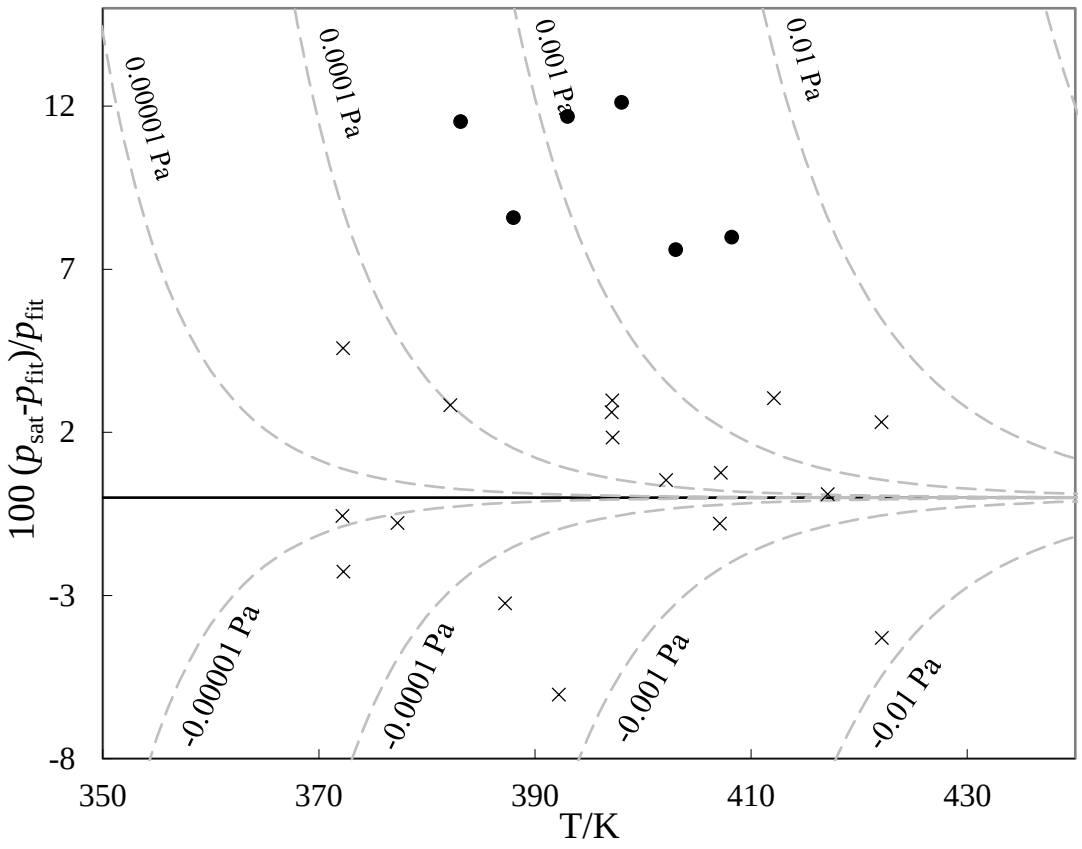

Fig. S22. Experimental vapor pressure deviations from the fitting equation for 9,9'-bifluorenyl in Table S9. Here: ● – from *Rakus et al.* [30], × - this work.

Table S10. Compilation of data on enthalpies of sublimation $\Delta_{cr}^{g}H_{m}^{\circ}$ of 9,9'-bifluorenyl.

Experiment[a]	Method[b]	T-Range	T_{avg}	$\Delta_{cr}^{g}H_{m}^{\circ}(T_{avg})$	$\Delta_{cr}^{g}H_{m}^{\circ}$(298.15K)[c]	p_{sat}[d]
		K	K	kJ mol^{-1}	kJ mol^{-1}	nPa
Rakus *et al.* 2008 [30]	T	383.1 – 408.2	395.4	131.9	138.2±4.5	23.3
This Work 2019	T	372.2 – 422.1	395.6	133.6	139.5±4.7	18.5
					138.8±3.3[e]	20.9[f]

[a] Author and year of publication. [b] Methods: T = transpiration. [c] Enthalpies of sublimation were adjusted according to *Chickos et al.* [9] with $\Delta_{cr}^{g}C_{p,m}^{\circ}$ and $C_{p,m}^{\circ}$(cr), stated in Table S2. Uncertainties are expressed as expanded uncertainty with confidence level of 0.95 (k = 2). [d] Vapor pressure at 298.15 K. [e] Weighted average value, calculated using uncertainty as the weighing factor. [f] Average value.

In this study vapor pressures of 9,9'-bifluorenyl were measured with the transpiration method in the temperature range of 372.2 – 422.1 K. From the results a value of enthalpy of sublimation at 298.15 K was derived to be 139.5±4.7 kJ mol^{-1}. The complete set of measured *p-T* data and resulting *Clausius-Clapeyron* equation for vapor pressures of 9,9'-bifuorenyl are presented in Table S9 and illustrated together with other literature *p-T* values in Figure S21.

There is only one literature source available for comparison. In the study of *Rakus et al*. [30], vapor pressures were also measured by transpiration method. The results of own and literature data are compiled in Table S10. In the work of *Rakus et al.* [30], the derived enthalpy of sublimation at 298.15 K (138.2±4.5 kJ mol^{-1}) matches the results, obtained in this work (139.5±4.7 kJ mol^{-1}) within the interval of uncertainties. The extrapolated vapor pressures at 298.15 K in the work of *Rakus et al.* [30] and this study are respectively 23.3 nPa and 18.5 nPa. Deviation of experimental literature values from the work of *Rakus et al.* [30] from *p-T*-equation derived from *p-T*-data obtained in this work (Table S9) is illustrated in Figure S22.

From these two datasets, average weighted value of enthalpy of sublimation at 298.15 K (138.8±3.3 kJ mol^{-1}) and arithmetic average of vapor pressure at 298.15 K (20.9 nPa) were derived.

S7. GC/MS parameters

Compilation of VO-GC/MS parameters used for transpiration experiments

GC/MS	*Shimadzu QP2010SE*® with *LabSolution* GCMSsolution v4.11
Injector	Atas Optic 4 with Evolution Workstation v4.1
Liner	10 mm V2A stainless steel tube, 5 mm wall thickness, equipped with silanized glass wool (2 mm injection needle penetration into wool)
Restriction	0.05 mm capillary, 10.53 mm length (Restek #10097)
Column connector	*SGE Siltite µ-Union*® (Restek #073562)
Analytical columns	*Restek RTX-TNT 1*® (3 m, 0.53 mm, 1.5 µm)
Oven program	DEMP 1: 40 °C (hold 0.10 min) → 150 °C (rate 60 °C min^{-1})
	TEP 2: 40 °C (hold 0.10 min) → 80 °C (rate 45 °C min^{-1}) → 80 °C (hold 1 min)

	Malathion 3: 40 °C (hold 0.10 min) → 240 °C (rate 60 °C min^{-1}) → 240 °C (hold 0.1 min)
	MS 4: 40 °C (hold 0.10 min) → 280 °C (rate 120 °C min^{-1}) → 280 °C (hold 0.5 min)
Injector head pressure	90 kPa
Virtual column	100 m, 0.25 µm film thickness, 0.20 mm i.d. (entry for GCMSsolution)
Column flow	3.92 mL min^{-1}
Split ratio	150.0 (entered in LabSolutions GCMSsolution)
Purge flow	10 mL min^{-1}
Injection volume	1 µL
Ion source	200 °C
MS interface	200 °C
MS	SIM mode (event Time 100 ms)
	DEMP 1: 0.60 – 1.00 min; m/z: 79.
	Naphthalene: 1.00 – 1.90 min; m/z: 128 (standard).
	TEP 2: 0.61 – 1.62 min; m/z: 99.
	Naphthalene: 1.62 – 1.90 min; m/z: 128 (standard).
	Malathion 3: 0.51 – 2.65 min; m/z: 57.
	Hexadecane: 2.65 – 3.50 min; m/z: 125 (standard).
	MS 4: 0.51 – 1.40 min; m/z: 120.
	Anthracene: 1.40 – 2.00 min; m/z: 178 (standard).
	m/z: quantification ion.

S8. HPLC/DAD parameters

HPLC	*Shimadzu Promenence*® with LC-20AD pump module and SPD-M20A Diode Array Detector; software *LabSolutions v*5.86
Analytical column	*Phenomenex Kinetex*® (2.6 µm Biphenyl, 100 Å, 150 × 4.6 mm)
Oven temperature	45°C
Program	
Naphthalene	Injection volume: 1 µL Total Flow: 1.00 mL/min Mobile phase: 75 % MeCN, 25 % Water

	Time: 6 min
	Channel 1 wavelength: 274 nm (Naphthalene)
	Retention time 1: 2.198 min
	Channel 2 wavelength: 294 nm (standard, DNAN)
	Retention time 2: 1.973 min
Anthracene	Injection volume: 1 µL
	Total Flow: 1.00 mL/min
	Mobile phase: 75 % MeCN, 25 % Water
	Time: 6 min
	Channel 1 wavelength: 250 nm (Anthracene)
	Retention time 1: 2.785 min
	Channel 2 wavelength: 294 nm (standard, DNAN)
	Retention time 2: 1.973 min
Perylene	Injection volume: 10 µL
	Total Flow: 1.00 mL/min
	Mobile phase: 90 % MeOH, 10 % Chloroform
	Time: 6 min
	Channel 1 wavelength: 251 nm (Perylene)
	Retention time 1: 2.815 min
	Channel 2 wavelength: 251 nm (standard, Anthracene)
	Retention time 2: 2.149 min
9,9’ – Bifluorenyl	Injection volume: 1 µL
	Total Flow: 1.00 mL/min
	Mobile phase: 90 % MeOH, 10 % Chloroform
	Time: 6 min
	Channel 1 wavelength: 265 nm (9,9’– Bifluorenyl)
	Retention time 1: 2,640 min
	Channel 2 wavelength: 251 nm (standard, Anthracene)
	Retention time 2: 2.149 min

References

[1] T. Schönberger, Toxichem Krimtech 79 (2012) 81.

[2] M.E. Wieser, N. Holden, T.B. Coplen, J.K. Böhlke, M. Berglund, W.A. Brand, P. De Bièvre, M. Gröning, R.D. Loss, J. Meija, Pure Appl. Chem. 85 (2013) 1047-1078.

[3] A. Reichmuth, S. Wunderli, M. Weber, V.R. Meyer, Microchim. Acta 148 (2004) 133-141.

[4] M. Weber, C. Hellriegel, A. Rück, R. Sauermoser, J. Wüthrich, Accredit. Qual. Assur. 18 (2013) 91-98.

[5] V.N. Emel’yanenko, S.P. Verevkin, J. Chem. Thermodyn. 85 (2015) 111-119.

[6] S.P. Verevkin, A.Y. Sazonova, V.N. Emel’yanenko, D.H. Zaitsau, M.A. Varfolomeev, B.N. Solomonov, K.V. Zherikova, Journal of Chemical & Engineering Data 60 (2015) 89-103.

[7] J.S. Chickos, S. Hosseini, D.G. Hesse, J.F. Liebman, Structural Chemistry 4 (1993) 271-278.

[8] W. Acree Jr, J.S. Chickos, J. Phys. Chem. Ref. Data 45 (2016) 033101.

[9] W. Acree, J.S. Chickos, J. Phys. Chem. Ref. Data 39 (2010) 043101.

[10] J.E. Hurst, B. Keith Harrison, Chem. Eng. Commun. 112 (1992) 21-30.

[11] A.B. Butrow, J.H. Buchanan, D.E. Tevault, J. Chem. Eng. Data 54 (2009) 1876-1883.

[12] G. Kosolapoff, J. Chem. Soc. (1955) 2964-2965.

[13] A. Brozena, J.H. Buchanan, R.W. Miles Jr, B.R. Williams, M.S. Hulet, J. Chem. Eng. Data 59 (2014) 2649-2659.
[14] M.J. Cavalier, Ann. Chem. Phys. (1899) 449-576.
[15] D.P. Evans, W.C. Davies, W.J. Jones, J. Chem. Soc. (1930) 1310-1313.
[16] Y.-H. Kim, J.E. Woodrow, J.N. Seiber, J. Chromatogr. A 314 (1984) 37-53.
[17] W. Gückel, G. Synnatschke, R. Rittig, Pestic. Sci. 4 (1973) 137-147.
[18] W. Eichler, Handbuch der Insektizidkunde VEB Verlag Volk und Gesundheit, Berlín, 1965.
[19] R.M. Stephenson, S. Malanowski, D. Ambrose, Handbook of the thermodynamics of organic compounds, Elsevier (1987).
[20] G. Schrader, Die Entwicklung neuer insektizider Phosphorsäure-Ester, Verlag Chemie (1963).
[21] D.A. Hinckley, T.F. Bidleman, W.T. Foreman, J.R. Tuschall, Journal of Chemical and Engineering Data 35 (1990) 232-237.
[22] W. Perkow, Die Insektizide, Hüthig (1968).
[23] D.E. Tevault, L.C. Buettner, K.L. Crouse, Report: Vapor Pressure of Methyl Salicylate and n-Hexadecane, Edgewood Chemical Biological Center Aberdeen Proving Ground [US] (2014).
[24] J. Matthews, J. Sumner, E. Moelwyn-Hughes, Trans. Faraday Soc. 46 (1950) 797-803.
[25] W. Ramsay, S. Young, J. Chem. Soc. Trans. 47 (1885) 640-657.
[26] M.A. Althoff, K. Grieger, M.A. Härtel, K.L. Karaghiosoff, T.M. Klapötke, M. Metzulat, J. Phys. Chem. A 121 (2017) 2603-2609.
[27] J. McCullough, H. Finke, J. Messerly, S. Todd, T. Kincheloe, G. Waddington, J. Phys. Chem. 61 (1957) 1105-1116.
[28] M. Radomska, R. Radomski, Thermochim. Acta 40 (1980) 405-414.
[29] W.-K. Wong, E.F. Westrum Jr, Mol. Cryst. Liq. Cryst. 61 (1980) 207-228.
[30] K. Rakus, S.P. Verevkin, J. Schätzer, H.-D. Beckhaus, C. Rüchardt, Chem. Ber. 127 (1994) 1095-1103.
[31] Thermodynamics Research Center, Selected values of properties of chemical compounds, Texas A&M University, College Station, Texas (1997).
[32] O.V. Dorofeeva, Thermodynamic Properties of Polycyclic Aromatic Hydrocarbons in the Gas Phase, Institute for High Temperatures, USSR Academy of Sciences (1988).
[33] K. Růžička, M. Fulem, V. Růžička, J. Chem. Eng. Data 50 (2005) 1956-1970.
[34] S.P. Verevkin, A.Y. Sazonova, V.N. Emel'yanenko, D.H. Zaitsau, M.A. Varfolomeev, B.N. Solomonov, K.V. Zherikova, J. Chem. Eng. Data 60 (2014) 89-103.
[35] D. Ambrose, I.J. Lawrenson, C.H.S. Sprake, J. Chem. Thermodyn. 7 (1975) 1173-1176.
[36] M.J.S. Monte, L.M.N.B.F. Santos, M. Fulem, J.M.S. Fonseca, C.A.D. Sousa, J. Chem. Eng. Data 51 (2006) 757-766.
[37] M.A. Siddiqi, R.A. Siddiqui, B. Atakan, J. Chem. Eng. Data 54 (2009) 2795-2802.
[38] L.M.N.B.F. Santos, L.M.S.S. Lima, C.F.R.A.C. Lima, F.D. Magalhães, M.C. Torres, B. Schröder, M.A.V. Ribeiro da Silva, J. Chem. Thermodyn. 43 (2011) 834-843.
[39] J.L. Goldfarb, E.M. Suuberg, J. Chem. Eng. Data 53 (2008) 670-676.
[40] R. Bender, V. Bieling, G. Maurer, J. Chem. Thermodyn. 15 (1983) 585-594.
[41] X. Chen, V. Oja, W.G. Chan, M.R. Hajaligol, J. Chem. Eng. Data 51 (2006) 386-391.
[42] M.A.V. Ribeiro da Silva, M.J.S. Monte, L.M.N.B.F. Santos, J. Chem. Thermodyn. 38 (2006) 778-787.
[43] V. Oja, E.M. Suuberg, J. Chem. Eng. Data 43 (1998) 486-492.
[44] P.C. Hansen, C.A. Eckert, J. Chem. Eng. Data 31 (1986) 1-3.
[45] A.B. Macknick, J.M. Prausnitz, J. Chem. Eng. Data 24 (1979) 175-178.
[46] C.G. De Kruif, J. Chem. Thermodyn. 12 (1980) 243-248.
[47] L. Malaspina, R. Gigli, G. Bardi, J. Chem. Phys. 59 (1973) 387-394.
[48] M.V. Roux, M. Temprado, J.S. Chickos, Y. Nagano, J. Phys. Chem. Ref. Data 37 (2008) 1855-1996.
[49] J.D. Kelley, F.O. Rice, J. Phys.Chem. 68 (1964) 3794-3796.
[50] R. Gigli, M. L, G. Bardi, Ann. Chim. 63 (1973) 627-633.
[51] H. Hoyer, W. Peperle, Z. Elektrochem 62 (1958) 61-66.
[52] H. Inokuchi, S. Shiba, T. Handa, H. Akamatu, Bull. Chem. Soc. Jpn. 25 (1952) 299-302.
[53] J.S. Chickos, P. Webb, G. Nichols, T. Kiyobayashi, P.-C. Cheng, L. Scott, J. Chem. Thermodyn. 34 (2002) 1195-1206.

[54] K. Nass, D. Lenoir, A. Kettrup, Angew. Chem. Int. Ed. 34 (1995) 1735-1736.

5.2. Measurements of RDX and TNX (Article 2)

Article 2: Experimental Vapor Pressures of Hexahydro-1,3,5-trinitro1,3,5-triazine (RDX) and Hexahydro-1,3,5-trinitroso-1,3,5-triazine (TNX)

The results were published in *Propellants, Explosives, Pyrotechnics* [111] and are open-access. DOI: doi.org/10.1002/prep.202000098.

Figure 24. Cover picture in the journal *Propellants, Explosives, Pyrotechnics* (2020): transpiration method set-up.

Full Paper

Propellants, Explosives, Pyrotechnics

DOI: 10.1002/prep.202000098

Experimental Vapor Pressures of Hexahydro-1,3,5-trinitro-1,3,5-triazine (RDX) and Hexahydro-1,3,5-trinitroso-1,3,5-triazine (TNX)

Greta Bikelytė,[a] Martin A. C. Härtel,[a] and Thomas M. Klapötke*[a]

Abstract: In this work experimental vapor pressures of hexahydro-1,3,5-trinitro-1,3,5-triazine (RDX) and hexahydro-1,3,5-trinitroso-1,3,5-triazine (TNX) were measured with transpiration method. Corresponding enthalpies of sublimation were determined to be (130.9 ± 2.1) kJ mol^{-1} and (108.1 ± 1.6) kJ mol^{-1}, respectively. Along with the experimental data fitting equations are reported and *p-T* data extrapolated to 298.15 K to be 0.71 μPa for RDX and 823 μPa for TNX.

Keywords: Vapor Pressure · High explosives · Gas-saturation · Enthalpy of sublimation

1 Introduction

With the increase of reported terrorist attacks throughout last decades, there is a great scientific interest in the detection of potentially hazardous materials [1]. Vapor pressure is a vital parameter when it comes to gas-phase detection of such materials. Extensive efforts have been given throughout the years to determine vapor pressures of most common explosives. Two comprehensive reviews on vapor pressures have been published by *Östmark et al.* [2] and *Ewing et al.* [3]. These reviews emphasize on the need of experimental vapor pressures over a broad temperature range, also yielding other thermodynamic properties, such as enthalpy of sublimation/vaporization. Unfortunately, the reported vapor pressures of explosives often differ significantly. Since the release of these reviews, several studies have been published by our group with the aim of providing reliable experimental vapor pressure data on a variety of explosives [4].

One of the most commonly used high explosives hexahydro-1,3,5-trinitro-1,3,5-triazine (RDX) has great importance in military use: it is one of the main ingredients in most commonly used explosive mixture compositions [5]. It has relatively low sensitivity and high thermal stability. Regardless the wide use of this high explosive, obtaining experimental vapor pressures of RDX has been hindered by the fact that RDX possesses a very low vapor pressure. Several attempts have been made in the past, however, most of the results in various literature sources are inconsistent, as discussed below. For this reason, this work focused on the determination of reliable experimental vapor pressures of RDX in a temperature range from 342.4 to 397.1 K.

As a result of wide use of RDX in military applications, the degradation of the chemical has been studied extensively. It has been shown that under environmental conditions nitro groups of RDX tend to transform into nitroso derivatives or cleave the N-NO_2 bonds producing labile products [6]. None of the decomposition products are known to occur naturally, therefore, the detection of them can indicate the current or past presence of RDX [7]. One of the nitroso derivatives hexahydro-1,3,5-trinitroso-1,3,5-triazine (TNX) could be a signature compound when detecting the presence of RDX in the environment. Moreover, this compound is known in the amateur chemist scene and in the past has been used in improvised explosive devices (IED) [8]. For these reasons, experimental vapor pressures in a temperature range from 312.6 to 357.1 K are reported in this work.

2 Experimental Section

2.1 Materials

Caution! RDX and TNX are toxic and should be handled with caution! Proper protective measures (gloves, safety

[a] *G. Bikelytė, M. A. C. Härtel, T. M. Klapötke*
Department of Chemistry
Ludwig-Maximilian University of Munich
Butenandtstr. 5–13, 81377 Munich (Germany)
**e-mail: tmk@cup.uni-muenchen.de*
Homepage: http://www.hedm.cup.uni-muenchen.de

Supporting information for this article is available on the WWW under https://doi.org/10.1002/prep.202000098

goggles, laboratory coats, etc.) should always be used during handling of the compounds.

RDX was synthesized according to the procedure described in the thesis of *Steeman* [9]. TNX was prepared according to the procedure described in the work of *Rothstein et al.* [10]. The purity of the compounds used in this study (Figure 1) was tested by EA, ^{1}H-, ^{13}C-, ^{14}N-NMR, and HPLC-DAD techniques. Purity data are disclosed in the Table 1. For further details see Supporting Information.

2.2 Transpiration Method

The vapor pressure of the compounds was measured using the transpiration method, which was described in detail before [11]. Between 0.5 and 1 g of analyte was used to coat 1 mm diameter glass beads. In the case of RDX, the compound was dissolved in acetone and added to the glass beads. The resulting suspension was dried in a rotational evaporator until the solvent is completely evaporated and then transferred into a thermostatted glass saturator. In case of TNX, compound was carefully layered with beads directly into the saturator. A dry nitrogen stream was passed through the temperature-controlled saturator and the transported analyte was collected in a glass tube, immersed in a cooling trap. The amount of collected analyte was determined by HPLC-DAD analysis using a suitable internal standard. Further information about the methods used is provided in the Supporting Information. The validity of the experimental setup in conjunction with the HPLC-DAD instrument was tested previously with several reference materials of well-established vapor pressures (naphthalene, anthracene, etc.) [11a].

The calculation of vapor pressure p_{sat} at the temperature of saturator T_{exp} relies on Dalton's law of partial pressures (under assumption that the volume of the analyte in the gas phase is negligible) and the Ideal Gas Law:

$$p_{sat}(T_{exp}) = \frac{m_a R T_{amb}}{M V_{amb}} \quad (1)$$

p_{sat}: vapor pressure of the analyte [Pa], T_{exp}: temperature of the saturator [K], m_a: mass of the analyte [kg], T_{amb}: ambient temperature [K], V_{amb}: volume of the carrier gas at the ambient conditions [m^3], M: molecular weight of the analyte [kg mol^{-1}], R: universal gas constant 8.314469 J mol^{-1} K^{-1}.

Resulting experimental *p-T* values are fitted according to equation 2:

$$\ln\left(\frac{p_{sat}}{p^{\circ}}\right) - \frac{\Delta_{cr}{}^{g}C^{\circ}_{p,m}}{R} ln\frac{T}{T_0} = A - \frac{B}{T} \quad (2)$$

p°: reference pressure (1 Pa), $\Delta_{cr}{}^{g}C^{\circ}_{p,m}$: molar heat capacity difference between crystalline (cr) and gaseous phase (g) at constant pressure [J mol^{-1} K^{-1}], T: temperature [K], T_0: reference temperature [K], A/B: fitting coefficients (A: unitless coefficient [ ], B: [K]).

Calculation of molar enthalpy of sublimation $\Delta_{cr}{}^{g}H^{\circ}_{m}$ at temperature T was performed using the equation 3:

$$\Delta_{cr}{}^{g}H^{\circ}_{m}(T) = RB + \Delta_{cr}{}^{g}C^{\circ}_{p,m} \quad (3)$$

This approach was used to analyse both own and literature data.

The molar heat capacity at constant pressure $C^{\circ}_{p,m}$ for RDX was available in the literature [12]. The value for TNX was obtained with the empirical increment approach by *Hurst et al.* [13]. Molar heat capacity differences were obtained by a procedure described by *Chickos et al.* [14]. The values are detailed in Table 2.

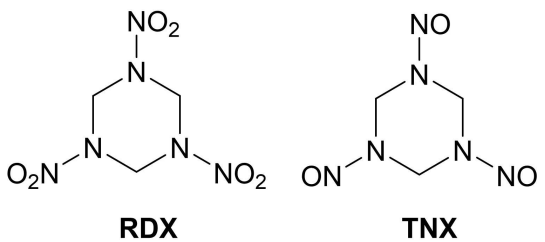

Figure 1. Compounds studied in this work: hexahydro-1,3,5-trinitro-1,3,5-triazine (RDX) and hexahydro-1,3,5-trinitroso-1,3,5-triazine (TNX).

Table 1. Purity of the compounds investigated.

Substance	CAS#	Purity[a]
RDX	121-82-4	0.999
TNX	13980-04-6	0.999

[a] Mass fraction purity was determined by HPLC-DAD.

Table 2. Molar heat capacities and their differences at T = 298.15 K.

Compound	$C^{\circ}_{p,m}(cr)$ Calc. J mol^{-1} K^{-1}	$C^{\circ}_{p,m}(cr)$ Exp. J mol^{-1} K^{-1}	$-\Delta^{g}_{cr}C^{\circ}_{p,m}$ J mol^{-1} K^{-1}
RDX	(259.2)[a]	248.9 [12]	38.1[c]
TNX	214.8[b]	n.a.	33.0[c]

Values in parentheses were not used for calculation of molar heat capacity differences. n.a.: not available. [a] Derived from the molecular increments procedure described by *Chickos et al.* [15]. [b] Calculated according to the empirical increment approach by *Hurst et al.* [13]. [c] Calculated by $-^{g}_{cr}C^{\circ}_{p,m} = 0.75 + C^{\circ}_{p,m}(cr) \times 0.15$ [14].

3 Results and Discussion

3.1 RDX

The sublimation behavior of RDX was measured in the temperature range of 342.4 – 397.1 K. The absolute vapor pressures p_{sat} and thermodynamic properties of sublimation obtained by the transpiration method are compiled in Table 3. Several datasets of vapor pressures are available in the literature. A comparison of own data with literature experiments regarding the enthalpies of sublimation is compiled in Table 4. Figure 2 shows a *Clausius-Clapeyron* plot of the own and literature *p-T* data for the sublimation of RDX.

There have been several attempts to measure vapor pressures of RDX in the past. Some of the first reported experimental values were obtained by *Edwards* [16] by Knudsen effusion method and *Rosen and Dickinson* [17] by Langmuir effusion technique. In this work, the corresponding experimental *p-T* data from the works of *Edwards* [16] and *Rosen and Dickinson [17]* were used to derive enthalpies of sublimation at 298.15 K: (114.8 ± 5.4) kJ mol^{-1} and (131.8 ± 3.5) kJ mol^{-1}, respectively.

In several studies, the vapor pressure of RDX was measured in order to prove validity of newly developed methods. The work by *John et al.* [18] applied isotopic dilution method. The fitting equation was obtained from vapor pressures at three temperatures and the resulting enthalpy of sublimation, 59.2 kJ mol^{-1} (derived in this work by equations 2 and 3) does not agree with any other reported literature data (see Table 4). Moreover, as mentioned in the report by *Östmark et al.* [2], the results in the provided graph do not match the reported fitting equation. *Hikal et al.* [19] implemented an UV-absorbance technique on thin nanofilms of common explosives (TNT and RDX). The measurements of RDX were conducted at two different wavelengths (209 and 243 nm) and they yielded different enthalpies of sublimation at 298.15 K. Furthermore, it is not clear which set of results was used to form the resulting fitting equation.

In 1978, *Cundall et al.* [23] reported a fitting equation for the vapor pressures of RDX in the temperature range from 343.4 to 447.4 K. Three years later a corrigendum was issued with corrected equation coefficients and the resulting enthalpy of sublimation is 137.8 kJ mol^{-1}. Another fitting equation of *R. Stimac* was reported as a personal communication in the study of *Eiceman et al.* [21]. The study reports that the experiment was conducted by adsorbing the vapors and analysing them by Ion Mobility Spectrometry (IMS). Unfortunately, no experimental temperature range is provided. The study of *Eiceman et al.* [21] calculated the values for three different temperatures and, in this work, we plot the corresponding fitting equation in this temperature range.

One of the most recent studies on the vapor pressures of the RDX is a study by *Felix-Rivera et al.* [20], conducted with isothermal thermogravimetric analysis (TGA). The work provides no experimental *p-T* data, solely a fitting equation of the relationship of mass loss vs. the temperature. The resulting enthalpy of sublimation, 101.9 kJ mol^{-1}, does not agree with the majority of the other literature values for reasons stated before [4a].

Deviations of experimental literature values from *p-T*-equation derived from *p-T* data obtained in this work (Table 3) are illustrated in Figure 3.

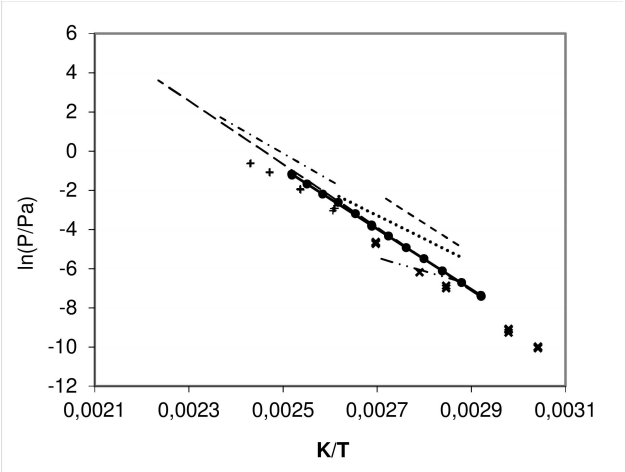

Figure 2. Experimental vapor pressure values of **RDX** in comparison with literature values. Here • and solid line – from this work, ···· line from *Felix-Rivera et al.* [20], – – – line from *Hikal et al.* [19], – · – · line from *R. Stimac* [21], — — line from *Cundall et al.* [22], – · · – · · line from *John et al.* [18], × from *Rosen and* Dickinson [17], + – from *Edwards* [16].

3.2 TNX

The sublimation behavior of TNX was measured in the temperature range of 312.6 – 357.1 K. The absolute vapor pressures p_{sat} and thermodynamic properties of sublimation obtained by the transpiration method are compiled in Table 3.

Only one experimental *p-T* dataset is available in the literature. A comparison of own data with the results of the work of *Pepekin et al.* [24] is presented in Table 5 and Figure 4. In the work of *Pepekin et al.* [24], vapor pressures were measured with the Knudsen effusion method in the temperature range from 325.2 to 360.2 K. No experimental *p-T* data was disclosed, solely a fitting equation without specifying the units of pressure and resulting calculated enthalpy of sublimation at average temperature was reported (112.5 ± 0.8 kJ mol^{-1}). In this work, we assume that the results were reported in Torr and Figure 4 depicts the differences between the vapor pressures measured in this work and the results from a fitting equation reported by *Pepekin et al.* [24].

Table 3. Absolute vapor pressures p_{sat} and thermodynamic properties of sublimation of RDX and TNX obtained by the transpiration method in this work.

RDX: $\Delta_{cr}^{g}H_{m}^{\circ}$ (298.15 K) = (130.9 ± 2.1) kJ mol^{-1}

$\ln\frac{p_{sat}}{p^0} = \frac{359.2}{R} - \frac{142206.8}{RT} - \frac{38.1}{R}ln\frac{T}{298.15\ K}$

T_{exp} [a]	m [b]	V_{N2} [c]	T_{amb} [d]	Gasflow	p_{sat} [e]	u(p_{sat}) [f]	$\Delta_{cr}^{g}H_{m}^{\circ}$	$\Delta_{cr}^{g}S_{m}^{\circ}$
[K]	[µg]	[dm^3]	[K]	[dm^3 h^{-1}]	[mPa]	[mPa]	[kJ mol^{-1}]	[J mol^{-1} K^{-1}]
342.4	6.72	123	297.3	5.12	0.61	0.01	129.15	219.9
342.4	5.09	93.5	297.1	3.89	0.61	0.01	129.15	219.9
342.4	6.63	117	299.7	4.90	0.64	0.02	129.15	220.3
342.4	5.31	93.6	299.7	3.88	0.64	0.02	129.15	220.2
347.3	12.7	117	299.1	4.89	1.21	0.03	128.97	219.8
352.3	24.1	123	300.7	4.95	2.21	0.05	128.78	219.0
357.2	8.01	21.9	300.4	4.90	4.11	0.10	128.60	218.6
362.1	76.4	118	299.0	4.90	7.25	0.17	128.41	217.9
367.1	132	114	300.7	4.93	13.1	0.3	128.22	217.5
371.9	11.0	5.64	296.2	5.45	21.7	0.5	128.04	216.7
372.0	11.9	6.00	297.2	4.86	22.0	0.5	128.04	216.8
372.0	47.6	23.1	300.8	4.96	23.2	0.6	128.04	217.1
376.9	17.4	4.75	299.4	3.90	41.1	1.0	127.86	217.0
382.1	8.87	1.38	301.5	3.93	72.8	1.7	127.66	216.6
387.0	6.88	0.68	298.1	2.73	112	3	127.48	215.5
392.0	11.5	0.68	298.7	2.74	188	4	127.29	215.1
397.0	34.7	1.30	298.3	4.89	297	7	127.10	214.3
397.0	38.4	1.46	298.4	5.83	294	7	127.10	214.3
397.1	18.8	0.69	299.0	2.74	307	7	127.10	214.6

TNX: $\Delta_{cr}^{g}H_{m}^{\circ}$ (298.15 K) = (108.1 ± 1.6) kJ mol^{-1}

$\ln\frac{p_{sat}}{p^0} = \frac{336.5}{R} - \frac{117926.7}{RT} - \frac{33.0}{R}ln\frac{T}{298.15\ K}$

T_{exp} [a]	m [b]	V_{N2} [c]	T_{amb} [d]	Gasflow	p_{sat} [e]	u(p_{sat}) [f]	$\Delta_{cr}^{g}H_{m}^{\circ}$	$\Delta_{cr}^{g}S_{m}^{\circ}$
[K]	[mg]	[dm^3]	[K]	[dm^3 h^{-1}]	[mPa]	[mPa]	[kJ mol^{-1}]	[J mol^{-1} K^{-1}]
312.6	0.04	82.8	296.1	3.50	6.13	0.13	107.62	206.2
312.6	0.03	78.7	296.4	4.85	6.14	0.13	107.62	206.2
317.7	0.07	80.5	296.3	4.81	11.9	0.2	107.45	205.6
322.6	0.03	19.0	296.4	4.84	21.9	0.5	107.29	205.1
327.6	0.22	75.1	296.3	4.84	40.6	0.8	107.13	204.7
332.5	0.05	9.35	296.4	4.84	72.7	1.5	106.97	204.2
337.4	0.04	4.75	296.4	4.83	130	3	106.80	203.9
337.4	0.05	5.40	296.2	4.83	128	3	106.80	203.7
337.4	0.04	4.76	296.4	4.84	129	3	106.80	203.8
342.3	0.05	3.40	297.4	4.86	217	4	106.64	203.1
347.2	0.05	2.01	297.6	4.83	376	8	106.48	202.8
352.1	0.05	1.21	296.3	4.84	637	13	106.32	202.5
357.0	0.09	1.21	296.3	4.84	1029	21	106.16	201.9
357.1	0.09	1.21	296.3	4.84	1045	22	106.15	201.9
357.1	0.09	1.21	296.4	4.85	1023	21	106.15	201.7
357.1	0.09	1.21	296.6	4.85	1009	21	106.15	201.6

[a] Saturation temperature ($u(T)$ = 0.1 K). [b] Mass of transferred sample. [c] Volume of nitrogen ($u(V)$ = 0.005 dm^3) used to transfer m ($u(m)$ = 0.0001 g) of the sample. [d] T_{amb} is the temperature of the soap bubble meter used for measurement of the gas flow. [e] Vapor pressure at temperature T, calculated from the m and the residual vapor pressure at the condensation temperature calculated by an iteration procedure; p° = 1 Pa. [f] Expressed as standard uncertainties, more details are given in Supporting Information. Uncertainties of sublimation enthalpies are expressed as expanded uncertainties (k = 2) and they were derived according to the procedures reported in [11a, 25].

Table 4. Compilation of data on enthalpies of sublimation $\Delta^{g}_{cr}H^{\circ}_{m}$ of RDX.

Experiment[a]	Method[b]	*T*-Range K	T_{avg} K	$\Delta^{g}_{cr}H^{\circ}_{m}(T_{avg})$ kJ mol^{-1}	$\Delta^{g}_{cr}H^{\circ}_{m}$(298.15 K)[c] kJ mol^{-1}	p_{sat}[d] µPa
Felix-Rivera *et al.* 2011 [20]	TGA, O	348.0–383.0	365.1	99.4	[101.9]	[13.67]
Hikal *et al.* 2011 [19]	UV, O	348.2–368.2	353.0	128.5	[130.8]	[4.42]
R. Stimac 1997 [21]	IMS, O	–	–	–	[118.8]	[5.36]
Cundall *et al.* 1981 [22][g]	K, O	343.4–447.4	393.1	134.2	[137.8]	[0.45]
John *et al.* 1975 [18]	ID, O	347.2–369.2	357.6	56.9	[59.2]	[45.33]
Rosen *et al.* 1969 [17]	L	328.9–370.9	346.5	129.9	131.8 ± 3.5	0.31
Edwards 1953 [16]	K	383.2–411.7	398.7	111.1	114.8 ± 5.4	2.04
This Work	T	342.4–397.1	367.4	128.2	130.9 ± 2.1	0.71
					129.5 ± 1.7[e]	1.02[f]

Values in brackets were not used in further analysis. [a] First author and year of publication. [b] Methods: O: Equation only, T: Transpiration Method, TGA: Isothermal Thermogravimetric Method, K: Knudsen effusion, UV: UV-absorbance spectroscopy, IMS: Ion Mobility Spectroscopy, L: Langmuir Effusion, ID: Isotopic Dilution, IMS: Ion Mobility Spectrometry. [c] Enthalpies of sublimation were derived using the equation (3) and adjusted according to *Chickos et al.* [26]: $\Delta^{g}_{cr}C^{\circ}_{p,m} = 38.1$ J mol^{-1} K^{-1} from DCS measurement of $C^{\circ}_{p,m}$(cr) = 248.9 J mol^{-1} K^{-1} by *Krien et al.* [12]. Uncertainty for enthalpy of sublimation is expressed as expanded uncertainty with confidence level of 0.95 ($k = 2$). [d] Vapor pressure at 298.15 K.[e] Weighted average value, calculated using uncertainty as the weighing factor. [f] Average value. [g] Corrigendum of work in 1978 [23].

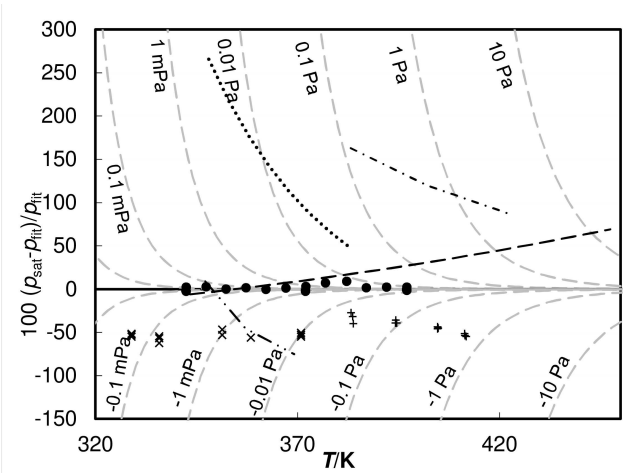

Figure 3. Experimental vapor pressure p_{sat} deviations from the derived fitting equation p_{fit} for **RDX** in Table 3. Here • and solid line – from this work, ···· line from *Felix-Rivera et al.* [20], – · – · line from *R. Stimac* [21], — — line from *Cundall et al.* [22], – · · – · · line from *John et al.* [18], × – from *Rosen and* Dickinson [17],+ – from *Edwards* [16]. Results from *Hikal et al.* [19] possess extremely big deviations from other literature results and, therefore, are not depicted in this graph.

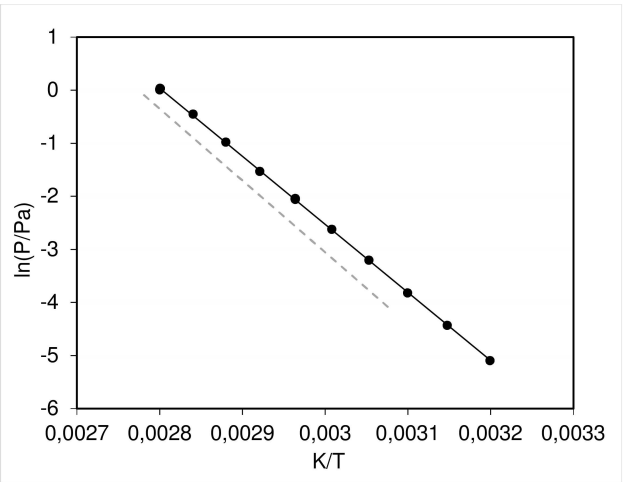

Figure 4. Experimental vapor pressure values of **TNX** in comparison with literature values. Here • and solid line – from this work, dashed grey line – from *Pepekin et al.* [24].

Table 5. Compilation of data on enthalpies of sublimation $\Delta^{g}_{cr}H^{\circ}_{m}$ of **TNX.**

Experiment[a]	Method[b]	*T*-Range K	T_{avg} K	$\Delta^{g}_{cr}H^{\circ}_{m}(T_{avg})$ kJ mol^{-1}	$\Delta^{g}_{cr}H^{\circ}_{m}$(298.15 K)[c] kJ mol^{-1}	p_{sat}[d] µPa
Pepekin et al. 1974 [24]	K, O	325.2–360.2	342.3	112.6	114.0	376
This Work	T	312.6–357.1	337.3	106.9	108.1 ± 1.6	823

[a] First author and year of publication. [b] Methods: T: Transpiration, K: Knudsen effusion, O: Equation only. [c] Enthalpies of sublimation were derived using the equation (3) and adjusted according to *Chickos et al.* [14] with values of $^{g}_{cr}C^{\circ}_{p,m}$ and $C^{\circ}_{p,m}$(cr), stated in Table 2. Uncertainty for enthalpy of sublimation is expressed as expanded uncertainty with confidence level of 0.95 ($k = 2$). [d] Vapor pressure at 298.15 K.

4 Conclusion

In this study, new experimental vapor pressures for one of the most commonly used explosive RDX and its environmental decomposition product TNX, which is also known as common homemade explosive, were measured using the transpiration method. *p-T* fitting equations for RDX in the temperature range from 342.4 to 397.1 K and TNX in the temperature range from 312.6 to 357.0 K are also reported. These equations were extrapolated to yield vapor pressures and enthalpies of sublimation at ambient conditions (0.71 μPa, (130.9 ± 2.1) kJ mol^{-1} for RDX; 823 μPa, (108.1 ± 1.6) kJ mol^{-1} for TNX). Results were compared with existing *p-T* data in the literature. In case of RDX, several data sets are available, however, most of the vapor pressure data is inconsistent. This could be associated with the fact that RDX is extremely low-volatile. New reported experimental vapor pressures should introduce more certainty in the thermodynamic description of this important compound. As for TNX, only one set of experimental vapor pressures has been recorded in the past and the results considerably differ. Since the vapor pressures of TNX are significantly higher than of its mother compound, it could allow more efficient detection of the past or current presence of explosive RDX in environmental conditions.

Acknowledgements

For financial support of this work by Ludwig-Maximilian University (LMU), the Office of Naval Research (ONR) under grant no. ONR N00014-19-1-2078, the Strategic Environmental Research and Development Program (SERDP) under contract no. W912HQ19C0033 and the DAAD (German Academic Exchange Service) [grant no. 57299294] is gratefully acknowledged. We would like to thank Prof. Dr. Sergey Verevkin (University of Rostock) for help with establishing the transpiration method at our laboratory. Open access funding enabled and organized by Projekt DEAL.

References

[1] A. M. Rouhi, Government, Industry Efforts Yield Array Of Tools To Combat Terrorism, *Chemical & Engineering News Archive* **1995**, *73*, 10–19.

[2] H. Östmark, S. Wallin, H. G. Ang, Vapor pressure of explosives: a critical review, *Propellants Explos. Pyrotech.* **2012**, *37*, 12–23.

[3] R. G. Ewing, M. J. Waltman, D. A. Atkinson, J. W. Grate, P. J. Hotchkiss, The vapor pressures of explosives, *TrAC Trends Anal. Chem.* **2013**, *42*, 35–48.

[4] a) G. Bikelytė, M. Härtel, J. Stierstorfer, T. M. Klapötke, A. A. Pimerzin, S. P. Verevkin, Benchmark properties of 2-, 3-and 4-nitrotoluene: Evaluation of thermochemical data with complementary experimental and computational methods, *J. Chem. Thermodyn.* **2017**, *111*, 271–278; b) M. A. Härtel, T. M. Klapötke, B. Stiasny, J. Stierstorfer, Gas-phase Concentration of Triacetone Triperoxide (TATP) and Diacetone Diperoxide (DADP), *Propellants Explos. Pyrotech.* **2017**, *42*, 623–634; c) M. A. Härtel, T. M. Klapötke, J. Stierstorfer, L. Zehetner, Vapor Pressure of Linear Nitrate Esters Determined by Transpiration Method in Combination with VO-GC/MS, *Propellants Explos. Pyrotech.* **2019**, *44*, 484–492; d) M. A. C. Härtel, T. M. Klapötke, V. N. Emel'yanenko, S. P. Verevkin, Aliphatic nitroalkanes: Evaluation of thermochemical data with complementary experimental and computational methods, *Thermochim. Acta* **2017**, *656*, 151–160.

[5] T. M. Klapötke, *Chemistry of High-Energy Materials*, De Gruyter, Berlin, **2019**, pp. 60–69.

[6] a) N. McCormick, J. H. Cornell, A. Kaplan, Biodegradation of Hexahydro-1,3,5-Trinitro-1,3,5-Triazine, *Appl. Environ. Microbiol.* **1981**, *42*, 817–823; b) D. Fournier, A. Halasz, J. Spain, P. Fiurasek, J. Hawari, Determination of key metabolites during biodegradation of hexahydro-1,3,5-trinitro-1,3,5-triazine with Rhodococcus sp. strain DN22, *Appl. Environ. Microbiol.* **2002**, *68*, 166–172.

[7] L. Paquet, F. Monteil-Rivera, P. B. Hatzinger, M. E. Fuller, J. Hawari, Analysis of the key intermediates of RDX (hexahydro-1,3,5-trinitro-1,3,5-triazine) in groundwater: occurrence, stability, and preservation, *J. Environ. Monit.* **2011**, *13*, 2304–2311.

[8] a) E. National Academies of Sciences, Medicine, *Reducing the Threat of Improvised Explosive Device Attacks by Restricting Access to Explosive Precursor Chemicals*, The National Academies Press, Washington, DC, **2018**; b) M. M. Houck, *Materials analysis in forensic science*, Academic Press/ Elsevier, Amsterdam; Boston, **2016**.

[9] F. X. Steemann, *Beiträge zur Chemie energetischer Amin-, Nitramin- und Tetrazolverbindungen*, Dissertation, LMU München Thesis, **2009**.

[10] S. A. Rothstein, P. Dubé, S. R. Anderson, An Improved Process Towards Hexahydro-1,3,5-trinitroso-1,3,5-triazine (TNX), *Propellants Explos. Pyrotech.* **2017**, *42*, 126–130.

[11] a) G. Bikelytė, M. A. Härtel, T. M. Klapötke, B. Krumm, A. Sadaunykas, Experimental thermochemical data of CWA simulants: Triethyl phosphate, diethyl methylphosphonate, malathion and methyl salicylate, *J. Chem. Thermodyn.* **2020**, *143*, 106043; b) M. Härtel, *Studies towards the gas-phase detection of hazardous materials by vapor pressure measurements with the transpiration method in combination with vacuum outlet GC/MS*, Dissertation Thesis, LMU München **2017**.

[12] G. Krien, H. H. Licht, J. Zierath, Thermochemical investigation of nitramines., *Thermochim. Acta* **1973**, *6*, 465–472.

[13] J. E. Hurst, B. K. Harrison, Estimation of Liquid and Solid Heat Capacities Using a Modified Kopp's Rule , *Chem. Eng. Commun.* **1992**, *112*, 21–30.

[14] W. Acree, J. S. Chickos, Phase Transition Enthalpy Measurements of Organic and Organometallic Compounds. Sublimation, Vaporizationand Fusion Enthalpies From 1880 to 2010, *J. Phys. Chem. Ref. Data* **2010**, *39*, 043101.

[15] W. Acree Jr, J. S. Chickos, Phase transition enthalpy measurements of organic and organometallic compounds. Sublimation, vaporization, and fusion enthalpies from 1880 to 2015. Part 1. C1–C10, *J. Phys. Chem. Ref. Data* **2016**, *45*, 033101.

[16] G. Edwards, The vapour pressure of cyclo-trimethylene-trinitramine (cyclonite) and pentaerythritol-tetranitrate, *Trans. Faraday Soc.* **1953**, *49*, 152–154.

[17] J. M. Rosen, C. Dickinson, Vapor pressures and heats of sublimation of some high-melting organic explosives, *J.l Chem. Eng. Data* **1969**, *14*, 120–124.

[18] G. S. John, J. McReynolds, W. Blucher, A. Scott, M. Anbar, Determination of the concentration of explosives in air by isotope dilution analysis, *Forensic science* **1975**, *6*, 53–66.

[19] W. M. Hikal, J. T. Paden, B. L. Weeks, Thermo-optical determination of vapor pressures of TNT and RDX nanofilms, *Talanta* **2011**, *87*, 290–294.
[20] H. Félix-Rivera, M. L. Ramírez-Cedeño, R. A. Sánchez-Cuprill, S. P. Hernández-Rivera, Triacetone triperoxide thermogravimetric study of vapor pressure and enthalpy of sublimation in 303–338 K temperature range, *Thermochim. Acta* **2011**, *514*, 37–43.
[21] G. Eiceman, D. Preston, G. Tiano, J. Rodriguez, J. Parmeter, Quantitative calibration of vapor levels of TNT, RDX, and PETN using a diffusion generator with gravimetry and ion mobility spectrometry, *Talanta* **1997**, *45*, 57–74.
[22] R. B. Cundall, T. F. Palmer, C. E. C. Wood, Corrigendum *J. Chem. Soc., Faraday Trans 1* **1981**, *77*, 711–712.
[23] R. B. Cundall, T. F. Palmer, C. E. C. Wood, Vapour pressure measurements on some organic high explosives, *J. Chem. Soc., Faraday Trans* **1978**, *74*, 1339–1345.
[24] V. I. Pepekin, Y. N. Matyushin, Y. A. Lebedev, Thermochemistry of N-nitro- and N -nitrosoamines of the alicyclic series, *Bulletin of the Academy of Sciences of the USSR, Division of chemical science* **1974**, *23*, 1707–1710.
[25] a) S. P. Verevkin, A. Y. Sazonova, V. N. Emel'yanenko, D. H. Zaitsau, M. A. Varfolomeev, B. N. Solomonov, K. V. Zherikova, Thermochemistry of Halogen-Substituted Methylbenzenes, *J. Chem. Eng. Data* **2015**, *60*, 89–103; b) V. N. Emel'yanenko, S. P. Verevkin, Benchmark thermodynamic properties of 1,3-propanediol: Comprehensive experimental and theoretical study, *J. Chem. Thermodyn.* **2015**, *85*, 111–119.
[26] J. S. Chickos, W. E. Acree, Enthalpies of Vaporization of Organic and Organometallic Compounds, 1880–2002, *J. Phys. Chem. Ref. Data* **2003**, *32*, 519–878.

Manuscript received: April 20, 2020
Revised manuscript received: May 27, 2020
Version of record online: July 28, 2020

Experimental Vapor Pressures of Hexahydro-1,3,5-trinitro-1,3,5-triazine (RDX) and Hexahydro-1,3,5-trinitroso-1,3,5-triazine (TNX)

Greta Bikelytė, Martin A. C. Härtel, Thomas M. Klapötke.

SUPPORTING INFORMATION

S1. Purity assessment

Elemental analysis (CHNS) was performed with an *Elementar Vario Micro* instrument. NMR spectra were measured with a *Bruker* AVANCE 400 MHz instrument.

1.1 Purity assessment results

Results of the purity assessment are presented in the following: Figure S1 and Table 1 for **RDX** and Figures S2, S3 and Table 2 for **TNX**.

In the case of TNX, different chemical environments of the protons induced by fixed nitroso groups yield different peaks for each of the hydrogens. This behaviour has been previously reported in several literature sources [1; 2].

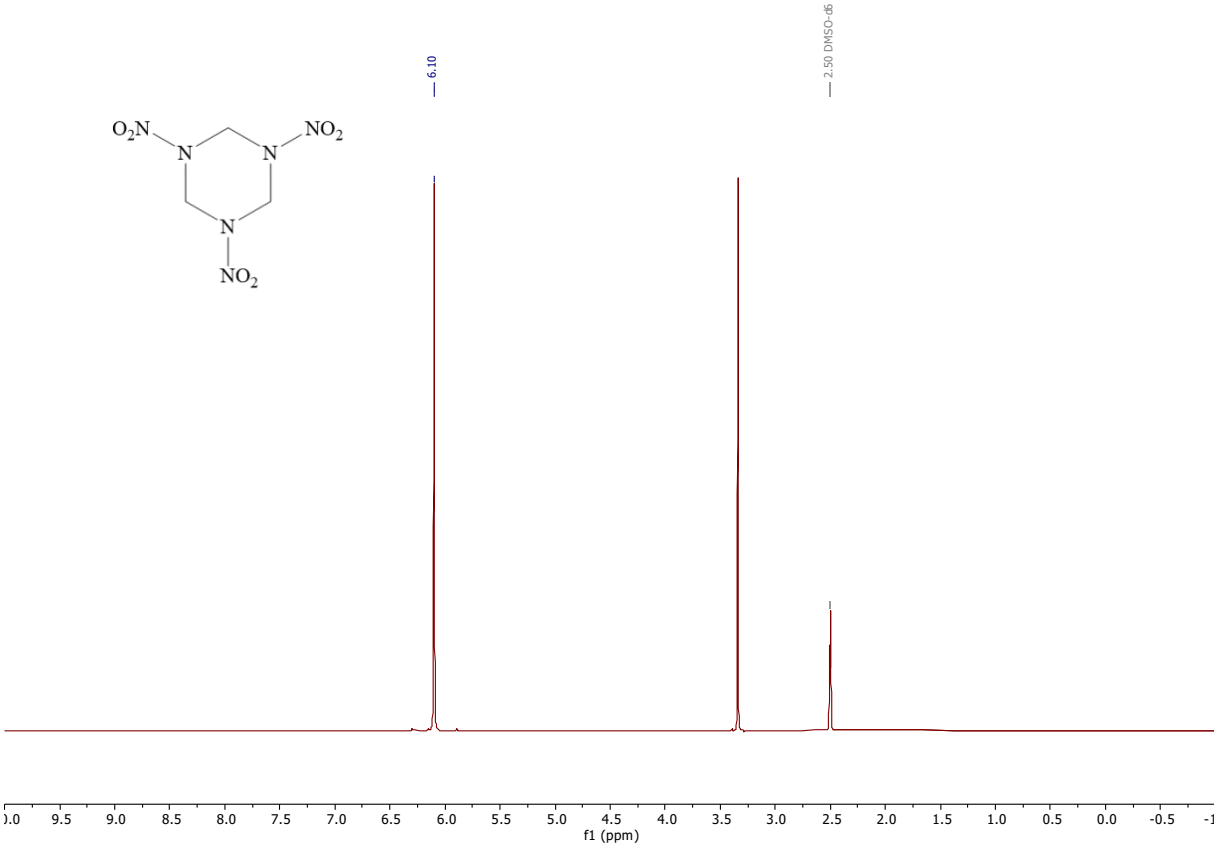

Figure S1. ^{1}H-NMR spectrum of **RDX**.

Table 1. Results of NMR and EA experiments for **RDX**.

^{1}H – NMR	(DMSO-d_6, 400 MHz): δ = 6.10 (s, 6H, CH_2) ppm.
^{13}C – NMR	(DMSO-d_6, 101 MHz): δ = 61.2 (CH_2) ppm.
^{14}N – NMR	(DMSO-d_6, 29 MHz): δ = -34 ppm.
EA	Calc.: C 16.22, H 2.72, N 37.84 %; Found: C 16.39, H 2.58, N 37.66 %.

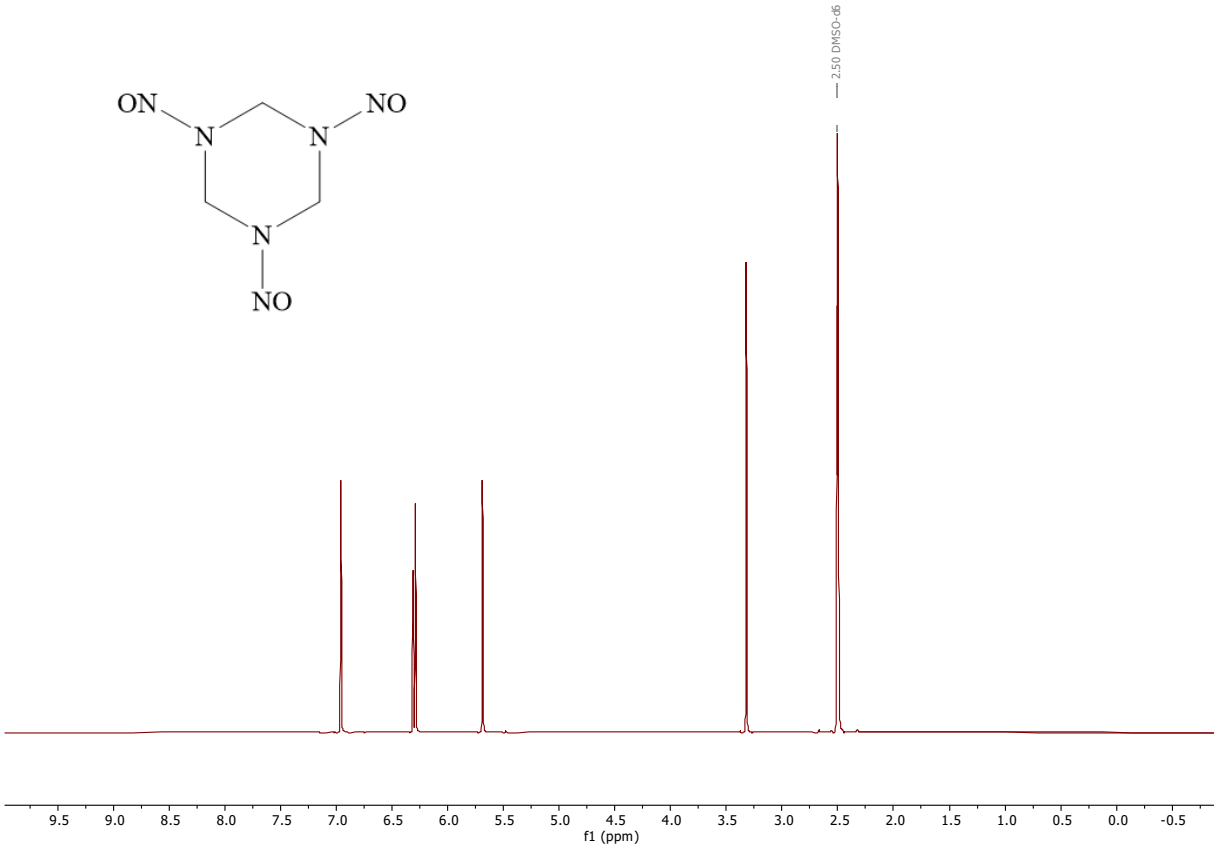

Figure S2. ^{1}H-NMR spectrum of **TNX**.

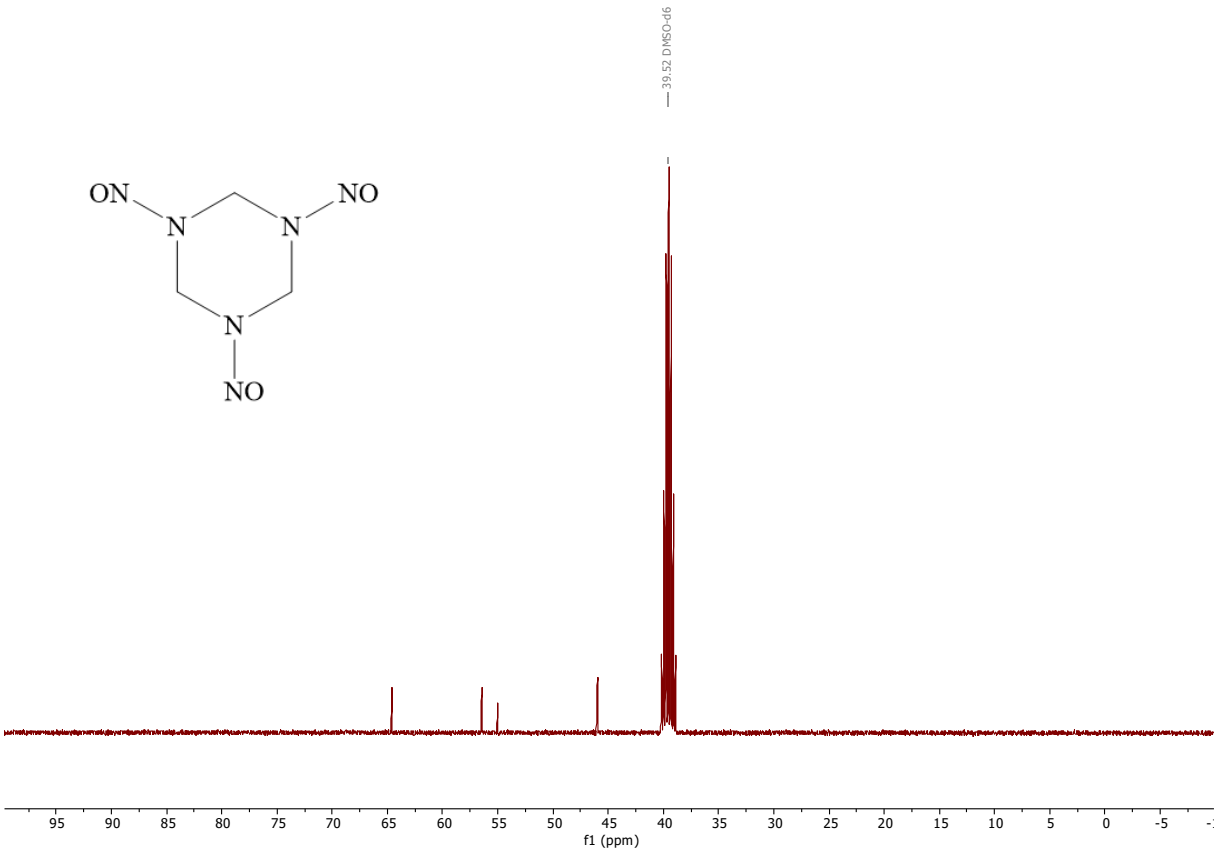

Figure S3. ^{13}C-NMR spectrum of **TNX**.

Table 2. Results of NMR and EA experiments for **TNX**.

^{1}H – NMR	(DMSO-d_6, 400 MHz): δ = 4.96 (s, CH_2), 6.31 (s, CH_2), 6.29 (s, CH_2), 5.69 (s, CH_2) ppm.
^{13}C – NMR	(DMSO-d_6, 101 MHz): δ = 64.59 (CH_2), 56.44 (CH_2), 55.01 (CH_2), 45.96 (CH_2) ppm.
EA	Calc.: C 20.69, H 3.47, N 48.27 %; Found: C 20.67, H 3.42, N 48.37 %.

S2. Estimation of standard vapor pressure uncertainties

The calculation of standard uncertainties of vapor pressure measurements was partially based on the previously reported process by *Verevkin et al.* [3]. Calculation of combined standard uncertainty includes the uncertainty of mass of the analyte ($u(m_{An})$), mass of the reference material ($u(m_{Ref})$), volumes of calibrated pycnometers for preparation of the standard solutions for analyte $u(V_{Std})$ and reference material $u(V_{Ref})$, uncertainties introduced by standard addition – uncertainty of the syringe calibration $u(V_{Syringe})$ and uncertainty of smallest injection into the sample with a syringe $u(V_{inj})$, GC analysis (for calibration and determination) ($u(HPLC)$), transporting gas volume uncertainty ($u(V_{gas})$), uncertainties of the thermostat $u(T_{Therm})$, saturator $u(T_{Satur})$ and ambient $u(T_{Amb})$ temperatures uncertainties ($u(T)$). Here an example of uncertainty calculation for vapor pressures for TNX are provided:

$$u_r(p) = \frac{u(p)}{p}$$

$$u_r(m, mass) = \sqrt{u_r^2(m_{An}) + u_r^2(m_{Ref})} = \sqrt{(\frac{0.0001\ g}{0.0488\ g})^2 + (\frac{0.0001\ g}{0.0965\ g})^2} = 0.002$$

$$u_r(V, pycnometers) = \sqrt{u_r^2(V_{An}) + u_r^2(V_{Ref})} = \sqrt{(\frac{0.01\ ml}{100\ ml})^2 + (\frac{0.01\ ml}{100\ ml})^2} = 0.00014$$

$$u_r(V, standard\ addition) = \sqrt{u_r^2(V_{Syringe}) + u_r^2(V_{inj})} = \sqrt{\left(\frac{0.01\ \mu l}{100\ \mu l}\right)^2 + \left(\frac{0.1\ \mu l}{24\ \mu l}\right)^2}$$
$$= 0.0047$$

$$u_r(HPLC) = \sqrt{u_r^2(calibr) + u_r^2(analysis)} = \sqrt{0.01^2 + 0.01^2} = 0.014$$

$$u_r(T, temperature) = \sqrt{u_r^2(T_{Amb}) + u_r^2(T_{Therm}) + u_r^2(T_{Satur})}$$
$$= \sqrt{\left(\frac{0.2\ K}{298.15\ K}\right)^2 + \left(\frac{0.2\ K}{312.55\ K}\right)^2 + \left(\frac{0.01\ K}{312.55\ K}\right)^2} = 0.0009$$

$$Combined\ standard\ uncertainty\ u_r$$
$$= \sqrt{u_r^2(m) + u_r^2(V, pycnometers) + u_r^2(V, standard\ addition) + u_r^2(HPLC) + u_r^2(T)}$$
$$= 0.0206 = 2.06\%$$

S3. HPLC/DAD parameters

3.1 RDX

HPLC	*Shimadzu Prominence*® with LC-20AD pump module and SPD-M20A Diode Array Detector; software *LabSolutions v*5.86
Analytical column	*Phenomenex Kinetex*® (2.6 µm Biphenyl, 100 Å, 150 × 4.6 mm)
Oven temperature:	40°C
Program	
RDX	Injection volume: 1 µL Total Flow: 0.60 mL/min Mobile phase: 55 % MeCN, 45 % Water Time: 10 min Channel 1 wavelength: 240 nm (RDX) Retention time 1: 3.90 min Channel 2 wavelength: 266 nm (standard, naphthalene) Retention time 2: 7.03 min

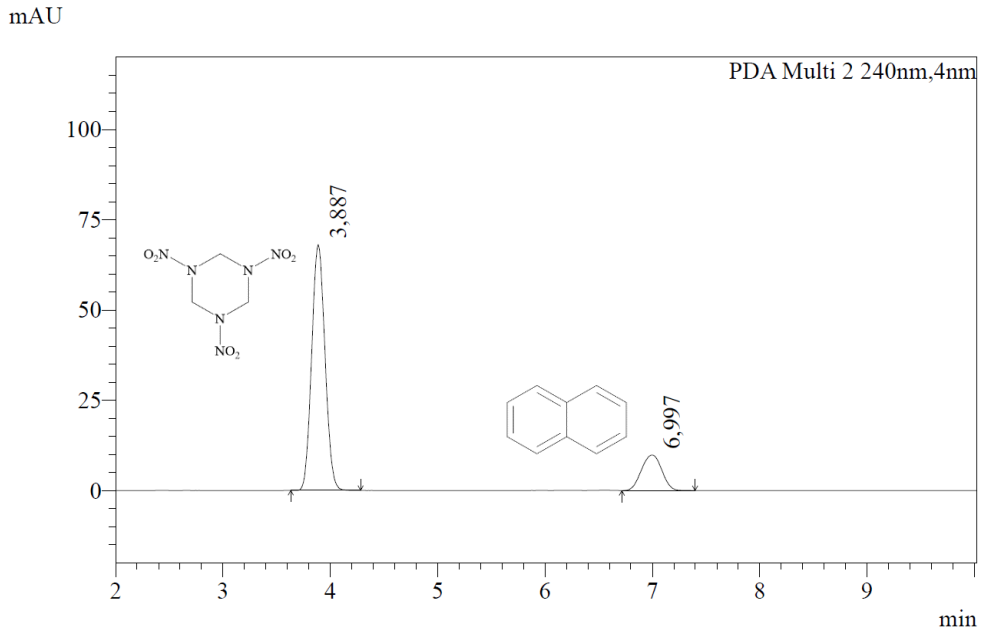

Figure S4. Chromatogram of RDX (retention time 3.887 min) and naphthalene (retention time 6.997 min), measured with a method, described in S3.1 (240 nm).

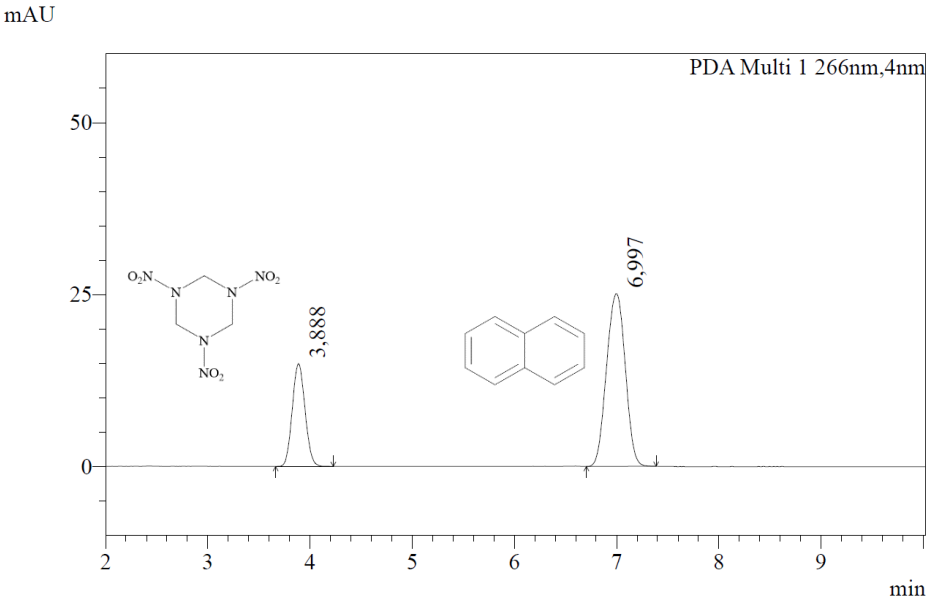

Figure S5. Chromatogram of RDX (retention time 3.887 min) and naphthalene (retention time 6.997 min), measured with a method, described in S3.1 (266 nm).

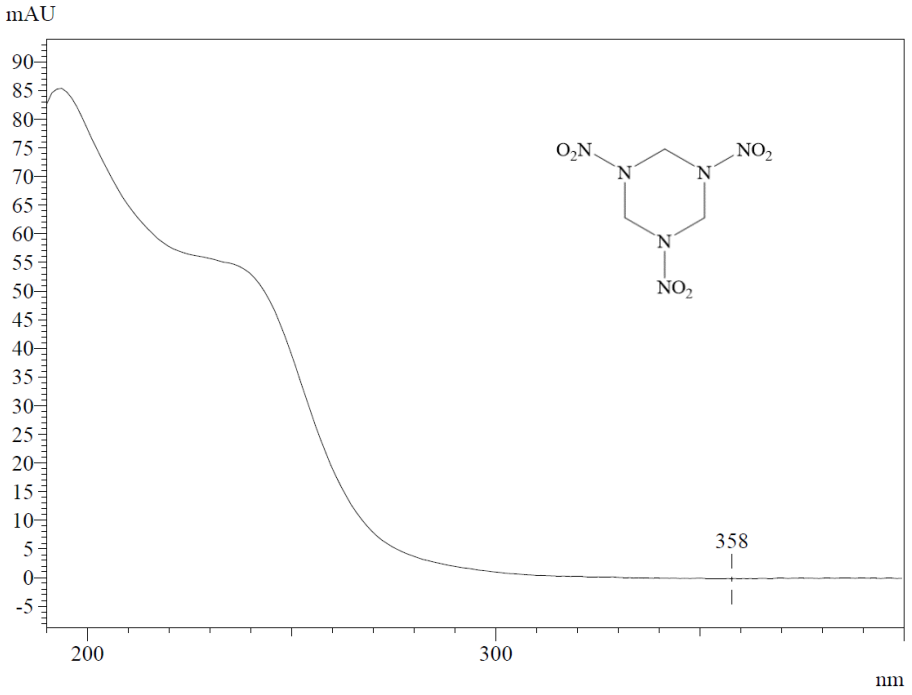

Figure S6. Absorption spectrum of RDX (retention time 3.887 min) measured with a method, described in S3.1.

3.2 TNX

HPLC	*Shimadzu Promenence*® with LC-20AD pump module and SPD-M20A Diode Array Detector; software *LabSolutions v*5.86
Analytical column	*Phenomenex Kinetex*® (2.6 µm Biphenyl, 100 Å, 150 × 4.6 mm)
Oven temperature:	40°C
Program	
TNX	Injection volume: 1 µL Total Flow: 1.00 mL/min Mobile phase: 15 % MeCN, 85 % Water

Time: 10 min
Channel 1 wavelength: 233 nm (TNX)
Retention time 1: 9.04 min
Channel 2 wavelength: 266 nm (standard, 1-nitro-pyrazole)
Retention time 2: 5.20 min

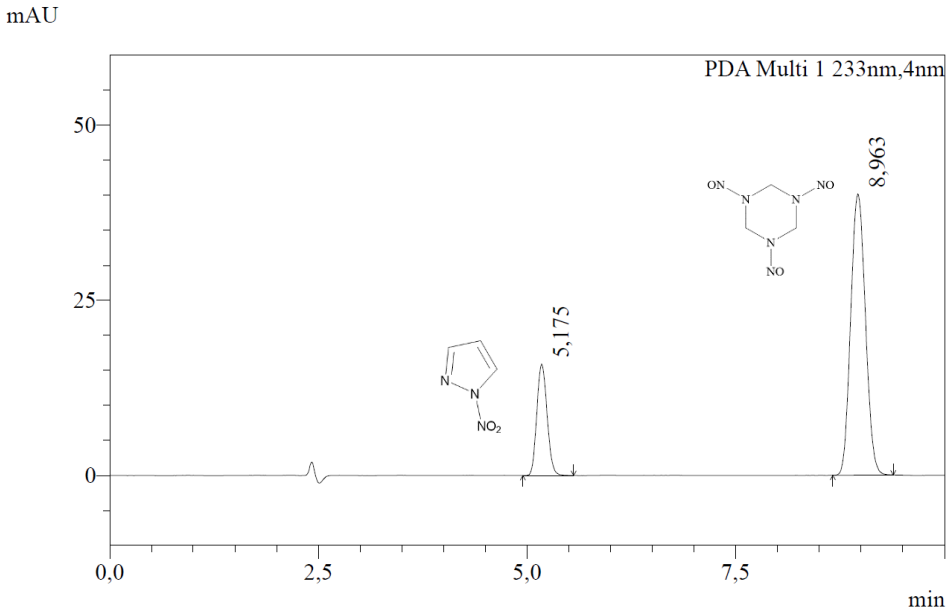

Figure S6. Chromatogram of TNX (retention time 8.963 min) and 1-nitro-pyrazole (retention time 5.175 min), measured with a method, described in S3.2 (233 nm).

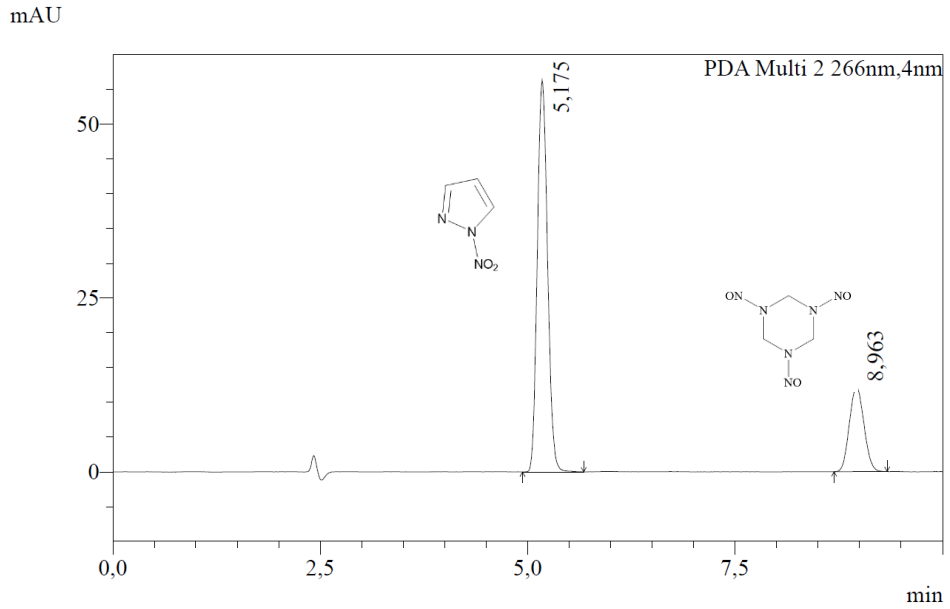

Figure S7. Chromatogram of TNX (retention time 8.963 min) and 1-nitro-pyrazole (retention time 5.175 min), measured with a method, described in S3.2 (266 nm).

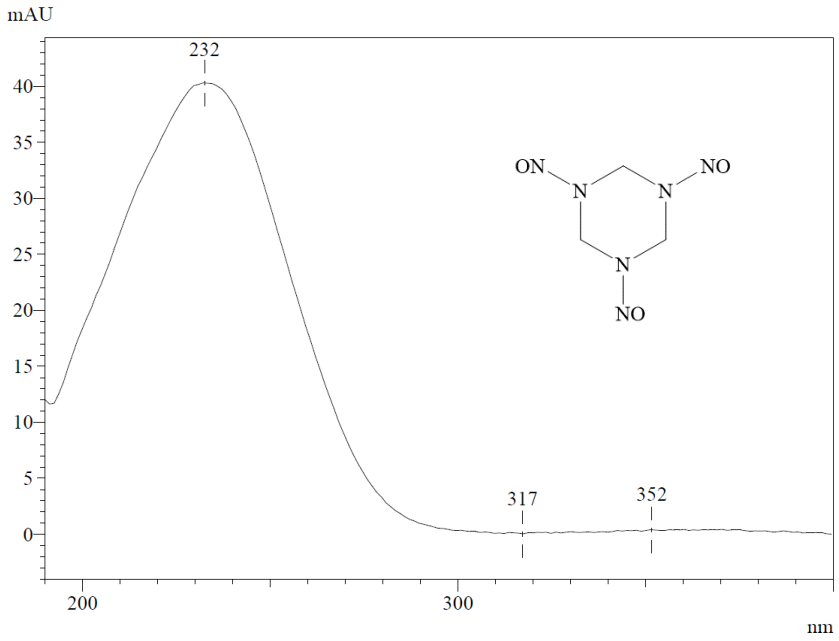

Figure S8. Absorption spectrum of TNX (retention time 8.963 min) measured with a method, described in S3.2.

References

[1] S.A. Rothstein, P. Dubé, S.R. Anderson, Propellants Explos. Pyrotech. 42 (2017) 126-130.
[2] A.T. Nielsen, D.W. Moore, M.D. Ogan, R.L. Atkins, J. Org. Chem. 44 (1979) 1678-1684.
[3] V.N. Emel'yanenko, S.P. Verevkin, J. Chem. Thermodyn. 85 (2015) 111-119.

5.3.Measurements of NENAs (Article 3)

Article 3: Thermodynamic Properties of Energetic Plasticizers: Experimental Vapor Pressures of Methyl-, Ethyl-, and Butyl-Nitroxyethyl Nitramines

The results were published in *Journal of Chemical and Engineering Data* [76] and are reprinted with permission. Copyright (2021) American Chemical Society. DOI: doi.org/10.1021/acs.jced.0c01014.

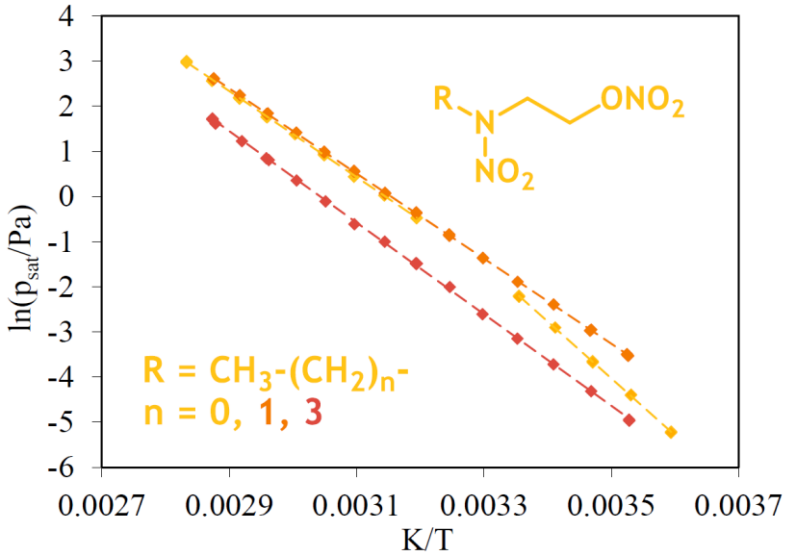

Figure 25. Graphical abstract from the Article 3 [76].

Journal of Chemical&Engineering Data

pubs.acs.org/jced Article

Thermodynamic Properties of Energetic Plasticizers: Experimental Vapor Pressures of Methyl-, Ethyl-, and Butyl-Nitroxyethyl Nitramines

Greta Bikelytė, Martin A. C. Härtel, Marcel Holler, Andreas Neuer, and Thomas M. Klapötke*

Cite This: https://doi.org/10.1021/acs.jced.0c01014 Read Online

ACCESS | Metrics & More | Article Recommendations | Supporting Information

ABSTRACT: In this work, experimental vapor pressures of the commonly used energetic plasticizers methyl-NENA, ethyl-NENA, and butyl-NENA were measured for the first time with a transpiration method. The $p-T$ fitting equations and the corresponding molar enthalpies of phase transitions at 298.15 K are reported: the molar enthalpies of sublimation and vaporization of methyl-NENA were measured to be 104.5 ± 0.9 and 82.0 ± 1.1 kJ·mol^{-1}, respectively. The consistency of these results was examined by the differential scanning calorimetry experiment, which yielded the molar enthalpy of fusion at 298.15 K to be 23.8 ± 0.3 kJ·mol^{-1}. The molar enthalpies of vaporization at 298.15 K for ethyl- and butyl-NENAs were derived to be 79.8 ± 0.4 and 85.9 ± 0.5 kJ·mol^{-1}, respectively. The $p-T$ fitting equations were extrapolated at 298.15 K, and the corresponding results were reported in this work.

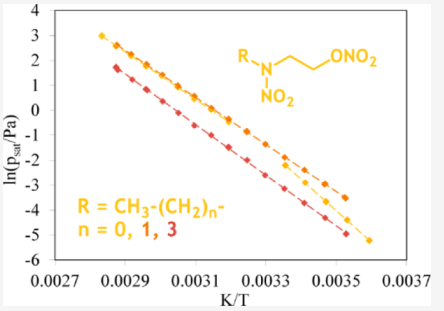

1. INTRODUCTION

In the applications of energetic materials, plasticizers are essential for successful functioning of many different systems.

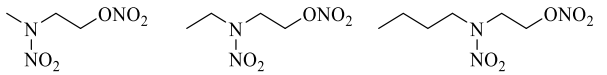

Figure 1. Chemical structures of compounds under investigation: Me-NENA, Et-NENA, and Bu-NENA.

In gun propellants, they allow the gelation of nitrocellulose (NC) and production of extruded or cast grains. In the field of cast-cured materials such as explosive charges for warheads or composite rocket propellant grains, plasticizers fulfill multiple purposes: during mixing and casting, they reduce the viscosity of the formulation. After curing, the elasticity of the rubbery material is considerably improved even at temperatures below −50 °C.[1] Handling and use of energetic systems in extremely low temperature conditions is an important standard requirement that can hardly be attained without plasticizers.

A rather narrow selection of substances is being implemented as plasticizers for energetic materials on industrial scale.[2] Typical energetic plasticizers are nitrate esters. Nitrate esters release significant amounts of energy during combustion and decompose to products of low molecular weight, which raises performance parameters such as specific impulse or impetus in comparison to inert plasticizers. The downsides of nitrate esters include their inherent and self-accelerating instability in combination with high sensitivity to impact, friction, and heat, which make them quite dangerous to handle. In addition, they possess a tendency to migrate slowly within and even out of the final product and are generally toxic.[3,4]

In search of a replacement for nitrate ester plasticizers, a series of different concepts have been investigated.[2,5−9] Among the most promising families of substances are molecules with a 2-nitroxyethyl nitramine functionality, commonly named NENA.[10−15] A series of NENAs with different alkyl chains have been elucidated and is commercially available. By choosing the length of the alkyl chain, properties such as heat of formation, sensitivity, or melting point can be adjusted. The most commonly used on an industrial scale are methyl-, ethyl-, and butyl-NENAs—in pure form or as the eutectic mixture of 58% Me-NENA and 42% Et-NENA, also called MEN-42. Bu-NENA and MEN-42 show excellent plasticizing capabilities for NC and polymers such as glycidyl azide polymer (GAP), polyesters, or polyethers. In contrast to nitrate esters, they are less toxic and slightly less sensitive to shock and friction while providing improved mechanical properties and comparable performance.[11,15,16] A prominent example of commercial use of NENAs lies in the development of smoke-free, high-performance rocket propellants based on nitramines incorporated in GAP.[17] By utilizing Bu-NENA or

Received: December 3, 2020
Accepted: March 3, 2021

Table 1. Mass Fraction Purity P_{An} of the Compounds Investigated in This Work as Determined by the ^{1}H-qNMR Technique

substance	IUPAC name	CAS #	source	stated purity	$P_{An} \pm U(P_{An})^a$
Me-NENA	methyl-(nitro)[2-(nitrooxy)ethyl]amine	17096-47-8	Bayern-Chemie	"100%"	1.003 (±0.005)
Et-NENA	ethyl-(nitro)[2-(nitrooxy)ethyl]amine	85068-73-1	Bayern-Chemie	"100%"	0.975 (±0.004)
Bu-NENA	butyl-(nitro)[2-(nitrooxy)ethyl]amine	82486-82-6	Bayern-Chemie	"100%"	0.989 (±0.004)

[a]Expanded uncertainties are reported with a confidence level of 0.95 (k = 2).

MEN-42, the low-temperature properties of the GAP binder could be greatly improved while obtaining promising safety and performance characteristics. Additionally, NC-based gun propellants with Bu-NENA are reported to exhibit improved energetics, insensitivity, and mechanical properties.[11]

During the manufacturing process of composite rocket propellants, the propellant slurry is mixed for extended periods of time and finally cast at elevated temperatures while applying vacuum to the machinery. This prohibits the entrapment of gasses in the final propellant.[1] To avoid unwanted extraction of components and changes in the formulation, it must be assured that the substances used show a vapor pressure low enough not to evaporate in significant amounts during processing. Regardless, there is a scarcity of available literature data regarding the volatility of alkyl-NENA compounds: a sole study that discusses the volatility of alkyl-NENAs is a work by Cartwright[10] and it lacks any absolute values of the experimental data. Hence, this work is focused on the determination of reliable experimental vapor pressures and the corresponding thermodynamic properties of three of the most widely used alkyl-NENA compounds (Figure 1): Me-NENA, Et-NENA, and Bu-NENA. For this purpose, the transpiration (gas saturation) method was employed.

2. EXPERIMENTAL SECTION

2.1. Materials. All the compounds investigated in this study were obtained by donation from the company Bayern-Chemie GmbH. The purity of the compounds used in this study was tested by elemental analysis and ^{1}H-qNMR techniques. Purity determined with the ^{1}H-qNMR technique is reported in Table 1. For further information on purity assessment, please see the Supporting Information.

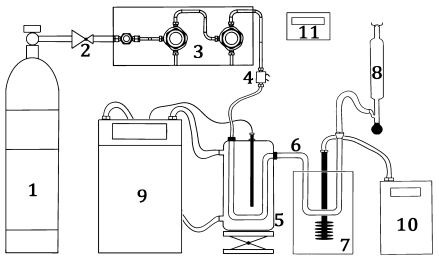

Figure 2. Transpiration method experimental set-up: nitrogen reservoir (1), pressure reduction valve (2), drying module (3), mass flow controller (4), saturator (5), condensation tube (6), cooling trap (7), soap film flow meter (8), thermostat (9), immersion cooler (10), and thermobarometer (11).

2.2. Transpiration Method. The vapor pressure of the compounds of interest was measured using the transpiration (gas saturation) method. The experimental set-up of this method is depicted in Figure 2. For the validation of the experimental set-up, several reference materials of well-defined vapor pressures were measured, and the results were reported previously.[18]

Table 2. Estimated Molar Heat Capacities $C^\circ_{p,m}$(l/cr) and Their Differences $\Delta^g_{l/cr}C^\circ_{p,m}$ of Alkyl-NENA Compounds (T = 298.15 K)

compound	$C^\circ_{p,m}$(cr)[a]	$-\Delta^g_{cr}C^\circ_{p,m}$[b]	$C^\circ_{p,m}$(l)[a]	$-\Delta^g_{l}C^\circ_{p,m}$[c]
	J·mol^{-1}·K^{-1}	J·mol^{-1}·K^{-1}	J·mol^{-1}·K^{-1}	J·mol^{-1}·K^{-1}
Me-NENA	208.9	32.1	274.2	81.9
Et-NENA			305.7	90.1
Bu-NENA			337.2	98.3

[a]Calculated according to the empirical increment approach by Hurst and Harrison.[19] [b]Calculated by $-\Delta^g_{cr}C^\circ_{p,m} = 0.75 + C^\circ_{p,m}(cr) \times 0.15$.[20] [c]Calculated by $-\Delta^g_{l}C^\circ_{p,m} = 10.58 + C^\circ_{p,m}(l) \times 0.26$.[20]

The core of the experimental set-up is a custom-made cylindrical glass vessel—saturator (**5**), which contains an inner channel and an outer chamber. The inner channel was filled with around 35 g of small glass beads mixed with 0.5−1 g of analyte. During the transpiration experiment, the carrier gas (**1**, nitrogen, Air Liquide, Stickstoff HG Flüssig, 99.999 vol % purity, <3 ppm O_2/H_2O) flowed through a pressure reduction valve (**2**) and a gas-drying module (**3**, Swagelok, consisting of one T-type particulate filter SS-4TF-05 and two SS-FCB coalescing particle filters) and entered the inner chamber of the saturator (**5**). The flow rate of the carrier gas was controlled by a mass flow controller (**4**, Natec Sensors GmbH, MC-100 CCM) and determined with a soap film flow meter (**8**, Hewlett Packard, no. 0101-0113). In the inner channel, the flowing (now purified) carrier gas reached the state of saturation with the vapors of the analyte. The outer chamber of the saturator (**5**) was filled with thermal fluid (ethylene glycol, 50% aqueous), and its temperature was controlled by a thermostat (**9**, Huber, Ministat 230 with external class A PT-100 temperature sensor). The ambient conditions were determined with a thermobarometer (**11**, Greisinger, GFTB 200). For a defined interval of time, the transported saturated vapors of the analyte were collected in a condensation tube (**6**), which was placed in a cooling trap (**7**, isopropanol, 243 K) and cooled by an immersion cooler (**10**, Huber, TC45E). The amount of analyte collected in the condensation tube was quantified using chromatographic techniques: vacuum outlet−gas chromatography/mass spectrometry (GC/MS) (Shimadzu, GC/MS QP2010SE) or high-performance liquid chromatography-diode array detection (HPLC-DAD) (Shimadzu, Prominence with an LC-20AD pump module and a SPDM20A Diode Array Detector) by means of internal standard calibration. Chromatographic conditions and methods are detailed in the Supporting Information.

The absolute values of vapor pressure p_{sat} at the temperature of the saturator T can be calculated using the ideal gas law

$$p_{sat}(T) = \frac{mRT_{amb}}{MV_{amb}} \quad (1)$$

where p_{sat} is the vapor pressure of the analyte, in Pa; T is the temperature of the saturator, in K; m is the mass of the analyte collected in the condenser tube, in kg; T_{amb} is the ambient

https://doi.org/10.1021/acs.jced.0c01014
J. Chem. Eng. Data XXXX, XXX, XXX−XXX

Table 3. Experimental Conditions Resulting in Absolute Vapor Pressures p_{sat} and Thermodynamic Properties of Sublimation (Molar Enthalpy of Sublimation $\Delta^g_{cr}H^\circ_m$ and Molar Entropy of Sublimation $\Delta^g_{cr}S^\circ_m$) Obtained from the Measurements of Me-NENA by the Transpiration Method[g]

Me-NENA: $\Delta^g_{cr}H^\circ_m$ (298.15 K) = 104.5 ± 0.9 kJ·mol^{-1}

$$\ln p_{sat}/p^0 = \frac{364.3}{R} - \frac{114056.2}{RT} - \frac{32.1}{R}\ln\frac{T}{298.15K}$$

T[a]	m[b]	V_{N2}[c]	T_{amb}[d]	flow	p_{sat}[e]	$u(p_{sat})$[f]	$\Delta^g_{cr}H^\circ_m(T)$	$\Delta^g_{cr}S^\circ_m(T)$
K	mg	dm^3	K	dm^3·h^{-1}	mPa	mPa	kJ·mol^{-1}	J·mol^{-1}·K^{-1}
278.2	0.03	85	295.0	3.6	5.35	0.11	105.1	238.60
278.3	0.03	71	295.3	3.0	5.47	0.11	105.1	238.78
278.3	0.02	62	295.1	2.6	5.34	0.11	105.1	238.56
283.2	0.06	68	295.6	3.6	12.4	0.3	105.0	238.45
283.2	0.05	66	295.6	3.6	12.2	0.3	105.0	238.26
288.1	0.03	16	294.8	3.6	25.3	0.5	104.8	237.48
288.1	0.14	78	295.3	3.6	25.7	0.5	104.8	237.60
288.1	0.04	21	296.1	3.6	26.1	0.5	104.8	237.73
293.1	0.03	7.3	295.8	3.6	54.8	1.1	104.7	237.20
298.1	0.04	4.8	295.5	3.6	109.5	2.3	104.5	236.46
298.1	0.10	13	295.1	3.6	108.5	2.3	104.5	236.39
298.1	0.04	5.1	295.9	3.6	111.1	2.3	104.5	236.57

[a]Saturation temperature [$u(T)$ = 0.1 K]. [b]Mass of the transferred sample condensed at 243 K. [c]Volume of nitrogen [$u(V)$ = 0.005 dm^3] used to transfer m [$u(m)/m$ = 0.015] of the sample. [d]T_{amb} is the temperature of the soap film flow meter used for the measurement of the gas flow. [e]Vapor pressure at temperature T, calculated from m, and residual vapor pressure at the condensation temperature, calculated by an iteration procedure; p° = 1 Pa. [f]Relative standard uncertainty with confidence level 0.68 (k = 1) for p was calculated to be $u(p)/p$ = 0.0208 (see the Supporting Information). [g]Experimental conditions: T—saturation temperature, m—mass of the transferred sample, V_{N_2}—volume of the carrier gas, and T_{amb}—ambient temperature. [h]The uncertainties for T, V, and m are standard uncertainties. The uncertainty of the molar enthalpy of sublimation is the standard uncertainty with a confidence level of 0.68 (k = 1), calculated including uncertainties of vapor pressure, uncertainties from the fitting equation, and the uncertainty of temperature adjustment to T = 298.15 K. Detailed information on the methods of calculations was published previously.[21,22]

temperature, in K; R is the universal gas constant 8.314462, in J·mol^{-1}·K^{-1}; M is the molecular weight, in kg·mol^{-1}; and V_{amb} is the volume of the carrier gas measured at ambient conditions, in m^3.

Equation 1 is valid under the assumption that the volume of the analyte (V_a) in the gaseous phase is negligibly small in comparison to the volume of the carrier gas (V_{N_2}) and the validity of Dalton's law of partial pressures (eq 2).

$$V_{N_2} \gg V_a; \qquad \text{in } V_{amb} = V_{N_2} + V_a \tag{2}$$

where V_a is the volume of the analyte, in m^3, and V_{N_2} is the volume of the carrier gas, in m^3.

These assumptions allow the determination of V_{amb} from the flow rate of the carrier gas stream and the duration of the measurement.

The resulting experimental $p-T$ values are fitted according to eq 3

$$\ln\left(\frac{p_{sat}}{p^\circ}\right) - \frac{\Delta^g_{cr/l}C^\circ_{p,m}}{R}\ln\frac{T}{T_0} = A - \frac{B}{T} \tag{3}$$

where p° is the reference pressure (1 Pa), $\Delta^g_{cr/l}C^\circ_{p,m}$ is the molar heat capacity difference between the crystalline (cr) or liquid (l) and gaseous phase (g) at a constant pressure, in J·mol^{-1}·K^{-1}, T is the temperature, in K, T_0 is the reference temperature, in K, and A/B are the fitting coefficients (A: unitless; B: in K).

The calculation of molar enthalpy of sublimation or vaporization $\Delta^g_{cr/l}C^\circ_m$ at temperature T was performed using eq 4

$$\Delta^g_{cr/l}H^\circ_m(T) = RB + \Delta^g_{cr/l}C^\circ_{p,m}T \tag{4}$$

The molar entropies of vaporization or sublimation were calculated according to eq 5

$$\Delta^g_{cr/l}S^\circ_m(T) = RA \tag{5}$$

The molar heat capacities at a constant pressure $C^\circ_{p,m}$ for all the compounds were not available in the literature and were obtained with the empirical increment approach by Hurst and Harrison.[19] The molar heat capacity differences were obtained by a procedure described by Acree and Chickos.[20] The values are detailed in Table 2.

3. RESULTS AND DISCUSSION

Experimental vapor pressures and thermodynamic characteristics such as molar enthalpies of phase transition $\Delta^g_{cr/l}H^\circ_m(T)$ and molar entropies of phase transition $\Delta^g_{cr/l}S^\circ_m(T)$ are reported in this section, in Tables 3, 4, 6, and 7.

3.1. Me-NENA. The transpiration experiment for the compound Me-NENA was conducted in two different temperature ranges since the compound undergoes phase transition at an ambient temperature range.

3.1.1. Sublimation. The sublimation behavior of Me-NENA was measured in the temperature range of T = 278.2−298.1 K. The collected mass m was determined with an HPLC-DAD device. The absolute vapor pressures p_{sat} and the thermodynamic properties of sublimation obtained by the transpiration method are compiled in Table 3.

3.1.2. Vaporization. The vaporization behavior of Me-NENA was measured in the temperature range of T = 313.0−353.0 K. The collected mass m was determined with the GC/MS device. The absolute vapor pressures p_{sat} and the

https://doi.org/10.1021/acs.jced.0c01014
J. Chem. Eng. Data XXXX, XXX, XXX−XXX

Table 4. Experimental Conditions Resulting in Absolute Vapor Pressures p_{sat} and Thermodynamic Properties of Vaporization (Molar Enthalpy of Vaporization $\Delta_l^g H_m^\circ$ and Molar Entropy of Vaporization $\Delta_l^g S_m^\circ$) Obtained from the Measurements of Me-NENA by the Transpiration Method[g]

Me-NENA: $\Delta_l^g H_m^\circ$ (298.15 K) = 82.0 ± 1.1 kJ·mol^{-1}

$$\ln p_{sat}/p^0 = \frac{340.1}{R} - \frac{106464.1}{RT} - \frac{81.9}{R}\ln\frac{T}{298.15K}$$

T[a]	m[b]	V_{N2}[c]	T_{amb}[d]	flow	p_{sat}[e]	$u(p_{sat})$[f]	$\Delta_l^g H_m^\circ(T)$	$\Delta_l^g S_m^\circ(T)$
K	mg	dm^3	K	dm^3·h^{-1}	Pa	Pa	kJ·mol^{-1}	J·mol^{-1}·K^{-1}
313.0	0.04	1.06	296.2	4.2	0.624	0.013	80.83	158.6
313.0	0.05	1.21	296.3	4.8	0.623	0.013	80.83	158.5
313.1	0.04	0.91	296.5	3.6	0.618	0.013	80.82	158.5
318.1	0.08	1.21	295.8	4.8	1.02	0.02	80.41	157.3
323.0	0.13	1.21	296.1	4.8	1.55	0.03	80.01	155.6
328.0	0.21	1.21	297.5	4.8	2.59	0.05	79.61	154.9
328.0	0.17	1.01	296.0	4.0	2.49	0.05	79.60	154.6
328.0	0.17	1.01	296.1	4.0	2.53	0.05	79.60	154.6
333.0	0.24	0.91	297.7	3.6	3.98	0.08	79.20	153.6
333.0	0.32	1.21	296.4	4.8	3.99	0.08	79.19	153.6
337.9	0.35	0.91	297.5	3.6	5.80	0.12	78.79	152.1
338.0	0.47	1.21	296.1	4.8	5.83	0.12	78.78	152.0
342.9	0.53	0.90	297.6	3.6	8.72	0.18	78.38	150.9
343.0	0.73	1.21	297.2	4.9	8.95	0.19	78.37	151.0
348.1	1.05	1.21	297.5	4.8	12.9	0.3	77.96	149.6
353.0	1.16	0.86	296.3	3.4	20.1	0.4	77.56	149.0
353.0	1.12	0.86	295.6	3.4	19.4	0.4	77.56	148.6
353.0	1.14	0.86	296.0	3.4	19.7	0.4	77.56	148.8

[a]Saturation temperature [$u(T)$ = 0.1 K]. [b]Mass of the transferred sample condensed at 243 K. [c]Volume of nitrogen [$u(V)$ = 0.005 dm^3] used to transfer m [$u(m)/m$ = 0.015] of the sample. [d]T_{amb} is the temperature of the soap film flow meter used for the measurement of the gas flow. [e]Vapor pressure at temperature T, calculated from m, and residual vapor pressure at the condensation temperature, calculated by an iteration procedure; p° = 1 Pa. [f]Relative standard uncertainty with confidence level 0.68 (k = 1) for p was calculated to be $u(p)/p$ = 0.0210 (see the Supporting Information). [g]Experimental conditions: T—saturation temperature, m—mass of the transferred sample, V_{N_2}—volume of the carrier gas, and T_{amb}—ambient temperature. [h]The uncertainties for T, V, and m are standard uncertainties. The uncertainty of the molar enthalpy of vaporization is the standard uncertainty with a confidence level of 0.68 (k = 1), calculated including uncertainties of vapor pressure, uncertainties from the fitting equation, and the uncertainty of temperature adjustment to T = 298.15 K. Detailed information on the methods of calculations was published previously.[21,22]

Table 5. Compilation of Data on Molar Phase Transition Enthalpies $\Delta_{l/cr}^{g/l} H_m^\circ$ of Me-NENA at the Reference Temperature T_{ref} (p° = 0.1 MPa)

	T_{ref}	$\Delta_{cr}^{l} H_m^\circ(T_{ref})$	$\Delta_l^g H_m^\circ(T_{ref})$	$\Delta_{cr}^{g} H_m^\circ(T_{ref})$
	K	kJ·mol^{-1}	kJ·mol^{-1}	kJ·mol^{-1}
Me-NENA	309.9 ± 0.5[a]	24.4 ± 0.2[a]		
	298.15	23.8 ± 0.3[b]	82.0 ± 1.1[c]	104.5 ± 0.9[c]

[a]Expressed as standard uncertainties, reported above. [b]Standard uncertainty of the temperature adjustment of the molar enthalpy of fusion from the temperature of fusion T_{fus} to the reference temperature introduced an additional estimated uncertainty of one-third of the total adjustment.[20] [c]Expressed as standard uncertainties.

thermodynamic properties of vaporization obtained by the transpiration method are compiled in Table 4.

3.1.3. Data Verification with Enthalpy of Fusion. The validity of the obtained molar enthalpies of phase transitions of Me-NENA could be tested by investigating the relationship between the molar enthalpies of sublimation $\Delta_{cr}^g H_m^\circ$, vaporization $\Delta_l^g H_m^\circ$, and fusion $\Delta_{cr}^l H_m^\circ$, provided that all enthalpies in eq 6 are referenced to the same temperature (the reference temperature is 298.15 K in this work)[23]

$$\Delta_{cr}^l H_m^\circ(T_{ref}) = \Delta_{cr}^g H_m^\circ(T_{ref}) - \Delta_l^g H_m^\circ(T_{ref}) \quad (6)$$

The molar enthalpy of fusion at melting temperature $\Delta_{cr}^l H_m^\circ(T_{fus})$ of Me-NENA was measured with a differential scanning calorimeter (Mettler Toledo 822), which was calibrated with high-purity indium (melting point T_0 = 430.0 K and enthalpy of fusion ΔH_{ref} = 29.0 J·g^{-1}). For all the measurements, an empty crucible was used as a reference. The thermal behavior of Me-NENA was investigated at a heating rate of 5 K·min^{-1} under nitrogen flow. The differential scanning calorimetry (DSC) measurements were repeated twice, the temperature of phase change was determined from the peak onset, and the integration was executed with a straight line for a baseline. The measured values agreed within the experimental uncertainties $u(\Delta_{cr}^l H_m^\circ)$ = 0.2 kJ·mol^{-1} for the molar enthalpy of fusion and $u(T)$ = 0.5 K for the melting temperature (T_{fus}). The measured temperature of fusion (309.9 ± 0.5 K) fits in the wide interval of temperatures reported in the literature (304−314 K).[13,24,25]

The resulting molar enthalpy of fusion at the melting temperature was adjusted to 298.15 K using eq 7

https://doi.org/10.1021/acs.jced.0c01014
J. Chem. Eng. Data XXXX, XXX, XXX−XXX

Table 6. Experimental Conditions Resulting in Absolute Vapor Pressures p_{sat} and Thermodynamic Properties of Vaporization (Molar Enthalpy of Vaporization $\Delta_l^g H_m^\circ$ and Molar Entropy of Vaporization $\Delta_l^g S_m^\circ$) Obtained from the Measurements of Et-NENA by the Transpiration Method[g]

Et-NENA: $\Delta_l^g H_m^\circ$ (298.15 K) = 79.8 ± 0.4 kJ·mol^{-1}

$$\ln p_{sat}/p^0 = \frac{342.1}{R} - \frac{106649.2}{RT} - \frac{90.1}{R}\ln\frac{T}{298.15K}$$

T[a]	m[b]	V_{N2}[c]	T_{amb}[d]	flow	p_{sat}[e]	$u(p_{sat})$[f]	$\Delta_l^g H_m^\circ(T)$	$\Delta_l^g S_m^\circ(T)$
K	mg	dm^3	K	dm^3·h^{-1}	Pa	Pa	kJ·mol^{-1}	J·mol^{-1}·K^{-1}
283.6	0.14	65.0	298.4	3.6	0.0293	0.0006	81.1	160.94
283.7	0.15	68.6	296.0	3.6	0.0298	0.0006	81.1	160.93
283.7	0.09	38.9	295.6	2.4	0.0304	0.0007	81.1	161.02
288.3	0.30	79.8	298.0	4.8	0.0523	0.0011	80.7	159.57
288.5	0.30	80.1	295.6	4.8	0.0513	0.0011	80.7	159.18
293.3	0.08	12.0	297.8	4.8	0.0915	0.0020	80.2	157.90
298.3	0.08	7.5	298.0	4.8	0.151	0.003	79.8	156.04
303.2	0.10	5.4	296.0	4.7	0.255	0.006	79.3	154.59
303.2	0.08	4.3	297.6	4.8	0.257	0.006	79.3	154.65
308.1	0.10	3.3	296.0	4.7	0.418	0.009	78.9	153.07
308.1	0.10	3.3	296.1	4.7	0.433	0.009	78.9	153.36
308.2	0.12	4.0	296.6	4.8	0.428	0.009	78.9	153.19
313.1	0.08	1.6	297.8	4.8	0.690	0.015	78.4	151.72
313.1	0.08	1.6	299.7	4.8	0.705	0.015	78.4	151.88
313.2	0.22	4.4	298.8	4.8	0.696	0.015	78.4	151.70
318.0	0.13	1.7	296.1	4.7	1.06	0.02	78.0	150.09
318.0	0.13	1.7	296.1	4.7	1.07	0.02	78.0	150.12
318.0	0.13	1.7	296.1	4.7	1.09	0.02	78.0	150.26
322.9	0.18	1.4	297.1	4.7	1.74	0.04	77.6	149.01
323.0	0.15	1.2	296.6	4.7	1.77	0.04	77.5	149.10
323.1	0.15	1.2	299.0	4.8	1.74	0.04	77.5	148.94
327.9	0.23	1.2	297.5	4.7	2.68	0.06	77.1	147.62
328.0	0.23	1.2	296.6	4.7	2.70	0.06	77.1	147.62
328.0	0.23	1.2	298.5	4.8	2.67	0.06	77.1	147.47
332.7	0.36	1.2	295.8	4.7	4.13	0.09	76.7	146.50
337.7	0.58	1.3	296.0	4.7	6.32	0.14	76.2	145.28
338.0	0.54	1.2	299.9	4.8	6.25	0.13	76.2	145.00
342.8	0.82	1.2	300.0	4.8	9.46	0.20	75.8	143.93
347.7	0.88	0.9	296.5	3.5	13.71	0.30	75.3	142.67
347.7	0.89	0.9	300.3	3.6	13.69	0.30	75.3	142.63
347.8	0.87	0.9	300.2	3.6	13.40	0.29	75.3	142.43
347.9	1.17	1.2	299.1	4.8	13.47	0.29	75.3	142.40

[a]Saturation temperature [$u(T)$ = 0.1 K]. [b]Mass of the transferred sample condensed at 243 K. [c]Volume of nitrogen [$u(V)$ = 0.005 dm^3] used to transfer m [$u(m)/m$ = 0.015] of the sample. [d]T_{amb} is the temperature of the soap film flow meter used for the measurement of the gas flow. [e]Vapor pressure at temperature T, calculated from m, and residual vapor pressure at the condensation temperature, calculated by an iteration procedure; p° = 1 Pa. [f]Relative standard uncertainty with confidence level 0.68 (k = 1) for p was calculated to be $u(p)/p$ = 0.0216 (see the Supporting Information). [g]Experimental conditions: T—saturation temperature, m—mass of the transferred sample, V_{N_2}—volume of the carrier gas, and T_{amb}—ambient temperature. [h]The uncertainties for T, V, and m are standard uncertainties. The uncertainty of the molar enthalpy of vaporization is the standard uncertainty with a confidence level of 0.68 (k = 1), calculated including uncertainties of vapor pressure, uncertainties from the fitting equation, and the uncertainty of temperature adjustment to T = 298.15 K. Detailed information on the methods of calculations was published previously.[21,22]

$$\Delta_{cr}^{l} H_m^\circ(T_{ref}/\mathrm{K})/(\mathrm{J\cdot mol^{-1}}) = \Delta_{cr}^{l} H_m^\circ(T_{fus}/\mathrm{K})/(\mathrm{J\cdot mol^{-1}}) - [(\Delta_{cr}^{g} C_{p,m}^\circ/\mathrm{J\cdot K^{-1}\cdot mol^{-1}}) - (\Delta_{l}^{g} C_{p,m}^\circ/\mathrm{J\cdot K^{-1}\cdot mol^{-1}})]\cdot[(T_{fus}/\mathrm{K}) - (T_{ref}/\mathrm{K})] \quad (7)$$

The results are presented in Table 5.

The calculation according to eq 6, $\Delta_{cr}^{l} H_m^\circ$ (298.15 K) = 104.5 ± 0.9 kJ·mol^{-1} −82.0 ± 1.1 kJ·mol^{-1} = 22.5 ± 1.4 kJ·mol^{-1}, shows an agreement (within the combined experimental uncertainty) with the individually measured calorimetric value of $\Delta_{cr}^{l} H_m^\circ$(298.15 K) = 23.8 ± 0.3 kJ·mol^{-1}. The agreement of the results supports the consistency of the molar phase transition enthalpies for Me-NENA achieved in this work (Tables 3 and 4).

3.2. Et-NENA. The vaporization behavior of Et-NENA was measured in the temperature range of T = 283.6−347.9 K. The collected mass m was determined with the GC/MS device. The absolute vapor pressures p_{sat} and the thermodynamic properties of vaporization obtained by the transpiration method are compiled in Table 6.

3.3. Butyl-NENA. The vaporization behavior of Bu-NENA was measured in the temperature range of T = 283.4 to 348.0 K. The collected mass m was determined with the HPLC-DAD

https://doi.org/10.1021/acs.jced.0c01014
J. Chem. Eng. Data XXXX, XXX, XXX−XXX

Table 7. Experimental Conditions Resulting in Absolute Vapor Pressures p_{sat} and Thermodynamic Properties of Vaporization (Molar Enthalpy of Vaporization $\Delta_l^g H_m^\circ$ and Molar Entropy of Vaporization $\Delta_l^g S_m^\circ$) Obtained from the Measurements of Bu-NENA by the Transpiration Method[g]

Bu-NENA: $\Delta_l^g H_m^\circ$ (298.15 K) = 85.9 ± 0.5 kJ·mol^{-1}

$$\ln p_{sat}/p^0 = \frac{360.3}{R} - \frac{115222.9}{RT} - \frac{98.3}{R}\ln\frac{T}{298.15K}$$

T[a]	m[b]	V_{N2}[c]	T_{amb}[d]	flow	p_{sat}[e]	$u(p_{sat})$[f]	$\Delta_l^g H_m^\circ(T)$	$\Delta_l^g S_m^\circ(T)$
K	mg	dm^3	K	dm^3·h^{-1}	Pa	Pa	kJ·mol^{-1}	J·mol^{-1}·K^{-1}
283.4	0.02	35	299.9	1.8	0.0070	0.0001	87.4	171.26
283.5	0.05	86	297.7	4.8	0.0070	0.0001	87.4	171.18
283.5	0.03	50	296.9	2.7	0.0071	0.0001	87.4	171.37
288.3	0.03	24	296.6	4.8	0.0134	0.0003	86.9	169.74
293.3	0.03	16	297.9	4.8	0.0242	0.0005	86.4	167.86
298.3	0.02	6.8	298.6	4.8	0.0429	0.0009	85.9	166.08
303.2	0.03	4.5	299.2	4.9	0.074	0.002	85.4	164.28
308.0	0.04	3.2	296.6	4.8	0.135	0.003	84.9	163.37
313.0	0.04	2.0	297.2	4.8	0.226	0.005	84.5	161.73
313.1	0.06	3.3	303.6	4.9	0.225	0.005	84.4	161.60
313.1	0.08	4.4	296.8	4.8	0.227	0.005	84.4	161.62
313.1	0.04	2.0	296.8	4.8	0.224	0.005	84.4	161.52
313.1	0.06	3.2	298.4	4.8	0.228	0.005	84.4	161.66
313.2	0.06	3.2	299.0	4.8	0.228	0.005	84.4	161.61
318.0	0.04	1.2	297.5	4.8	0.368	0.008	84.0	159.95
322.9	0.11	2.4	301.4	4.9	0.541	0.011	83.5	157.68
327.7	0.10	1.3	297.2	4.8	0.897	0.019	83.0	156.66
332.7	0.14	1.2	303.2	4.9	1.43	0.03	82.5	155.26
337.6	0.23	1.2	297.9	4.8	2.24	0.05	82.0	154.01
338.0	0.23	1.2	300.1	4.8	2.34	0.05	82.0	153.90
342.5	0.34	1.2	297.9	4.8	3.41	0.07	81.6	152.63
347.4	0.50	1.2	297.9	4.8	5.03	0.10	81.1	151.08
347.9	0.56	1.2	297.0	4.8	5.54	0.12	81.0	151.38
348.0	0.57	1.2	297.6	4.8	5.64	0.12	81.0	151.47
348.0	0.55	1.2	300.7	4.8	5.51	0.11	81.0	151.27

[a]Saturation temperature [$u(T$ = 0.1 K]. [b]Mass of the transferred sample condensed at 243 K. [c]Volume of nitrogen [$u(V)$ = 0.005 dm^3] used to transfer m [$u(m)/m$ = 0.015] of the sample. [d]T_{amb} is the temperature of the soap film flow meter used for the measurement of the gas flow. [e]Vapor pressure at temperature T, calculated from m, and residual vapor pressure at the condensation temperature, calculated by an iteration procedure; p° = 1 Pa. [f]Relative standard uncertainty with confidence level 0.68 (k = 1) for p was calculated to be $u(p)/p$ = 0.0208 (see the Supporting Information). [g]Experimental conditions: T—saturation temperature, m—mass of the transferred sample, V_{N_2}—volume of the carrier gas, and T_{amb}—ambient temperature. [h]The uncertainties for T, V, and m are standard uncertainties. The uncertainty of the molar enthalpy of vaporization is the standard uncertainty with a confidence level of 0.68 (k = 1), calculated including uncertainties of vapor pressure, uncertainties from the fitting equation, and the uncertainty of temperature adjustment to T = 298.15 K. Detailed information on the methods of calculations was published previously.[21,22]

device. The absolute vapor pressures p_{sat} and the thermodynamic properties of vaporization obtained by the transpiration method are compiled in Table 7.

3.4. Comparison. The experimental $p-T$ data of the compounds of interest are depicted in Figure 3. The corresponding thermodynamic properties are compiled in Table 8.

Evaluation of the experimental $p-T$ data of all the alkyl-NENA compounds, measured in this work, reveals that the vaporization behavior of Me-NENA and Et-NENA is comparable. As can be seen in Table 8, the molar enthalpies of vaporization at 298.15 K for these compounds almost match within the experimental uncertainties. The molar enthalpy of vaporization has been shown to have a linear dependency on the number of carbon atoms in an aliphatic chain.[26,27] This phenomenon explains the increase of the molar enthalpy of vaporization for the Bu-NENA compound in comparison to short-chain length Me-NENA and Et-NENA.

As shown, the absolute vapor pressures of Me- and Et-NENAs are nearly indistinguishable, Et-NENA having slightly higher vapor pressure values. Little to no data is present in the literature to support the observed behavior: no studies report the experimental boiling points since the measurements are hindered by the exothermal decomposition of alkyl-NENA compounds; however, it should be noted that the temperatures of fusion T_{fus} of alkyl-NENA compounds are significantly lowered with every additional carbon atom in the alkyl chain [Me-NENA: 309.9 ± 0.5 K, from this work; Et-NENA: 274–278 K;[28] and Bu-NENA: 245–246 K[28]]. It can be speculated that in the case of a shorter alkyl group, the chemical structure and the corresponding charge distribution in Me-NENA induce an additional dipole moment affecting the intermolecular interactions. In this regard, the behavior of vaporization partially agrees with the results of thermogravimetric analysis (TGA) of alkyl-NENA compounds, reported in the work of Cartwright,[10] which mainly focuses on the volatility of the propellant compositions containing several plasticizers, includ-

https://doi.org/10.1021/acs.jced.0c01014
J. Chem. Eng. Data XXXX, XXX, XXX−XXX

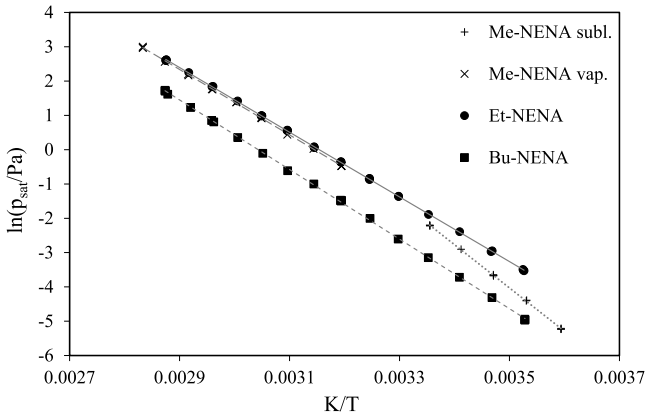

Figure 3. Comparison of the experimental vapor pressure values of alkyl-NENA compounds measured in this work. Here, + and dotted line—Me-NENA, sublimation; × and long dashed line—Me-NENA, vaporization; ● and solid line—Et-NENA; and ■ and dashed line—Bu-NENA.

ing the group of alkyl-NENAs. This work graphically reports the isothermal TGA experiment results on neat alkyl-NENA compounds, not disclosing any absolute values for the mass loss rate. The graph depicts a general vaporization behavior, showing that Et-NENA has a higher mass loss rate than Me-NENA and that agrees with the results of this work. Surprisingly, the same graph also shows that the rate of mass loss for Bu-NENA is higher than that for Me-NENA and that does not align with the results reported in this work. For this reason, the isothermal TGA experiment was repeated here in an attempt to replicate the conditions and data from ref 10. The illustration of the results and experimental conditions are reported in the Supporting Information. In the repeated experiment, Bu-NENA has a significantly lower mass loss rate than the other two compounds analyzed. These observations lead to the assumption that the results of the isothermal TGA experiment in the work of Cartwright[10] might be erroneous in terms of indexing of the analytes in the graph.

4. CONCLUSIONS

In this study, the experimental vapor pressures and the resulting molar enthalpies of phase transitions for alkyl–NENAs were reported for the first time. The thermodynamic properties of compounds Me-NENA, Et-NENA, and Bu-NENA were measured in an ambient temperature range using the transpiration (gas saturation) method.

In the case of Me-NENA, two $p-T$ fitting equations were reported: the sublimation behavior was investigated in the temperature range of 278.2–298.1 K, resulting in the molar enthalpy of sublimation at 298.15 K equal to 104.5 ± 0.9 kJ·mol^{-1}; the vaporization experiments were performed in the temperature range of 313.0–353.0 K with the corresponding molar enthalpy of vaporization at 298.15 K equal to 82.0 ± 1.1 kJ·mol^{-1}. To verify the validity of the derived molar enthalpies of phase transition of Me-NENA, a DSC experiment was performed and the molar enthalpy of fusion at 298.15 K was determined. The resulting value (23.8 ± 0.3 kJ·mol^{-1}) agrees with the derived difference of experimentally determined molar enthalpies of sublimation and vaporization (22.5 ± 1.4 kJ·mol^{-1}) within the experimental uncertainties, confirming the consistency of the experimental results.

For Et-NENA, the $p-T$ fitting equation was reported in the temperature range of 283.6–347.9 K, yielding the molar enthalpy of vaporization at 298.15 K to be 79.8 ± 0.4 kJ·mol^{-1}. In the case of Bu-NENA, the experimental results were reported in the temperature range of 283.4–348.0 K. The resulting enthalpy of vaporization at 298.15 K was derived to be 85.9 ± 0.5 kJ·mol^{-1}.

The results of this study fill an evident gap in the knowledge of the thermodynamic properties of the alkyl-NENA compounds and may assist in the optimization of the manufacturing process of propellant mixtures.

■ ASSOCIATED CONTENT

Supporting Information

The Supporting Information is available free of charge at https://pubs.acs.org/doi/10.1021/acs.jced.0c01014.

Purity assessment of the compound, TGA experiments, and details of the quantification methods (PDF)

■ AUTHOR INFORMATION

Corresponding Author

Thomas M. Klapötke − *Department of Chemistry, Ludwig-Maximilian University of Munich, 81377 Munich, Germany;* orcid.org/0000-0003-3276-1157; Email: tmk@cup.uni-muenchen.de

Authors

Greta Bikelytė − *Department of Chemistry, Ludwig-Maximilian University of Munich, 81377 Munich, Germany;* orcid.org/0000-0001-6305-627X

Table 8. Comparison of Thermodynamic Properties of the Compounds Me-NENA, Et-NENA, and Bu-NENA Obtained in This Work: Vapor Pressure p_{sat} and Molar Enthalpies of Phase Transition $\Delta^{g}_{l/cr}H^{\circ}_{m}$ at the Average Experimental Temperature T_{avg} and at 298.15 K[a]

experiment[b]	T-range	T_{avg}	$\Delta^{g}_{l/cr}H^{\circ}_{m}(T_{avg})$[c]	$\Delta^{g}_{l/cr}H^{\circ}_{m}$ (298.15 K)[c]	p_{sat}[d]
	K	K	kJ·mol^{-1}	kJ·mol^{-1}	mPa
Me-NENA subl.	278.2–298.1	287.6	104.9 ± 0.5	104.5 ± 0.9	112
Me-NENA vap.	313.0–353.0	332.7	79.3 ± 0.3	82.0 ± 1.1	130
Et-NENA	283.6–347.9	315.6	78.4 ± 0.2	79.8 ± 0.4	153
Bu-NENA	283.4–348.0	315.8	84.3 ± 0.2	85.9 ± 0.5	43.1

[a]Subl.: sublimation, vap.: vaporization. [b]Molar enthalpy of sublimation or vaporization at an average temperature. [c]Molar enthalpies of sublimation and vaporization were adjusted according to Acree and Chickos[20] with values of $\Delta^{g}_{l/cr}C^{\circ}_{p,m}$, $C^{\circ}_{p,m}$(cr), and $C^{\circ}_{p,m}$(l) stated in Table 2. Uncertainties for molar enthalpies of phase transition at average and reference temperatures are expressed as standard uncertainties. [d]Vapor pressure at 298.15 K extrapolated from the $p-T$-data using eq 3.

https://doi.org/10.1021/acs.jced.0c01014
J. Chem. Eng. Data XXXX, XXX, XXX−XXX

Martin A. C. Härtel − *Department of Chemistry, Ludwig-Maximilian University of Munich, 81377 Munich, Germany;* orcid.org/0000-0001-8247-5314
Marcel Holler − *Bayern-Chemie GmbH, 84544 Aschau Am Inn, Germany*
Andreas Neuer − *Department of Chemistry, Ludwig-Maximilian University of Munich, 81377 Munich, Germany;* orcid.org/0000-0001-6614-4734

Complete contact information is available at: https://pubs.acs.org/10.1021/acs.jced.0c01014

Notes

The authors declare no competing financial interest.

■ ACKNOWLEDGMENTS

For the financial support of this work, Ludwig-Maximilian University (LMU), the Office of Naval Research (ONR) under grant no. ONR N00014-19-1-2078, the Strategic Environmental Research and Development Program (SERDP) under contract no. W912HQ19C0033, and the DAAD (German Academic Exchange Service) (grant no. 57299294) are gratefully acknowledged. Moreover, we would like to acknowledge the company Bayern-Chemie GmbH for providing the compounds for this study, Elena Reinhardt for great effort with synthetic chemistry, and Maurus Völkl for the help in improving the experimental set-up.

■ REFERENCES

(1) Davenas, A. The Main Families and Use of Solid Propellants. In *Solid Rocket Propulsion Technology*; Davenas, A., Ed.; Pergamon: Amsterdam, 1993; Chapter 8, pp 329−367.
(2) Kumari, D.; Balakshe, R.; Banerjee, S.; Singh, H. Energetic plasticizers for gun & rocket propellants. *Rev. J. Chem.* **2012**, *2*, 240−262.
(3) Vogelsanger, B. Chemical stability, compatibility and shelf life of explosives. *Chimia* **2004**, *58*, 401−408.
(4) Trache, D.; Tarchoun, A. F. Analytical Methods for Stability Assessment of Nitrate Esters-Based Propellants. *Crit. Rev. Anal. Chem.* **2019**, *49*, 415−438.
(5) Badgujar, D. M.; Talawar, M. B.; Zarko, V. E.; Mahulikar, P. P. New directions in the area of modern energetic polymers: An overview. *Combust. Explos. Shock Waves* **2017**, *53*, 371−387.
(6) Damse, R. S.; Singh, A.; Singh, A. Evaluation of energetic plasticisers for solid gun propellant. *Def. Sci. J.* **2008**, *58*, 86.
(7) Ghoroghchian, F.; Bayat, Y.; Abrishami, F. Compatibility of energetic plasticizers with the triblock copolymer of polypropylene glycol-glycidyl azide polymer-polypropylene glycol (PPG-GAP-PPG). *J. Polym. Eng.* **2020**, *40*, 797−805.
(8) Provatas, A. *Energetic Polymers and Plasticisers for Explosive Formulations: A Review of Recent Advances*; DSTO Aeronautical and Maritime Research Laboratory, 2000.
(9) Singh, A.; Radhakrishnan, S.; Vijayalakshmi, R.; Talawar, M. B.; Kumar, A.; Kumar, D. Screening of polymer-plasticizer systems for propellant binder applications: an experimental and simulation approach. *J. Energ. Mater.* **2019**, *37*, 365−377.
(10) Cartwright, R. V. Volatility of NENA and other energetic plasticizers determined by thermogravimetric analysis. *Propellants, Explos. Pyrotech.* **1995**, *20*, 51−57.
(11) Chakraborthy, T. K.; Raha, K. C.; Omprakash, B.; Singh, A. A study on gun propellants based on butyl-NENA. *J. Energ. Mater.* **2004**, *22*, 41−53.
(12) Damse, R. S.; Omprakash, B.; Tope, B. G.; Chakraborthy, T. K.; Singh, A. Study of N-n-butyl-N-(2-nitroxyethyl) nitramine in RDX based gun propellant. *J. Hazard. Mater.* **2009**, *167*, 1222−1225.
(13) Izsák, D.; Klapötke, T. M. Characterization of the Energetic Plasticizer Methyl-NENA. *Z. Anorg. Allg. Chem.* **2011**, *637*, 2135−2141.
(14) Rao, K. P. C.; Sikder, A. K.; Kulkarni, M. A.; Bhalerao, M. M.; Gandhe, B. R. Studies on n-Butyl Nitroxyethylnitramine (n-BuNENA): Synthesis, Characterization and Propellant Evaluations. *Propellants, Explos. Pyrotech.* **2004**, *29*, 93−98.
(15) Yuan, S.; Luo, Y. Mechanical Properties of HTPE/Bu-NENA Binder and the Kinetics of Bu-NENA Evaporation. *Cent. Eur. J. Energ. Mater.* **2020**, *17*, 119.
(16) Lemos, M. F.; Bohn, M. A. DMA of polyester-based polyurethane elastomers for composite rocket propellants containing different energetic plasticizers. *J. Therm. Anal. Calorim.* **2018**, *131*, 595−600.
(17) Deschner, T.; Løkke, E. A.; Kristensen, T. E.; Jensen, T. L.; Unneberg, E. Insensitive Minimum Smoke Propellants for Tactical Missiles In *Insensitive Munition and Energetic Materials Symposium IMEMTS*; IMEMTS: Portland, OR, USA; 2018.
(18) Bikelytė, G.; Härtel, M. A.; Klapötke, T. M.; Krumm, B.; Sadaunykas, A. Experimental thermochemical data of CWA simulants: Triethyl phosphate, diethyl methylphosphonate, malathion and methyl salicylate. *J. Chem. Thermodyn.* **2020**, *143*, 106043.
(19) Hurst, J. E.; Harrison, B. K. Estimation of Liquid and Solid Heat Capacities Using a Modified Kopp's Rule. *Chem. Eng. Commun.* **1992**, *112*, 21−30.
(20) Acree, W.; Chickos, J. S. Phase Transition Enthalpy Measurementsof Organic and Organometallic Compounds. Sublimation, Vaporizationand Fusion Enthalpies From 1880 to 2010. *J. Phys. Chem. Ref. Data* **2010**, *39*, 043101.
(21) Emel'yanenko, V. N.; Verevkin, S. P. Benchmark thermodynamic properties of 1,3-propanediol: Comprehensive experimental and theoretical study. *J. Chem. Thermodyn.* **2015**, *85*, 111−119.
(22) Verevkin, S. P.; Sazonova, A. Y.; Emel'yanenko, V. N.; Zaitsau, D. H.; Varfolomeev, M. A.; Solomonov, B. N.; Zherikova, K. V. Thermochemistry of halogen-substituted methylbenzenes. *J. Chem. Eng. Data* **2014**, *60*, 89−103.
(23) Bikelytė, G.; Härtel, M.; Stierstorfer, J.; Klapötke, T. M.; Pimerzin, A. A.; Verevkin, S. P. Benchmark properties of 2-, 3-and 4-nitrotoluene: Evaluation of thermochemical data with complementary experimental and computational methods. *J. Chem. Thermodyn.* **2017**, *111*, 271−278.
(24) Blomquist, A. T.; Fiedorek, F. T. Nitramines U.S. Patent 2,485,855 A, 1949.
(25) Blomquist, A. T.; Fiedorek, F. T. Process of preparing nitroxy alkyl nitramines U.S. Patent 2,678,946 A, 1954.
(26) Nagrimanov, R. N.; Samatov, A. A.; Nasyrova, T. M.; Buzyurov, A. V.; Mukhametzyanov, T. A.; Schick, C.; Solomonov, B. N.; Verevkin, S. P. Long-chain linear alcohols: Reconciliation of phase transition enthalpies. *J. Chem. Thermodyn.* **2020**, *146*, 106103.
(27) Verevkin, S. P.; Zaitsau, D. H.; Emel'yanenko, V. N.; Yermalayeu, A. V.; Schick, C.; Liu, H.; Maginn, E. J.; Bulut, S.; Krossing, I.; Kalb, R. Making Sense of Enthalpy of Vaporization Trends for Ionic Liquids: New Experimental and Simulation Data Show a Simple Linear Relationship and Help Reconcile Previous Data. *J. Phys. Chem. B* **2013**, *117*, 6473−6486.
(28) Simmons, R. NENAs—New Energetic Plasticizers In *ADPA International Symposium on Energetic Materials Technology*; NENA: Orlando, FL; 1994.

SUPPORTING INFORMATION

Thermodynamic Properties of Energetic Plasticizers: Experimental Vapor Pressures of Methyl-, Ethyl-, and Butyl-Nitroxyethyl Nitramines

Greta Bikelytė,[†] Martin A. C. Härtel,[†] Marcel Holler,[‡] Andreas Neuer,[†] Thomas M. Klapötke[†]*

*e-mail: tmk@cup.uni-muenchen.de

[†]Department of Chemistry

Ludwig-Maximilian University of Munich

Butenandtstr. 5–13, 81377 Munich (Germany)

Homepage: http://www.hedm.cup.uni-muenchen.de

[‡]Bayern-Chemie GmbH

Liebigstrasse 17, Postfach 1131, 84544 Aschau am Inn, Germany

S1. Purity assessment

Elemental analysis (CHNS) was performed with an *Elementar Vario Micro* instrument. ^{1}H-NMR spectra were measured with a *Bruker* AVANCE 400 MHz instrument and the processing was done with *MestReNova* v. 12.0.1-20560 software. The peaks were integrated excluding the sattelites. The ^{1}H-qNMR experiments were executed and results were processed with a procedure, described previously [1]. For these compounds a certified reference material 1,3,5-trimethoxybenzene was used (*Sigma-Aldrich*, Product no. 74599, 99.96% mass fraction purity).

1.1 Purity assessment results

Results of the purity assessment are presented in the following. The peaks used for the purity assessment are marked in the spectra and underlined in the Tables S1-S3.

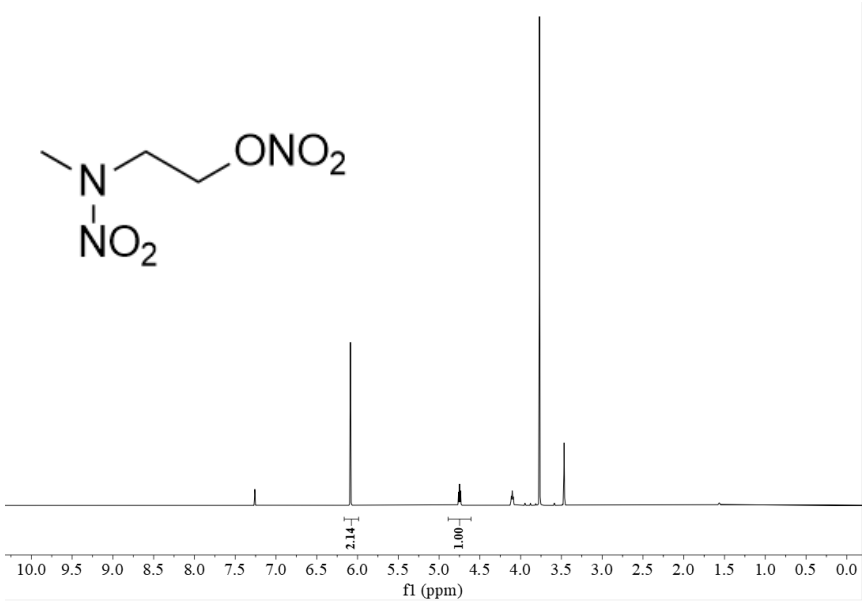

Fig. S1. ^{1}H-NMR spectrum of **Me-NENA.**

Table S1. Results of NMR and EA experiments for **Me-NENA**.

^{1}H – qNMR	($CDCl_3$, 400 MHz): δ = <u>4.74 (t, 2H, O–C*H*$_2$)</u>, 4.10 (t, 2H, N–C*H*$_2$), 3.45 (s, 3H, C*H*$_3$) ppm. 1,3,5-Trimethoxybenzene, **CRM** ($CDCl_3$, 400 MHz): <u>δ = 6.09 (s, 3H, C*H*)</u>, 3.77 (s, 9H, C*H*$_3$).
^{13}C – NMR	($CDCl_3$, 101 MHz): δ = 69.2 (O–*C*H$_2$), 50.3 (N–*C*H$_2$), 40.2 (*C*H$_3$), ppm.
^{14}N – NMR	($CDCl_3$, 29 MHz): δ = -29.5 (N–*N*O$_2$), -46.0 (O–*N*O$_2$) ppm.
EA	Calc.: C 21.82, H 4.27, N 25.25 %; Found: C 21.80, H 4.29, N 25.06 %.

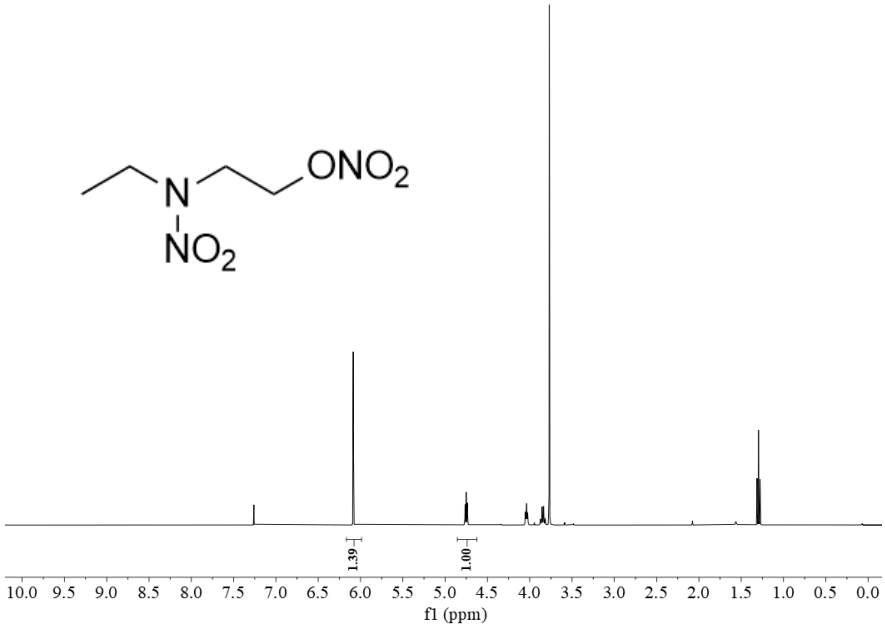

Fig. S2. ^{1}H-NMR spectrum of **Et-NENA.**

Table S2. Results of NMR and EA experiments for **Et-NENA**.

^{1}H – NMR	($CDCl_3$, 400 MHz): δ = 4.73 (t, 2H, O–C*H*$_2$–CH_2), 4.03 (t, 2H, N–C*H*$_2$–CH_2), 3.82 (q, 2H, C*H*$_2$–CH_3), 1.58 (t, 3H, C*H*$_3$) ppm. 1,3,5-Trimethoxybenzene, **CRM** ($CDCl_3$, 400 MHz): δ = 6.09 (s, 3H, C*H*), 3.77 (s, 9H, C*H*$_3$).
^{13}C – NMR	($CDCl_3$, 101 MHz): δ = 69.2 (O–*C*H_2), 48.6 (N–*C*H_2), 48.0 (*C*H_2–CH_3), 11.3 (*C*H_3) ppm.
^{14}N – NMR	($CDCl_3$, 29 MHz): δ = -30.4 (N–*N*O_2), -45.3 (O–*N*O_2) ppm.
EA	Calc.: C 26.82, H 5.06, N 23.46 %; Found: C 27.32, H 5.05, N 23.12 %.

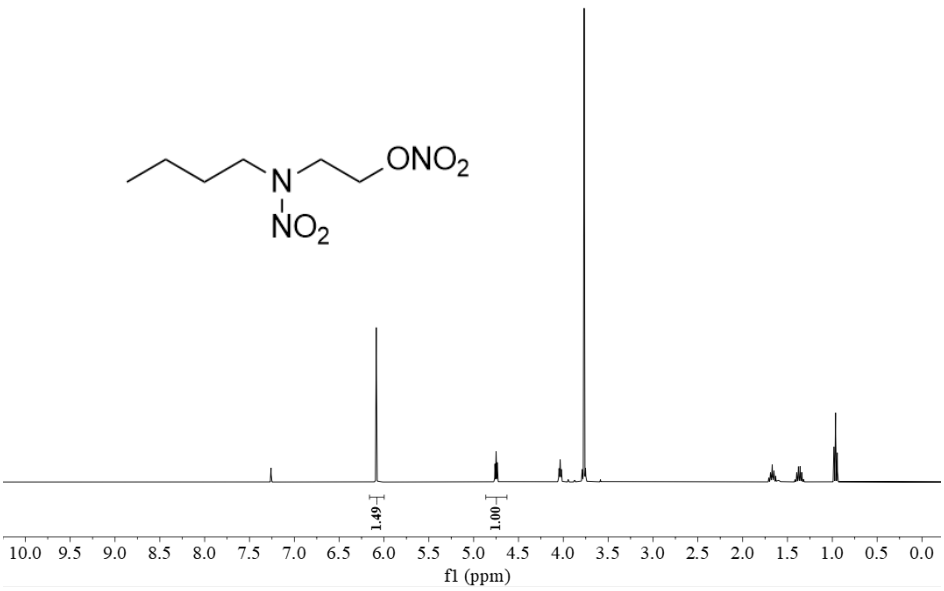

Fig. S3. ^{1}H-NMR spectrum of **Bu-NENA.**

Table S3. Results of NMR and EA experiments for **Bu-NENA**.

^{1}H – NMR	($CDCl_3$, 400 MHz): δ = 4.73 (t, 2H, O–C*H*$_2$–CH_2), 4.03 (t, 2H, N–C*H*$_2$–CH_2), 3.75 (t, 2H, C*H*$_2$–CH_2–CH_2–CH_3), 1.64 (m, 2H, CH_2–C*H*$_2$–CH_2–CH_3), 1.35 (m, 2H, C*H*$_2$–CH_3), 0.94 (t, 3H, C*H*$_3$) ppm. 1,3,5-Trimethoxybenzene, **CRM** ($CDCl_3$, 400 MHz): δ = 6.09 (s, 3H, C*H*), 3.77 (s, 9H, C*H*$_3$).
^{13}C – NMR	($CDCl_3$, 101 MHz): δ = 69.2 (O–*C*H_2), 52.9 (N–*C*H_2), 49.0 (*C*H_2–CH_2–CH_2–CH_3), 28.6 (CH_2–*C*H_2–CH_2–CH_3), 19.9 (*C*H_2–CH_3), 13.6 (*C*H_3) ppm.
^{14}N – NMR	($CDCl_3$, 29 MHz): δ = -30.3 (N–*N*O_2), -45.6 (O–*N*O_2) ppm.
EA	Calc.: C 34.78, H 6.32, N 20.28 %; Found: C 34.68, H 6.56, N 20.16 %.

S2. Assessment of the uncertainties

The calculation of standard uncertainties of vapor pressure measurements was previously discussed elsewhere [1, 2]. The calculation of combined standard uncertainties for measured vapor pressure values includes several contributions from various sources: uncertainty of mass of the analyte ($u(m_{An})$), mass of the reference material ($u(m_{Ref})$), volumes of the pycnometers ($u(V_{Pyc})$), volumes of the standard solutions ($u(V_{Std})$), uncertainties introduced by standard addition into the sample ($u(V_{Add})$), chromatographic analysis (for calibration and determination) ($u(GC/HPLC)$), transporting gas volume uncertainty ($u(V_{gas})$), saturator and ambient temperatures uncertainties ($u(T)$) and the uncertainty of purity of the materials ($u(P_{An})$). Experimental vapor pressures measured in this work are reported together with standard uncertainties of confidence level 0.68 (k = 1).

S3. TGA experiment

In this work an isothermal TGA experiment was conducted for the purpose of comparison of own results with the previously reported results by Cartwright [3]. The experiment was performed using a *Perkin Elmer TGA4000* device with dry nitrogen as purge gas. The device crucible was filled with 17 to 27 mg of compound under investigation, heated to initial temperature (set temperature 373.15 K, sample temperature 371.48 K) and run for extensive period of time under 20 ml·min^{-1} purge gas.

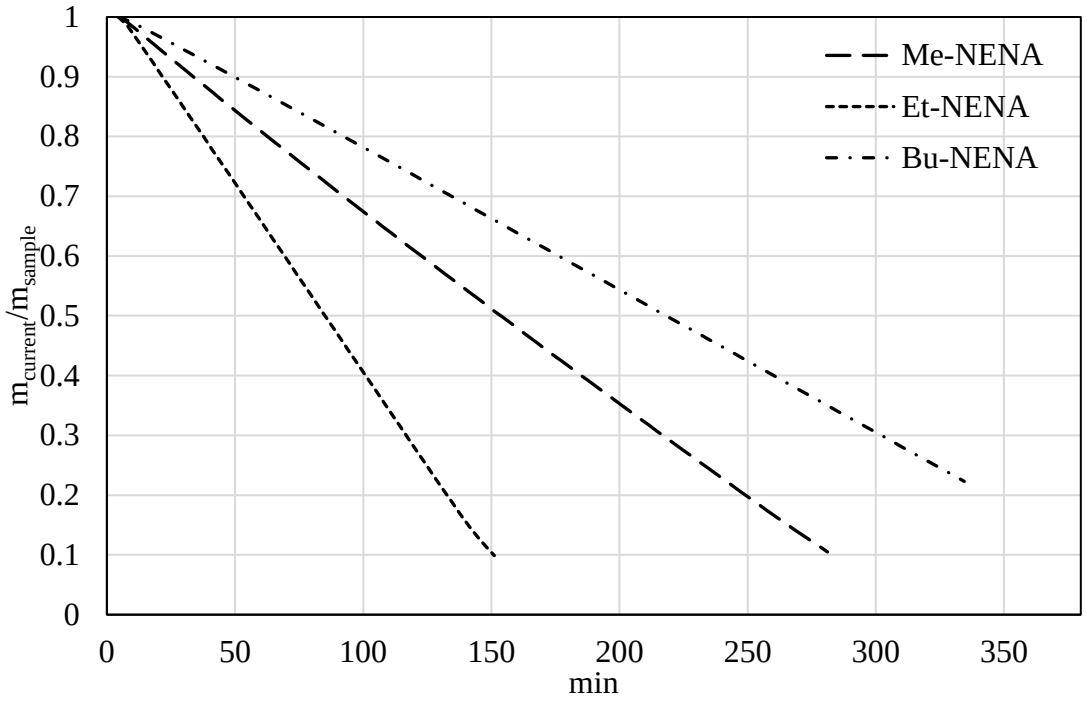

Fig. S4. Results of Me-, Et- and Bu-NENA compounds in isothermal TGA experiment, sample temperature 371.48 K. Here: long dashed line – Me-NENA, dashed line – Et-NENA, dashed-dotted line – Bu-NENA.

S4. GCMS/HPLC-DAD parameters

Compilation of VO-GC/MS parameters used for transpiration experiments:

GC/MS	*Shimadzu QP2010SE*® with *LabSolution* GCMSsolution v4.11
Injector	Atas Optic 4 with Evolution Workstation v4.1
Liner	10 mm V2A stainless steel tube, 5 mm wall thickness, equipped with silanized glass wool (2 mm injection needle penetration into wool)
Restriction	0.05 mm capillary, 10.53 mm length (Restek #10097)
Column connector	*SGE Siltite µ-Union*® (Restek #073562)
Analytical column	*Restek RTX-TNT 1*® (3 m, 0.53 mm, 1.5 µm)
Oven program	Me-NENA, vaporization: 40 °C (hold 0.10 min) → 215 °C (rate 60 °C min^{-1}), total program time 3.02 min. Et-NENA: 40 °C (hold 0.10 min) → 215 °C (rate 60 °C min^{-1}), total program time 3.02 min.
Injector head pressure	97 kPa
Virtual column	100 m, 0.25 µm film thickness, 0.20 mm i.d. (entry for GCMSsolution)

Column flow	3.97 mL min^{-1}
Split ratio	150.0 (entered in LabSolutions GCMSsolution)
Purge flow	10 mL min^{-1}
Injection volume	1 µL
Ion source	200 °C
MS interface	200 °C
MS	SIM mode (event time 100 ms)
	Me-NENA: 1.20 – 1.80 min; m/z: 43.1. Retention time: 1.50 min.
	Hexadecane (standard): 1.90 – 3.00 min; m/z: 57.1. Retention time: 2.28 min.
	Et-NENA: 1.20 – 2.00 min; m/z: 46.0. Retention time: 1.63 min.
	Hexadecane (standard): 2.00 – 3.00 min; m/z: 57.1 Retention time: 2.28 min.
	m/z: quantification ion.

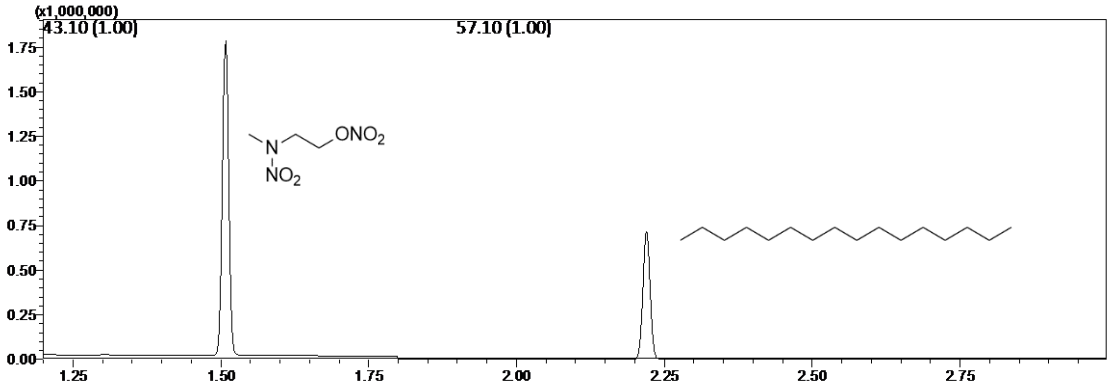

Fig. S5. GC/MS chromatogram of Me-NENA (retention time 1.50 min, m/z = 43.10) and standard hexadecane (retention time 2.28 min, m/z = 57.10), measured with a method, described in S4.

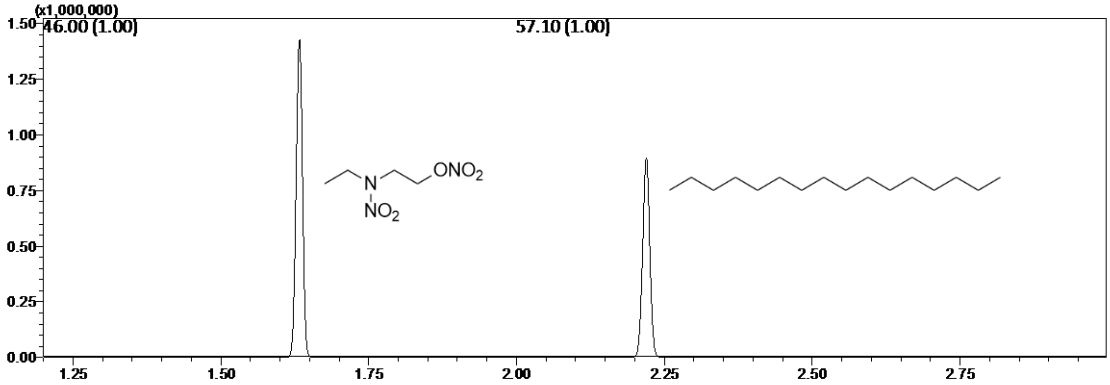

Fig. S6. GC/MS chromatogram of Et-NENA (retention time 1.63 min, m/z = 46.00) and standard hexadecane (retention time 2.28 min, m/z = 57.10), measured with a method, described in S4.

HPLC	*Shimadzu Prominence*® with LC-20AD pump module and SPD-M20A Diode Array Detector; software *LabSolutions v*5.86
Analytical column	*Phenomenex Kinetex*® (2.6 µm Biphenyl, 100 Å, 150 × 4.6 mm)
Oven temperature:	40°C
Program	
Me-NENA, sublimation	Injection volume: 1 µL Total Flow: 0.75 mL/min Mobile phase: 70 % MeOH, 30 % Water Time: 7.5 min Channel 1 wavelength: 238 nm (Me-NENA) Retention time: 2.90 min Channel 2 wavelength: 275 nm (standard, naphthalene) Retention time: 6.29 min
Bu-NENA	Injection volume: 1 µL Total Flow: 0.85 mL/min Mobile phase: 65 % MeOH, 35 % Water Time: 10 min Channel 1 wavelength: 241 nm (Bu-NENA) Retention time: 5.09 min Channel 2 wavelength: 275 nm (standard, naphthalene) Retention time: 7.55 min

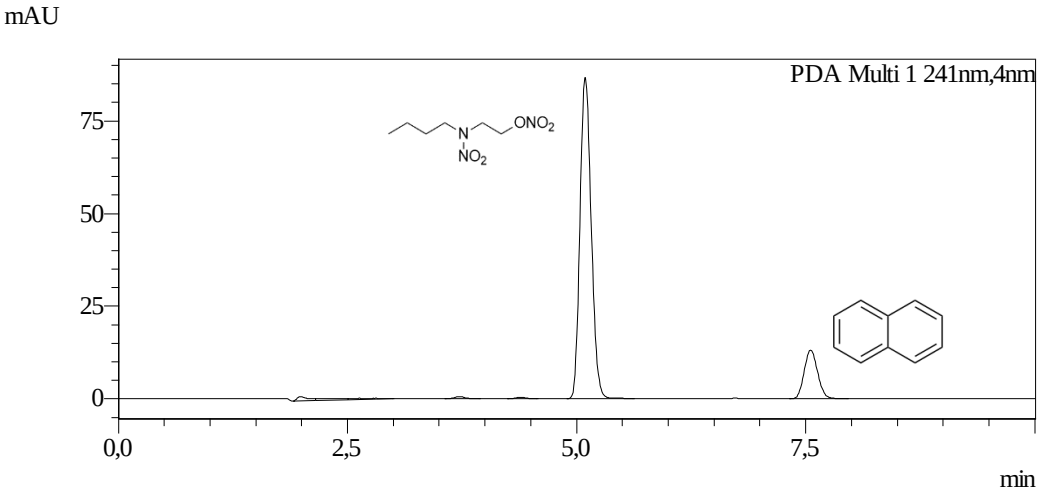

Fig. S7. HPLC-DAD chromatogram of Bu-NENA (retention time 5.09 min, integration wavelength λ = 241 nm) and standard naphthalene (retention time 7.55 min, integration wavelength λ = 275 nm), measured with a method, described in S4.

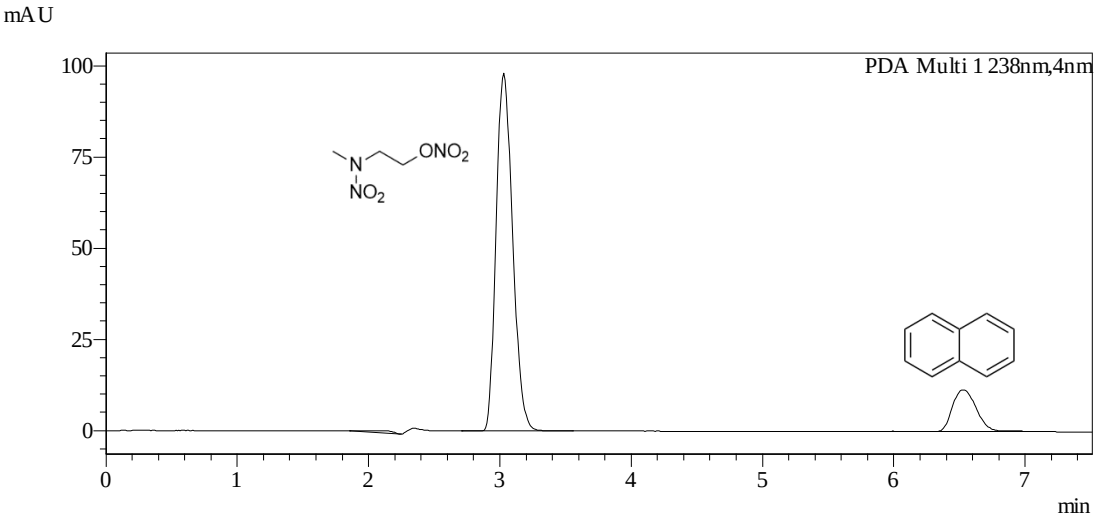

Fig. S8. HPLC-DAD chromatogram of Me-NENA (retention time 2.9 min, integration wavelength λ = 238 nm) and standard naphthalene (retention time 7.55 min, integration wavelength λ = 275 nm), measured with a method, described in S4.

1. Bikelytė, G.; Härtel, M. A.; Klapötke, T. M.; Krumm, B.; Sadaunykas, A., Experimental thermochemical data of CWA simulants: Triethyl phosphate, diethyl methylphosphonate, malathion and methyl salicylate. *J. Chem.Thermodyn.* **2020,** 143, 106043.
2. Bikelytė, G.; Härtel, M. A.; Klapötke, T. M., Experimental Vapor Pressures of Hexahydro-1, 3, 5-trinitro-1, 3, 5-triazine (RDX) and Hexahydro-1, 3, 5-trinitroso-1, 3, 5-triazine (TNX). *Propellants Explos. Pyrotech.* **2020,** 45, (10), 1573-1579.
3. Cartwright, R., Volatility of NENA and other energetic plasticizers determined by thermogravimetric analysis. *Propellants Explos. Pyrotech.* **1995,** 20, (2), 51-57.

5.4. Measurements of Organic Azides (Article 4)

Article 4: Thermodynamics of organic azides: experimental vapor pressures of organic polyazido compounds measured with the transpiration method

The results were published in *Fluid Phase Equilibria* (2021) [112] and are reprinted with permission. DOI: doi.org/10.1016/j.fluid.2021.113222.

Fluid Phase Equilibria 549 (2021) 113222

Contents lists available at ScienceDirect

Fluid Phase Equilibria

journal homepage: www.elsevier.com/locate/fluid

Thermodynamics of organic azides: Experimental vapor pressures of organic polyazido compounds measured with the transpiration method ☆

Greta Bikelytė, Alexander G. Harter, Martin A.C. Härtel, Stefanie B. Heimsch, Thomas M. Klapötke*

Department of Chemistry, Ludwig-Maximilian University of Munich, Butenandtstr. 5–13, 81377 Munich Germany

ARTICLE INFO

Article history:
Received 22 March 2021
Revised 3 September 2021
Accepted 9 September 2021
Available online 11 September 2021

Keywords:
Vapor pressure
Organic azides
Gas-saturation
Vaporization enthalpy

ABSTRACT

In this study experimental vapor pressures of several organic azides including 1,3-diazidopropan-2-ol (1,3-DAP, CAS: 57011-48-0), 2,3-diazidopropan-2-ol (2,3-DAP, CAS: 67880-10-8) and geminal diazido group containing 1,3–diethyl-2,2-diazidomalonate (DE-DAM, CAS: 168207-98-5) were measured for the first time using the transpiration method. The study provides *p-T* fitting equations and corresponding molar enthalpies of vaporization, adjusted to 298.15 K: (72.6 ± 0.5) kJ mol^{-1} for 1,3-DAP, (75.2 ± 0.6) kJ mol^{-1} for 2,3-DAP and (76.0 ± 1.1) kJ mol^{-1} for DE-DAM.

1. Introduction

The organic azides are useful as building blocks in “click” chemistry [1,2], in pharmaceuticals [3], energetic materials [3–5] and many other applications [3]. In the field of energetic materials, the introduction of the azide functional group in the composition of potential energetic materials can result in “greener”, more environmentally friendly solutions since the combustion of the azide functional group containing materials is smokeless and produces environmentally harmless molecular nitrogen. However, the -N_3 group not only raises the energetic load of the compound, but often causes a significant increase in the sensitivity towards friction and impact [6]. The sensitivity of the compounds might hinder the determination of experimental thermodynamic parameters, such as molar enthalpies of phase transitions or molar enthalpy of formation, which are important for the assessment of the performance of potential high energy materials [7]. As a result, in recent years a considerable amount of effort was invested in the development of the computational methods to predict the thermochemical properties of the organic azides [6–11]. The development of the methods relies heavily on the availability of high-quality experimental thermodynamic data. Consequently, in the past decade several published studies aimed to provide new reliable data and to eliminate the existent disarray in experimental thermodynamic properties of organic azides [12,13]. Moreover, the relatively “young” class of compounds containing geminal diazides have remained an uninvestigated area in terms of their thermodynamic behaviors [14].

Recently our research group executed investigations on the performance of several organic azides [15,16]. Therefore, a group of relatively insensitive organic polyazido compounds, including two diazido propanols, 1,3-diazidopropan-2-ol (1,3-DAP) and 2,3-diazidopropan-2-ol (2,3-DAP), and a malonic ester with a geminal diazido group 1,3–diethyl-2,2-diazidomalonate (DE-DAM), were chosen for the determination of thermodynamic properties using the transpiration method (Fig. 1).

2. Materials and methods

2.1. Materials

CAUTION! 1,3-DAP, 2,3-DAP and DE-DAM are energetic materials with sensitivity to various stimuli. While we encountered no issues in the handling of these materials, we encourage to employ additional protective measures (Kevlar gloves, hearing protections, face shields, etc.) during the handling of all of the compounds at all times including vapor pressure measurements.

☆ Homepage: http://www.hedm.cup.uni-muenchen.de

* Corresponding author.
E-mail address: tmk@cup.uni-muenchen.de (T.M. Klapötke).

https://doi.org/10.1016/j.fluid.2021.113222
0378-3812/

List of symbols

p_{sat}	saturated vapor pressure, in Pa (Eq. (1))
p°	reference pressure, in Pa (Eq. (2))
m	mass of the analyte collected during the transpiration experiment, in kg (Eq. (1))
T_{amb}	ambient temperature, in K (Eq. (1))
T	temperature, in K (Eq. (1))
T_0	Reference temperature, in K (Eq. (2))
V_{N_2}	volume of carrier gas at ambient conditions, in m^3 (Eq. (1))
$C^{\circ}_{p,m}$	standard heat capacity at constant pressure, in $J{\cdot}mol^{-1}{\cdot}K^{-1}$ (Table 2)
$\Delta^g_l C^{\circ}_{p,m}$	difference of molar heat capacities at constant pressure, in $J{\cdot}mol^{-1}{\cdot}K^{-1}$ (Eq. (2))
$\Delta^g_l H^{\circ}_m$	standard molar enthalpy of vaporization, in $J{\cdot}mol^{-1}$ (Eq. (3))
$\Delta^g_l S^{\circ}_m$	standard molar entropy of vaporization, in $J{\cdot}mol^{-1}$ (Eq. (4))

All of the compounds investigated in this study were synthesized by procedures, described previously in the literature. The 1,3-DAP and 2,3-DAP compounds were produced according to the methods described in Farhanullah et al. and Samrin et al., respectively [17,18]. Compound DE-DAM was prepared according to the synthetic path described in the study of Erhart et al. [19]. The purity of the compounds used in this study was investigated with the elemental analysis and ^{1}H NMR spectroscopy and is reported in Table 1. Further information on purity assessment is provided in the Supporting Information.

Before the transpiration experiment took place, a sample conditioning step within the experimental setup was executed by subjecting the sample to the carrier gas stream at ambient and elevated temperatures (315–320 K) for 2–3 h each, in order to remove moisture and possible volatile impurities.

2.2. Transpiration method

The measurements of the experimental vapor pressures were executed with the transpiration method described previously [20]. The method relies on the determination of the amount of the analyte in a saturated carrier gas stream. To facilitate the saturation conditions, a generous amount of the compound of interest (0.5–1 g) is homogenously coated on the surface of the 1 mm diameter glass beads, which are placed in a temperature-regulated glass vessel, the so-called saturator. Given that the flow of the carrier gas is relatively slow (1–5 $dm^3{\cdot}h^{-1}$), the carrier gas stream enters the glass vessel and, upon the contact with the analyte, gets saturated. The saturation state is demonstrated by the independence of the analytical results and flow rate at the lowest experimental temperature. To determine the amount of the vapors of the analyte, present in the gas phase, the gas stream exits the saturator into a detachable glass tube, which is immersed in a cooling bath (isopropanol, 243 K). The vapors of the analyte condense on the glass walls and the amount of the analyte collected over a specific period of time is quantified by a chromatographic technique (HPLC-DAD, Shimadzu, Prominence® with LC-20AD pump module and SPDM20A Diode Array Detector). For the chromatographic methods please refer to the Supporting Information.

Table 1
Origin and mass fraction purity P_{An} of the compounds investigated in this work.

Substance	IUPAC name	CAS #	P_{An} [a]
1,3-DAP	1,3-diazidopropan-2-ol	57011-48-0	>0.98
2,3-DAP	2,3-diazidopropan-1-ol[b]	67880-10-8	>0.95
DE-DAM	1,3-diethyl-2,2-diazidomalonate	168207-98-5	>0.98

[a] Purity P_{An} of the samples as mass fraction, estimated from the ^{1}H NMR, were clean spectra could be associated with the purity of >0.98 (m/m). The conservative estimations were backed up by elemental analyses. [b]*ee* not determined.

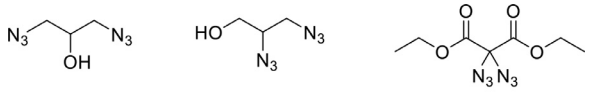

1,3-DAP 2,3-DAP DE-DAM

Fig. 1. The compounds of interest, that were analyzed in this work: 1,3-DAP, 2,3-DAP and DE-DAM.

Table 2
The estimated molar heat capacities $C^{\circ}_{p,m}$ and their differences of the organic azides, investigated in this work (T = 298.15 K).

Compound	$C^{\circ}_{p,m}(l)$ [a]	$-\Delta^g_l C^{\circ}_{p,m}$ [b]
	$J{\cdot}mol^{-1}{\cdot}K^{-1}$	$J{\cdot}mol^{-1}{\cdot}K^{-1}$
1,3-DAP	327.5	95.7
2,3-DAP	327.5	95.7
DE-DAM	458.0	129.7

[a] Calculated according to the group contribution method by *Acree and Chickos* [22]. Group values for azide functional group were obtained from experimental heat capacity values by *Fagley and Myers* [23].
[b] Calculated by $-\Delta^g_l C^{\circ}_{p,m} = 10.58 + C^{\circ}_{p,m}(l) \times 0.26$ [21].

Experimental conditions including temperature of the saturator T (in K), ambient temperature T_{amb} (in K), volume of the carrier gas V_{N_2} (in m^3) along with the amount of the analyte collected during the transpiration experiment m (in kg) are inserted into modified equation of the Ideal Gas Law (Eq. (1)), which allows the calculation of absolute vapor pressure p_{sat} (in Pa).

$$p_{sat}(T) = \frac{mRT_{amb}}{MV_{N_2}} \tag{1}$$

Here R is universal gas constant 8.314462 $[J{\cdot}mol^{-1}{\cdot}K^{-1}]$; M: molecular weight $[kg{\cdot}mol^{-1}]$. The validity of the Eq. (1) relies on the Dalton's law of partial pressures and the assumption that the volume of the vapors of the analyte is negligible in comparison to the volume of the carrier gas. The relationship between the absolute vapor pressures and the experimental temperature is described by a fitting equation:

$$\ln\left(\frac{p_{sat}}{p^{\circ}}\right) - \frac{\Delta^g_l C^{\circ}_{p,m}}{R} ln\frac{T}{T_0} = A - \frac{B}{T} \tag{2}$$

Here $p^{\circ}$is the reference pressure (in Pa), T_0 is the reference temperature (in K), A and B are fitting coefficients (A is unitless, B in K). Molar heat capacity differences between liquid (l) and gaseous phase (g) at constant pressure $\Delta^g_l C^{\circ}_{p,m}$ for the compounds of interest were calculated using the procedure described by *Acree and Chickos* [21]. The molar heat capacities $C^{\circ}_{p,m}(l)$, required for this calculation were obtained via group contribution method by Acree and Chickos [22]. The values are detailed in Table 2.

The determined *p-T* datasets allow the determination of the molar enthalpy of vaporization $\Delta^g_l H^{\circ}_m$ and molar entropy of vaporization $\Delta^g_l S^{\circ}_m$ at temperature T according to the equations

$$\Delta^g_l H^{\circ}_m(T) = RB + \Delta^g_l C^{\circ}_{p,m} T \tag{3}$$

$$\Delta^g_l S^{\circ}_m(T) = \frac{\Delta^g_l H^{\circ}_m(T)}{R} + Rln\left(\frac{p_{sat}}{p^{\circ}}\right) \tag{4}$$

Here $p^{\circ}$is the standard pressure (0.1 MPa).

For the evaluation of the uncertainties of molar enthalpies of vaporization $\Delta^g_l H^{\circ}_m(T)$, experimental vapor pressures were fitted

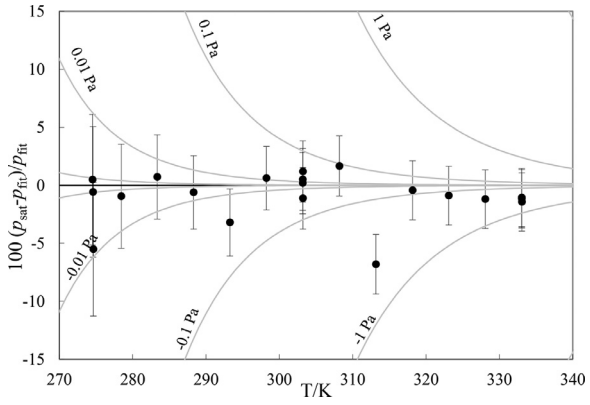

Fig. 2. Experimental vapor pressure (•) deviations from the derived fitting equation for 1,3-DAP in Table 3. Dashed lines display the absolute deviation in pressure. Error bars are the standard uncertainties as reported in Table 3.

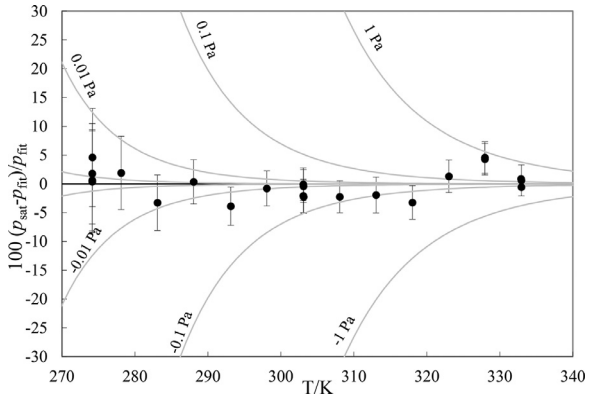

Fig. 3. Experimental vapor pressure (•) deviations from the derived fitting equation for 2,3-DAP in Table 4. Dashed lines display the absolute deviation in pressure. Error bars are the standard uncertainties as reported in Table 4.

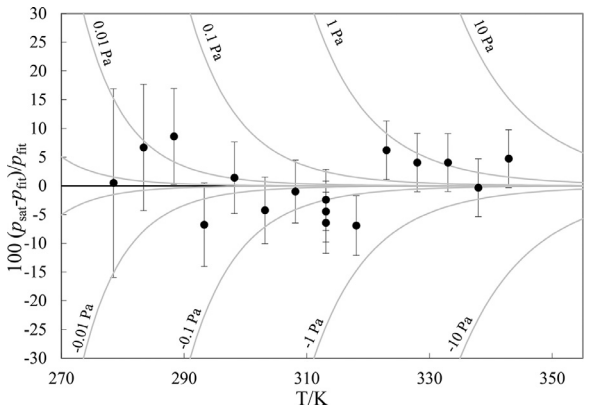

Fig. 4. Experimental vapor pressure (•) deviations from the derived fitting equation for DE-DAM in Table 5. Dashed lines display the absolute deviation in pressure. Error bars are the standard uncertainties as reported in Table 5.

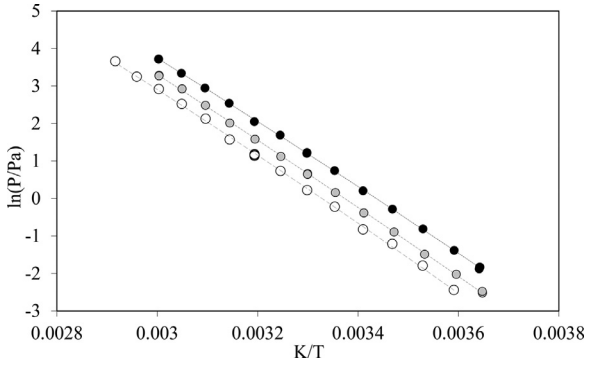

Fig. 5. Comparison of the experimental vapor pressures of diazidopropanols: • and dashed black line for 1,3 – DAP; • and dashed dark gray line for 2,3- DAP; ○ and dashed light gray line for DE-DAM.

to the linear equation $\ln p = f(T^{-1})$ using the method of least squares. The resulting enthalpies of vaporization, their corresponding uncertainties and the uncertainties introduced by the approximation were included in the calculations of the uncertainties of $\Delta_l^g H_m^\circ(T)$ (Eq. (2)) [24].

3. Results and discussion

The results of the transpiration experiments performed as described above are reported in the Tables 3 – 5 together with the fitting functions according to Eq. (2) and molar enthalpies of vaporization, adjusted to 298.15 K. The correcponding *p-T* data is also plotted in the Figure 5.

Visualizations of the experimental vapor pressure deviations from fitting equations are provided in Figs. 2, 3, and 4. The experimental vapor pressures of DE-DAM exhibit significantly higher deviations from the fitting equation (Eq. (2)) than for 1,3-DAP and 2,3-DAP and for this reason standard vapor pressure uncertainties for DE-DAM were increased by a factor of two.

If fitted to the *Clarke-Glew* equation [27] (Eq. (5)), where vapor pressures are directly related to the thermodynamic functions of vaporization, the fitting equation yields a theoretically impossible positive $\Delta_l^g C_{p,m}^\circ$value.

$$R\ln\left(\frac{p_{sat}}{p^0}\right) = \frac{-\Delta_l^g G_m^\circ(\theta)}{\theta} - \Delta_l^g H_m^\circ(\theta)\left(\frac{1}{\theta}-\frac{1}{T}\right) + \Delta_l^g C_{p,m}^\circ(\theta)\left(\frac{\theta}{T}-1+ln\left(\frac{T}{\theta}\right)\right) \quad (5)$$

Here p_{sat} is the vapor pressure (in Pa) at the temperature T, p° is the standard pressure (0.1 MPa), θ is an arbitrary reference temperature (in this work θ = 298.15 K), $\Delta_l^g C_{p,m}^\circ$ is the difference in the isobaric molar heat capacities between gaseous and liquid states, $\Delta_l^g H_m^\circ$ is the molar enthalpy of vaporization and $\Delta_l^g G_m^\circ$ is the difference in Gibbs energy between gaseous and liquid states.

Reduction of the experimental data-set at high and low temperatures eliminated this inconsistency and the remaining data points are presented in Table 5 and Fig. 4. The full experimental vapor pressure data-set of DE-DAM is reported in table S4 and deviation plot is depicted in figure S4. The resulting molar enthalpies of vaporization at 298.15 K derived from reduced and full *p-T*-datasets (76.0 kJ·mol^{-1} and 76.2 kJ·mol^{-1}, respectively) agree within the experimental uncertainties.

The thermodynamic properties, derived in this work for 1,3-DAP, 2,3-DAP and DE-DAM, are compiled in the Table 6. There are notable differences in the vaporization behavior of the diazidopropanols: the molar enthalpy of vaporization at 298.15 K of 1,3-DAP has a lower value (72.6 ± 0.5 kJ·mol^{-1}) in comparison to the value of 2,3-DAP (75.2 ± 0.6 kJ·mol^{-1}) and there is an obvious difference in absolute vapor pressures in the whole experimental temperature range, with the compound 1,3-DAP having higher vapor pressures. The reasoning behind these results could be that the compound 2,3-DAP is less symmetrical and, consequently, more polar than 1,3-DAP. Also, it is known that the hydrogen bond formation in the primary alcohol group (2,3-DAP) is less sterically hindered compared to the bond formation at the secondary alcohol group (1,3-DAP) [28]. With respect to that, more hydrogen bonds can be expected for 2,3-DAP. The increase of the molecule polar-

Table 3
1,3-DAP (liq): experimental conditions and resulting absolute vapor pressures p_{sat} obtained by the transpiration method in this work.

$\Delta_l^g H_m^\circ$ (298.15 K) = (72.6 ± 0.5) kJ mol^{-1}

$\ln\left(\frac{p_{sat}}{p^0}\right) = \frac{345.3}{R} - \frac{101.171.93}{RT} - \frac{95.7}{R} ln\frac{T}{298.15K}$

T[a] K	m[b] mg	V_{N2}^c dm³	T_{amb}[d] K	Gasflow dm³·h^{-1}	p_{sat}[e] Pa	$u(p_{sat})$[f] Pa
274.5	0.13	14	295.9	3.6	0.161	0.009
274.6	0.26	28	299.8	1.6	0.160	0.009
274.6	0.12	14	295.9	4.8	0.153	0.009
278.4	0.41	28	295.6	1.6	0.251	0.011
283.4	0.15	5.6	295.5	4.8	0.445	0.016
288.3	0.12	2.8	296.0	4.8	0.753	0.024
293.3	0.09	1.2	296.0	4.8	1.23	0.04
298.2	0.17	1.4	295.8	4.8	2.10	0.06
303.2	0.24	1.2	295.3	4.9	3.38	0.09
303.2	0.24	1.2	295.2	4.8	3.37	0.09
303.2	0.24	1.2	295.3	4.8	3.41	0.09
303.2	0.24	1.2	298.8	4.9	3.34	0.09
308.2	0.38	1.2	296.6	4.8	5.43	0.14
313.2	0.55	1.2	302.0	4.9	7.77	0.20
318.2	0.45	0.6	299.9	2.4	12.7	0.3
323.1	0.51	0.5	295.5	1.8	19.0	0.5
328.1	0.75	0.5	297.1	1.8	28.2	0.7
333.1	0.99	0.4	298.5	1.6	41.2	1.0
333.1	1.09	0.5	298.8	1.6	41.3	1.0
333.1	0.99	0.4	300.0	1.7	41.2	1.0

[a] Saturation temperature ($u(T)$ = 0.1 K). [b] Mass of transferred sample condensed at 243 K. [c] Volume of nitrogen ($u(V)$ = 0.01 dm^3) used to transfer m ($u(m)/m$ = 0.015) of the sample. [d] T_{amb} is the temperature of the soap film flowmeter used for measurement of the gas flow. [e] Vapor pressure at temperature T, obtained from the mass m and the residual vapor pressure at the condensation temperature, calculated by an iteration procedure; p° = 1 Pa. [f] Standard uncertainties were calculated with u(p/Pa) = 0.005 + 0.025(p/Pa). The uncertainties for T, V and m are standard uncertainties. The determination of the u(m) included the evaluation of the uncertainties associated with the preparation of internal standard solutions (caused by weighing and pycnometers), volumetric standard addition, chromatographic calibration and determination. The uncertainty of the molar enthalpy of vaporization (at 298.15 K) is the standard uncertainty with a confidence level of 0.68, calculated including uncertainties of vapor pressure, the uncertainties from the fitting equation and the uncertainty of temperature adjustment to T = 298.15 K. Detailed information on the methods of calculations was published previously [25; 26].

ity and the hydrogen bonds lowers the vapor pressure of a compound. Similar behavior can be observed for analogous aliphatic compounds, where the molar enthalpy of vaporization for pentan-3-ol (CAS: 584-02-1, 53.2 kJ·mol^{-1} [22; 29]) is slightly lower than of 2-methyl-1-butanol (CAS: 137-32-6, 54.1 kJ·mol^{-1} [30,31]).

As expected, the compound DE-DAM showed both lower vapor pressures and higher molar enthalpies of vaporization in comparison to the diazidopropanols, investigated in this work (Table 6).

Literature research revealed that only few studies discuss the vapor pressures of the compounds containing multiple azido groups [12,32]. The work by Lee et al. [32] provides, as stated by the researchers, "approximate" results on the p-T-data for several aliphatic chains with terminal azido groups. In the work by Verevkin et al. [12] the results of Lee et al. were processed to yield the molar enthalpies of vaporization at 298.15 K and a correlation between the $\Delta_l^g H_m^\circ$(298.15 K) and the carbon number in the aliphatic chain was derived. However, no experimental p-T-data are available for the -OH group containing aliphatic diazido-compounds, or, in fact, any of the compounds investigated in this work. One noteworthy datapoint available for 1,3-DAP is a boiling point, reported in the work of Isaev et al. [33] and it is depicted in the Figure S5 in the Supporting Information. The measured boiling point lies closely to the extrapolated fitting equation from the results achieved in this work (Table 3). Additionally, this is the first

Table 4
2,3-DAP (liq): experimental conditions and resulting absolute vapor pressures p_{sat} obtained by the transpiration method in this work.

$\Delta_l^g H_m^\circ$ (298.15 K) = (75.2 ± 0.6) kJ mol^{-1}

$\ln\left(\frac{p_{sat}}{p^0}\right) = \frac{349.3}{R} - \frac{103.721.26}{RT} - \frac{95.7}{R} ln\frac{T}{298.15K}$

T[a] K	m[b] mg	V_{N2}^c dm³	T_{amb}[d] K	Gasflow dm³·h^{-1}	p_{sat}[e] Pa	$u(p_{sat})$[f] Pa
274.2	0.07	14	297.7	4.8	0.082	0.007
274.2	0.32	66	296.2	3.6	0.081	0.007
274.2	0.15	32	296.6	2.0	0.081	0.007
274.2	0.21	42	298.0	2.4	0.084	0.007
278.1	0.07	8.7	297.2	4.8	0.133	0.008
283.1	0.06	4.4	297.1	4.8	0.226	0.011
288.1	0.06	2.3	296.4	4.8	0.410	0.015
293.1	0.07	1.6	296.3	4.8	0.680	0.022
298.1	0.09	1.2	296.2	4.8	1.17	0.03
303.1	0.14	1.2	296.0	4.8	1.94	0.05
303.1	0.14	1.2	296.2	4.8	1.91	0.05
303.1	0.14	1.2	295.9	4.8	1.94	0.05
303.1	0.14	1.2	297.1	4.8	1.91	0.05
308.1	0.22	1.2	295.4	4.8	3.07	0.08
313.0	0.35	1.2	296.8	4.8	4.87	0.13
318.0	0.54	1.2	296.5	4.8	7.49	0.19
323.0	0.87	1.2	297.0	4.8	12.0	0.3
328.0	0.80	0.7	295.2	2.8	18.6	0.5
328.0	0.79	0.7	295.3	2.8	18.6	0.5
332.9	1.14	0.7	295.4	2.8	26.7	0.7
333.0	1.14	0.7	295.3	2.8	26.7	0.7
333.0	1.12	0.7	295.2	2.8	26.3	0.7

For table legend please refer to Table 3.

Table 5
DE-DAM (liq): experimental conditions and resulting absolute vapor pressures p_{sat} obtained by the transpiration method in this work.

$\Delta_l^g H_m^\circ$ (298.15 K) = (76.0 ± 1.1) kJ mol^{-1}

$\ln\left(\frac{p_{sat}}{p^0}\right) = \frac{382.6}{R} - \frac{114.672.99}{RT} - \frac{129.7}{R} ln\frac{T}{298.15K}$

T[a] K	m[b] mg	V_{N2}^c dm³	T_{amb}[d] K	Gasflow dm³·h^{-1}	p_{sat}[e] Pa	$u(p_{sat})$[f] Pa
278.5	0.67	78	296.3	4.8	0.09	0.01
283.4	0.50	30	296.4	4.8	0.17	0.02
288.3	0.52	18	296.2	4.8	0.30	0.02
293.3	0.51	12	297.1	4.8	0.44	0.03
298.2	0.51	6.4	296.8	4.8	0.80	0.05
303.2	0.45	3.6	297.1	4.8	1.25	0.07
308.1	0.50	2.4	297.7	4.8	2.08	0.11
313.1	0.47	1.5	297.4	4.8	3.26	0.17
313.1	0.50	1.6	296.4	4.8	3.13	0.17
313.1	0.51	1.6	296.3	4.8	3.20	0.17
318.1	0.58	1.2	296.5	4.8	4.83	0.25
323.0	1.00	1.2	297.5	4.8	8.40	0.43
328.0	1.49	1.2	297.0	4.8	12.5	0.6
333.0	2.22	1.2	296.5	4.8	18.5	0.9
338.0	3.09	1.2	297.5	4.8	25.8	1.3
342.9	7.15	1.9	297.2	4.8	38.9	2.0

[a] Saturation temperature ($u(T)$ = 0.1 K). [b] Mass of transferred sample condensed at 243 K. [c] Volume of nitrogen ($u(V)$ = 0.01 dm^3) used to transfer m ($u(m)/m$ = 0.015) of the sample. [d] T_{amb} is the temperature of the soap film flowmeter used for measurement of the gas flow. [e] Vapor pressure at temperature T obtained from the m and the residual vapor pressure at the condensation temperature, calculated by an iteration procedure; p° = 1 Pa. [f] Standard uncertainties were calculated with u(p/Pa) = 0.01 + 0.05(p/Pa). The uncertainties for T, V and m are standard uncertainties. The determination of the u(m) included the evaluation of the uncertainties associated with the preparation of internal standard solutions (caused by weighing and pycnometers), volumetric standard addition, chromatographic calibration and determination. The uncertainty of the molar enthalpy of vaporization (at 298.15 K) is the standard uncertainty with a confidence level of 0.68, calculated including uncertainties of vapor pressure, the uncertainties from the fitting equation and the uncertainty of temperature adjustment to T = 298.15 K. Detailed information on the methods of calculations was published previously [25; 26].

Table 6
Compilation of the thermodynamic data on 1,3-DAP, 2,3-DAP and DE-DAM, derived from *p-T*-data obtained in this work.

Experiment	T-Range	T_{avg}	$\Delta_l^g H_m^\circ(T_{avg})$ [a]	$\Delta_l^g H_m^\circ$(298.15 K) [b]	p_{sat} [c]
	K	K	kJ·mol^{-1}	kJ·mol^{-1}	Pa
1,3-DAP	274.5 – 333.1	302.1	72.3 ± 0.5	72.6 ± 0.5	2.05
2,3-DAP	274.2 – 333.0	301.6	74.9 ± 0.6	75.2 ± 0.6	1.19
DE-DAM[d]	278.5 – 342.9	309.8	74.7 ± 1.0	76.0 ± 1.1	0.79

[a] Molar enthalpies of vaporization at average temperature, derived by the linear data approximation $\ln p = f(T^{-1})$ and for the purpose of calculation of u($\Delta_l^g H_m^\circ$) from the Eq. (3). [b] Molar enthalpies of vaporization were adjusted according to Acree and Chickos [21] with values of $\Delta_l^g C_{p,m}^\circ$ and $C_{p,m}^\circ$(l), stated in Table 2. The uncertainty of molar enthalpy of vaporization is expressed as standard uncertainty with the confidence level of 0.68. [c]The calculated vapor pressure at 298.15 K, according to the fitting equations reported in the Tables 3–5. [d] Results obtained from reduced data-set, as explained above.

time that experimental vapor pressures and corresponding thermodynamic properties are reported for a geminal diazido- compound.

4. Conclusions

This study discusses the vaporization behavior of several compounds from a rarely thermodynamically investigated organic polyazido group: 1,3-diazidopropanol (1,3-DAP), 2,3-diazidopropanol (2,3-DAP) and 1,3–diethyl-2,2-diazidomalonate (DE-DAM). Their experimental vapor pressures were measured using the transpiration method. It is the first time the thermodynamic properties are reported for a compound, containing a geminal diazido- group (DE-DAM). The experimental *p-T*-datasets were obtained in the ambient temperature range and their corresponding *p-T* fitting equations were derived and reported. The achieved data allowed the determination of the molar enthalpies of vaporization and saturation vapor pressures at 298.15 K. The reported thermodynamic data could contribute to achieve a better understanding of the vaporization behavior of the azido- group containing organic compounds and improve the existent thermochemical parameter estimation methods for the compounds containing multiple azido groups.

Declaration of Competing Interest

The authors declare that they have no known competing financial interests or personal relationships that could have appeared to influence the work reported in this paper.

CRediT authorship contribution statement

Greta Bikelytė: Conceptualization, Formal analysis, Investigation, Writing – original draft, Writing – review & editing, Visualization, Validation. **Alexander G. Harter:** Resources, Writing – review & editing. **Martin A.C. Härtel:** Writing – review & editing, Supervision. **Stefanie B. Heimsch:** Resources, Writing – review & editing. **Thomas M. Klapötke:** Writing – review & editing, Supervision, Project administration, Funding acquisition.

Acknowledgments

For financial support of this work Ludwig-Maximilian University (LMU), the Office of Naval Research (ONR) [grant no. ONR N00014-19-1-2078], the Strategic Environmental Research and Development Program (SERDP) [contract no. W912HQ19C0033] and the DAAD (German Academic Exchange Service) [grant no. 57299294] are gratefully acknowledged. We would also like to thank Prof. Dr. Sergey P. Verevkin for the tremendous help establishing transpiration method in our group. Lastly, I would like to thank Andreas Neuer for his input during the time of his internship in our group.

Supplementary materials

Supplementary material associated with this article can be found, in the online version, at doi:10.1016/j.fluid.2021.113222.

References

[1] M. Meldal, F. Diness, Recent fascinating aspects of the CuAAC click reaction, Trends Chem. 2 (2020) 569–584, doi:10.1016/j.trechm.2020.03.007.
[2] Y. Takayama, K. Kusamori, M. Nishikawa, Click chemistry as a tool for cell engineering and drug delivery, Molecules 24 (2019) 172, doi:10.3390/molecules24010172.
[3] S. Bräse, K. Banert, Organic azides: Syntheses and Applications, John Wiley & Sons, 2010, doi:10.1002/9780470682517.
[4] T.M. Klapötke, Chemistry of High-Energy Materials, Walter de Gruyter GmbH & Co KG, Berlin, 2019.
[5] T. Lenz, T.M. Klapötke, M. Mühlemann, J. Stierstorfer, About the azido derivatives of pentaerythritol tetranitrate, Prop., Explos., Pyrotech. 46 (2021) 723, doi:10.1002/prep.202000265.
[6] O.V. Dorofeeva, O.N. Ryzhova, M.A. Suntsova, Accurate prediction of enthalpies of formation of organic azides by combining G4 theory calculations with an isodesmic reaction scheme, J. Phys. Chem. A 117 (2013) 6835–6845, doi:10.1021/jp404484q.
[7] M.H. Keshavarz, Improved prediction of heats of sublimation of energetic compounds using their molecular structure, J. Hazard. Mater. 177 (2010) 648–659, doi:10.1016/j.jhazmat.2009.12.081.
[8] M.J. McQuaid, H. Sun, D. Rigby, Development and validation of COMPASS force field parameters for molecules with aliphatic azide chains, J. Comput. Chem. 25 (2004) 61–71, doi:10.1002/jcc.10316.
[9] M. Jafari, M.H. Keshavarz, M.R. Noorbala, M. Kamalvand, A reliable method for prediction of the condensed phase enthalpy of formation of high nitrogen content materials through their gas phase information, ChemistrySelect 1 (2016) 5286–5296, doi:10.1002/slct.201601184.
[10] M.S. Elioff, J. Hoy, J.A. Bumpus, Calculating heat of formation values of energetic compounds: a comparative study, Adv. Phys. Chem. 2016 (2016) 1–11, doi:10.1155/2016/5082084.
[11] M.J. McQuaid, B.M. Rice, Report: Computational Chemistry-Based Enthalpy-of–Formation, Enthalpy-of-Vaporization, and Enthalpy-of-Sublimation Predictions for Azide-Functionalized Compounds, Army Research Lab Aberdeen Proving Ground MD Weapons and Materials Research Directorate, 2006.
[12] S.P. Verevkin, V.N. Emel'yanenko, M. Algarra, J.M. López-Romero, F. Aguiar, J.E. Rodriguez-Borges, J.C.E. da Silva, Vapor pressures and enthalpies of vaporization of azides, J. Chem. Thermodyn. 43 (2011) 1652–1659, doi:10.1016/j.jct.2011.05.028.
[13] V.N. Emel'yanenko, M. Algarra, J.C.G. Esteves da Silva, J. Hierrezuelo, J.M. López-Romero, S.P. Verevkin, Thermochemistry of organic azides revisited, Thermochim. Acta 597 (2014) 78–84, doi:10.1016/j.tca.2014.10.015.
[14] A.P. Häring, S.F. Kirsch, Synthesis and chemistry of organic geminal di- and triazides, Molecules 20 (2015) 20042–20062, doi:10.3390/molecules201119675.
[15] M. Claßen, S.B. Heimsch, T.M. Klapötke, Synthesis and characterization of new azido esters derived from malonic acid, Propellants Explos. Pyrotech. 44 (2019) 1515–1520, doi:10.1002/prep.201900285.
[16] S.B. Heimsch, Azido Liquids as Potential Hydrazine Replacements in a Hypergolic Bipropulsion System, LMU Munich, 2020, doi:10.5282/edoc.26932.
[17] T. Farhanullah, E.-J. Kang, E.-C. Yoon, S. Choi, J.Lee Kim, 2-[2-Substituted-3-(3,4-dichlorobenzylamino)propylamino]-1H-quinolin-4-ones as Staphylococcus aureus methionyl-tRNA synthetase inhibitors, Eur. J. Med. Chem. 44 (2009) 239–250, doi:10.1016/j.ejmech.2008.02.021.
[18] F. Samrin, A. Sharma, I.A. Khan, S. Puri, Synthesis and antibacterial activity of new diaryldiamines, J. Heterocycl. Chem. 49 (2012) 1391–1397, doi:10.1002/jhet.1040.
[19] H. Erhardt, A.P. Häring, A. Kotthaus, M. Roggel, M.L. Tong, P. Biallas, M. Jübermann, F. Mohr, S.F. Kirsch, Geminal diazides derived from 1, 3-dicarbonyls: a

protocol for synthesis, J. Org. Chem. 80 (2015) 12460–12469, doi:10.1021/acs.joc.5b02328.
[20] G. Bikelytė, M.A. Härtel, T.M. Klapötke, B. Krumm, A. Sadaunykas, Experimental thermochemical data of CWA simulants: triethyl phosphate, diethyl methylphosphonate, malathion and methyl salicylate, J. Chem. Thermodyn. 143 (2020) 106043, doi:10.1016/j.jct.2019.106043.
[21] W. Acree, J.S. Chickos, Phase transition enthalpy measurementsof organic and organometallic compounds. sublimation, vaporizationand fusion enthalpies from 1880 to 2010, J. Phys. Chem. Ref. Data 39 (2010) 043101, doi:10.1063/1.3309507.
[22] W. Acree Jr, J.S. Chickos, Phase transition enthalpy measurements of organic and organometallic compounds. Sublimation, vaporization and fusion enthalpies from 1880 to 2015. Part 1. C1− C10, J. Phys. Chem. Ref. Data 45 (2016) 033101, doi:10.1063/1.4948363.
[23] T.F. Fagley, H.W. Myers, The heats of combustion of cyclopentyl and cyclohexyl azides, J. Am. Chem. Soc. 76 (1954) 6001–6003 10.1021/ja01652a031.
[24] S.P. Verevkin, A.Y. Sazonova, V.N. Emel'yanenko, D.H. Zaitsau, M.A. Varfolomeev, B.N. Solomonov, K.V. Zherikova, Thermochemistry of halogen-substituted methylbenzenes, J. Chem. Eng. Data 60 (2015) 89–103, doi:10.1021/je500784s.
[25] V.N. Emel'yanenko, S.P. Verevkin, Benchmark thermodynamic properties of 1,3-propanediol: comprehensive experimental and theoretical study, J. Chem. Thermodyn. 85 (2015) 111–119, doi:10.1016/j.jct.2015.01.014.
[26] S.P. Verevkin, A.Y. Sazonova, V.N. Emel'yanenko, D.H. Zaitsau, M.A. Varfolomeev, B.N. Solomonov, K.V. Zherikova, Thermochemistry of halogen-substituted methylbenzenes, J. Chem. Eng. Data 60 (2014) 89–103, doi:10.1021/je500784s.
[27] E.C.W. Clarke, D.N. Glew, Evaluation of thermodynamic functions from equilibrium constants, Trans. Faraday Soc. 62 (1966) 539–547, doi:10.1039/TF9666200539.
[28] D. Kulikov, S.P. Verevkin, A. Heintz, Enthalpies of vaporization of a series of aliphatic alcohols: experimental results and values predicted by the ERAS-model, Fluid Ph. Equilibria 192 (2001) 187–207, doi:10.1016/S0378-3812(01)00633-1.
[29] A.D. Peschenko, O.V. Shvaro, V.I. Zubkov, Thermodyn. Org. Soedin. (Gorky) 39 (1988) 41.
[30] K.G. McCurdy, K.J. Laidler, Heats of vaporization of a series of aliphatic alcohols, Can. J. Chem. 41 (1963) 1867–1871, doi:10.1139/v63-274.
[31] S.P. Verevkin, V.N. Emel'yanenko, V. Diky, C.D. Muzny, R.D. Chirico, M. Frenkel, New group-contribution approach to thermochemical properties of organic compounds: hydrocarbons and oxygen-containing compounds, J. Phys. Chem. Ref. Data 42 (2013) 033102, doi:10.1063/1.4815957.
[32] A. Lee, C.K. Law, A. Makino, Aerothermochemical studies of energetic liquid materials: 3. Approximate determination of some thermophysical and thermochemical properties of organic azides, Combust. Flame 78 (1989) 263–274, doi:10.1016/0010-2180(89)90016-3.
[33] B. Isaev, S. Kanashin, M. Kozhukh, N. Tokarev, Combustion of some organic azides, chemical physics of combustion and explosion. chemical reaction kinetics, in: Proc. VI All-Union Symp. on Combustion and Explosion, Alma-Ata, 1980, pp. 97–101.

SUPPORTING INFORMATION

Thermodynamics of organic azides: experimental vapor pressures of organic polyazido compounds measured with the transpiration method

*Greta Bikelytė, Alexander G. Harter, Martin A. C. Härtel, Stefanie B. Heimsch, Thomas M. Klapötke**

Department of Chemistry
Ludwig-Maximilian University of Munich
Butenandtstr. 5–13, 81377 Munich (Germany)
*e-mail: tmk@cup.uni-muenchen.de

S1. Purity assessment

Elemental analysis (CHNS) of the liquid samples were performed with an *Elementar Vario El* instrument. ^{1}H-NMR spectra were measured with a *Bruker* AVANCE 400 MHz instrument and the processing was done with *MestReNova* v. 12.0.1-20560 software. Results of the purity assessment are presented in the following.

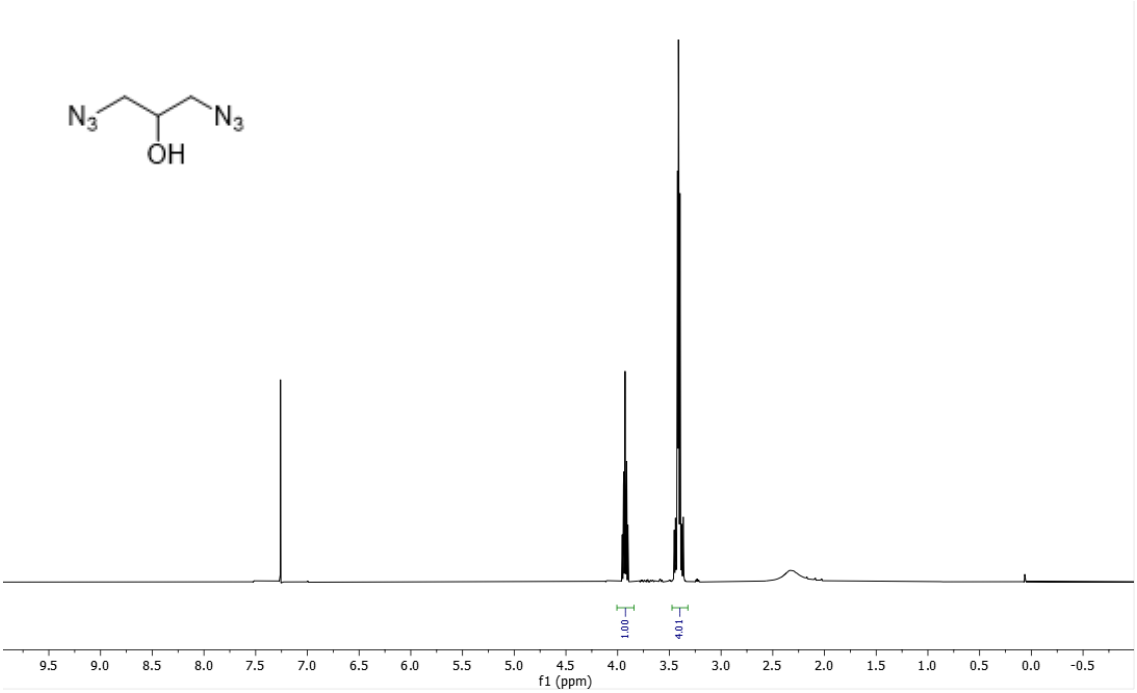

Figure S1. ^{1}H-NMR spectrum of **1,3-DAP**.

1,3-DAP: **^{1}H NMR** ($CDCl_3$, 400 MHz): δ = 3.9 (q, 1H, C*H*), 3.4-3.3 (m, 4H, CH_2), 2.3 (s, 1H, −O*H*) ppm. **^{13}C NMR** ($CDCl_3$, 101 MHz): δ = 69.7 (*C*H_2−OH), 54.0 (*C*H_2−N_3) ppm. **^{14}N NMR** ($CDCl_3$, 29 MHz): δ = −134 (N_β), −170 (N_β). **EA**: Calcd.: C 25.35, H 4.26, N 59.13 %; Found: C 25.05, H 3.99, N 59.04 %.

Table S1. Peak integrals for ^{1}H-NMR spectrum of **1,3-DAP** in Fig. S1.

δ range	Integral (normalized)	Integral (absolute)
4.01 .. 3.84	1.00	286012.37
3.47 .. 3.32	4.01	1150154.36

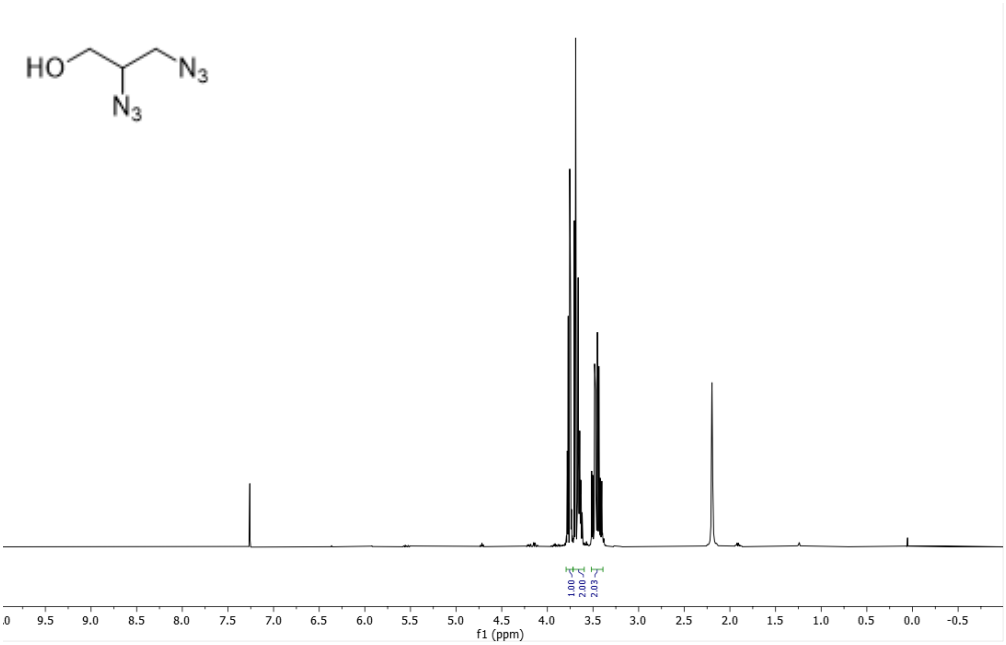

Figure S2. ^{1}H-NMR spectrum of enantiomeric mixture for compound **2,3-DAP**, *ee* not defined**.**

2,3-DAP: **^{1}H NMR** ($CDCl_3$, 400 MHz): δ = 3.82-3.72 (m, 1H), 3.7-3.6 (m, 2H), 3.5-3.4 (m, 2H), 2.2 (s, 1H, −O*H*) ppm. **^{13}C NMR** ($CDCl_3$, 101 MHz): δ = 62.7 (*C*H_2−OH), 62.7 (*C*H−N_3), 51.6 (*C*H_2−N_3) ppm. **^{14}N NMR** ($CDCl_3$, 29 MHz): δ = −134 ($N_β$), −135 ($N_β$), −169 (Nγ) ppm. **EA**: Calcd.: C 59.13, H 4.26, N 25.35 %; Found: C 58.71, H 3.92, N 25.58 %.

Table S2. Peak integrals for ^{1}H-NMR spectrum of **2,3-DAP** in Fig. S2.

δ range	Integral (normalized)	Integral (absolute)
3.79 .. 3.72	1.00	472590.20
3.72 .. 3.60	2.00	944603.83
3.52 .. 3.39	2.03	957175.81

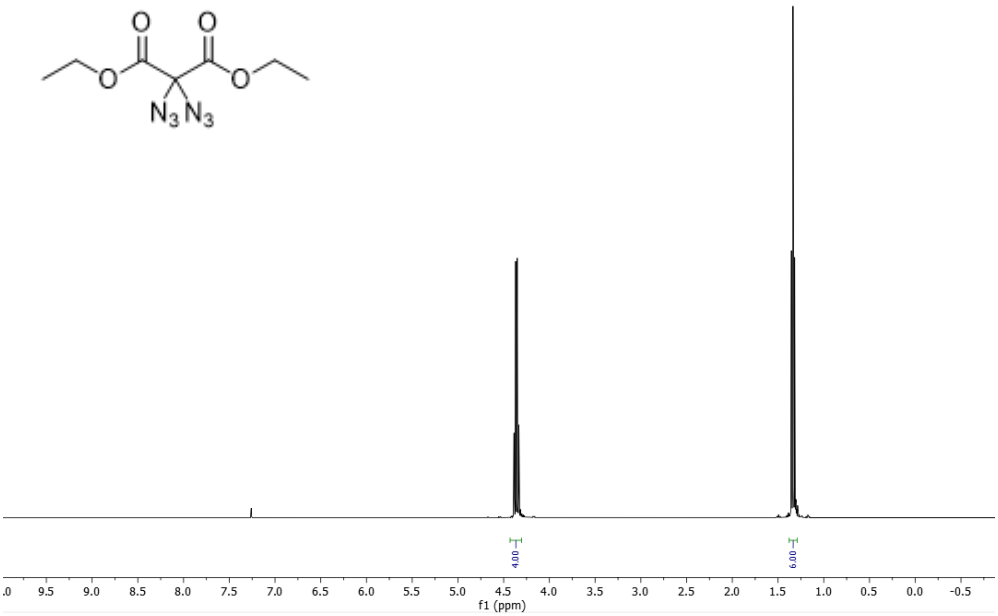

Figure S3. [1]H-NMR spectrum of **DE-DAM.**

DE-DAM: **^{1}H NMR** ($CDCl_3$, 400 MHz): δ = 4.4 (q, 4H, CH_2CH$_3$), 1.3 (t, 6H, CH_3) ppm. **^{13}C NMR** ($CDCl_3$, 101 MHz): δ = 163.6 (*C*O$_2$Et), 80.0 (*C*(N$_3$)$_2$), 64.2 (*C*H$_2$CH$_3$), 14.0 (OCH$_2$*C*H$_3$) ppm. **^{14}N NMR** ($CDCl_3$, 29 MHz): δ = −141 (N$_\beta$), −156 (Nγ) ppm. **EA**: Calcd.: C 34.70, H 4.16, N 34.71 %; Found: C 34.97, H 3.75, N 33.01 %.

Table S3. Peak integrals for [1]H-NMR spectrum of DE-DAM in Fig. S3.

δ range	Integral (normalized)	Integral (absolute)
4.43 .. 3.30	4.00	1304431.14
1.38 .. 1.29	6.00	1958122.41

S2. Experimental results of DE-DAM

Table S4. DE-DAM: experimental conditions and resulting absolute vapor pressures p_{sat} obtained by the transpiration method in this work.

$\Delta_l^g H_m^\circ$ (298.15 K) = (76.2 ± 2.2) kJ mol^{-1}

$$\ln\left(\frac{p_{sat}}{p^0}\right) = \frac{383.7}{R} - \frac{114870.37}{RT} - \frac{129.7}{R} ln\frac{T}{298.15K}$$

T[a]	m[b]	V_{N2}[c]	T_{amb}[d]	Gasflow	p_{sat}[e]	$u(p_{sat})$[f]
K	mg	dm³	K	dm³·h^{-1}	Pa	Pa
274.6[g]	0.41	69	297.4	4.8	0.06	0.01
274.6[g]	0.46	79	296.7	4.8	0.06	0.01

274.6[g]	0.42	72	298.0	4.0	0.06	0.01
274.7[g]	0.44	70	297.6	3.0	0.06	0.01
278.5	0.67	78	296.3	4.8	0.09	0.01
283.4	0.50	30	296.4	4.8	0.17	0.02
288.3	0.52	18	296.2	4.8	0.30	0.02
293.3	0.51	12	297.1	4.8	0.44	0.03
298.2	0.51	6.4	296.8	4.8	0.80	0.05
303.2	0.45	3.6	297.1	4.8	1.25	0.07
308.1	0.50	2.4	297.7	4.8	2.08	0.11
313.1	0.47	1.5	297.4	4.8	3.26	0.17
313.1	0.50	1.6	296.4	4.8	3.13	0.17
313.1	0.51	1.6	296.3	4.8	3.20	0.17
318.1	0.58	1.2	296.5	4.8	4.83	0.25
323.0	1.00	1.2	297.5	4.8	8.40	0.43
328.0	1.49	1.2	297.0	4.8	12.5	0.6
333.0	2.22	1.2	296.5	4.8	18.5	0.9
338.0	3.09	1.2	297.5	4.8	25.8	1.3
342.9	7.15	1.9	297.2	4.8	38.9	2.0
347.7[g]	5.86	1.0	296.2	3.0	59.0	3.0
347.7[g]	4.43	0.8	296.2	3.0	59.5	3.0
347.7[g]	4.43	0.8	296.2	3.0	59.3	3.0
347.8[g]	4.47	0.7	296.5	3.0	60.2	3.0
347.9[g]	4.38	0.7	296.4	3.0	59.1	3.0
352.9[g]	9.40	1.1	296.8	4.5	83.4	4.2
353.1[g]	6.11	0.7	296.5	2.4	84.7	4.2

[a] Saturation temperature ($u(T)$ = 0.1 K). [b] Mass of transferred sample condensed at 243 K. [c] Volume of nitrogen ($u(V)$ = 0.01 dm^3) used to transfer m ($u(m)/m$ = 0.015) of the sample. [d] T_{amb} is the temperature of the soap film flowmeter used for measurement of the gas flow. [e] Vapor pressure at temperature T obtained from the m and the residual vapor pressure at the condensation temperature, calculated by an iteration procedure; $p°$ = 1 Pa. [f] Standard uncertainties were calculated with u(p/Pa) = 0.01 +0.05(p/Pa). The uncertainties for T, V and m are standard uncertainties. The determination of the u(m) included the evaluation of the uncertainties associated with the preparation of internal standard solutions (caused by weighing and pycnometers), volumetric standard addition, chromatographic calibration and determination.The uncertainty of the molar enthalpy of vaporization (at 298.15 K) is the standard uncertainty with a confidence level of 0.68, calculated including uncertainties of vapor pressure,

uncertainties from the fitting equation and the uncertainty of temperature adjustment to T = 298.15K. Detailed information on the methods of calculations was published previously [1; 2]. [g]Values not included for the determination of the fitting equation and molar enthalpies of vaporization.

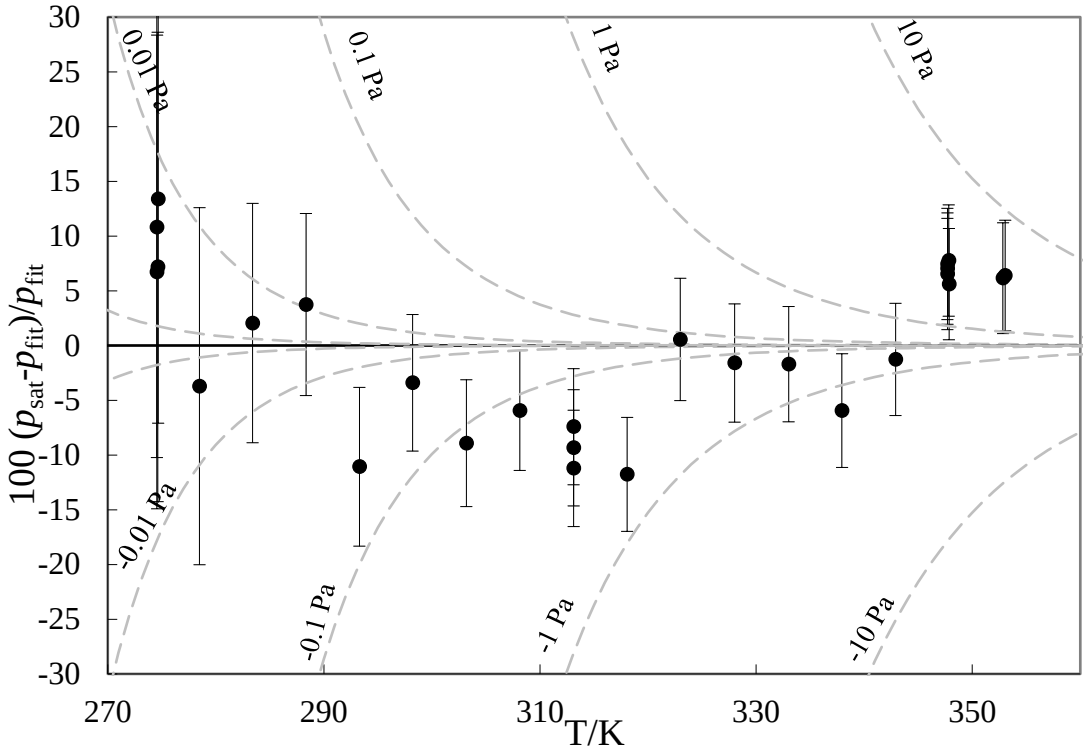

Figure S4. Experimental vapor pressure (●) deviations from the derived fitting equation for DE-DAM in Table S1. Dashed lines display the absolute deviation in pressure. Error bars are the standard uncertainties as reported in Table S1.

S3. Comparisons to other literature data

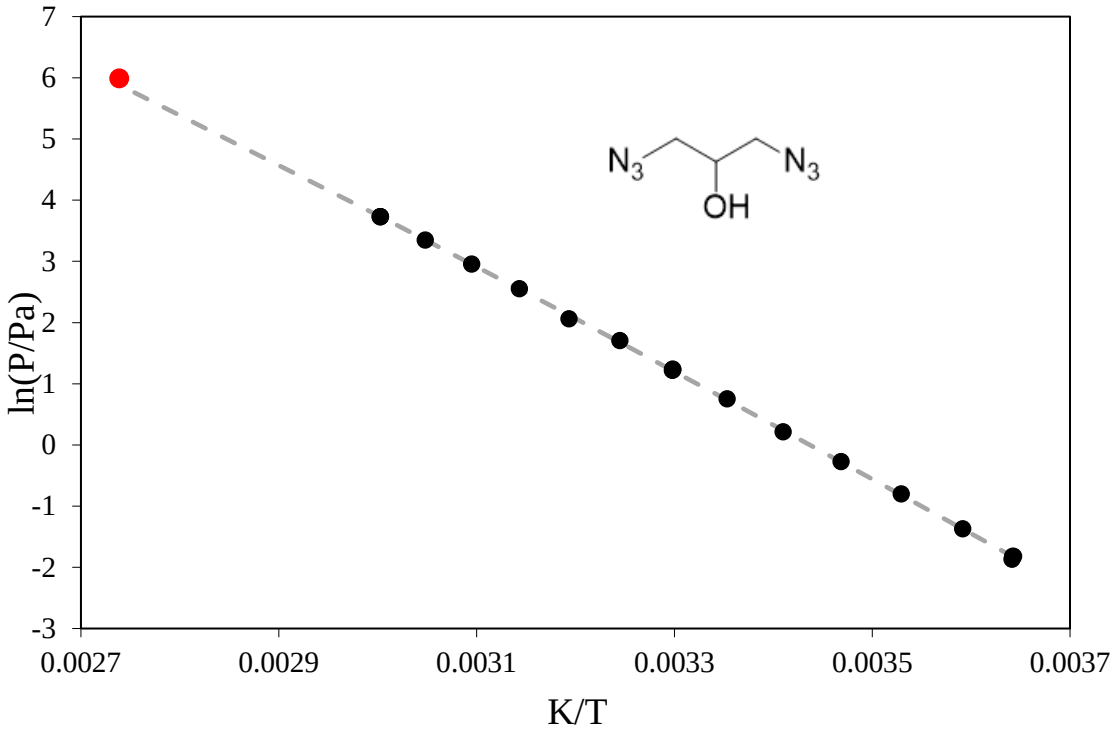

Figure S5. Experimental vapor pressures of 1,3-DAP from this work (●) and the derived fitting equation from the Table 3 (dashed line) in comparison with the boiling point (at reduced pressure of 3 mmHg) from the work of *Isaev et al.* [3] (●).

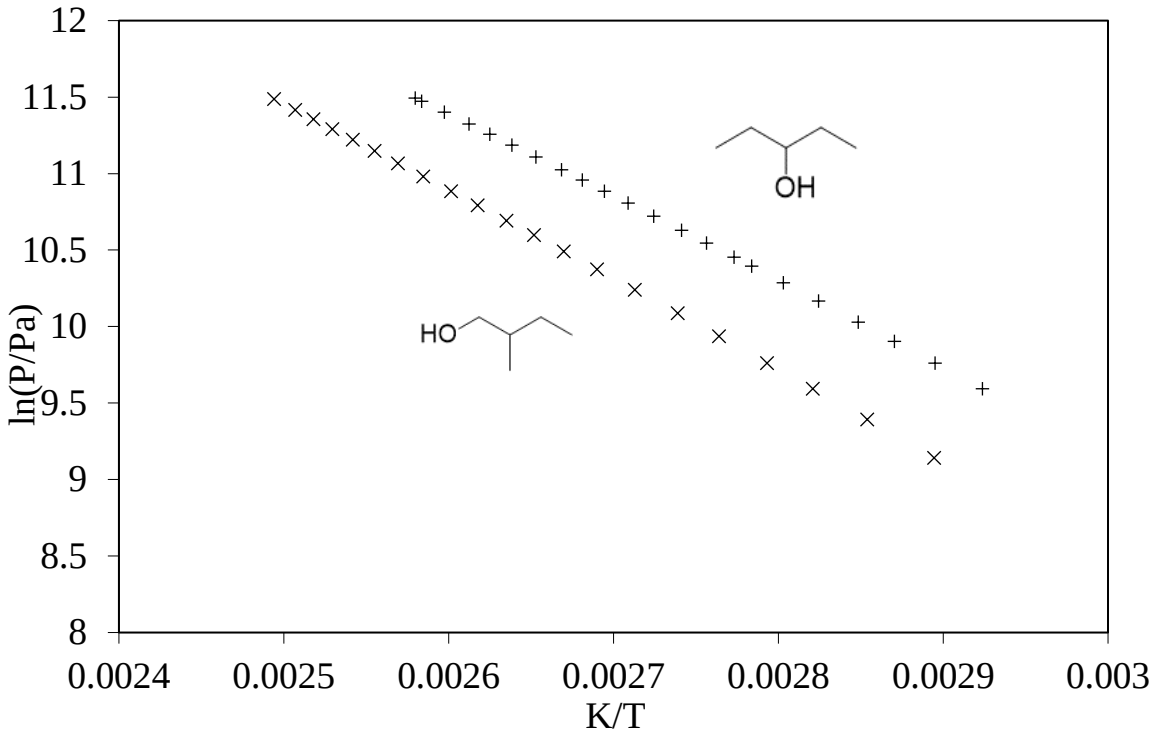

Figure S6. Experimental vapor pressures as of aliphatic analogues for diazidopropanols investigated in this work: 3-pentanol (+) and 2-methyl-1-butanol (×), as reported in the work by *Čenský et al.* [4].

S4. HPLC-DAD parameters

HPLC	*Shimadzu Prominence*® with LC-20AD pump module and SPD-M20A Diode Array Detector; software *LabSolutions v*5.86
Analytical column	*Phenomenex Kinetex*® (2.6 µm Biphenyl, 100 Å, 150 × 4.6 mm)
Oven temperature:	40°C
Program	
1,3-DAP	Injection volume: 1 µL Total Flow: 0.75 mL/min Mobile phase: 25 % MeOH, 75 % Water Time: 15 min Channel 1 wavelength: 212 nm (1.3-DAP) Retention time: 6.0 min Channel 2 wavelength: 232 nm (standard, RDX) Retention time: 13.6 min
2,3-DAP	Injection volume: 1 µL Total Flow: 0.75 mL/min Mobile phase: 25 % MeOH, 75 % Water Time: 15 min Channel 1 wavelength: 212 nm (2.3-DAP) Retention time: 6.4 min Channel 2 wavelength: 232 nm (standard, RDX) Retention time: 13.5 min
DE-DAM	Injection volume: 1 µL Total Flow: 0.95 mL/min Mobile phase: 60 % MeOH, 40 % Water Time: 10 min Channel 1 wavelength: 212 nm (DE-DAM) Retention time: 8.4 min Channel 2 wavelength: 280 nm (standard, 4-MNT) Retention time: 6.2 min

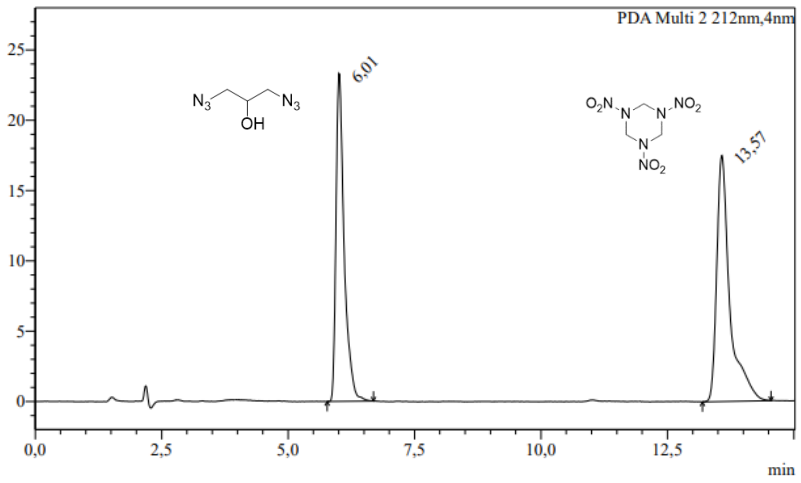

Figure S6. HPLC-DAD chromatogram of 1,3-DAP (retention time 6.01 min, integration wavelength λ = 212 nm) and standard RDX (retention time 13.57 min, integration wavelength λ = 212 nm), measured with a method, described in this section.

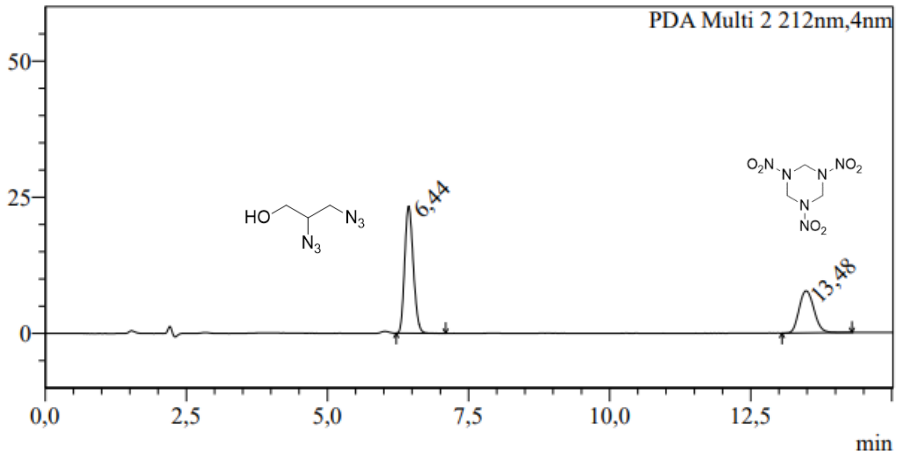

Figure S7. HPLC-DAD chromatogram of 2.3- DAP (retention time 6.44 min, integration wavelength λ = 212 nm) and standard RDX (retention time 13.48 min, integration wavelength λ = 232 nm), measured with a method, described in this section.

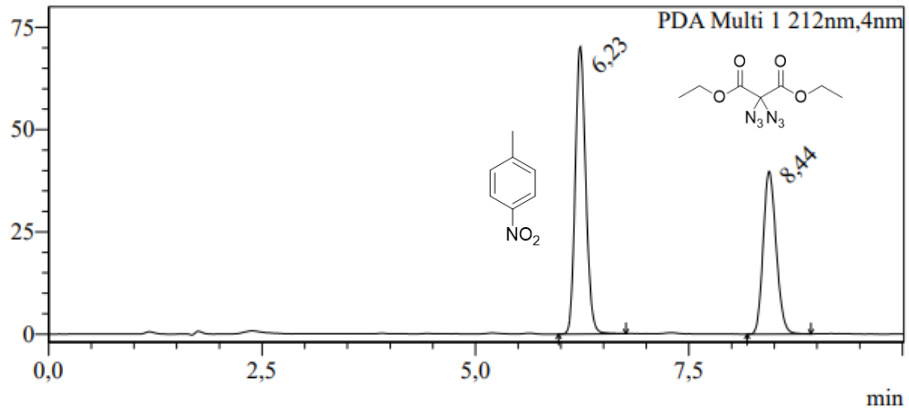

Figure S8. HPLC-DAD chromatogram of DE-DAM (retention time 8.40 min, integration wavelength λ = 212 nm) and standard 4-MNT (retention time 6.21 min, integration wavelength λ = 280 nm), measured with a method, described in this section.

[1] V.N. Emel'yanenko, S.P. Verevkin, Benchmark thermodynamic properties of 1,3-propanediol: Comprehensive experimental and theoretical study, J. Chem. Thermodyn. 85 (2015) 111-119. http://dx.doi.org/10.1016/j.jct.2015.01.014.

[2] S.P. Verevkin, A.Y. Sazonova, V.N. Emel'yanenko, D.H. Zaitsau, M.A. Varfolomeev, B.N. Solomonov, K.V. Zherikova, Thermochemistry of halogen-substituted methylbenzenes, J. Chem. Eng. Data 60 (2014) 89-103. https://doi.org/10.1021/je500784s.

[3] B. Isaev, S. Kanashin, M. Kozhukh, N. Tokarev, Combustion of some organic azides, Chemical Physics of Combustion and Explosion. Chemical Reaction Kinetics, Proc. VI All-Union Symp. On Combustion and Explosion, Alma-Ata, 1980, pp. 97-101.

[4] M. Čenský, P. Vrbka, K. Růžička, M. Fulem, Vapor pressure of selected aliphatic alcohols by ebulliometry. Part 2, Fluid Phase Equilibria 298 (2010) 199-205. https://doi.org/10.1016/j.fluid.2010.06.020.

5.5. Measurements of phlegmatized TATP mixtures (Article 5)

Article 5: Phlegmatization of TATP and HMTD with Activated Charcoal as Training Aid for Explosive Detection Dogs

The results were published in the journal *Propellants, Explosives, Pyrotechnics* (2022) [113] and are reprinted with permission. Copyright (2022) John Wiley and Sons, New York, NY. DOI: doi.org/10.1002/prep.202100057.

Full Paper

Propellants, Explosives, Pyrotechnics

doi.org/10.1002/prep.202100057

Phlegmatization of TATP and HMTD with Activated Charcoal as Training Aid for Explosive Detection Dogs

Isabel Wilhelm,[b] Greta Bikelytė,[c] Michael Wittek,[b] Martin Andreas Christian Härtel,*[a] Dirk Röseling,[b] and Thomas Matthias Klapötke[c]

Abstract: Both TATP and HMTD could be phlegmatized by coprecipitation with active charcoal resulting in mixtures with a nominal content of 40 wt-% (d40-TATP) and 10 wt-% (d10-HMTD), respectively. In terms of impact and friction sensitivity for both peroxides a content of 40 wt-% resulted in >30 Nm impact sensitivity and >360 N friction sensitivity. Both phlegmatized peroxides passed the Koenen Tube and Thermal Stability Test according to the UN recommendation on the transport of dangerous goods test manual. Investigations with a process mass spectrometer indicate that d40-TATP can produce a saturated TATP headspace at least in the same time as the same amount of pure TATP. Measurements with the transpiration method demonstrated that the vapor pressure p_{sat} at 298.15 K of d40-TATP (2.3 Pa) and d32.7-TATP (0.9 Pa) is lower than that of pure TATP (6.7 Pa). Headspace SPME-GC/MS measurements revealed that the active charcoal does not contribute to the vapor profile of the training aid. Both d40-TATP and d10-HMTD were tested as training aids for explosive detection dog teams (EDD). In both differentiation track and realistic environment scenarios a detection rate of 100% could be achieved by German Federal Police EDD with a false positive rate of solely 3%.

Keywords: Peroxides · Explosive Detection · Canine Training Aid · Explosive Detection Dogs · Vapor Pressure

1 Introduction

Triacetone triperoxide (TATP) is a notorious explosive that was discovered accidentally by *Wolffenstein* [1] in 1895. With respect to its high vapor pressure and extreme sensitivity towards impact and friction, the explosive neither finds military nor civil application. Dry TATP is reported to have a higher impact (0.1 J) and friction sensitivity (0.05 N) than the crude product from the aqueous synthesis (0.5 J, 0.2 N) that is stabilized by trace amounts of water [2]. Despite that, the compound is a homemade explosive that is illegally synthesized by both amateur chemists and terrorists, which is reflected by numerous incidents [3–5]. Due to the dangerous popularity of the illicit use of TATP and hexamethylene triperoxide diamine (HMTD) law enforcements units are urged to train their explosive detection dog teams (EDD) for the detection of peroxide explosives like TATP and HMTD. Regarding the sensitivity of the peroxides, training for EDD is frequently performed with training aids that contain TATP or HMTD (mostly in trace amounts) with numerous commercial, patented products available. These include microamounts of the peroxide explosives coated on porous metal [6–7] and proprietary mixtures with phlegmatization agents [8–12]. Recent research work dealing with the phlegmatization of TATP/HMTD for canine training aids includes a study using ionic liquids as an inert matrix [2] (commercially available at the Diehl Defence GmbH & Co. KG) and the microencapsulation of TATP in polymers [13–15]. The latter development has been commercialized in form of a microsphere heater system [15]. The vapor sensing of explosive materials has been reviewed by *Lefferts* and *Castell* [16] including animal olfaction approaches like EDD. For the training of an EDD it is essential to both train the detection of confined explosives, as well as large bulk amounts of explosive material. Whilst confined explosives (e.g., well-sealed pipe bomb) release solely trace amounts of explosive vapor into the air, large open bulk amounts (e.g., a trolley filled with explosive) release a "cloud" of vapor with high concentration. If the latter scenario is not trained properly, the EDD may be overcharged by the presence of the vapor "cloud", which possibly results in inability of the EDD to locate the explosive or even non-detection. This phenomenon is called "large amount problem"[17].

Canine training aids have been reviewed in detail by *Simon et al.* [18]. Commercially available HMTD training aids

[a] *M. A. C. Härtel*
Research and Testing
German Federal Police Headquarters
Schwartauer Landstr. 1–5, 23554 Lübeck, Germany
**e-mail: martin.haertel@polizei.bund.de*
[b] *I. Wilhelm, M. Wittek, D. Röseling*
Energetic Materials–Safety and Security Research
Fraunhofer Institute for Chemical Technology
Joseph-von-Fraunhofer Strasse 7, 76327 Pfinztal, Germany
[c] *G. Bikelytė, T. M. Klapötke*
Ludwig-Maximilians-Universität München
Department of Chemistry
Butenandtstr. 5–13, 81377 Munich, Germany

have been characterized [19] without disclosing the brand. The results indicate headspace variation of bulk HMTD vs. commercial training aids that contain HMTD and diatomaceous earth [8–11]. Multiple research efforts [20–24] focus on the development and characterization of canine training aids, which are, to the best knowledge of the authors, not commercially available.

The majority of the commercially available canine training aids mentioned before remain to be products with proprietary ingredients, production processes (e.g., used solvents) and sparse public availability of (peer-reviewed) characterization data including the characterization of the vaporization behaviour and headspace profile.

In order to ensure the proper training of EDD for the detection of large bulk amounts of the highly sensitive peroxide explosives TATP and HMTD the German Federal Police commissioned the Fraunhofer Institute for Chemical Technology with the development of a training aid for both TATP and HMTD that is safe to handle and can be used for the training of large bulk amount scenarios of both compounds. It was our intention to publish the results without prior patenting to give the international EDD training community access to an open-source canine training aid for peroxide explosives with public availability of the synthetic procedure and extensive characterization data.

The task was realized by phlegmatization of both peroxides with activated charcoal. The resulting materials were characterized in terms of handling safety (impact and friction sensitivity), security testing (Koenen Tube Test, Thermal Stability Test), toxicity (Lumistox test) and detectability with EDD provided by German Federal Police. With respect to the difficult gas phase behaviour of HMTD [19, 25–27] solely the volatility of the TATP training aid was investigated by vapor pressure measurements with the transpiration method (performed at the University of Munich) and by real-time concentration monitoring with a process mass spectrometer. Additionally, the headspace composition of the TATP and HMTD training aids was investigated with SPME-GC/MS (solid phase microextraction gas chromatography mass spectroscopy).

2 Experimental Section

Within the framework of the development of the training aid one of the main tasks was to find a stabilizing additive that would not contribute to the odor profile of the peroxides, but would decrease the friction and impact sensitivity of the peroxides so that they could be used for safe handling in training. Activated charcoal was selected because of its odorless characteristic. A lot of other materials were tried to be used as additive materials (e.g., molecular sieve, silica gel, diatomaceous earth). Some materials (e.g., diatomaceous earth) were excluded with respect to their characteristic smell (perceived olfactorally by the experimenter), some materials have even increased the friction and impact sensitivity (e.g., sand). Within the stabilization agent screening performed in this work active charcoal provided the best results and its peroxide mixtures were further characterized.

Chemicals: Hydrogen peroxide (30 %, p.a. stab.) and citric acid (without further purification) were obtained from Carl Roth GmbH + Co. KG. Activated Charcoal (SUPELCO, puriss., p.a., powder) was obtained from Sigma Aldrich. Acetone ($\geq$ 99 %, technical) and hydrochloric acid (37 %, Reag. Ph. Eur.) were obtained from VWR International GmbH. Urotropin (for synthesis) was obtained from Merck KGaA.

2.1 Synthesis of TATP on Activated Charcoal: d40-TATP

15.0 mL of acetone were cooled down to about −10 to −5 °C, then 9.0 mL hydrogen peroxide were added within 45 minutes while cooling and stirring constantly. Afterwards 1.0 mL of hydrochloric acid (37 %) was added dropwise under cooling in an ice-salt bath in the temperature range of −10 °C to −5 °C and stirring within 5 minutes. The solution was stirred for 45 minutes in the ice-salt bath and then slowly warmed up to room temperature. The TATP, which precipitated overnight, was filtered and washed with distilled water until the filtrate reached a neutral pH value. The TATP was dried at room temperature overnight. The procedure yielded ~3.0 g of pure TATP.

These 3.0 g of TATP were diluted in 15.0 mL acetone and 4.5 g of activated charcoal were slowly added while stirring. The mixture was stirred for one hour, followed by addition of 50 mL distilled water. The mixture was filtered and dried overnight at room temperature in a fume hood (Figure 1). The procedure yielded ~7.5 g TATP/activated charcoal-mixture with 40 wt.–% of TATP in the mixture (d40-TATP), as determined via GC-FID, method specified in 2.6.2.

Figure 1. Dried homogeneous TATP/activated charcoal-mixture d40-TATP on top of a filter paper (circular, folded once).

2.3 Synthesis of HMTD on Activated Charcoal: d40-HMTD, d10-HMTD and d5-HMTD

16.0 mL of hydrogen peroxide were cooled down to −10 to −5 °C, then 8.0 g urotropin were added within 30 minutes keeping the temperature below −5 °C by the use of an ice-salt bath and stirring constantly. After an additional 20 minutes, 8.0 g of citric acid was added within the time span of 30 minutes. The solution was stirred another 20 minutes until the acid was dissolved. Then, while maintaining the cool conditions, 6.0 g of activated charcoal was added within 20 minutes. The resulting suspension was stirred for another 60 minutes in the ice-salt bath (−10 °C to −5 °C) and then slowly warmed up to room temperature. HMTD/activated charcoal precipitated overnight and was filtered and washed with distilled water until neutrality of the filtrate was reached. The HMTD/activated charcoal-mixture was dried overnight at room temperature in a fume hood (Figure 2). The procedure yielded ~9.6 g HMTD/activated charcoal-mixture with 40 wt.–% of HMTD in the mixture (d40-HMTD), as determined via HPLC, method specified in 2.4.

12.5 g of the 40 % HMTD/activated charcoal (d40-HMTD) were well mixed with 37.5 g pure activated charcoal to obtain 50.0 g of a 10 % HMTD/activated charcoal-mixture (d10-HMTD). To obtain 50.0 g of a 5 % mixture (d5-HMTD), 6.25 g of 40 % HMTD/activated charcoal were mixed with 43.75 g pure activated charcoal.

Figure 2. Dried homogeneous HMTD/activated charcoal-mixture d40-HMTD on top of a filter paper (circular, folded once).

Table 1. HPLC method eluent gradient.

Time min	B %	Flow mL/min
0	17	0.6
8	90	0.6
9	90	0.6
10	17	0.6

2.4 High Performance Liquid Chromatography (HPLC)

The content of HMTD in the mixtures was determined using a HPLC device (1290 Infinity) by Agilent.

HPLC conditions. Column: Kinetex 2.6 μm Biphenyl 100 × 4.6 mm with C18 pre-column (Phenomenex); Eluent: Water (A): Acetonitrile (B), 83 : 17 (Table 1); Flow: 0.6 mL/min; Detection: 200 nm (DAD); Injection volume: 5 μL; Column temperature: 308.15 K; Analysis time: 10 min.

2.5 Impact and Friction Sensitivity

The impact sensitivity was determined by the BAM (Bundesanstalt für Materialprüfung - Federal Institute for Material Testing) Fallhammer test 3(a)(ii) and likewise the friction sensitivity was determined with BAM Friction test 3(b)(i) in accordance with the UN Recommendation on the Transport of Dangerous Goods, Manual of Tests and Criteria [28].

2.6 Gas Chromatography

2.6.1 SPME-GC/MS Analysis

The pure activated charcoal and the mixture with TATP was analyzed via SPME-GC/MS (Gas Chromatograph 7890 B and Mass Spectrometer 5977 A by Agilent; PAL autosampler by CTC Analytics). The SPME-GC/MS analysis was performed using the following parameters:

GC/MS conditions. Column: HP-5MS, 30 m × 0.25 mm ID, × 0.25 μm film; Liner: 2 mm, Siltek coated (Restek); Oven: 343.15 K–4 min, 10 K/min–563.15 K; Inj.-Temperature: 523.15 K, split-ratio 6; mass spectrometer: scan, 10–500 amu.

SPME conditions. Fiber: 65 μm Polydimethylsiloxane (PDMS) / DVB (Divinylbenzene) (Supelco); Incubation: 5 min at 318.15 K; Extraction: 5 min at 318.15 K; Desorption: 5 min at 523.15 K.

The activated charcoal mixture with HMTD was analyzed via SPME-GC/MS as well. (Gas Chromatograph 7890 A and Mass Spectrometer 5975 C by Agilent; PAL autosampler by CTC Analytics). This analysis was performed with the following parameters:

GC/MS conditions. Column: HP–5 MS, 30 m x 0.25 mm ID, x 0.25 μm film; Liner: 2 mm, Siltek coated (Restek)

Oven: 323.15 K–3 min, 15 K/min–553.15 K; Inj.-Temperature: 533.15 K, split-ratio 10; mass spectrometer: scan, 10–500 amu.

SPME conditions. Fiber: 50/30 μm DVB / CARBOXEN-PDMS (Divinylbenzene/ Carboxen/ Polydimethylsiloxane) (Supelco); Incubation: 30 min at 323.15 K; Extraction: 15 min at 323.15 K; Desorption: 5 min at 533.15 K.

2.6.2 GC-FID TATP Content Determination[M1]

The activated charcoal mixture with TATP was analyzed via GC (Agilent 6890N) using following parameters:

Column: Supelco Equity – 5, 30m x 0.32mm ID x 1µm film; Liner: 4 mm, Siltek coated (Agilent); Oven: 333.15 K – 3 min, 10 K/min – 523.15 K; Inj.-Temperature: 423.25 K, split-ratio 20; flow: He, 2 mL/min; Detection: 523.15 K; FID: H_2/Air – 30/400 ml/min, Make-up Gas – 25 mL/min.

Sample preparation:

Approximately 10 mg of the TATP/activated charcoal samples were weighed into a 10 ml flask and filled with acetone. The flasks were then placed in an ultrasonic bath for 10 minutes and then the liquid phase was filtered off.

2.7 Security Testing: Koenen Tube Test and Thermal Stability

The Koenen Tube Test is used to determine the sensitivity of solid and liquid substances to the effect of intense heat under confinement. The requirements for the test method are listed in the UN Recommendation on the Transport of Dangerous Goods, Manual of Tests and Criteria, Koenen Tube Test 2(b) [28]. Samples of the test material are confined in a steel tube fitted with an orifice plate at the top end with varying vent hole diameters. The steel tube is heated along its entire length by four burners which are positioned around the tube (Figure 3). The vent hole diameter is decreased from 20 mm until the increased confinement causes a reaction to burst the tube. The limiting diameter is determined as the largest diameter at which an explosion is observed.

2.8 Thermal Stability

The thermal stability test type 3(c)(i) according to the UN Recommendation on the Transport of Dangerous Goods, Manual of Tests and Criteria [28] has been carried out. This test procedure is used to measure the stability of a substance when it is exposed to higher temperatures in order to determine if the substance is too dangerous for transportation. A 50 g sample is filled into a beaker, covered and placed in an oven. The oven is heated up to 348.15 K and the sample is left there for 48 hours or until an ignition or explosion occurs.

If the substance shows no signs of reaction in this test, it can be considered thermally stable. If the test result is "positive (+)", the substance should be considered as thermally unstable for transportation.

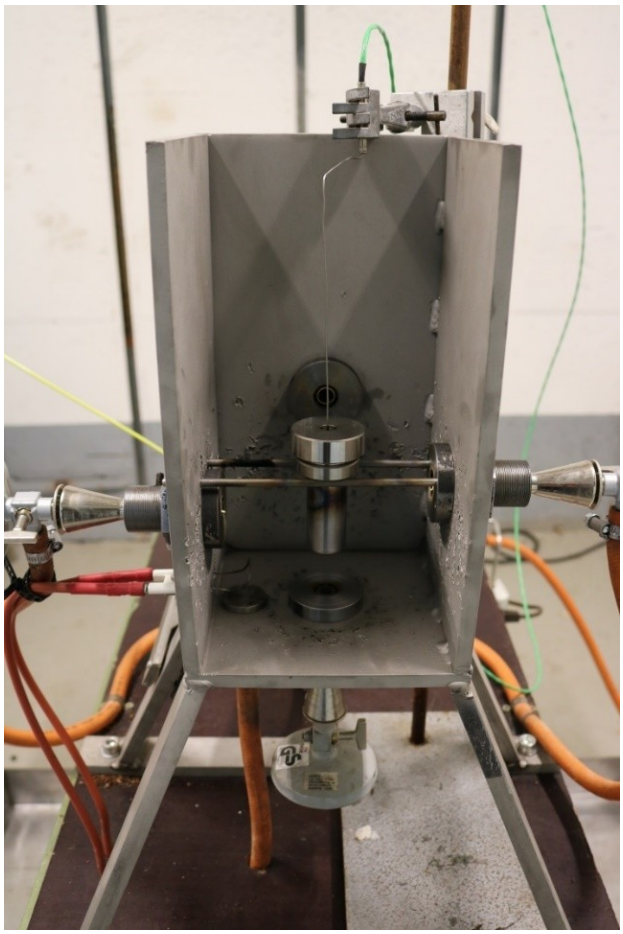

Figure 3. Koenen Tube Test Apparatus.

2.9 Accelerating Rate Calorimeter (ARC)

A dilution series for the HMTD/activated charcoal mixture was analyzed by ARC. The Accelerating Rate Calorimetry method is used for the detection of thermally induced decomposition reactions [29].

The measurements were performed in an Accelerated Rate Calorimeter (ARC ES) from Thermal Hazard Technology using the following parameters:

Weighing 300 mg, with a phi factor of approx. 7 (phi factor sample plus vessel without pressure transducer).

The sample vessel is made of titanium; Start temperature: 313.15 K; Final temperature: 513.15 K; Step size: 5 K; Sensitivity: 0.2 K/min; Waiting time: 10 min.

2.10 LUMIStox Test for Toxicity

The luminescent bacteria test was performed to estimate the acute toxicity of HMTD and TATP. This test was carried out with the LUMIStox 300 instrument from Dr. Lange. In combination with the LUMIStherm incubation block it

meets the technical requirements of DIN 38412 L34/L341 and the international standard DIN EN ISO 11348 [30, 31]. In the luminescent bacteria test, the ability of the marine bacteria *Vibrio fischeri* to glow under optimal growth conditions (bioluminescence) is used. Toxic substances cause a reduction in bioluminescence, which is proportional to the toxicity of the sample. The toxicity of the sample is expressed as G_L value [32], a dilution factor.

0.2 g of the peroxide explosives were suspended in a 2% NaCl solution. After 3 days the suspension was filtered. The G_L value is then determined with the filtrate obtained in the luminescent bacteria test. The reported solubility of TATP in water is 177 mg L^{-1} (22 °C) [33]. According to *Matyáš* and *Pachman* [34], the solubility of HMTD in water is 100 mg L^{-1}.

2.11 Process Mass Spectrometer Measurements

In this experiment, the spread of TATP and d40-TATP in the gas phase was compared. Since d40-TATP is to be used to enable gas phase experiments under safe conditions, the time until saturation of the gas phase is reached, is valuable information. Since the saturation time depends on various external parameters such as temperature [35], humidity, gas volume, packaging, etc., the experimental setup was configured to minimize the fluctuation of these parameters. TATP and d40-TATP were laid out in a closed gas volume and the increase of concentration in the gas phase was monitored. The aim of the experiments was to verify that the mixture, which is safe to handle, shows a similar behaviour in comparison to pure TATP.

Method: The diffusion rate of any substance into the gas phase depends on the total surface area. In order to obtain the same macroscopic surface, both the TATP and d40-TATP were laid out in the same open cardboard box in DIN A4 format (297 x 210 mm). Larger agglomerates were carefully crushed so that the particle size was optically identical for d40-TATP and pure TATP. 100 g of pure TATP and 100 g of d40-TATP (40 wt.–% pure TATP) were used.

An acrylic glass cuboid (aquarium) with a volume of 150 litres was used to confine the closed gas volume (Figure 4). The cuboid has a removable cover that allows to put the TATP or the mixture into the chamber. It also has 9 inlets each closed with an Agilent long-life, non-stick inlet septum made from silicone polymers. 3 of the inlets are on the lid and 3 on each of the two smaller sides.

The concentration of TATP in the aquarium was monitored with a Pfeiffer MS OmniStar GSD 320 O mass spectrometer using the secondary electron multiplier (SEM). For monitoring the concentration in the gas phase, mass channels, that were only influenced by TATP, were selected. During the electron impact ionization of the TATP, the fragments with the following mass to charge ratios should have the highest intensity according to the literature: *m/z* 43, 58, 59 and 75 [36]. For both TATP and d40-TATP a signal increase in channels 43, 58 and 59 could be observed.

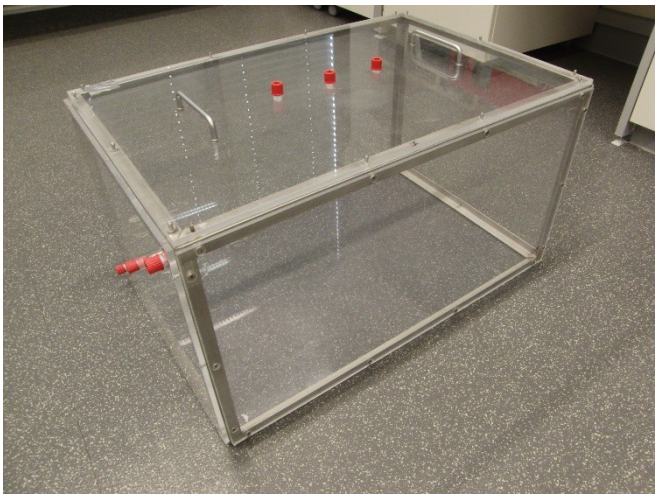

Figure 4. Glass cuboid used for the process mass spectrometer measurements.

Acetone is used in the synthesis of TATP and d40-TATP. Since the synthesis of TATP involves chemical precipitation with water and a subsequent additional drying process, it is very unlikely that residues of acetone will remain. However, since acetone decomposes into the same fragments with mass to charge ratios 43 and 58 during ionization [37] (Figure 5), the results of TATP and TATP/activated carbon were compared with an identical experiment carried out with 1 mL acetone. The spreading time of acetone is many times faster than that of TATP and acetone showed no signal in the m/z 59 channel. With TATP and d40-TATP, however, all channels 43, 58 and 59 showed the same concentration trends. Considering all these aspects, it is relatively safe to assume that the resulting signals in the *m/z* 43, 58, and 59 channels can be allocated to the presence of TATP.

The aquarium was filled with ambient air, and the relative humidity during the experiments averaged at about 40%. The temperature was 24 °C.

Experimental: Before TATP or d40-TATP were laid out into the aquarium, the aquarium was cleaned thoroughly with distilled water and flushed with pure Nitrogen for a couple of hours. The lid was closed and the concentration was monitored with the mass spectrometer. No change in the background signal of the aquarium could be detected between the two measurements, ensuring an identical starting point for the experiments.

The respective substance was positioned into the aquarium and the lid was closed. The measurement was continued until saturation was achieved for several hours (Figure 6).

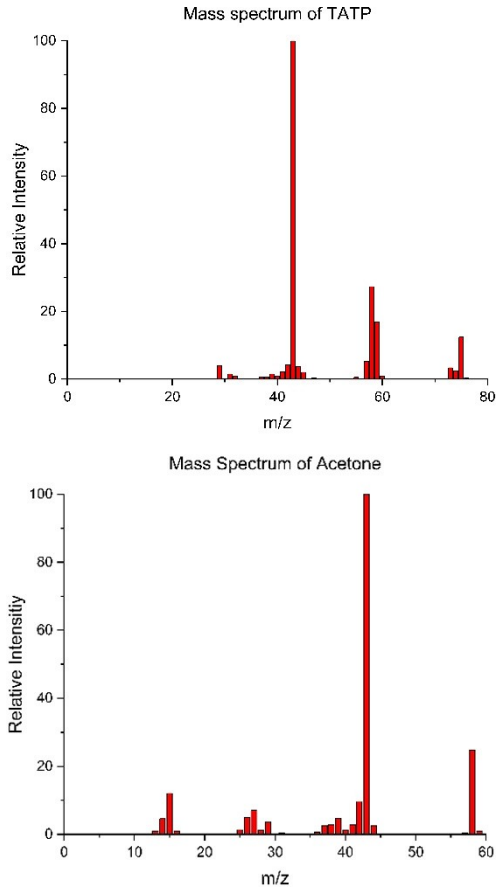

Figure 5. Mass spectra of TATP (above) and acetone (below). Data extracted from [36] and [37].

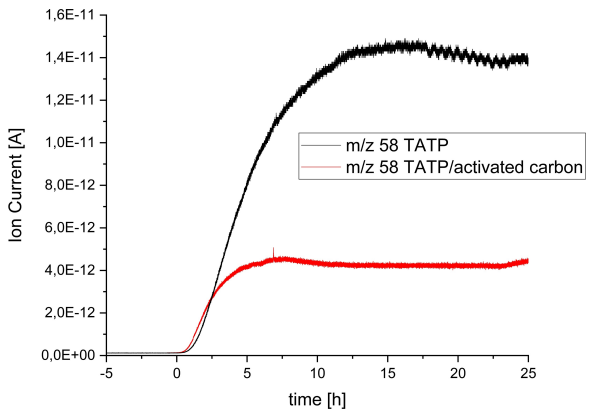

Figure 6. Comparison of the concentration increase of TATP and TATP/activated charcoal (d40-TATP). The graph with the lower final ion current corresponds to d40-TATP. The time zero represents the time at which the respective substance was placed in the aquarium and the lid was closed.

2.12 Vapor Pressure Measurements using the Transpiration Method

In order to investigate the thermochemical properties of developed phlegmatized mixtures, vapor pressures of mixtures d40-TATP and d32.7-TATP were measured using the transpiration method. This method has been successfully implemented for the measurements of vapor pressures of various energetic materials, including pure TATP [38]. The same experimental procedure that was used to determine the vapor pressures of pure TATP in the work of *Härtel et al.* [38] was also replicated in this work.

The working principle of the transpiration method has been thoroughly discussed in the literature [39]. In this work, the experimental setup was filled with TATP/activated charcoal-mixtures prepared according to the procedure, described in section 2.1. The gas saturation was confirmed by replicate measurements at different carrier gas flowrates resulting in the same derived vapor pressure. The quantification of the analytes was carried out with vacuum-outlet gas chromatography coupled with mass spectrometer (VO-GC/MS) [40] using a Shimadzu QP2010 SE device. Along with the obtained experimental *p-T* data, corresponding thermodynamic parameters and fit-functions in a form of a modified Clarke-Glew equation [41] were derived. Table 2 provides the isobaric molar heat capacities and their differences for TATP, which are necessary for the adjustment of the molar enthalpies of sublimation to the reference temperature (298.15 K) according to the procedure discussed in the work of *Chickos et al.* [42].

2.13 Explosive Detection Dog Trials

As part of the desensitization study of HMTD and TATP a test was carried out with explosive detection dog teams (EDD). For this purpose, several EDD were provided by the German Federal Police, who tested the detection of both the pure substances and the safe-to-handle mixtures at Fraunhofer ICT over a period of 3 days. The following dogs took part in the testing: two German Shepherds (both female, 4 and 5 years old), two X–Mechelaars (both male, 3 and 4 years old), one Dutch Herder (male, 7 years old) and one Malinois (female, 7 years old). All dogs participated in the tests, except for day 3: the Malinois and one German Shepherd dog (4 years old) did not participate due to a police operation. The dogs were trained before according to

Table 2. Molar heat capacities and their differences at constant pressure ($T = 298.15$ K).

Compound	$C^{\circ}_{p,m}(cr)$ J mol^{-1} K^{-1}	$-\Delta^{g}_{cr}C^{\circ}_{p,m}$ [a] J mol^{-1} K^{-1}
TATP	271.8 [43]	41.5

[a] Calculated by $-\Delta^{g}_{cr}C^{\circ}_{p,m} = 0.75 + 0.15 \times C^{\circ}_{p,m}(cr)$ [44].

BRAS 170, which is a restricted German Federal Police internal guideline. The training of the dogs includes by routine the presence of numerous distractors (gloves, human scent, etc.) in search scenarios.

A differentiation track was used to test the detection of pure (1.0 g) and phlegmatized substances (3 g) in a time-efficient manner (Figure 7). In this test, easily accessible odor samples are placed at regular intervals on a wooden beam. The EDD have to identify the samples with the explosives in between different samples. Pure activated charcoal has been used as distractor odor sample: one of 15 samples contained an explosive (training aid) amongst samples with pure activated charcoal and blank samples. All of the tests were carried out in a single-blind fashion. This means that, besides the test assessor, neither the dog nor the handler knew where the explosive was located. The location of the target was randomly chosen and changed between every dog. The sample preparation included 5 minutes of soak time prior to testing.

Furthermore, various training aid samples were hidden in different scenarios: 40.0 g d10-HMTD in a locker of a dressing room, 40.0 g d10-HMTD in the trunk of a car and 70.0 g d40-TATP in an engine compartment of a car and had to be found by the EDDs. The training aids were laid out 5 minutes in advance.

Figure 7. Top: Training at a differentiation track, bottom: Signal position of an EDD for detection of a compound.

3 Results and Discussion

3.1 Impact and Friction Sensitivity

The materials were tested according the UN Recommendation on the Transport of Dangerous Goods, Manual of Tests and Criteria [28] (Table 3).

The test result is considered "positive (+)" if the lowest impact energy at which at least one "explosion" occurs in six trials is 2 Nm or less and the substance is considered too dangerous for transport in the form in which it was tested. Otherwise, the result is considered "negative (−)".

The test result for the friction test is considered "positive (+)" if the lowest friction load at which one "explosion" occurs in six trials is less than 80 N and the substance is considered too dangerous for transport in the form in which it was tested. Otherwise, the test result is considered "negative (−)".

Pure TATP and HMTD are extremely sensitive against friction and impact. The pure explosives are very dangerous and extreme caution is required when handling these substances.

Table 3 shows that the mixtures with the activated charcoal are significantly less sensitive than the pure peroxide explosives. Therefore, the handling of the mixtures is much safer compared to the pure peroxide explosives.

3.2 Headspace SPME-GC/MS Analysis of TATP on Activated Charcoal

A headspace SPME-GC/MS analysis of pure activated charcoal was performed. Figure 8 shows the resulting chromatogram.

The big peak at the beginning of the chromatogram is a ghost peak caused by air (maximum peak height at 3.7×10^6). The second peak at 18 minutes is caused by column bleeding, a common degradation process of the stationary phase. The resulting chromatogram of the headspace SPME-GC/MS analysis of the activated charcoal did

Table 3. Impact and friction sensitivity of pure and desensitized substances.

	Impact Sensitivity Nm	Result +/–	Friction Sensitivity N	Result +/–
pure TATP	0.03–1.00	+	< 5.0	+
d40-TATP	> 30.0	–	> 360.0	–
pure HMTD	0.20–1.00	+	< 5.0	+
d40-HMTD	> 30.0	–	> 360.0	–
d10-HMTD	> 30.0	–	> 360.0	–
d5-HMTD	> 30.0	–	> 360.0	–

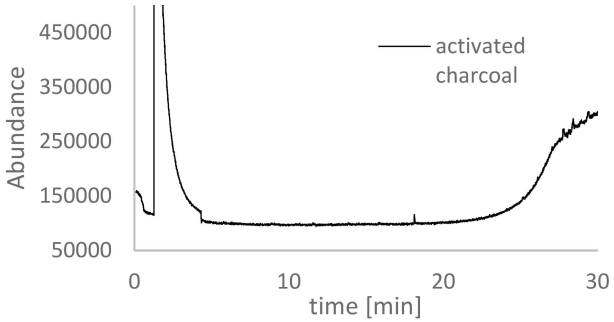

Figure 8. GC chromatograms of pure activated charcoal.

not reveal the presence of further compounds, therefore the activated charcoal does not influence the odor signature of the peroxide explosive mixtures.

The chromatogram of the TATP/activated charcoal-mixture TATP-d40 in Figure 9 contains the ghost peak caused by air and an explicit peak for TATP at a retention time of 8 minutes. No peaks that correspond to impurities or decomposition products are present in the chromatogram.

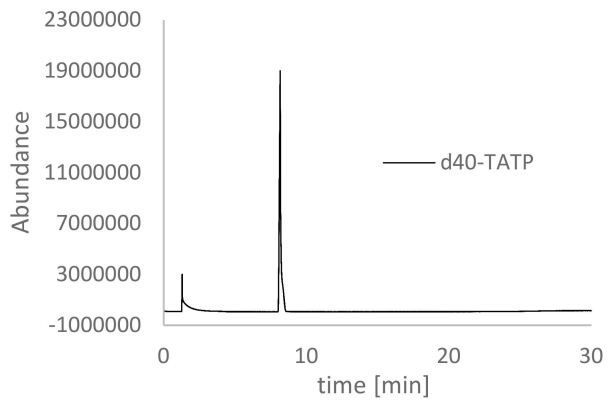

Figure 9. GC chromatogram of d40-TATP.

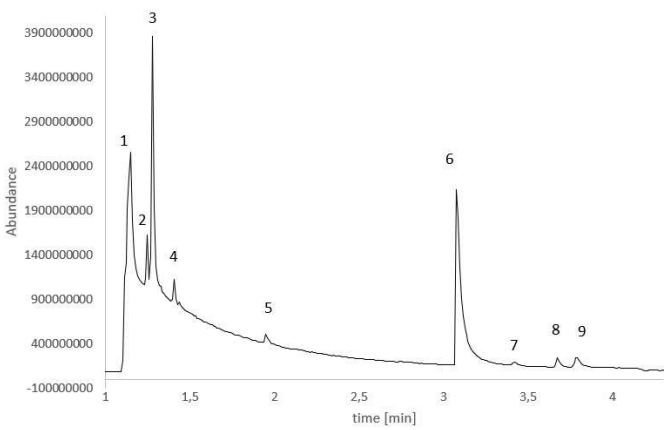

Figure 10. SPME-GC/MS chromatogram of d10-HMTD.

As it is stated in the literature, the odor profile of HMTD is complex. [19, 25–27]. Using headspace SPME-GC/MS, degradation products of HMTD could be identified in the headspace of the HMTD mixture. The first peak in the chromatogram (Figure 10) is caused by air. The following degradation products of HMTD were found in the gas phase: formamide (2), formic acid (3), acetic acid (4) and dimethylformamide (6). The peaks 5, 7, 8 and 9 are siloxanes, caused by column bleeding. The qualitative headspace profile of the HMTD mixture agrees with the components found in the headspace profile of laboratory-grade and clandestine HMTD with different ages [19]. The non-detection of formaldehyde and trimethylamine, quantitative aspects of the headspace composition and ageing effects must be further investigated for the training aid presented in this work in comparison to the work by *Simon and DeGreeff* [19].

3.3 Security Testing: Koenen Tube Test, Thermal Stability

3.3.1 Koenen Tube Test

The Koenen Tube Test was performed for d40-TATP and d-40-HMTD.

For d40-TATP, explosions occurred at 2 and 3 mm vent hole diameters (Figure 11). With a nozzle diameter of 5 mm, no explosion was observed for three times. Therefore the limiting diameter of d40-TATP according to the UN test manual is 3 mm.

The results of the Koenen test for d40-HMTD indicate that the material has a limited vent hole diameter of less than 1 mm (Figure 12). However, during the tests it was observed that the mixture was blown out very fast from the steel tube after a few seconds at low thermal stress (about 370 K).

3.3.2 Thermal Stability

The test was carried out with 50.0 g of d40-TATP. Due to its density, the mixture did not fit into the 50 mL beaker proposed in the test manual. Only 14 g of the substance would fit into it. After consultation with BAM the mixture was placed in a 250 mL beaker (plane, without spout) and covered with a watch glass. The beaker was placed in an oven at 348.15 K for 48 hours. During the 48 h, no ignition or explosion took place. Weighing of the mixture indicated that a weight loss of 1.34 % had occurred. The result of the thermal stability test for d40-TATP is "negative (−)", so it is considered as thermally stable for transportation.

Likewise, the test was also performed with 50.0 g of d40-HMTD. Already after 2 hours in the oven, a deflagration of the mixture could be observed, similar to the observations made within the Koenen test. d40-HMTD must therefore be classified as "positive (+)", so the substance should be considered thermally unstable for transport.

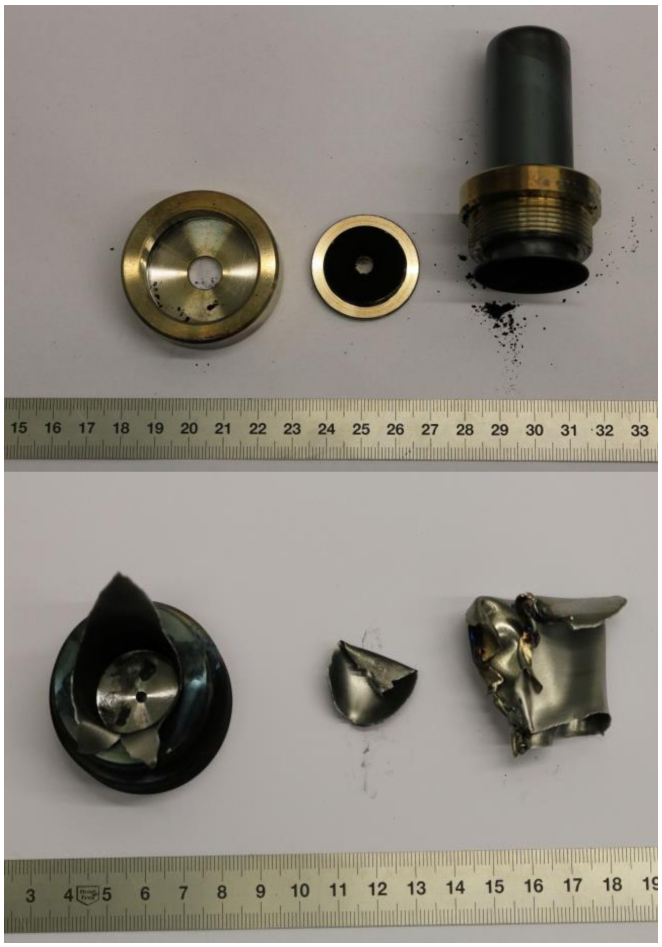

Figure 11. Steel tubes after testing with d40-TATP. Top: 5 mm vent hole diameter (no explosion, the orifice plate and the steel tube is intact), bottom: 3 mm vent hole diameter (with explosion, the steel tube is destroyed, the orifice plate is still intact).

Figure 12. Steel tubes after testing with d40-HMTD. Top: 20 mm vent hole diameter of the orifice plate, the steel tube and the plate are still intact; bottom: 1 mm vent hole diameter; orifice plate and steel tube are both intact.

Based on this result, ARC (Accelerating Rate Calorimeter) [29] analysis of d40-HMTD was carried out. In addition, a dilution series for the HMTD/activated charcoal mixture was also analyzed by ARC. The dilution was performed as described in part 2.2.

The analysis by the adiabatic calorimeter (Figure 13) shows that the 40% HMTD/activated charcoal mixture achieves a high self-heating rate (900 K/min). In order to suppress this self-heating, active charcoal dilutions of the HMTD activated carbon mixture were examined. The 5%, 10% and 20% HMTD/activated charcoal mixtures show only low self-heating rates above 363.15 K and 353.15 K respectively (max. ~0.1 K/min).

Based on the ARC results, the thermal stability test was performed again with 50.0 g of a 5% HMTD/activated charcoal mixture. No inflammation or explosion was detected during the 48 h in the oven. Weight loss of the mixture was 1.8%. The result of d5-HMTD is "negative (−)".

The thermal stability test was also performed with the 10% HMTD/activated charcoal mixture. Again, no inflammation or explosion could be observed during the 48 h. The weight loss of the mixture was 2.1%. The result of d10-HMTD is "negative (−)". So, both d5-HMTD and d10-HMTD are considered as thermally stable for transportation.

3.4 LUMIStox Testing for Toxicity

The LUMIStox Test was performed for TATP and HMTD.

TATP has a G_L value of 1:2 and is classified as non-toxic (Table 4). The lowest achievable G_L value is 1:2 with respect to the measurement procedure. Therefore, TATP does not cause any effect on the luminescent bacteria at the lowest possible dilution level.

The first dilution level of HMTD with a light transmission of less than 20% was 1:64 and thus corresponds to the G_L value. The sample containing HMTD is classified as moder-

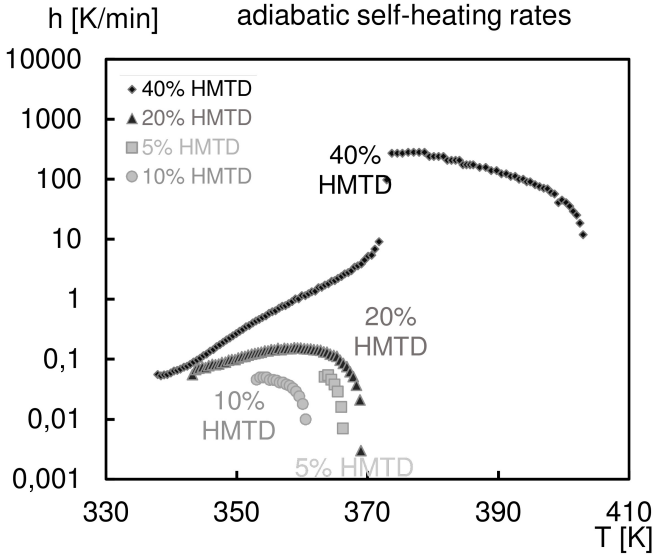

Figure 13. Adiabatic self-heating rates of HMTD/activated charcoal mixtures.

Table 4. G_L results of TATP and HMTD.

	G_L
triacetone triperoxide (TATP) + 2% NaCl-Solution	1:2
hexamethylene triperoxide diamine (HMTD) + 2% NaCl-Solution	1:64

ately toxic according to the classification by Wang [32], a hazard is assumed if the G_L value greater than 1:8 is exceeded.

3.5 Process Mass Spectrometer Measurements

The asymptotic nature of curves during saturation (Figure 6) combined with the signal noise makes it difficult to define the point at which saturation is reached. To compare the two experiments, the time when 10% and 90% of the maximum signal was reached were determined.

The data (Table 5) show that for TATP 90% saturation was reached after about 9–10 hours, whereas for d40-TATP this took half of the time, namely 4–5 hours. The saturation point of 10% was reached after about 2 hours for TATP, and after about 1 hour for d40-TATP. The absolute signal level for TATP was 3.5 times higher for TATP than for d40-TATP.

The observed differences between both TATP variants can be explained by several reasons. First, the absolute amount of TATP was different in both experiments, specifically 40 g vs. 100 g. It should also be mentioned that first the TATP experiment and then the experiment with TATP/activated charcoal was performed. A possible explanation for the faster speed of saturation in the second experiment could be that the walls of the aquarium were saturated by adsorption of TATP in the first experiment. Possibly the walls could not adsorb as much TATP since they were already loaded, although cleaning was performed between the measurements. The TATP in the gas phase in the experiment with d40-TATP was possibly not adsorbed on the walls anymore, which might have led to a faster gas phase saturation.

On the other hand, the faster saturation time could be explained by a larger surface area of the d40-TATP in comparison to TATP. Due to the mixture with activated charcoal, the surface area of the TATP with activated charcoal could potentially be larger than that of pure TATP. Therefore, the time to saturation is shorter due to the larger surface area for interactions between TATP molecules and the gas phase.

Another reason could be the reproducibility of the experiment. Since the vapor pressure and the spreading time in the gas phase are very sensitive to changes in external factors, the difference in gas spreading could be due to fluctuations during both experiments. For example, it was observed that the concentration of TATP in the gas phase could be correlated with the incident solar light during the day and therefore varied by about +/−10%.

It should be noted that the mass spectrometer could not be calibrated as there was no calibration gas generator available for calibration. Therefore, the absolute signal level cannot be correlated with a specific concentration, but the deviation in signal level is most probably not caused exclusively by the possible loss of sensitivity of the mass spectrometer during this period alone. If the concentration for

Table 5. Comparison of signal levels and corresponding times of TATP and d40-TATP.

	TATP			**d40-TATP**		
	m/z 43	m/z 58	m/z 59	m/z 43	m/z 58	m/z 59
Baseline [pA]	0.5	0.1	0.1	0.8	0.1	0.1
saturated signal [pA]	58.0	13.9	0.6	18.2	4.3	0.3
10% saturated signal [pA]	6.3	1.5	0.1	2.5	0.5	0.1
90% saturated signal [pA]	52.2	12.5	0.5	16.5	3.9	0.3
t_10% saturated signal [h]	1.9	1.9	1.8	1.0	1.0	1.0
t_90% saturated signal [h]	9.3	9.1	9.8	4.4	4.1	4.9

Table 6. d40-TATP: absolute vapor pressures p_{sat} and thermodynamic properties of sublimation obtained by the transpiration method in this work.

d40-TATP: $\Delta^g_{cr}H^\circ_m$ (298.15 K) = 80.2 ± 0.5 kJ mol^{-1}

$\ln p_{sat}/p^0 = \frac{317.4}{R} - \frac{92612.5}{RT} - \frac{41.5}{R} ln \frac{T}{298.15\ K}$

T_{exp} [a] K	m [b] µg	V_{N_2} [c] dm^3	T_{amb} [d] K	Gasflow dm^3 h^{-1}	p_{sat} [e] Pa	$u(p_{sat})$ [f] Pa	$\Delta^g_{cr}H^\circ_m$ kJ mol^{-1}	$\Delta^g_{cr}S^\circ_m$ J mol^{-1} K^{-1}
274.5	30.6	2.54	297.4	2.0	0.14	0.01	81.58	184.9
274.5	21.6	1.74	298.2	2.3	0.14	0.01	80.17	180.0
274.5	19.1	1.59	297.9	1.6	0.14	0.01	80.17	179.7
279.0	21.9	0.98	298.0	2.0	0.25	0.01	79.98	179.5
279.1	21.0	0.98	296.7	2.0	0.24	0.01	79.98	179.0
283.7	19.2	0.49	297.7	2.0	0.44	0.02	79.79	178.7
288.5	32.6	0.49	298.0	2.0	0.74	0.02	79.59	177.7
293.4	58.6	0.49	297.3	2.0	1.33	0.04	79.39	177.2
293.4	56.9	0.49	298.1	2.0	1.29	0.04	79.39	177.0
293.4	58.1	0.49	298.0	2.0	1.32	0.04	79.39	177.2
298.2	97.2	0.49	297.2	2.0	2.21	0.06	79.19	176.4
303.1	162	0.49	298.0	2.0	3.70	0.10	78.98	175.8
307.9	263	0.49	296.6	2.0	5.98	0.17	80.20	179.6
307.9	274	0.49	297.4	2.0	6.23	0.18	80.20	179.9
312.7	498	0.52	297.9	2.0	10.6	0.3	80.00	179.8
312.7	454	0.49	298.0	2.0	10.3	0.3	80.00	179.5

[a] Saturation temperature ($u(T) = 0.1$ K). [b] Mass of transferred sample condensed at 243 K. [c] Volume of nitrogen ($u(V) = 0.005$ dm^3) used to transfer m ($u(m)/m = 1.5\%$) of the sample. [d] T_{amb} is the temperature of the soap film flowmeter used for measurement of the gas flow. [e] Vapor pressure at temperature T, calculated from the m and the residual vapor pressure at the condensation temperature, calculated by an iteration procedure; $p^\circ = 1$ Pa. [f] Standard uncertainty in p was calculated with u(p/Pa) = 0.005 + 0.025(p/Pa) for p < 5 Pa and u(p/Pa) = 0.025 + 0.025(p/Pa) for p > 5 to 3000 Pa.

TATP was higher, this could be explained by leaks from the aquarium. The aquarium is far from being gas-tight and the lid was only loosely put on to avoid any forces during opening and closing.

The comparison of these preliminary aquarium experiments of pure TATP and d40-TATP has shown that d40-TATP needed roughly half the time for saturation of the cuboid atmosphere and produced a 3.5 times smaller signal at the mass spectrometer. Due to the sensitive characteristics of gas spreading, such as the discussed factors of wall adsorption and sunlight, further experiments need to be conducted to obtain a more conclusive picture. To get more insight into the comparison of the vaporization behaviour of bulk TATP and the phlegmatized d40-TATP under well-controlled (calibrated, gas-tight) conditions we performed vapor pressure measurements of the active charcoal mixtures d40-TATP and d32.7-TATP.

3.6 Vapor Pressure Measurements

The obtained *p-T* values, experimental conditions, their uncertainties and the corresponding thermodynamic properties of TATP in the mixtures d40-TATP and d32.7-TATP, obtained by vapor pressure measurements with the transpiration method are compiled in Tables 6 and 7.

The uncertainties for T, V and m are standard uncertainties. Uncertainty of the enthalpy of sublimation is the standard uncertainty, calculated including uncertainties of vapor pressure, uncertainties from the fitting equation and the uncertainty of temperature adjustment to $T = 298.15$ K. Detailed information on the methods of calculations was published previously [45–46].

Comparison of experimental vapor pressures of pure TATP [38] and the phlegmatized mixtures, measured in this work are presented in the Table 8 and Figure 14.

It was observed that lowering the amount of TATP in the mixture with activated charcoal decreases the vapor pressure p_{sat} at 298.15 K (6.7 Pa for pure TATP, 2.3 Pa for d40-TATP and 0.9 Pa for d32.7-TATP) and increases the mo-

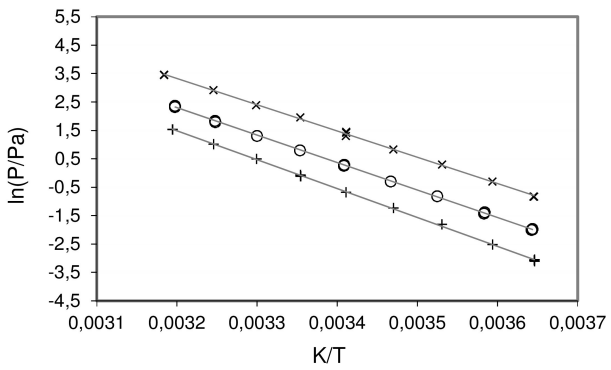

Figure 14. Experimental vapor pressures of the TATP in TATP/activated charcoal-mixtures in comparison with the literature values. Here ×–*Härtel et al.* [38], ○–d40-TATP from this work, + – d32.7-TATP from this work. Solid lines represent the linear fits.

Table 7. d32.7-TATP: absolute vapor pressures p_{sat} and thermodynamic properties of sublimation obtained by the transpiration method in this work.

d32.7-TATP: $\Delta_{cr}^{g}H_m^{\circ}$ (298.15 K) = 84.4 ± 0.5 kJ mol^{-1}

$\ln p_{sat}/p^0 = \frac{323.8}{R} - \frac{96732.9}{RT} - \frac{41.5}{R} ln \frac{T}{298.15\ K}$

T_{exp} [a] K	m [b] µg	V_{N_2} [c] dm^3	T_{amb} [d] K	Gasflow dm^3 h^{-1}	p_{sat} [e] Pa	$u(p_{sat})$ [f] Pa	$\Delta_{cr}^{g}H_m^{\circ}$ kJ mol^{-1}	$\Delta_{cr}^{g}S_m^{\circ}$ J mol^{-1} K^{-1}
274.3	12.3	3.05	297.1	2.0	0.05	0.01	85.35	189.7
274.3	11.8	2.78	298.0	1.4	0.05	0.01	85.35	190.1
274.3	8.5	2.06	299.7	2.2	0.05	0.01	85.35	189.9
278.3	5.1	0.70	297.9	2.0	0.08	0.01	85.18	189.5
283.3	7.4	0.50	299.0	2.0	0.16	0.01	84.98	189.3
288.2	13.2	0.50	298.4	2.0	0.29	0.01	84.77	188.2
293.2	22.9	0.50	298.2	2.0	0.51	0.02	84.57	187.2
298.1	40.4	0.50	298.9	2.0	0.90	0.02	84.36	186.4
298.1	40.2	0.50	299.3	2.0	0.90	0.03	84.36	186.3
298.1	41.4	0.50	299.4	2.0	0.93	0.03	84.36	186.6
298.2	50.2	0.60	298.8	2.0	0.94	0.03	84.36	186.7
303.1	74.4	0.51	299.2	2.0	1.6	0.1	84.15	186.1
308.1	125	0.50	299.0	2.0	2.8	0.1	83.95	185.2
313.1	210	0.51	300.1	2.0	4.6	0.1	83.74	184.5
313.1	211	0.51	299.3	2.0	4.7	0.1	83.74	184.6
313.1	209	0.50	299.7	2.0	4.6	0.1	83.74	184.5

[a] Saturation temperature ($u(T)$ = 0.1 K). [b] Mass of transferred sample condensed at 243 K. [c] Volume of nitrogen ($u(V)$ = 0.005 dm^3) used to transfer m ($u(m)/m$ = 1.5 %) of the sample. [d] T_{amb} is the temperature of the soap film flowmeter used for measurement of the gas flow. [e] Vapor pressure at temperature T, calculated from the m and the residual vapor pressure at the condensation temperature, calculated by an iteration procedure; p° = 1 Pa. [f] Standard uncertainty in p was calculated with u(p/Pa) = 0.005 + 0.025(p/Pa) for p < 5 Pa.

Table 8. Compilation of data on molar enthalpies of sublimation $\Delta_{cr}^{g}H_m^{\circ}$ of TATP and its phlegmatized mixtures.

Experiment	Method[a]	T-Range K	$\Delta_{cr}^{g}H_m^{\circ}$(298.15 K)[b] kJ mol^{-1}	p_{sat} [c] Pa
pure TATP [38]	T	274.3–314.1	76.7 ± 0.7	6.7
d40-TATP	T	274.5–312.7	80.1 ± 0.5	2.3
d32.7-TATP	T	274.3–313.1	84.4 ± 0.5	0.9

[a] Method: T = transpiration. [b] Enthalpies of sublimation were adjusted according to Acree and Chickos [44] with values of $\Delta_{cr}^{g}C_{p,m}^{\circ}$ and $C_{p,m}^{\circ}$(cr), stated in Table 4. Uncertainty for molar enthalpy of sublimation is expressed as standard uncertainty. [c] Vapor pressure at 298.15 K.

lar enthalpy of sublimation at 298.15 K (76.7 ± 0.7 kJ mol^{-1} for pure TATP, 80.1 ± 0.5 kJ mol^{-1} for d40-TATP and 84.4 ± 0.5 kJ mol^{-1} for d32.7-TATP) which can be attributed to absorption phenomena. This demonstrates that the volatility of the TATP in the TATP/activated charcoal-mixtures is rather sensitive to the compound concentration. For the simulation of the vaporization behavior of pure TATP with active charcoal mixtures the content should be chosen as high as feasible in terms of handling safety.

Measurements with the transpiration method demonstrated that the vapor pressure p_{sat} at 298.15 K of d40-TATP (2.3 Pa) and d32.7-TATP (0.9 Pa) is lower than that of pure TATP (6.7 Pa) but in the same order of magnitude with a strong dependency on the TATP-content in the mixture.

The results agree with the process mass spectrometer measurements (section 3.5) which indicated that d40-TATP has a lower volatility than the pure bulk material regarding the lower signal intensity (ion current) of d40-TATP in comparison to the bulk material in Figure 6.

3.7 Explosive Detection Dog Trials

Day 1:

On the first day 7 Explosive Detection Dog Teams (EDD) were available. For the start of the training at the differentiation track 1.0 g HMTD (pure substance) was used. In the afternoon, 40.0 g of the HMTD-activated charcoal mixture (d40-HMTD) were hidden in a desk container in the building for free search. The mixture was found by each team. Furthermore, in the afternoon, 1.0 g of TATP (pure substance) was hidden in a handbag placed in a room to check the detection abilities for TATP. Again, the explosive was detected and located by all teams.

Day 2:

On the second day also 7 EDD were available. The differentiation track was set up: The samples, containing one of the safe-to-handle TATP/HMTD mixtures, were placed. The quantity of d40-HMTD and d40-TATP was 3.0 g. The differ-

entiation track experiments were continued on day 3, the results of both days are summarized in Table 9.

Day 3:

5 EDD were available on day 3. The differentiation track experiments were continued. The results are shown in Table 9. The safe mixtures of HMTD and TATP were found with a total detection rate of 100 %. Afterwards 3 realistic environment tasks were prepared for exercise: 40.0 g of d40-HMTD in the trunk of a car, 70 g of d40-TATP in the engine compartment of a car and 40 g of d40-HMTD in the locker of a dressing room. All safe explosive formulations were found by all teams.

Both TATP and HMTD were detected with a rate of 100 % by the EDD in their safe mixtures.

TATP/activated charcoal and HTMD/activated charcoal mixtures were found by all teams resulting in a global detection rate throughout all tests of 100 %. A total of 168 blank sample vials, which were in some cases filled with activated charcoal as distractor, were used, 5 of which were indicated as explosives by the sniffer dog. Thus, a false positive alarm rate of 3 % was observed. (Table 10).

4 Conclusion

Both TATP and HMTD could be phlegmatized by coprecipitation with active charcoal resulting in mixtures with a nominal content of 40 wt-% (d40-TATP) and 10 wt-% (d10-HMTD), respectively. In terms of impact and friction sensitivity for both peroxides a content of 40 wt-% resulted in >30 Nm impact sensitivity and >360 N friction sensitivity. Both phlegmatized peroxides were tested according to the UN recommendation on the transport of dangerous goods test manual. (Koenen Tube Test and Thermal Stability). For the Koenen Tube Test a limiting diameter of 3 mm was determined for d40-TATP and 1 mm was determined for d40-HMTD. The thermal stability test for d40-TATP resulted in a weight loss of 1.34 % (pass ("-")). For d40-HMTD the thermal stability test resulted in a deflagration (fail ("+")), whilst for d10-HMTD the test was passed with a weight loss of 2.1 %. In terms of toxicity TATP was classified as non-toxic and HMTD as moderately toxic for aquatic organisms by the LUMIstox test. The volatility of the phlegmatized TATP was further investigated. Investigations with a process mass spectrometer indicate that d40-TATP is likely to produce a saturated atmosphere at least in the same time as the same amount of pure TATP. Despite that it should be noted that the process mass spectrometer experiment was only performed once and remeasurements should be carried out to check for reproducibility of the results. Measurements with the transpiration method demonstrated that the vapor pressure p_{sat} at 298.15 K of d40-TATP (2.3 Pa) and d32.7-TATP (0.9 Pa) is lower than that of pure TATP (6.7 Pa) but in the same order of magnitude with a strong dependency on the TATP-content in the mixture. Headspace SPME-GC/MS measurements revealed that the active charcoal does not contribute to the vapor profile of the training aid. Finally, both d40-TATP and d10-HMTD were tested as training aids for EDD. In both differentiation track and realistic environment scenarios a detection rate of 100 % could be achieved by EDD of German Federal Police with a false positive rate of solely 3 %. It should be noted that the published results did not verify whether dogs that have never been conditioned for the detection of HMTD and TATP will detect the bulk materials after exclusive conditioning with the developed training aids. The authors encourage appropriate authorities for bilateral exchange. Consequently, a promising canine training aid for both TATP and HMTD was developed. It has the potential for enabling both trace and bulk amount detection scenarios and was reported without prior patenting of the technology. First tests towards a UN transport classification for dangerous goods were performed and will be continued. For a deeper understanding of the gas phase release of bulk and phlegmatized TATP quantitative vapor analysis will be performed in the near future.

Table 9. Detection rate for the safe mixtures.

	d40-TATP	d40-HMTD
Counts	12	15
Notification/Signal	12	15
Detection rate	100 %	100 %

Table 10. Summarized results for all scenarios of the explosive dog detection trials.

	Blank sample	Safe mixtures
Counts	168	27
Notification/Signal	5	27
Failure rate	3 %	–
Detection rate	–	100 %

Acknowledgements

For financial support for the work in Ludwig-Maximilian University (LMU), the Office of Naval Research (ONR) under grant no. ONR N00014-19-1-2078, the Strategic Environmental Research and Development Program (SERDP) under contract no. W912HQ19 C0033 and the DAAD (German Academic Exchange Service) [grant no. 57299294] are gratefully acknowledged.

Data Availability Statement

The data that support the findings of this study are available from the corresponding author upon reasonable request.

References

[1] R. Wolffenstein, Ueber die Einwirkung von Wasserstoffsuperoxyd auf Aceton und Mesityloxyd. *Berichte der deutschen chemischen Gesellschaft* **1895**, *28* (2), 2265–2269.

[2] D. Lubczyk, A. Hahma, M. Brutschy, C. Siering, S. R. Waldvogel, A. New Reference Material, Safe Sampling of Terrorists Peroxide Explosives by a Non-Volatile Matrix. *Propellants, Explosives, Pyrotechnics* **2015**, *40* (4), 590–594.

[3] German police seize bomb, firearm in raid that foiled imminent Boston Marathon-style terror attack. http://news.nationalpost.com/news/world/german-police-seize-bomb-firearm-in-raid-that-foiled-imminent-boston-marathon-style-terror-attack accessed on 05/19/21.

[4] Paris suicide bombers used TATP, a powerful, homemade explosive: officials. http://www.nydailynews.com/news/world/paris-suicide-bombers-tatp-homemade-explosive-article-1.2435082 accessed on 05/19/21.

[5] 17-Jähriger hortete Sprengstoff. http://www.n-tv.de/panorama/17-Jaehriger-hortete-Sprengstoff-article334469.html. accessed on 05/19/21 (in German).

[6] P. Kaul, C. Becher, G. Holl, S. Maurer, A. Sündermann, U. Dülsner, EMPK® - novel training aids for explosives sniffer dogs. *Journal of Veterinary Behavior* **2012**, *7* (1), 55–56.

[7] https://explotech.de/de/produkte/empk.html accessed on 05/19/21.

[8] D.-T. T. Vu, *Process for producing non-detonable training aid materials for detecting explosives*, US Patent US 9,108,890 B2, Johns Hopkins University, **2013**.

[9] https://gallant.tech/pages/our-products accessed on 05/19/21.

[10] D. O. B. A. Adebimpe, *Methods for making scent simulants of chemical explosives, and compositions thereof*, US Patent US 8,444,881 B2, **2008**.

[11] http://scentlogix.com/s/explosives/ accessed on 05/19/21.

[12] https://www.sokksdogtraining.com/sokks-odours/sokks-explosives/ accessed on 05/20/21.

[13] J. C. Oxley, J. L. Smith, J. N. Canino, Insensitive TATP Training Aid by Microencapsulation. *Journal of Energetic Materials* **2015**, *33* (3), 215–228.

[14] J. C. Oxley, J. L. Smith, J. N. Canino, Systems and methods for providing non-detonatable explosives or explosive stimulant sources, US Patent US 9,784,723 B1, Council On Postsecondary Education Rhode Island Board of Education, **2014**.

[15] https://www.detectachem.com/products/microsphere-heater-system accessed on 05/19/21.

[16] M. J. Lefferts, M. R. Castell, Vapour sensing of explosive materials. *Analytical Methods* **2015**, *7* (21), 9005–9017.

[17] P. Kolla, Riechen Hunde Sprengstoff? *Polizei Verkehr + Technik* **2000**, *4*, 110–114 (in German).

[18] A. Simon, L. Lazarowski, M. Singletary, J. Barrow, K. Van Arsdale, T. Angle, P. Waggoner, K. Giles, A Review of the Types of Training Aids Used for Canine Detection Training. *Frontiers in Veterinary Science* **2020**, *7* (313).

[19] A. G. Simon, L. E. DeGreeff, Variation in the headspace of bulk hexamethylene triperoxide diamine (HMTD): Part II. Analysis of non-detonable canine training aids. *Forensic Chemistry* **2019**, *13*, 100155.

[20] R. J. Harper, J. R. Almirall, K. G. Furton, Identification of dominant odor chemicals emanating from explosives for use in developing optimal training aid combinations and mimics for canine detection. *Talanta* **2005**, *67* (2), 313–327.

[21] W. MacCrehan, M. Young, M. Schantz, T. Craig Angle, P. Waggoner, T. Fischer, Two-temperature preparation method for PDMS-based canine training aids for explosives. *Forensic Chemistry* **2020**, *21*, 100290.

[22] W. A. MacCrehan, M. Young, M. M. Schantz, Measurements of vapor capture-and-release behavior of PDMS-based canine training aids for explosive odorants. *Forensic Chemistry* **2018**, *11*, 58–64.

[23] S. Moore, W. MacCrehan, M. Schantz, Evaluation of vapor profiles of explosives over time using ATASS (Automated Training Aid Simulation using SPME). *Forensic Science International* **2011**, *212* (1), 90–95.

[24] T.-H. Ong, T. Mendum, G. Geurtsen, J. Kelley, A. Ostrinskaya, R. Kunz, Use of Mass Spectrometric Vapor Analysis To Improve Canine Explosive Detection Efficiency. *Analytical Chemistry* **2017**, *89* (12), 6482–6490.

[25] M. J. Aernecke, T. Mendum, G. Geurtsen, A. Ostrinskaya, R. R. Kunz, Vapor Pressure of Hexamethylene Triperoxide Diamine (HMTD) Estimated Using Secondary Electrospray Ionization Mass Spectrometry. *The Journal of Physical Chemistry A* **2015**, *119* (47), 11514–11522.

[26] L. E. DeGreeff, M. M. Cerreta, C. J. Katilie, Variation in the headspace of bulk hexamethylene triperoxide diamine (HMTD) with time, environment, and formulation. *Forensic Chemistry* **2017**, *4*, 41–50.

[27] J. C. Oxley, J. L. Smith, W. Luo, J. Brady, Determining the Vapor Pressures of Diacetone Diperoxide (DADP) and Hexamethylene Triperoxide Diamine (HMTD). *Propellants, Explosives, Pyrotechnics* **2009**, *34* (6), 539–543.

[28] United Nations: UN Recommendations on the Transport of Dangerous Goods. Manual of Tests and Criteria, New York and Genf, **2002**.

[29] D. I. Townsend, J. C. Tou, Thermal hazard evaluation by an accelerating rate calorimeter. *Thermochimica Acta* **1980**, *37* (3), 1–30.

[30] AbwV. 2004. Verordnung über Anforderungen an das Einleiten von Abwasser in Gewässer (Abwasserverordnung - AbwV): Anhang 22 Chemische Industrie. Bundesministerium für Justiz und Verbraucherschutz. **2004** (in German).

[31] HACH LANGE GMBH, Leuchtbakterientest nach DIN EN ISO 11348 Teil 2, LCK 480. **2019** (in German).

[32] Dr. Bruno Lange GmbH, LUMISTox 300: Bedienungsanleitung. Berlin **1998**, 1–46 (in German).

[33] C. Wang, Toxicity evaluation of reactivedyestuffs, auxiliaries and selected effluents in textile finishing industry to luminescent bacteria Vibrio fischeri. *Chemosphere* **2002**, *46*, 339.

[34] Walter, M. A., Herstellung und Charakterisierung Antikörper gegen Triacetontriperoxid (TATP). Mathematisch-Naturwissenschaftlichen Fakultät I, Humboldt-Universität zu Berlin, Dissertation, **2014** (in German).

[35] Matyáš, R.; Pachman, J.: Primary Explosives. Berlin Heidelberg, **2013**. DOI: 10.1007/978-3-642-28436–6.

[36] S. Alnemrat, J. P. Hooper, Predicting temperature-dependent solid vapor pressures of explosives and related compounds using a quantum mechanical continuum solvation model. *J. Phys. Chem.* **2013**, *117*, 2035–2043.

[37] National Institute of Standards and Technology. TATP. **2020**. Available at: https://webbook.nist.gov/cgi/cbook.cgi?ID=C17088378&Mask=200 accessed on 05/19/21.

[38] National Institute of Standards and Technology. Acetone. **2020**. Available at: https://webbook.nist.gov/cgi/cbook.cgi?ID=C67641&Type=IR-SPEC&Index=2 accessed on 05/19/21.

[39] M. A. Härtel, T. M. Klapötke, B. Stiasny, J. Stierstorfer, Gas-phase Concentration of Triacetone Triperoxide (TATP) and Diacetone Diperoxide (DADP). *Propellants, Explos., Pyrotech.* **2017**, *42* (6), 623–634.

[40] G. Bikelytė, M. A. Härtel, T. M. Klapötke, B. Krumm, A. Sadaunykas, Experimental thermochemical data of CWA simulants: Triethyl phosphate, diethyl methylphosphonate, malathion and methyl salicylate. *The Journal of Chemical Thermodynamics* **2020**, *143*, 106043.

[41] M. A. Härtel, T. M. Klapötke, J. Stierstorfer, L. Zehetner, Vapor Pressure of Linear Nitrate Esters Determined by Transpiration Method in Combination with VO-GC/MS. *Propellants, Explos., Pyrotech.* **2019**.

[42] E. C. W. Clarke, D. N. Glew, Evaluation of thermodynamic functions from equilibrium constants. *Transactions of the Faraday Society* **1966**, *62* (0), 539–547.

[43] J. S. Chickos, S. Hosseini, D. G. Hesse, J. F. Liebman, Heat capacity corrections to a standard state: a comparison of new and some literature methods for organic liquids and solids. *Structural Chemistry* **1993**, *4* (4), 271–278.

[44] R. Pilar, J. Pachman, R. Matyáš, P. Honcová, D. Honc, Comparison of heat capacity of solid explosives by DSC and group contribution methods. *Journal of Thermal Analysis and Calorimetry* **2015**, *121* (2), 683–689.

[45] W. Acree, J. S. Chickos, Phase Transition Enthalpy Measurementsof Organic and Organometallic Compounds. Sublimation, Vaporizationand Fusion Enthalpies From 1880 to 2010. *Journal of Physical and Chemical Reference Data* **2010**, *39* (4), 043101.

[46] V. N. Emel'yanenko, S. P. Verevkin, Benchmark thermodynamic properties of 1,3-propanediol: Comprehensive experimental and theoretical study. *The Journal of Chemical Thermodynamics* **2015**, *85*, 111–119.

[47] S. P. Verevkin, A. Y. Sazonova, V. N. Emel'yanenko, D. H. Zaitsau, M. A. Varfolomeev, B. N. Solomonov, K. V. Zherikova, Thermochemistry of halogen-substituted methylbenzenes. *J. Chem. Eng. Data* **2014**, *60* (1), 89–103.

Manuscript received: February 21, 2021
Revised manuscript received: October 17, 2021
Version of record online: ■■, ■■■

FULL PAPER

I. Wilhelm, G. Bikelytė, M. Wittek, M. A. C. Härtel, D. Röseling, T. M. Klapötke*

1 – 16

Phlegmatization of TATP and HMTD with Activated Charcoal as Training Aid for Explosive Detection Dogs

Abbreviations

AT	Acquisition time
CRDS	Cavity Ring Down Spectroscopy
DAD	Diode Array Detector
DAP	Diazidopropanol
DEDAM	1,3-diethyl-2,2-diazidomalonate
DEMP	Diethylmethy phosphonate
DSC	Differential scanninc calorimetry
EA	Elemental analysis
ECAC	European Civil Aviation Conference
EDD	Explosive Detection Dogs
ETD	Explosive Trace Detection
FID	Free induction decay
GC	Gas Chromatography
GCMS	Gas chromatography-Mass Spectrometry
GLP/GMP	Good laboratory and manufacturing practices
GPIB	General purpose interface bus
HME	Homemade explosive
HPLC	High performance liquid chromatography
IED	Improvised explosive device
IMS	Ion mobility spectrometry
LOD	Limit of detection
MEMS	Microelectromechanical systems

MOS	Metal Oxide Semiconductor
MS	Mass Spectrometry
MS	Methyl salicylate
NENA	Nitroxyethyl nitramine
NMR	Nuclear magnetic resonance
PETN	Pentaerythritol tetranitrate
PMT	Photomultiplier tube
p-T	Pressure-temperature
QCM	Quartz Crystal Microbalance
qNMR	Quantitative nuclear magnetic resonance
RDX	Hexahydro-1,3,5-trinitro1,3,5-triazine
RT	Room temperature
SERS	Surface-enhanced Raman Spectroscopy
TATP	Triacetone triperoxide
TEP	Triethyl phosphate
TGA	Thermogravimetric analysis
TNT	2,4,6-Trinitrotoluene
TNX	Hexahydro-1,3,5-trinitroso-1,3,5-triazine
TSA	US Transportation Security Association
VOC	Volatile organic compound
VP	Vapor pressure

List of Publications

Peer-reviewed publications

1. Bikelytė, G.; Härtel, M.; Stierstorfer, J.; Klapötke, T. M.; Pimerzin, A. A.; Verevkin, S. P., Benchmark properties of 2-, 3-and 4-nitrotoluene: Evaluation of thermochemical data with complementary experimental and computational methods. *J. Chem. Thermodyn.* **2017,** 111, 271-278.
2. Bikelytė, G.; Härtel, M. A.; Klapötke, T. M.; Krumm, B.; Sadaunykas, A., Experimental thermochemical data of CWA simulants: Triethyl phosphate, diethyl methylphosphonate, malathion and methyl salicylate. *J. Chem. Thermodyn.* **2020,** 143, 106043.
3. Bikelytė, G.; Härtel, M. A.; Klapötke, T. M., Experimental Vapor Pressures of Hexahydro-1, 3, 5-trinitro-1, 3, 5-triazine (RDX) and Hexahydro-1, 3, 5-trinitroso-1, 3, 5-triazine (TNX). *Propellants Explos. Pyrotech.* **2020,** 45, (10), 1573-1579.
4. Bikelytė, G.; Härtel, M. A. C.; Holler, M.; Neuer, A.; Klapötke, T. M., Thermodynamic Properties of Energetic Plasticizers: Experimental Vapor Pressures of Methyl-, Ethyl-, and Butyl-Nitroxyethyl Nitramines. *J. Chem. Eng. Data* **2021**, 66(4), 1709-1716.
5. Bikelytė, G.; Harter, A. G.; Härtel, M. A. C.; Heimsch, S. B.; Klapötke, T. M., Thermodynamics of organic azides: experimental vapor pressures of organic polyazido compounds measured with the transpiration method. **2021**, *Fluid Ph. Equilibria*, 549: 113222.
6. Wilhelm, I.; Bikelytė, G.; Wittek, M.; Härtel, M. A. C.; Klapötke, T. M., Phlegmatization of TATP and HMTD with Activated Charcoal as Training Aid for Explosive Detection Dogs *Propellants Explos. Pyrotech.* **2022**, 47(2): e202100057.
7. Küblböck, T.; Angé, G.; Bikelytė, G.; Pokorná, J.; Skácel, R.; Klapötke, T. M., Guanidinium 5,5′-Azotetrazolate: A Colorful Chameleon for Halogen-Free Smoke Signals. *Angewandte Chemie International Edition* **2020,** 59, (30), 12326-12330.

Poster presentations

1. Bikelytė, G. Härtel, M. A. C, Klapötke, T. M. Vapor pressure measurements of melt cast explosives with gas-saturation method, New Trends in Research of Energetic Materials, Proceedings of the Seminar, 21th, Pardubice, Czech Republic, 2018.

2. Bikelytė, G.; Härtel, M.; Stierstorfer, J.; Klapötke, T. M.; Pimerzin, A. A.; Verevkin, S. P., Benchmark properties of 2-, 3-and 4-nitrotoluene: evaluation of thermochemical data with complementary experimental and computational methods, XXII International Conference on Chemical Thermodynamics, Proceedings of the Seminar, 22th, Sankt Petersburg, Russia, 2018.

References

[1] "The road to the Manchester Arena bombing", available from: https://www.bbc.com/news/uk-51908280. Date accessed: 26 April 2021.
[2] The Queen v. Hashem Abedi, Jeremy Baker J.: Jeremy Baker J., (2020). https://www.judiciary.uk/wp-content/uploads/2020/08/Hashem-Abedi-Sentencing-Remarks-1.pdf.
[3] D. Anderson, Report: Attacks in London and Manchester between March and June 2017, (2017).
[4] "Manchester Arena attack: Bomb 'injured more than 800'" (2018), available from: https://www.bbc.com/news/uk-england-manchester-44129386. Date accessed: 28 April 2021.
[5] "Improvised Explosive Devices: Past, Present and Future" (2020), available from: https://reliefweb.int/report/world/improvised-explosive-devices-past-present-and-future. Date accessed: 28 April 2021.
[6] United States Bomb Data Center (USBDC), Report: Explosives Incident Report (EIR), (2019).
[7] J. Argomaniz, O. Bures, C. Kaunert, EU counter-terrorism and intelligence: A critical assessment, Routledge (2017).
[8] COUNCIL OF THE EUROPEAN UNION, Report: EU Action Plan on Enhancing the Security of Explosives, (2008).
[9] K.C. To, S. Ben-Jaber, I.P. Parkin, ACS Nano 14 (2020) 10804-10833.
[10] J.S. Caygill, F. Davis, S.P.J. Higson, Talanta 88 (2012) 14-29.
[11] K.E. Brown, M.T. Greenfield, S.D. McGrane, D.S. Moore, Anal. Bioanal. Chem. 408 (2016) 35-47.
[12] K.E. Brown, M.T. Greenfield, S.D. McGrane, D.S. Moore, Anal. Bioanal. Chem. 408 (2016) 49-65.
[13] D.S. Moore, Sens Imaging 8 (2007) 9-38.
[14] R.G. Ewing, M.J. Waltman, D.A. Atkinson, J.W. Grate, P.J. Hotchkiss, Trends Anal. Chem 42 (2013) 35-48.
[15] K.J. Albert, D.R. Walt, Anal. Chem 72 (2000) 1947-1955.
[16] National Research Council, Existing and potential standoff explosives detection techniques, National Academies Press (2004).
[17] H. Östmark, S. Wallin, H.G. Ang, Propellants Explos. Pyrotech. 37 (2012) 12-23.
[18] M.A. Härtel, T.M. Klapötke, B. Stiasny, J. Stierstorfer, Propellants, Explos., Pyrotech. 42 (2017) 623-634.
[19] S. O'Meara, A.M. Booth, M.H. Barley, D. Topping, G. McFiggans, Phys. Chem. Chem. Phys. 16 (2014) 19453-19469.
[20] A. Delle Site, J. Phys. Chem. Ref. Data 26 (1997) 157-193.
[21] S.P. Verevkin, PHASE CHANGES IN PURE COMPONENT SYSTEMS: LIQUIDS AND GASES, 1st ed., Elsevier B.V., Amsterdam, Netherlands (2005).
[22] K.A. Morrison, E.H. Denis, M.K. Nims, A.M. Broderick, R.C. Fausey, H.J. Rose, P.E. Gongwer, R.G. Ewing, J. Phys. Chem. A 125 (2021) 1279-1288.
[23] J.E. Brady, J.L. Smith, C.E. Hart, J. Oxley, Propellants, Explos., Pyrotech. 37 (2012) 215-222.
[24] "To cool datacenter servers, Microsoft turns to boiling liquid", available from: https://news.microsoft.com/innovation-stories/datacenter-liquid-cooling/. Date accessed: 26 April 2021.

[25] J.E. McFee, A.A. Faust, K.A. Pastor, Nuclear Instruments and Methods in Physics Research Section A: Accelerators, Spectrometers, Detectors and Associated Equipment 704 (2013) 131-139.
[26] S. Giannoukos, B. Brkić, S. Taylor, A. Marshall, G.F. Verbeck, Chem. Rev. 116 (2016) 8146-8172.
[27] J.W. Grate, R.G. Ewing, D.A. Atkinson, Trends Anal. Chem 41 (2012) 1-14.
[28] "Explosive Trace Detection (ETD) equipment", available from: https://www.ecac-ceac.org/activities/security/common-evaluation-process-cep-of-security-equipment. Date accessed: 5 March 2021.
[29] B.D. Piorek, S.J. Lee, M. Moskovits, C.D. Meinhart, Anal. Chem. 84 (2012) 9700-9705.
[30] M.J. Lefferts, M.R. Castell, Anal. Methods. 7 (2015) 9005-9017.
[31] U.S. Congress Office of Technology Assessment, Report: Technology Against Terrorism: Structuring Security, OTA-ISC-511, Washington, DC: U.S. Government Printing Office (1992).
[32] P. Kolla, Riechen Hunde Sprengstoff?, Polizei - Verkehr - Technik, 4/2000.
[33] J.C. Oxley, J.L. Smith, J.N. Canino, J. Energ. Mater. 33 (2015) 215-228.
[34] L. Cheng, Q.-H. Meng, A.J. Lilienthal, P. Qi, Meas Sci Technol (2021).
[35] Z. Long, L. Kou, M.J. Sepaniak, X. Hou, Rev. Anal. Chem. 32 (2013) 135-158.
[36] H. Ji, W. Zeng, Y. Li, Nanoscale 11 (2019) 22664-22684.
[37] "VAPORSENS NANOFIBER CHEMICAL SENSORS OVERVIEW", available from: https://www.vaporsens.com/nanofiber-sensor-technology. Date accessed: 4 March 2021.
[38] Transportation Security Association (TSA), Report: Air Cargo Screening Technology List (ACSTL), (2020).
[39] A. Sorribes-Soriano, M. de la Guardia, F.A. Esteve-Turrillas, S. Armenta, Anal. Chim. Acta 1026 (2018) 37-50.
[40] J. Kozole, J.R. Stairs, I. Cho, J.D. Harper, S.R. Lukow, R.T. Lareau, R. DeBono, F. Kuja, Anal. Chem. 83 (2011) 8596-8603.
[41] N. Hagan, I. Goldberg, A. Graichen, A. St. Jean, C. Wu, D. Lawrence, P. Demirev, J. Am. Soc. Mass Spectrom 28 (2017) 1531-1539.
[42] C. Kwan, A. Snyder, R. Erickson, P. Smith, W. Maswadeh, B. Ayhan, J. Jensen, J. Jensen, A. Tripathi, IEEE Sens. J. 10 (2010) 451-460.
[43] F. Meier, Data acquisition methods for next-generation mass spectrometry-based proteomics, Dissertation, LMU Munich, (2018).
[44] Á. Somogyi, Chapter 6 - Mass spectrometry instrumentation and techniques. in: K. Vékey, A. Telekes, A. Vertes, (Eds.), Medical Applications of Mass Spectrometry, Elsevier, Amsterdam, 2008, pp. 93-140.
[45] "Mass Analyzers", available from: https://chem.libretexts.org/Courses/BethuneCookman_University/BCU%3A_CH-346_Instrumental_Analysis/Mass_Spectrometry/Mass_Spectrometers_(Instrumentation)/Mass_Analyzers_(Mass_Spectrometry). Date accessed: 15 April 2021.
[46] W.R. de Araujo, T.M.G. Cardoso, R.G. da Rocha, M.H.P. Santana, R.A.A. Muñoz, E.M. Richter, T.R.L.C. Paixão, W.K.T. Coltro, Anal. Chim. Acta 1034 (2018) 1-21.
[47] P.I. Hendricks, J.K. Dalgleish, J.T. Shelley, M.A. Kirleis, M.T. McNicholas, L. Li, T.-C. Chen, C.-H. Chen, J.S. Duncan, F. Boudreau, R.J. Noll, J.P. Denton, T.A. Roach, Z. Ouyang, R.G. Cooks, Anal. Chem. 86 (2014) 2900-2908.
[48] D.T. Snyder, C.J. Pulliam, Z. Ouyang, R.G. Cooks, Anal. Chem. 88 (2016) 2-29.
[49] P.E. Leary, G.S. Dobson, J.A. Reffner, Appl. Spectrosc. 70 (2016) 888-896.
[50] R.G. Ewing, B.H. Clowers, D.A. Atkinson, Anal. Chem. 85 (2013) 10977-10983.

[51] P. Martínez-Lozano, J. Rus, G. Fernández de la Mora, M. Hernández, J. Fernández de la Mora, J. Am. Soc. Mass Spectrom 20 (2009) 287-294.
[52] A.P. Lister, W.J. Sellors, C.R. Howle, S. Mahajan, Anal. Chem. 93 (2021) 417-429.
[53] J.M. Sylvia, J.A. Janni, J.D. Klein, K.M. Spencer, Anal. Chem. 72 (2000) 5834-5840.
[54] Z. Chen, C. Xiao, W. Xiao, M. Qin, X. Liu, A review on several key problems of standoff trace explosives detection by optical-related technology, SPIE (2017).
[55] M. López-López, C. García-Ruiz, Trends Anal. Chem 54 (2014) 36-44.
[56] C. Muehlethaler, M. Leona, J.R. Lombardi, Anal. Chem. 88 (2016) 152-169.
[57] Z. Chen, M. Qin, C. Xiao, IEEE Access 8 (2020) 194925-194932.
[58] C. Ramos, P.J. Dagdigian, Appl. Opt. 46 (2007) 620-627.
[59] "Cavity Ring-Down Spectroscopy", available from: https://www.picarro.com/company/technology/crds. Date accessed: 4 March 2021.
[60] M. Todd, R. Provencal, T. Owano, B. Paldus, A. Kachanov, K. Vodopyanov, M. Hunter, S. Coy, J. Steinfeld, J. Arnold, Appl Phys B 75 (2002) 367-376.
[61] M.H. Barley, G. McFiggans, Atmos. Chem. Phys. 10 (2010) 749-767.
[62] R. Naef, W.E. Acree, Molecules 26 (2021) 1045.
[63] D. Ambrose, CHAPTER 13 - VAPOR PRESSURES. in: B. Le Neindre, B. Vodar, (Eds.), Experimental Thermodynamics, Butterworth-Heinemann, 1975, pp. 607-656.
[64] S.P. Verevkin, D.H. Zaitsau, C. Schick, F. Heym, Chapter 1 - Development of Direct and Indirect Methods for the Determination of Vaporization Enthalpies of Extremely Low-Volatile Compounds. in: S. Vyazovkin, N. Koga, C. Schick, (Eds.), Handbook of Thermal Analysis and Calorimetry, Elsevier Science B.V., 2018, pp. 1-46.
[65] M. Knudsen, Annalen der Physik 333 (1909) 75-130.
[66] G. Edwards, Trans. Faraday Soc. 49 (1953) 152-154.
[67] G. Edwards, Trans. Faraday Soc. 46 (1950) 423-427.
[68] R.B. Cundall, T. Frank Palmer, C.E.C. Wood, J. Chem. Soc., Faraday Trans.1 74 (1978) 1339-1345.
[69] R.B. Cundall, T.F. Palmer, C.E.C. Wood, J. Chem. Soc., Faraday Trans.1 77 (1981) 711-712.
[70] M. Härtel, Studies towards the gas-phase detection of hazardous materials by vapor pressure measurements with the transpiration method in combination with vacuum outlet GC/MS, Dissertation LMU München (2017).
[71] J.M. Rosen, C. Dickinson, J. Chem. Eng. Data 14 (1969) 120-124.
[72] M.A.C. Härtel, T.M. Klapötke, V.N. Emel'yanenko, S.P. Verevkin, Thermochim. Acta 656 (2017) 151-160.
[73] M.A. Härtel, T.M. Klapötke, J. Stierstorfer, L. Zehetner, Propellants, Explos., Pyrotech. (2019).
[74] G. Bikelytė, M. Härtel, J. Stierstorfer, T.M. Klapötke, A.A. Pimerzin, S.P. Verevkin, J. Chem. Thermodyn. 111 (2017) 271-278.
[75] M.A. Althoff, K. Grieger, M.A. Härtel, K.L. Karaghiosoff, T.M. Klapötke, M. Metzulat, J. Phys. Chem. A 121 (2017) 2603-2609.
[76] G. Bikelytė, M.A.C. Härtel, M. Holler, A. Neuer, T.M. Klapötke, J. Chem. Eng. Data (2021).
[77] V.R. Meyer, Practical high-performance liquid chromatography, John Wiley & Sons (2013).
[78] L.R. Snyder, J.J. Kirkland, J.W. Dolan, Inc., Hobeken, New Yersey, Canada (2010) 202.

[79] M.E. LaCourse, W.R. LaCourse, Chapter 17 - General instrumentation in HPLC*. in: S. Fanali, P.R. Haddad, C.F. Poole, M.-L. Riekkola, (Eds.), Liquid Chromatography (Second Edition), Elsevier, 2017, pp. 417-429.
[80] R. Blain, CHAPTER 3 - ABSORBANCE DETECTION. in: D. Parriott, (Ed.), A Practical Guide to HPLC Detection, Academic Press, San Diego, 1993, pp. 39-66.
[81] M. Swartz, J Liq Chrom Relat Tech 33 (2010) 1130-1150.
[82] D. Corradini, T.M. Phillips, Handbook of HPLC, CRC Press (Boca Raton), 2010.
[83] M. Cushman, G.I. Georg, U. Holzgrabe, S. Wang, J. Med. Chem. 57 (2014) 9219-9219.
[84] B. Diehl, U. Holzgrabe, Y. Monakhova, T. Schönberger, J. Pharm. Biomed. Anal. 177 (2020) 112847.
[85] G.F. Pauli, T. Gödecke, B.U. Jaki, D.C. Lankin, J. Nat. Prod. 75 (2012) 834-851.
[86] R.S. Phansalkar, C. Simmler, J. Bisson, S.-N. Chen, D.C. Lankin, J.B. McAlpine, M. Niemitz, G.F. Pauli, J. Nat. Prod. 80 (2017) 634-647.
[87] T. Gödecke, J.G. Napolitano, M.F. Rodríguez-Brasco, S.-N. Chen, B.U. Jaki, D.C. Lankin, G.F. Pauli, Phytochem Anal 24 (2013) 581-597.
[88] T. Schoenberger, Anal. Bioanal. Chem. 403 (2012) 247-254.
[89] F. Malz, H. Jancke, J. Pharm. Biomed. Anal. 38 (2005) 813-823.
[90] F. Malz, Chapter 2 - Quantitative NMR in the Solution State NMR. in: U. Holzgrabe, I. Wawer, B. Diehl, (Eds.), NMR Spectroscopy in Pharmaceutical Analysis, Elsevier, Amsterdam, 2008, pp. 43-62.
[91] T. Schoenberger, Report: Guideline for qNMR analysis, (2019).
[92] G.F. Pauli, S.-N. Chen, C. Simmler, D.C. Lankin, T. Gödecke, B.U. Jaki, J.B. Friesen, J.B. McAlpine, J.G. Napolitano, J. Med. Chem. 57 (2014) 9220-9231.
[93] G.F. Pauli, B.U. Jaki, D.C. Lankin, J. Nat. Prod. 68 (2005) 133-149.
[94] T. Schoenberger, Y. Monakhova, D. Lachenmeier, T. Kuballa, Guide to NMR Method Development and Validation – Part I: Identification and Quantification, (2014).
[95] T. Schönberger, Toxichem Krimtech 79 (2012) 81.
[96] M. Weber, C. Hellriegel, A. Rück, R. Sauermoser, J. Wüthrich, Accredit. Qual. Assur. 18 (2013) 91-98.
[97] A. Reichmuth, S. Wunderli, M. Weber, V.R. Meyer, Microchim. Acta 148 (2004) 133-141.
[98] "Atomic weights of the elements 2019", available from: www.ciaaw.org. Date accessed: 28 April 2021.
[99] J.S. Chickos, S. Hosseini, D.G. Hesse, J.F. Liebman, J. Struct. Chem. 4 (1993) 271-278.
[100] S.P. Verevkin, A.Y. Sazonova, V.N. Emel'yanenko, D.H. Zaitsau, M.A. Varfolomeev, B.N. Solomonov, K.V. Zherikova, J. Chem. Eng. Data 60 (2014) 89-103.
[101] W. Acree Jr, J.S. Chickos, J. Phys. Chem. Ref. Data 45 (2016) 033101.
[102] M. Radomska, R. Radomski, Thermochim. Acta 40 (1980) 405-414.
[103] O. Dorofeeva, L. Gurvich, Preprint l-238, IVTAN, Moscow (1988).
[104] J. McCullough, H. Finke, J. Messerly, S. Todd, T. Kincheloe, G. Waddington, J. Phys. Chem. 61 (1957) 1105-1116.
[105] T. Tables, Thermodynamic Research Center Data Project, Texas A&M University, College Station 971 (1974) 2605-2609.
[106] W. Acree, J.S. Chickos, J. Phys. Chem. Ref. Data 39 (2010) 043101.
[107] K. Rakus, S.P. Verevkin, J. Schätzer, H.-D. Beckhaus, C. Rüchardt, Chem. Ber. 127 (1994) 1095-1103.
[108] N.d. Kolossowsky, W. Udowenko, Zhur. Obshchei Khim. (1934) 1027-1033.
[109] J.E. Hurst, B. Keith Harrison, Chem. Eng. Commun. 112 (1992) 21-30.

[110] G. Bikelytė, M.A. Härtel, T.M. Klapötke, B. Krumm, A. Sadaunykas, J. Chem. Thermodyn. 143 (2020) 106043.
[111] G. Bikelytė, M.A. Härtel, T.M. Klapötke, Propellants Explos. Pyrotech. 45 (2020) 1573-1579.
[112] G. Bikelytė, A. G. Harter, M. A. Härtel, S. B. Heimsch, T. M. Klapötke, Fluid Ph. Equilibria, 549 (2021), 113222.
[113] I. Wilhelm, , G. Bikelytė, M. Wittek, M. A. C. Härtel, D. Röseling, T.M. Klapötke. Propellants Explos. Pyrotech. 47.2 (2022): e202100057.